MAX PLANCK INSTITUTE
OF MOLECULAR PHYSIOLOGY

technische universität
dortmund

Investigation of lncRNA GRASLND in the context of melanoma differentiation and IFNγ response

Dissertation

zur Erlangung des akademischen Grades des

Doktors der Naturwissenschaften

(Dr. rer. nat.)

der Fakultät Chemie und Chemische Biologie

der Technischen Universität Dortmund

vorgelegt von

Kim Denise Fischer, M. Sc.

geboren am 29.03.1995 in Bad Neuenahr-Ahrweiler

Dortmund, 06.01.2025

The work presented in this thesis was executed from June 2021 to December 2024 in the group of Dr. Jochen Imig and under the formal supervision of Prof. Dr. Dr. h.c. Herbert Waldmann at the Chemical Genomics Centre of the Max Planck Society, the Max Planck Institute of Molecular Physiology, and the Faculty of Chemistry and Chemical Biology at TU Dortmund University in Dortmund.

Die vorliegende Arbeit wurde von Juni 2021 bis Dezember 2024 in der Arbeitsgruppe von Dr. Jochen Imig und unter der formalen Aufsicht von Prof. Dr. Dr. h.c. Herbert Waldmann am Chemical Genomics Centre der Max-Planck-Gesellschaft, dem Max-Planck-Institut für Molekulare Physiologie und der Fakultät für Chemie und Chemische Biologie der TU Dortmund in Dortmund durchgeführt.

First Examiner/Erstgutachter: Prof. Dr. Dr. h.c. Herbert Waldmann

Second Examiner/Zweitgutachter: Prof. Dr. Carsten Watzl

Supervisor/Betreuer: Dr. Jochen Imig

Parts of the results of this dissertation are included in the following publication:

Die Ergebnisse dieser Dissertation sind zu Teilen in der folgenden Publikation enthalten:

Fischer, K. D., Tiwari, S., Thier, B., Qiu, L. C., Lin, T.-C., Paschen, A., Imig, J. “Long non-coding RNA GRASLND links melanoma differentiation and interferon-gamma response.“ *Frontiers in Molecular Biosciences* **2024**, 11,1471100. doi: 10.3389/fmolb.2024.1471100

Acknowledgements

First and foremost, I would like to express my sincere gratitude to my supervisor, Dr. Jochen Imig, for granting me the opportunity to work on this fascinating research topic and for his support and guidance throughout this 3.5 years PhD journey. While facing numerous challenges within this topic, his expertise and advice helped to shape the direction of my work and I am thankful for the opportunity to learn under his mentorship.

I would also like to extend my sincere appreciation to Prof. Herbert Waldmann for kindly taken over the role as my first examiner and his thorough evaluation of my dissertation. Moreover, he spearheaded the extension of CGC funding into a third phase, providing me and many other PhD candidates the opportunity to conduct research in this highly enriching scientific environment with exceptional projects.

I would like to extend my profound gratitude to Professor Carsten Watzl for kindly agreeing to serve as the second examiner. I deeply appreciate his expertise and insight in evaluating my dissertation.

A special and heartfelt thanks go to Prof. Annette Paschen from the University Hospital Essen for initially proposing the basis of my research project. She, together with her PhD student and later Postdoc, Dr. Beatrice Thier, gave exceptional effort and guidance to my research, which were instrumental in bringing this work to completion for publication. Their support has been truly indispensable and I deeply appreciated it.

I would like to extend my heartfelt thanks to my bachelor student Lin Christina Qiu not only for her outstanding contributions inside, but also outside the lab. Her dedication, enthusiasm, and commitment to the project were invaluable, and her scientific and mental support greatly enhanced the progress of my research (and well-being).

I would like to extend my gratitude to the former members of the Imig Lab, particularly Dr. Sama Shamloo, for her invaluable training, technical support, expertise, and thorough guidance, all of which played a significant role in shaping me as a researcher. Special thanks are extended to Dr. Evie Petroulia for her precious assistance with technical and experimental aspects, but most importantly for her friendship and mental support. My project would not have reached its current state without the exceptional support of the outstanding bioinformatician genius Shashank Tiwari, who has also become a great friend along the way. Thank you for everything. I would like to sincerely thank Dr. Jeffrey Schloßhauer, who joined the lab during the final year of my journey but made a significant impact in helping me bring everything to completion. Your invaluable pro-tips for publishing and help with almost every scientific question, combined with your friendship and emotional support, played a crucial role in this process, and I am deeply grateful for your presence during this pivotal time. I would like to extend my heartfelt thanks to all the other former members of the lab throughout the years: Dr. Alejandro Ulloa-Morales, Boris Simeonov, Katja Schamrin, Rajeha Perinbarajah, Sanat Mishra, Elnaz Banijamali and Lisa Kratzenbach. With all of you, there has always been a wonderful environment filled with

collaboration, support, and plenty of laughter. You made this journey not only productive but also truly enjoyable. Thank you for creating such a positive and inspiring atmosphere.

I am deeply grateful for the exceptional experimental support from Dr. Stefano Maffini and Nico Schmidt from Department 1 of the MPI Dortmund for the access and technical support to their fluorescence microscope and Dr. Daniel Summerer from the TU Dortmund for providing access to the flow cytometry instrument with special thanks to Dr. Tzu-Chen Lin for her extraordinary support of the measurement and data analysis. I really appreciated the help of Dr. Petra Janning from Department 4 of the MPI Dortmund and project group leader of the mass spectrometry group for her great support regarding the LC-MS-MS measurement and analysis. I also want to acknowledge Aylin Binici and Siska Führer from Department 4 of the MPI Dortmund for the help regarding the IncuCyte imaging system and the proteomics analysis, respectively. Further, I really appreciate Dr. Daniel Prumbaum for the access to the S2 lab and his consistent help with difficulties regarding S2 work. The general collaborative spirit in the institute were instrumental in advancing my research, and I truly appreciate your contributions.

I wish to express my appreciation to the CGC funding companies, particularly Pfizer for their commitment.

I would like to express my sincere gratitude to the IMPRS coordinators Christa Hornemann and Dr. Lucia Sironi for their steady support and dedication. Their guidance, organizational efforts, and commitment to fostering a positive learning environment have been invaluable throughout my doctoral journey.

My heartfelt thanks go to all the members of the CGC for fostering a collaborative and supportive environment. I would like to extend special appreciation to Sarah, Kai, Rachel, Neele, Kim, Siska and Lydia for their exceptional contributions throughout my PhD.

I would like to express my deepest gratitude to my study crew “Harter Kern”, with whom I had the privilege to study and share countless memories. Caro, Britta, Jan, Hannes, Jens, Sarah and Niko, your support, encouragement, and friendship over the past 10 years have been invaluable, both personally and academically.

My deepest gratitude goes to my family for their persistent support over the years. I am especially thankful to my parents, whose efforts and sacrifices allowed me to study and take this path. Their love and belief in me have meant the world.

Lastly, I would like to express my heartfelt appreciation to my partner Niko, who has been the greatest GRASLND Fan and my unwavering source of strength. Your belief in me, even when I felt stuck at a dead end, and your constant encouragement have meant more to me than words can express. Thank you for being my biggest fan and for always standing by my side.

This work is dedicated to the one whose silent fight and strength has guided my path. Experiencing this has encouraged me to contribute a tiny part to the understanding of this disease, with the hope that even the smallest effort may help in a battle that touches so many lives.

In loving memory of O. W.

Table of Contents

Abstract

Melanoma originates from the malignant transformation of melanocytes and represents the foremost cause of skin cancer-related mortality. The exceptionally poor survival prognosis, especially for patients in advanced disease stages, arises from its high metastatic potential, intratumoral heterogeneity and pronounced phenotypic plasticity. This latter characteristic is pivotal in driving tumor progression, metastatic spread and resistance to therapy. The primary treatment option for metastatic melanoma is immune checkpoint blockade (ICB) immunotherapy, which inhibits regulatory pathways to enhance the activation and function of cytotoxic T lymphocytes (CTLs) to recognize and attack tumor cells. ICB therapy has revolutionized the disease management and significantly improved long-term patient survival outcomes. Nonetheless, therapy resistance has become a widespread challenge and reduced the overall clinical success. Resistance mechanisms are primarily associated with a dysfunctional HLA class I-mediated antigen processing and presenting machinery (APM) or a loss of melanocytic differentiation antigens, which are generally recognized by CTLs. This loss is a result of cell dedifferentiation, a process known as phenotype switching and describes the cellular plasticity of melanoma cells to adapt to environmental cues through reversible transcriptional reprogramming, potentially facilitating evasion from CTL-mediated immune responses. Long non-coding RNAs (lncRNAs) have been implicated in crucial processes of melanomagenesis including immune escape mechanisms, but also proliferation, metastasis and drug resistance. Given their diverse regulatory functions, lncRNAs may also affect melanoma plasticity, yet their specific roles and underlying mechanisms remain largely unexplored.

In this study, lncRNA GRASLND was investigated for its potential relevance in melanoma pathogenesis, building on its prior description in mesenchymal stem cells (MSCs) as an inhibitor of the IFNγ signaling, a key immune pathway substantial for regulating the HLA class I-APM and thus immunogenicity towards CTLs, by direct interaction with interferon-induced, double-stranded RNA-activated protein kinase (PKR). GRASLND was found to be overexpressed in melanoma tumor samples, correlated to the differentiated melanoma cell state and contributing to poor clinical prognosis. RNAi-based GRASLND knockdown revealed a switch of a differentiated, melanocytic and highly proliferative cell state towards a dedifferentiated, highly invasive and slow-proliferating cell state. In addition, GRASLND was discovered as highly expressed in immunological “cold” tumors and demonstrated an inverse correlation with gene signatures of immune response activation and pro-inflammatory cellular processes, indicating an immune-regulatory role in melanoma. Significantly, a downregulation of GRASLND under IFNγ resulted in an increase of expression levels of IFNγ-stimulated genes (ISGs), including HLA-I surface protein expression, suggesting a suppressive effect of GRASLND on IFNγ signaling also in melanoma. Further, a GRASLND-PKR interaction, as reported in MSCs, was validated. These findings suggest an adaptive resistance mechanism of melanoma cells evading the immune system via suppression of IFNγ signaling. This appears to be driven by overexpression of lncRNA GRASLND, which likely contributes to this effect through its interaction with PKR. Thus, targeting this specific interaction might be promising to overcome a potential immune escape mechanism in melanoma.

Kurzzusammenfassung

Das Melanom entsteht durch die maligne Transformation von Melanozyten und stellen die Hauptursache für die mit Hautkrebs verbundene Sterblichkeit dar. Die schlechte Überlebensprognose, insbesondere für Patienten in fortgeschrittenen Krankheitsstadien, ist auf das hohe Metastasierungspotenzial, die intratumorale Heterogenität und die ausgeprägte phänotypische Plastizität zurück zuführen. Letztere ist entscheidend für das Fortschreiten des Tumors, die Ausbreitung von Metastasen und die Therapieresistenz. Die primäre Behandlungsoption für das metastasierte Melanom ist die Immun-Checkpoint-Blockade (ICB), die Regulationswege hemmt, um die Aktivierung und Funktion zytotoxischer T-Lymphozyten (CTLs) zur Erkennung und Bekämpfung von Tumorzellen zu verbessern. Die ICB-Therapie hat die Behandlung der Krankheit revolutioniert und die langfristigen Überlebensaussichten der Patienten erheblich verbessert. Dennoch hat sich die Therapieresistenz zu einer großen Herausforderung entwickelt und den klinischen Gesamterfolg verringert. Resistenzmechanismen sind in erster Linie mit einer dysfunktionalen HLA-Klasse-I-vermittelten Antigenprozessierungs- und präsentationsmaschinerie (APM) oder einem Verlust von melanozytären Differenzierungsantigenen verbunden, die normalerweise von CTLs erkannt werden. Dieser Verlust ist das Ergebnis einer Zell-Dedifferenzierung, einem Prozess, der als Phänotyp-Switching bekannt ist und die zelluläre Plastizität von Melanomzellen beschreibt, sich durch reversible transkriptionelle Umprogrammierung an Umweltreize anzupassen, und damit der CTL-vermittelten Immunreaktionen zu entgehen. Lange nichtkodierende RNAs (lncRNAs), sind in wesentliche Prozesse der Melanomagenese involviert, inklusive der Immunabwehr, aber auch der Proliferation, Metastasierung und Arzneimittelresistenz. Aufgrund ihrer vielfältigen regulatorischen Funktionen könnten lncRNAs auch die Plastizität des Melanoms beeinflussen, jedoch sind ihre spezifischen Rollen und Mechanismen noch weitgehend unerforscht.

In dieser Arbeit wurde die lncRNA GRASLND im Hinblick auf ihre potenzielle Relevanz in der Melanom-Pathogenese untersucht, basierend auf ihrer früheren Beschreibung in mesenchymalen Stammzellen (MSCs) als Inhibitor des IFNγ-Signalwegs, eines wichtigen Immunsignalwegs, der für die Regulierung der HLA-I-APM und damit der Immunogenität gegenüber CTLs wesentlich ist, durch direkte Interaktion mit der Interferon-induzierten, doppelsträngigen RNA-aktivierten Proteinkinase (PKR). GRASLND wurde im Melanom als überexprimiert und mit dem differenzierten Melanom-Zellstatus korrelierend nachgewiesen, es wurde auch gezeigt, dass es zu einer schlechten Prognose beiträgt. Die RNAi-basierte Ausschaltung von GRASLND zeigte einen Wechsel von einem differenzierten, melanozytären und stark proliferativen Zellstatus zu einem dedifferenzierten, stark invasiven und langsam proliferierenden Zellstatus. Darüber hinaus wurde festgestellt, dass GRASLND in immunologisch „kalten“ Tumoren stark exprimiert wird und eine umgekehrte Korrelation mit Gensignaturen der Aktivierung von Immunreaktionen und proinflammatorischen zellulären Prozessen aufweist, was auf eine immunregulatorische Rolle beim Melanom hinweist. Bemerkenswerterweise führte eine Herunterregulierung von GRASLND unter IFNγ zu einem Anstieg der Expressionsniveaus von IFNγ-stimulierten Genen (ISGs), einschließlich der Expression von HLA-I-Oberflächenproteinen, was auf eine unterdrückende Wirkung von GRASLND auf die IFNγ-Signalübertragung auch beim Melanom

hindeutet. Darüber hinaus wurde eine Interaktion zwischen GRASLND und PKR, wie sie bei MSCs berichtet wurde, bestätigt.

Diese Ergebnisse deuten darauf hin, dass Melanomzellen möglicherweise einen adaptiven Resistenzmechanismus einsetzen, um das Immunsystem zu umgehen, indem sie den IFNγ-Signalweg unterdrücken. Dieser Prozess scheint durch die Überexpression der lncRNA GRASLND angetrieben zu werden, die wahrscheinlich durch ihre Interaktion mit PKR zu diesem Effekt beiträgt. Daher könnte die gezielte Beeinflussung dieser spezifischen Interaktion vielversprechend sein, um einen potenziellen Mechanismus zur Umgehung des Immunsystems beim Melanom zu überwinden.

Abbreviations

Abbreviation	Meaning
3'UTR	3'-untranslated region
7mG	7-methyl guanosine
ACN	Acetonitrile
AJCC	American Joint Committee on Cancer
AMP	Antigen processing and presenting machinery
APCs	Antigen-presenting cells
AS-lncRNA	Antisense lncRNAs
ASO	Antisense Single-Stranded Oligonucleotide
BANCR	BRAF-Activated Non-Protein Coding RNA
BRAF	V-Raf Murine Sarcoma Viral Oncogene Homolog B
BRAFi	BRAF inhibitor
BSA	Bovine Serum Albumin
CASC15	Cancer Susceptibility Candidate 15
CDK4	Cyclin Dependent Kinase 4
CDKN2A	Cyclin Dependent Kinase Inhibitor 2A
ceRNA	Competitive endogenous RNA
CRISPR	Clustered Regularly Interspaced Short Palindromic Repeats
CRISPRa	CRISPR Activation
CRISPRi	CRISPR Interference
crRNA	CRISPR RNA
CSD	Chronically sun-damaged
CTLA-4	Cytotoxic T-Lymphocyte Antigen-4
CTLs	Cytotoxic T lymphocytes
dCas9	Catalytically dead Cas9
DDR	DNA damage repair
DMEM	Gibco Dulbecco's Modified Eagle's Medium
DSB	Double strand break
dsRNA	Double stranded RNA
DTT	Dithiothreitol
eIF2α	Eukaryotic Initiation Factor 2 alpha
EMT	Epithelial-to-mesenchymal transition
eRNAs	Enhancer RNAs
ESCC	Esophageal squamous cell carcinoma
FA	Formic acid
FBS	Fetal Bovine Serum
FC	Fold Change
FDA	Food and Drug Administration
FWD	Forward
GAGs	Glycosaminoglycans
GAPDH	Glyceraldehyde 3-phosphate Dehydrogenase
GEPIA	Gene Expression Profiling Interactive Analysis
GR	Glucocorticoid receptor
GRASLND	Glycosaminoglycan Regulatory Associated Long Non-coding RNA
GRASLND	Glycosaminoglycan Regulatory Associated Long Non-coding RNA
GSEA	Gene Set Enrichment Analysis
H3K27me3	Histone H3 lysine 27 trimethylation
HLA-I	Human leukocyte antigen class I
HOTAIR	HOX Transcript Antisense Intergenic RNA
ICB	Immune Checkpoint Blockade
ICI	Immune Checkpoint Inhibitor
IFNγ	Interferon gamma
IL-2	Interleukin-2
IL-6	Interleukin-6
ImmlncRNAs	Immune-related lncRNAs

ISGs	IFNγ-stimulated genes
ISR	Integrated stress response
JAK	Janus kinase
KRAB	Krüppel-associated box domain
LAG-3	Lymphocyte activation gene-3
LDH	Lactate dehydrogenase
LMP2	Low molecular weight protein 2
LNA	Locked nucleic acid
lncRNA	Long non-coding RNA
LPS	Lipopolysaccharides
MALAT1	Metastasis-associated lung adenocarcinoma transcript 1
MAPK	Mitogen-activated protein kinase
MDAs	Melanoma differentiation antigens
MEKi	MEK inhibitor
MHC II	Major histocompatibility complex (MHC) class II
miRNA	Micro RNA
MITF	Microphthalmia-associated Transcription Factor
MMP14	Matrix Metallopeptidase 14
mRNA	Messenger RNA
MSCs	Mesenchymal stem cells
NAST	Neoadjuvant systemic therapies
ncRNA	Non-coding RNA
NCSC	Neural crest stem cell
NEAT1	Nuclear Enriched Abundant Transcript 1
NF1	Neurofibromatosis type I
NGFR	Nerve Growth Factor Receptor
NHEJ	Non-homologous end joining
NRAS	Neuroblastoma RAS viral oncogene homolog
NS	Non-significant
PARP1	Poly(ADP-ribose) Polymerase 1
PBS	Phosphate Buffered Saline
PCA	Principal component analysis
PCR	Polymerase Chain Reaction
PD-1	Programmed Cell Death-1
PD-L1	Programmed Death-Ligand 1
PFS	Progression-free survival
piRNA	Piwi-interacting RNA
PKR	Interferon-induced, double-stranded RNA-activated protein kinase
Pol II	Polymerase II
PP1α	Protein phosphatase 1α
PRC1	Polycomb repressive complex 1
PRC2	Polycomb repressive complex 2
PROMPTs	Promoter upstream transcripts
pSTAT1	Phosphorylated STAT1
PTEN	Phosphatase and tensin homolog
PVDF	Polyvinylidene difluoride
RBP	RNA binding protein
REV	Reverse
RISC	RNA-induced silencing complex
RNAi	RNA Interference
RNase P	Ribonuclease P
RNA-Seq	RNA Sequencing
RNF144A-AS1	RNF144A antisense RNA 1
RNP	Ribonucleoprotein
ROS	Reactive oxygen species
rRNA	Ribosomal RNA
RT	Reverse Transcription
RTK	Receptor tyrosine kinase
SAM	Synergistic activation mediator

SAMMSON	Survival Associated Mitochondrial Melanoma Specific Oncogenic Non-coding RNA
SDS-PAGE	Sodium Dodecyl Sulfate Polyacrylamide Gel Electrophoresis
SEM	Standard error of mean
sgRNA	Single Guide RNA
shRNA	Small hairpin RNA
siRNA	Small interfering RNA
SKCM	Skin cutaneous melanoma
SLNB	Sentinel lymph node biopsy
SMC	"starved"-like melanoma cells
SMD	Staufen1 (STAU1)-mediated mRNA decay
snoRNA	Small nucleolar RNAs
snoRNPs	Small nucleolar ribonucleoprotein particle
snRNA	Small nuclear RNAs
SPRY4-IT1	Sprouty RTK signaling antagonist 4-intronic transcript 1
STAT1	Signal transducer and activator of transcription 1
STAT3	Signal transducer and activator of transcription 3
STAU1	Staufen homolog 1
STING	Stimulator of interferon genes
TBS	Tris Buffered Saline
TCGA	The Cancer Genome Atlas
TCR	T cell receptors
TEMED	Tetramethylethylenediamine
TERT	Telomerase Reverse Transcriptase
Tet	Tetracycline
TFA	Trifluoroacetic acid
TGFβ	Transforming growth factor β
TNFα	Tumor necrosis factor α
TNM	Tumor, Nodes, Metastasis
Tris	Tris(hydroxymethyl)aminomethane
tRNA	Transfer RNA
TSLNC8	Tumor suppressive long noncoding RNA on chromosome 8p12
TSS	Transcription start site
TUSC7	Tumor suppressor candidate 7
UV	Ultra violet
Xist	X-inactive specific transcript

1. Introduction

1.1 Melanoma

1.1.1 Origin and Staging

Cutaneous malignant melanoma is an aggressive and potentially lethal form of skin cancer that originates from pigment-producing, neural-crest derived, epidermal melanocytes. Hence, melanoma can develop in various melanocyte-containing tissues, including non-cutaneous sites like the oral mucosa, paranasal sinuses, the central nervous system and the eyes[1–3]. The transformation of melanocytes into metastatic melanoma can be described by different staging systems. The initial model proposed by Wallace H. Clark in 1969 is a risk assessment based on depth of tumor penetration in distinct skin layers. The Clark model consists of five levels, starting with level I, in which melanoma is restricted to the outermost epidermis. Levels II-IV describe the invasion from the papillary to the reticular dermis, while level V represents penetration into the subcutaneous tissues, associated with the greatest metastatic risk and the poorest prognosis[4]. One year later, Alexander Breslow conducted a study on 98 melanoma patients, considering not only the level of anatomical invasion but also the tumor thickness, or more precisely, the depth of invasion in millimeters, known as Breslow's depth. Breslow categorized the disease cases in four stages starting from stage I with tumors less than 0.75 mm in depth and ending with stage IV with melanomas > 4 mm. This study showed that the survival is greatly affected by both factors, tumor size and extent of its invasion, with deeper tumors indicating a poorer clinical outcome[5]. Nowadays, the gold standard for melanoma staging and patient outcome prediction in the clinics is the American Joint Committee on Cancer (AJCC) staging system, whose guidelines incorporate the Breslow's depth and additional key factors, such as ulceration, number of metastatic lymph nodes and site(s) of distant metastatic disease[6–8]. The most updated 8th edition is based on the international tumor-nodes-metastasis (TNM) classification, which is applied to nearly all solid tumors[8,9]. The T category incorporates tumor thickness and the presence of ulceration and mitosis. Subcategories of the N category includes the involvement and number of "clinically occult" or "clinically detected" regional metastatic lymph nodes. Lastly, the M category classifies patients with distant metastasis and considers levels of serum lactate dehydrogenase (LDH)[9,10], with elevated levels reflecting a high tumor burden and invasive activity[11]. The AJCC melanoma staging system integrates the TNM- and their subcategories to classify melanoma from Stage 0 (melanoma *in situ*) to Stage IV. Stages I and II indicate localized melanoma with no lymph node involvement, differing only in the thickness of the tumor. The presence of regional lymph node metastasis leads to the classification in Stage III. Advanced, Stage IV melanoma is characterized by the presence of distant metastases. The detailed AJCC melanoma staging allows clinicians to tailor treatment strategies, ranging from surgical excision to systemic therapies. Further, it aids in prognosis prediction and gives insights into survival probabilities and disease progression[7,12,13].

1.1.2 Risk Factors, Development and Progression

Melanoma is recognized as a multifaceted disease that develops through the combined effects of genetic predisposition and environmental influences. Among these, UV irradiation exposure stands out as the most critical environmental risk factor due to its mutagenic effects[14]. Intermittent sun exposure and past sunburn incidents, particularly during childhood, are established as the major modifiable risk factors for melanoma[15,16]. A significant non-modifiable risk factor is the quantity of moles, known as melanocytic or pigmented nevi, which are non-cancerous clusters of melanocytes or nevus cells. A meta-analysis demonstrated the increased risk of melanoma development correlated with the number of common and atypical nevi, highlighting the importance of monitoring and evaluating nevi as part of melanoma prevention and risk assessment[17]. Phenotypic features indicative of reduced melanin production, such as light complexion, light hair (blonde or red), light eye color, the presence of freckles and the tendency to sunburn are markers for a greater susceptibility to melanoma[18]. Furthermore, a family history of melanoma accounts for an increased risk, as approximately 8-12% of cases occur in individuals who have first-degree relatives affected by melanoma, either due to shared skin phenotypes or germline mutation. The most frequent germline mutations found in these families are in the tumor suppressor gene CDKN2A (p16), with less common occurrences of mutations in CDK4, which are both involved in cell cycle regulation[19–21]. Also a previous melanoma diagnosis significantly elevates the probability of developing a second melanoma[22,23].

The development of melanoma involves the transformation of melanocytes through genetic mutations upon UV-induced DNA damage. Cutaneous melanomas in Caucasians are generally divided into two major subtypes: those arising either from chronically sun-damaged (CSD) or from intermittently sun-exposed (non-CSD) skin. These subtypes are differentiated by variations in UV radiation exposure, anatomical location, patient age, and mutational burden[24–26] (Figure 1). The non-CSD melanomas are found on anatomical regions with moderate sun exposure, develop at a younger age (<55 years), often originate from nevi and exhibit a relatively lower mutational burden. These tumors frequently contain $BRAF^{V600E}$ mutation, which results in the formation of benign nevi that typically require further genetic alterations, such as TERT promoter mutations or CDKN2A loss to evolve into melanoma. In contrast, CSD melanomas are characterized by high mutational burdens, often occur in patients older than 55 years and primarily arise in anatomical regions with significant sun exposure, particularly the head and neck. These melanomas typically do not originate from pre-existing nevi, but rather from melanoma *in situ* or dysplastic lesions and are driven by a distinct set of mutations[26].

In advanced melanomas from both subtypes, various somatic mutations accumulate and impact genes that govern essential cellular functions, including proliferation (BRAF, NTAS, NF1), growth (PTEN, KIT), resistance to apoptosis (TP53), cell cycle (CDKN2A, encoding p16INK4A and p14ARF) and replicative life span (TERT). Consequently, the two key signaling pathways of mitogen-activated protein kinase (MAPK), also known as the Ras-Raf-MEK-ERK pathway and the phosphoinositol-3-kinase (PI3K)/AKT pathway are dysregulated and abnormally activated, regulating cell proliferation/survival and cellular homeostasis, respectively[26–29].

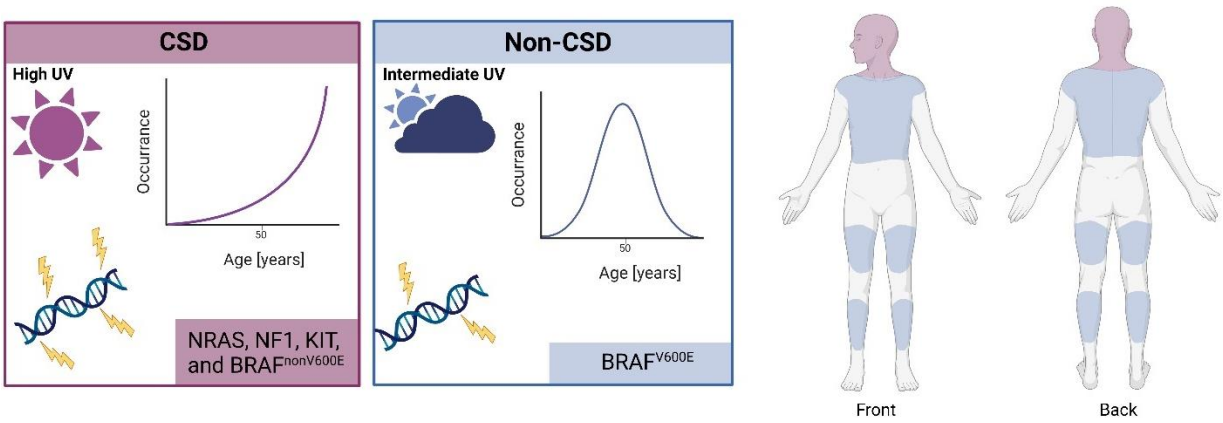

Figure 1: Chronically sun-damaged (CSD) and non-CSD melanoma subtypes. *CSD melanomas are found mainly in the head and neck, as these are areas with the highest degree of sun exposure. Thus, these tumors are characterized by a high mutational burden, frequently harboring mutations in NRAS, neurofibromin (NF1), KIT and BRAF (non-V600E), but develop later in life. In contrast, non-CSD melanomas manifest earlier in life in regions with moderate sun exposure. The mutation burden is relatively lower, with $BRAF^{V600E}$ being the predominant mutation. Figure was adapted from Shain et al.[26] and created using Biorender.com.*

Aberrant MAPK signaling is primarily attributed to mutations in BRAF or NRAS. B-Raf encoded by the BRAF gene is a serine/threonine kinase, that is activated by small GTPase Ras (Ras-GTP) and subsequently phosphorylates MEK. Roughly 50% of non-CSD melanomas contain a mutation in the BRAF gene, with over 90% occurring at codon 600. The predominant mutation is a point mutation resulting in the substitution of valine with glutamic acid (V600E), which causes constitutive kinase activation and renders it insensitive to negative feedback processes[27,30]. The second most prevalent mutation, V600K, accounts for approximately 10% of all melanomas with BRAF mutations, while V600M and V600R are rare[31,32]. Activating point mutations in the NRAS gene, coding for the small GTPase N-Ras are present in about 15-25% and the second most cause of a disrupted MAPK pathway signaling in cutaneous melanoma[27,33,34]. Activating mutations in the BRAF and NRAS genes are found to be mutually exclusive in the majority of melanomas[35,36] and in contrast to BRAF mutations, altered N-Ras function also leads to a dysregulation of the PI3K/AKT pathway[24]. An indirect and continuous activation of N-Ras can occur by a loss-of-function mutation of the gene encoding for the tumor suppressor protein neurofibromin 1 (NF1). NF1 acts as a negative regulator of the RAS/MAPK and PI3K/AKT signaling pathway by converting the active RAS-GTP to the inactive RAS-GDP form. In melanoma, NF1 is the third most altered gene occurring in 10-15% of tumors[27,37]. Both signaling pathways are triggered by direct binding of growth factors to the receptor tyrosine kinase (RTK) KIT. Activating alterations in the KIT genes are observed in a subset of malignant melanomas, as meta-analyzed by Gong *et al.*, stating an association with older age, acral, mucosal and CSD sites, but a negative correlation with non-CSD melanomas and a location on the extremities[38].

While these primary driver mutations are fundamental in melanoma development, various other critical genetic changes have been identified that influence the progression of the disease. These additional mutations are frequently found in advanced, metastatic melanoma, highlighting their role in the disease's spread. These include TERT promoter mutations that will enhance TERT transcriptional activity, thereby preserving telomere length and fostering cell immortalization and melanoma progression[39].

Furthermore, genetic alterations in the CDKN2A gene, which encodes the tumor suppressor proteins p16INK4A and p14ARF, result in enhanced melanoma invasion capacity and metastasis. As cell cycle regulators, a reduction in their activity, due to deletions, mutations, or promoter hypermethylation, leads to impaired cell cycle control and contributes to melanomagenesis[40]. Lastly, the dysregulation of the tumor suppressor phosphatase and tensin homolog (PTEN) is reported with a high prevalence (10-30%) in cutaneous melanoma. PTEN is a key molecule in a negative feedback mechanism of the PI3K/AKT signaling by counteracting PI3K activity. PTEN loss results in the constitutive activation of AKT and is linked to melanoma advancement[40,41].

1.1.3 MITF and Phenotype Switching

The transformation of melanocytes into melanoma is driven by a combination of genetic alterations and environmental factors, however, the transcription factor Microphthalmia-associated Transcription Factor (MITF) plays an essential role in the progression and aggressiveness of this lethal skin cancer. MITF is crucial for melanocyte development and functions by controlling the expression of genes involved in melanin-pigment production, cell cycle regulation, survival and melanocyte differentiation from neural crest cells, thus establishing itself as a key determinant of melanocyte identity[3,42,43]. In a key study, Keith S. Hoek and colleagues uncovered gene expression signatures of melanoma patient samples that define the metastatic potential and different melanoma phenotypic cell states[44]. The expression levels of MITF were found to be closely associated with the metastatic behavior of melanoma cells. Three melanoma sample cohorts were defined, with cohort A and C marked by MITF-high ($MITF^{high}$) and -low ($MITF^{low}$) expression, respectively, and cohort B displaying a heterogeneous gene expression pattern. The researchers discovered that the $MITF^{low}$ phenotype is more prone to metastasize, slow-growing and is associated with a heightened activity of invasion-related genes. In contrast, $MITF^{high}$ melanoma cells are highly proliferative and lowly invasive. A follow-up *in vivo* study demonstrated that melanoma cells can reversibly switch between the highly proliferative and differentiated, $MITF^{high}$ cell state and the invasive, slow-growing and dedifferentiated, $MITF^{low}$ state[45]. This cell state transition resembles the epithelial-to-mesenchymal transition (EMT), a process that aids to tumor metastasis by the loss of cell adhesion allowing tumor cells to detach their cellular structure and invade the basement membrane[46]. However, as melanocytes are not epithelial and their dedifferentiated phenotypes might not align with mesenchymal characteristics, the term “phenotype switching” is used in the melanoma context, initially proposed by Hoek *et al.* in 2008[45,47]. This study overturns the previously assumed unidirectionality of gene expression changes pointing towards a dynamic behavior and transcriptional signature plasticity. The tumor microenvironment with various internal and external signals modulates this phenotype switching, and this form of cellular plasticity appears to be essential for melanoma progression and metastasis (Figure 2)[45]. Unlike permanent genetic alterations, the phenotypic plasticity is marked by mostly reversible epigenetically driven remodeling of the transcriptome to allow flexibility and adaptability in response to various environmental stimuli[47], that include cellular stresses such as hypoxia, nutrient starvation and inflammation like transforming growth factor β (TGFβ) or tumor necrosis factor α (TNFα) signaling in melanoma by affecting MITF expression[48–53].

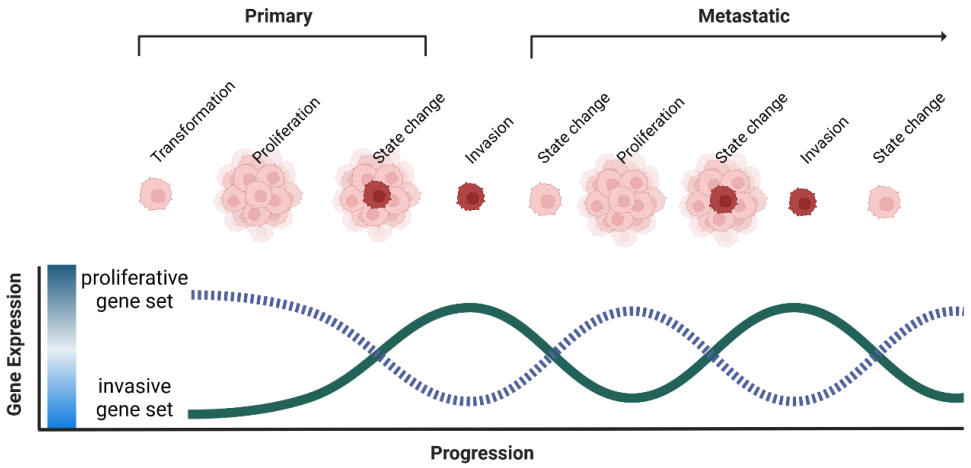

Figure 2: Model for melanoma metastases formation and progression based on alternating regulation of gene sets. *Melanoma cells in the primary tumor are characterized by the expression of the proliferative gene signature. Triggered by microenvironmental changes, proliferative cells undergo a cell state transition ('state change') to an invasive phenotype, characterized by the expression of a clearly distinct invasive gene set. Invasive melanoma cells spread through the bloodstream to a distant site, reverting to a proliferative cell state to form a metastasis. This cycle of phenotype switch accompanied with a change in the gene signature expression of proliferative and invasive genes is repeated during melanoma progression. Figure was adopted from Hoek et al.[45] and created using Biorender.com.*

A phenotype switch towards the invasive, dedifferentiated melanoma cell state not only correlates with increased metastatic potential, but is also closely associated with intrinsic and acquired resistance to targeted or immunotherapies[54] as explained in section 1.1.5 in more detail. Targeted therapy predominantly focuses on the inhibition of the MAPK signaling pathway. This approach primarily includes the use of inhibitors that target specific components, specifically BRAF and MEK. It has been reported that the absence of MITF is associated with decreased sensitivity to MAPK inhibitors (MAPKi), while its presence is crucial for effective drug responses[47,55]. In addition, a melanoma cell dedifferentiation is linked to reduced immunogenicity towards cytotoxic T lymphocytes (CTLs), leading to immunotherapy resistance[56,57]. These varying therapy sensitivities of different melanoma cell states, highlight the challenge for successful treatment. Nonetheless, this same phenotypic plasticity might present a strategy for therapeutic intervention, potentially promoting the transition of cells from a drug-resistant to a more drug-responsive state through targeting underlying mechanisms of phenotype switching. This underscores the critical need to identify undiscovered processes and factors that govern this cell state transition[47].

In recent years the oversimplistic model of a phenotype switch solely between a differentiated, MITF^{high} and a dedifferentiated, MITF^{low} cell state was redefined, as further cell states were identified. A gene expression analysis of melanoma samples by Tsoi *et al.* identified four subtypes for melanoma, categorized as classes C1-C4: the undifferentiated, neural crest-like, transitory, and melanocytic cell state, respectively[58]. Classes C1 and C4 thereby align with Hoek's MITF^{low} cohort C and MITF^{high} cohort A. The transitory class C3 exhibited MITF expression, but also displayed neural crest-like characteristics, linking it to Hoek's Cohort B[44]. The neural crest-like class C2 has been newly described and resembles the undifferentiated cell state C1 in terms of the absence of MITF and the high expression of the receptor tyrosine kinase (RTK) AXL, a marker for dedifferentation and drug resistance[55]. Classes

C1 and C2 are distinguished by their differential expression of the transcription factors SOX10 and SOX9. Specifically, Class C2 exhibits SOX10 expression and lacks SOX9 abundance. The opposite is observed for the undifferentiated C1 class, reflecting biological differences and diverse functional characteristics. Further, C2 is characterized by the presence of the neural crest lineage-specifying transcription factor and RTK Nerve Growth Factor Receptor (NGFR), which was reported to be associated with T cell and immunotherapy resistance[58,59]. In a pivotal study, Wouters *et al.* examined the intermediate state, which corresponds to Tsoi's transitory class C3, to determine whether it represents a heterogeneous mixture of melanocytic and dedifferentiated cells or if it is characterized by stable, "mixed" gene regulatory networks. Indeed, a robust gene expression pattern for the intermediate state and no spontaneous switching of the cell state with a certain regularity was found. The intermediate state is regulated by a set of transcription factors and shows moderate MITF activity. In addition it harbors gene signatures of both, the melanocytic and the mesenchymal-like, dedifferentiated state, thus exhibiting both proliferative and invasive characteristics[60]. Rambow *et al.* subsequently built upon these findings using single-cell RNA-Seq on BRAF mutant *in vivo* pre-clinical melanoma models exposed to MAPKis[61]. Four distinct drug-tolerant phenotypic states were identified as invasive, neural crest stem cell (NCSC), "starved"-like melanoma cells (SMC), and pigmented melanoma transcriptomic states, and were observed to coexist within tumor lesions. These cell states resemble the phenotypes defined earlier as the undifferentiated ("invasive"), the neural crest-like ("NCSC") and the melanocytic ("pigmented") phenotype[58]. The SMC melanoma cell population exhibits intermediate levels of MITF expression, yet demonstrates significant downregulation of cancer cell metabolic patterns, along with indicators of nutrient deprivation. Of note, it is still uncertain whether the intermediate/transitory and starved (SMC) states are separate entities[47]. This study demonstrated, that in response to drug exposure, highly-proliferative MITF-expressing melanoma cells underwent phenotype switching towards the drug-tolerant "starved"-like state, followed by a transition either into a therapy-resistant strongly pigmented $MITF^{high}$ state ("hyperdifferentiated") or an $MITF^{low}$ state, which could correspond to either the drug-tolerant invasive or NCSC state. Abundance of the latter was initially relatively low in the untreated patient melanomas and drug-naïve patient-derived xenografts. However, upon treatment with MAPKi, NCSC cells became more prevalent, though their numbers decreased once the treatment was discontinued[61]. These findings underscore the urgent need for further research into how melanoma phenotype switching influences both, disease progression and drug resistance. Understanding the mechanisms behind this cell state transition thus becomes an essential melanoma research priority.

1.1.4 Melanoma Immunogenicity

Melanoma phenotype switching towards a dedifferentiated cell state is marked by a diminished immunogenicity towards CTLs, a main cause of tumor immune evasion and thus resistance to immunotherapy. CTLs target and kill tumor cells with precision. This selectivity is facilitated by the T cell receptor's (TCRs) binding to specific HLA class I (HLA-I) antigen complexes. Dedifferentiated melanoma cells lack the expression of melanoma differentiation antigens (MDAs), such as MITF target genes MelanA, gp100 and tyrosinase, required for effective anti-tumor immune response[53,57,62]. The cytotoxic

effects of CD8+ T cells that have recognized their cognate antigen on the tumor cell are mediated by the release of cytolytic granules or the activation of death receptors[63]. A key element of the anti-tumor response, particularly in halting tumor growth and triggering cell death, involves the secretion of interferon-gamma (IFNγ). IFNγ is a cytokine that plays a key role in inflammation, enhances anti-tumor activity through direct anti-proliferative and pro-apoptotic effects, the recruitment of additional immune cells, and the activation of pathways involved in the expression of proteins within the HLA-I-mediated antigen processing and presentation machinery (HLA-I-APM)[64–66]. The HLA-I-APM is critical for the presentation of intracellular antigens to CD8+ T cells, allowing the immune system to detect and respond to intracellular pathogens and tumor cells. This process contains several key steps: antigen uptake, antigen processing, loading of the processed antigen onto HLA-I molecules, and the expression of this complex on the cell surface for presentation to T cells (Figure 3)[67].

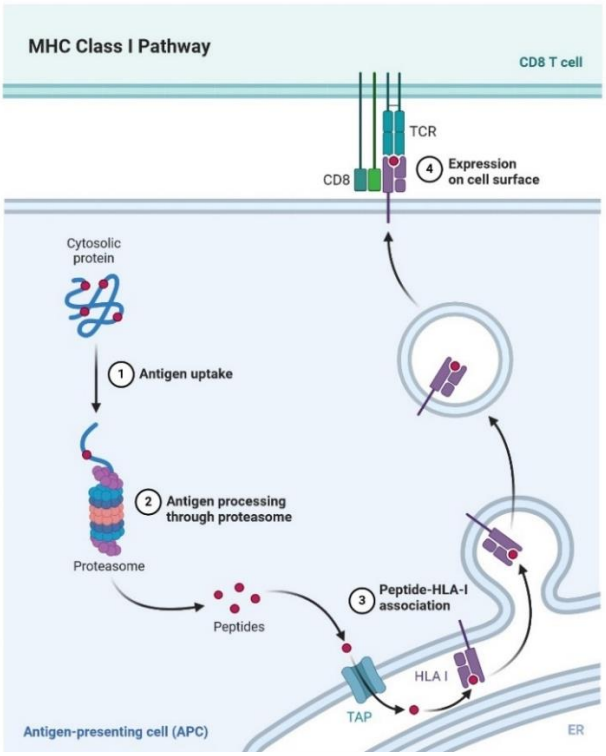

Figure 3: Mechanism of the HLA Class-I Antigen Processing and Presenting Machinery. *Tumor antigens are processed through the proteasome and transported into the ER lumen by the heterodimeric transporter associated with antigen processing complex (TAP1/TAP2). This is followed by the loading of the peptide onto the HLA-I molecule and the transfer to the cell surface via clathrin-independent endocytosis, where it gets presented to cytotoxic T cells. This figure is a template called "MHC Class I and II Pathways" made by Akiko Iwasaki using Biorender.com.*

Endogenous proteins are tagged with ubiquitin and subsequently degraded by cytosolic multi-subunit proteasome complexes, including the immunoproteasome. This process involves catalytic subunits low molecular weight protein 2 (LMP2), LMP7, and LMP10 for generating peptides. Activation of the immunoproteasome is stimulated mainly by IFNγ exposition. Generated antigen peptides are further transported to the ER lumen by the heterodimeric transporter associated with antigen processing (TAP) complex, where they are loaded onto β2M-associated HLA class-I heavy chain dimers. The peptide-HLA-I complex is shuttled from the ER to the Golgi apparatus and transported to the cell surface through

vesicular pathways for further recognition by TCRs of CD8+ T cells[67]. Foreign or irregular antigens, such as viral peptides or tumor-derived neoantigens, trigger T cell activation and an immune response. However, tumor cells, including melanoma, can develop strategies to evade this immune surveillance. Strategies involve downregulation of HLA-I molecules, mutations in components of the antigen-processing machinery (such as β2M, TAP1 and TAP2), or interferon signaling defects (JAK1/2 loss-of-function mutations), enabling them to avoid CTL recognition[68,69].

1.1.5 Treatment and Therapy Resistance

1.1.5.1 Surgery

The standard approach in melanoma treatment is the wide surgical excision of the primary tumor, focusing on the complete removal of the malignant lesion for local disease control and reduction of metastasis risks. For patients with melanoma *in situ* (stage 0) and localized cutaneous malignant melanoma (stage I and II), surgery is the most effective method with the majority being cured. The risk of localized melanoma recurrence is linked to the application of appropriate surgical margins, which are specified in guidelines based on several randomized trials and determined by Breslow thickness[70–72]. For further risk assessment, patients with advanced melanoma conditions are subjected to sentinel lymph node biopsy (SLNB). The presence of tumor-positive sentinel lymph nodes serves as a critical diagnostic and prognostic indicator, necessitating additional intervention through lymphadenectomy, which is the removal of (potentially) cancerous lymph nodes. The recommended melanoma stage III management protocol involves the excision of tumor and associated lymph node metastases with subsequent adjuvant systemic therapy, such as targeted therapy or immune checkpoint inhibition (ICI), as described below[72]. The last surgical intervention in melanoma is the curative metastasectomy, which is the excision of one or more metastatic sites and reported to improve the overall patient survival, especially by removal of treatment-resistant metastases[72,73].

1.1.5.2 Targeted Therapy

Targeted therapy has emerged as a pivotal approach in melanoma, utilizing drugs designed to specifically attack melanoma cells based on their unique genetic and molecular characteristics. This strategy aims to enhance treatment efficacy by selectively targeting the underlying oncogenic drivers, thereby improving patient outcomes and reducing side effects associated with a broader treatment[74,75]. Before 2011, advanced melanoma had very limited treatment options, with dacarbazine chemotherapy and high-dose interleukin-2 (IL-2), being the only available therapies[76–78]. These two agents remained the mainstays of melanoma treatment for decades, despite their modest effectiveness and significant side effects, highlighting the critical need for more effective therapeutic interventions during this period[79]. Targeted therapy revolutionized the treatment of advanced melanoma and was initiated by the discovery of the driver mutation in the BRAF gene (V600E), that is present in about 50% of melanomas[31,80]. A $BRAF^{V600}$ mutation leads to the constitutive activation of the MAPK signaling pathway, bypassing the

need for external signals to drive cell proliferation and survival (Figure 4). These findings prompted the mutation-driven drug development, resulting in the approval of vemurafenib, a BRAF inhibitor (BRAFi), as the first effective targeted therapy for $BRAF^{V600}$ harboring melanoma in 2011[79,80]. Two years later, the FDA approved dabrafenib, another BRAFi designed to target $BRAF^{V600}$-mutated melanoma, which significantly enhanced patient survival compared to the chemotherapy drug dacarbazine[81]. In the same year, trametinib was FDA-approved, an inhibitor for MEK (MEKi), which acts directly downstream of BRAF in the MAPK pathway. Trametinib showed superior outcomes in progression-free and overall survival compared to chemotherapy in patients with metastatic melanoma harboring a $BRAF^{V600E/K}$ mutation[82]. In patients with unresectable stage IIIC or stage IV melanoma holding one of those mutations, the combination of dabrafenib and trametinib, in contrast to dabrafenib monotherapy, led to a higher progression-free survival rate[83]. In the following years, additional MAPKi were released for clinical use, including encorafenib (BRAFi), cobimetinib (MEKi) and binimetinib (MEKi)[84]. Three BRAFi/MEKi combination therapies are currently approved including dabrafenib with trametinib, vemurafenib with cobimetinib and encorafenib with binimetinib. Overall, these BRAFi/MEKi combinations show similar efficacy, with response rates of 60% to 70% and 18-month progression-free survival (PFS) rates of 30% to 40%. The toxicity profiles of these combinations, however, vary. The primary benefit of these combinations lies in their ability to produce rapid responses, leading to significant tumor reduction in the majority of patients[85].

While this advancement towards more personalized melanoma treatment has improved both, life expectancy and quality of life, the emergence of resistance mechanisms remains a major challenge[86]. Resistance mechanisms to MAPK inhibition therapy are diverse and can be either intrinsic, adaptive or acquired. Intrinsic resistance occurs in about 20% of melanomas and denotes the pre-existing ability of melanoma cells to withstand drug treatment, making these tumors non-responsive from the beginning. Inherent genetic mutations and naturally released factors from stromal or tumor cells have been reported[87]. These include, among others, a PTEN loss that leads to the activation of both the MAPK and PI3K/AKT signaling pathways and plays a role in BRAFi resistance by inhibition of BIM-mediated apoptosis[88]. Further genetic alterations contributing to drug tolerance are cyclin D1 amplification, NF1 loss and mutations in the MEK and RAC1 gene[87,89–92]. Non-genetic factors include the stromal release of hepatocyte growth factor (HGF), which leads to the activation of HGF/c-MET signaling. This, in turn, reactivates MAPK signaling and promotes tolerance to MAPKi[93,94].

Adaptive resistance mechanisms occur as an immediate response to treatment after initial therapy sensitivity, and are characterized by transient and non-genetic alterations[84]. In reaction to MAPKi treatment, melanoma cells are capable of the loss of negative feedback loops, metabolic reprogramming or cell state transitions (phenotype switching) to become resistant to targeted therapy[87]. The switch from a proliferative and drug-sensitive $MITF^{high}$ to an invasive and drug-resistant $MITF^{low}$ phenotype, triggered by (micro-) environmental stresses, is an adaptive resistance mechanism to targeted therapy[95]. In addition, a low ratio of MITF/AXL expression represents an indicator for early resistance to targeted drugs. As *in vitro* studies have shown, combining AXL inhibitors with MAPKi significantly enhances tumor cell eradication[55].

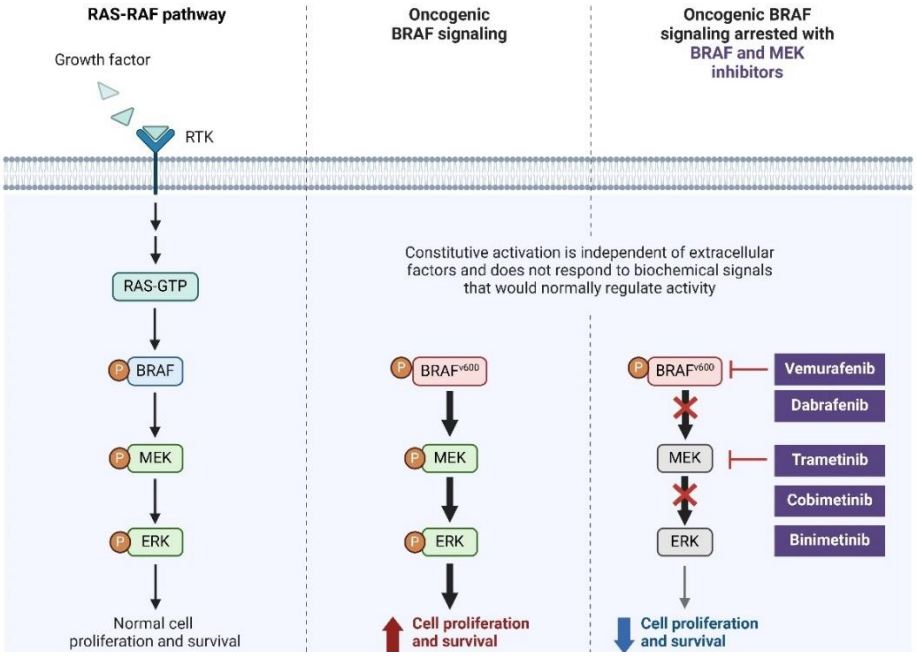

Figure 4: MAP kinase/ERK-signaling pathway and oncogenic signaling due to BRAF^{V600} mutations. *BRAF mutations of valine 600 as often observed in melanoma patients leads to constitutive activation of BRAF-signaling independent of extracellular factors, accompanied with uncontrolled cell proliferation and survival. FDA-approved BRAF or MEK inhibitors arrests BRAF signaling. Figure created using Biorender.com. Template 'Vemurafenib in oncogenic BRAF signaling pathway in melanoma' was used with slight changes.[31]*

Melanoma patients receiving mono- or combination-therapy initially exhibit a significant reduction in tumor size, however, this is frequently followed by the development of acquired resistances resulting in a relapse of tumor growth. In contrast to adaptive processes, these type of resistance mechanisms are typically indicated by stable genetic, and thus irreversible alterations that lead to reactivation or circumvention of MAPK signaling[87]. Reactivation of this pathway can be achieved by various genetic changes, such as mutations of NRAS and MEK genes, genetic BRAF amplification or aberrant BRAF splicing that can dimerize in a Ras-independent manner, to name a few[87,96–100]. As an additional strategy to resist MAPKi treatment, melanoma cells can switch to an alternative pathway, that are either the PI3K/AKT or WNT5A/β-catenin pathway, thus leading to drug resistance[87,101,102].

1.1.5.3 Immunotherapy

Immunotherapy represents a groundbreaking strategy in the treatment of advanced melanoma, harnessing the patient's own immune system to identify and destroy cancerous cells. Unlike traditional therapies that directly target the tumor, immunotherapy works by stimulating the immune system to recognize melanoma cells as threats. This innovative approach has significantly improved survival rates for patients with advanced melanoma, marking a major advance in oncology[103]. The success of immunotherapy against melanoma is mainly driven by the immunogenic nature of these tumors. As a result, melanoma cells have the capacity to provoke an immune response, making it more detectible by the immune system than other cancer types. This immunogenicity is indicated by a strong lymphocytic infiltration within melanoma tumors, that could induce partial or complete regression[104]. This attribute

has rendered melanoma a strategic target for immunotherapy, as the patient's immune system can be trained to recognize and eliminate these cells[103]. Immunotherapeutic treatment options are immune checkpoint inhibitors (ICIs), bispecific antibodies, cancer vaccines, oncolytic virotherapy and adoptive cell therapy[105].

Immune checkpoints are regulatory components within the immune system that control and modulate the immune response, preventing it from becoming overactive and causing damage to the body's own cells, a condition known as autoimmunity. Cytotoxic T lymphocyte-associated antigen-4 (CTLA-4), programmed death-1 (PD-1) and its ligand (PD-L1), and lymphocyte activation gene-3 (LAG-3) are key components of immune checkpoints. They act to downregulate CTLs and cancer cells can use this mechanism to reduce T cell activity and evade immune defenses. ICIs are monoclonal antibodies developed to target and block these inhibitory molecules, thereby enhancing immune cell activity and promoting tumor-suppressing effects[106].

As the pioneering immune checkpoint receptor to undergo clinical targeting, CTLA-4 is exclusively present on CD4+ and CD8+ T cells. It promotes an inhibitory signal for T cell activation, and thus immune response, by directly binding to its ligands, either the CD80 dimer or CD86 monomer, which are expressed on the surface of antigen-presenting cells (APCs)[107] (Figure 5). In 2011, the first monoclonal anti-CTLA4 antibody, ipilimumab received FDA-approval, which marked a milestone in melanoma management with a significant survival benefit in patients with advanced melanoma[108,109]. However, despite this high efficacy, nowadays monotherapy with ipilimumab is not the first-line treatment and is used in combination with other immunotherapy drugs[105]. Another immune repression mechanism that is targeted as part of ICI-mediated immunotherapy is the PD-1/PD-L1-axis. ICIs for both components, the Programmed Death-1(PD-1) and Programmed Death-Ligand 1 (PD-L1), are approved for melanoma treatment. PD-1 is a cell surface receptor on T cells that binds to its ligand PD-L1 or PD-L2 on tumor or other cells, causing cell cycle arrest and suppression of T cell activity[110] (Figure 5). Anti-PD-1 antibodies used in the clinic for metastatic melanoma treatment are nivolumab and pembrolizumab that show substantial patient's overall survival improvements[111–114]. An additional anti-PD-1 monoclonal antibody, spartalizumab, for the treatment of $BRAF^{V600}$ mutant, unresectable or metastatic melanoma is currently in a phase III trial[115] (Figure 5).

Despite its groundbreaking success in treating unresectable and metastatic melanoma, the ability of tumors to develop resistance remains a serious obstacle to long-term efficacy and patient outcomes. However, extensive research in recent years has uncovered mechanisms through which melanoma cells can escape immune system detection and develop resistance to immunotherapy treatments. A major immune evasion mechanism observed in melanoma is the modulation of the HLA-I-APM. This can be a result of a B2M mutation or deletion leading to a loss of HLA-I expression, escaping mutations in the IFNγ-JAK-STAT1 signaling or a dedifferentiation, i.e. the phenotype switching towards the $MITF^{low}$ cell state, causing the loss of melanocytic tumor antigen expression and presentation[56,116]. Building on recent discoveries, researchers are actively working on strategies to counteract resistance to immunotherapy. These efforts focus on turning immunologically "cold" into "hot" tumors and boosting the function of CTLs. This highlights the urgency of elucidating additional molecular details of immune evasion mechanisms in order to target them precisely and potentially overcome them in the future[116].

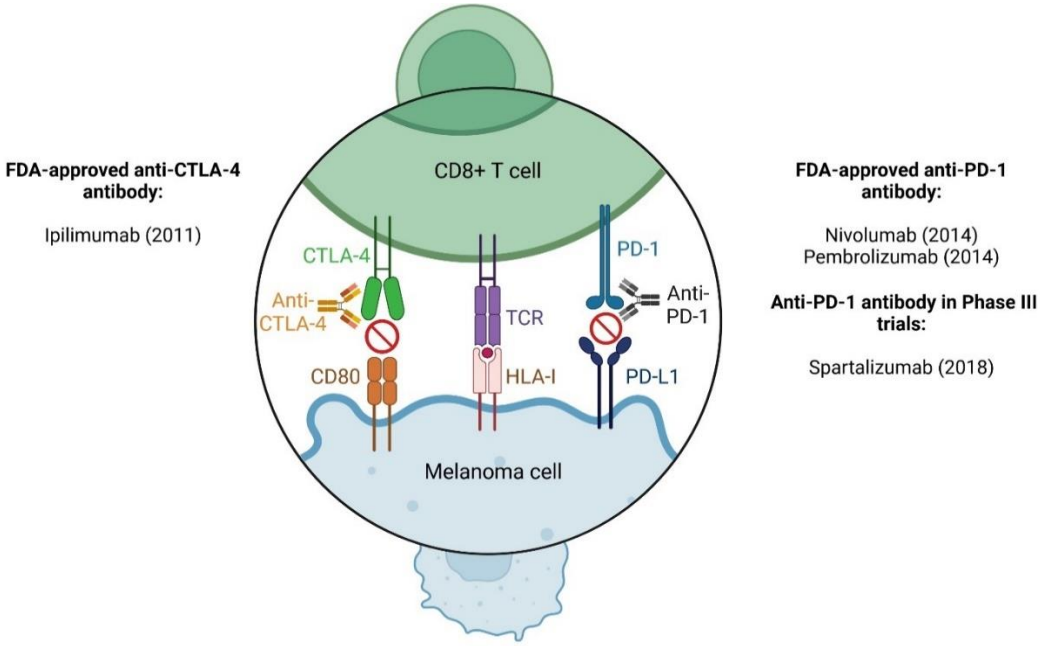

Figure 5: Principle of immune checkpoint inhibition immunotherapy. *PD-1 and CTLA-4 are immune checkpoint molecules expressed by T cells, which serve to inhibit immune responses. When these molecules interact with their ligands on tumor cells, they promote immune evasion. Immune checkpoint inhibitors, such as anti-CTLA-4 and anti-PD1 antibodies, counteract this effect by activating the immune response against tumor cells. Figure created with Biorender.com and partially adapted using the template 'Mechanisms of immune-related adverse events after immune checkpoint inhibitors immunotherapy' by Jamerson Silva available on Biorender.com.*

1.2 lncRNAs

1.2.1 Definition and Classification

Advances in genomic research over recent decades have uncovered the crucial roles of non-protein-coding RNA (ncRNA) molecules, once dismissed as insignificant and inaccurately labelled as "junk DNA" in the genomes of complex organisms. Non-coding transcripts longer than the arbitrarily chosen size cut-off of 200 nucleotides are defined as long non-coding RNA (lncRNA). This differentiates them from the majority of structural and small ncRNAs like ribosomal RNAs (rRNAs), transfer RNAs (tRNAs), microRNAs (miRNAs), small interfering RNAs (siRNAs) and piwi-interacting RNAs (piRNAs)[117]. Most lncRNAs are transcribed by polymerase II (Pol II) and thus undergo mRNA-like processing including 5' end 7-methyl guanosine (m7G) capping and polyadenylation at the 3' end to ensure stabilization[118]. However, recent discoveries have identified non-canonical RNA processing pathways for some lncRNAs, which contribute to their stabilization, including RNase P cleavage to generate a mature 3′ end for protection, as observed for lncRNA MALAT1[119,120]. Additionally, the capping by small nucleolar ribonucleoprotein particles (snoRNPs) and the formation of circular molecules are described, generating sno-lncRNAs and circular RNAs (circRNAs), respectively[119,121,122]. Besides classification based on the processing mechanism, lncRNAs can be categorized according to their relationship to protein-coding genes. This anatomical classification includes long intergenic non-coding RNAs (lincRNAs) that are generated from intergenic regions of the genome, which do not overlap with any protein-coding sequences. In contrast, antisense lncRNAs (AS-lncRNAs) can overlap with exons or introns of coding

genes and are transcribed from their opposite strand[123]. Often, these types of lncRNAs have an inherent benefit to regulate their sense genes[124]. Further, lncRNAs can be transcribed from promoter regions, thus termed promoter upstream transcripts (PROMPTs). PROMPTs are transcribed in antisense orientation to a high number of active protein coding genes spanning a length between 200-600 nucleotides. They are marked by a short half-life, due to fast degradation by the RNA nuclear exosome targeting (NEXT) complex[119,125–127]. Finally, lncRNAs generated from enhancer regions, which function as regulatory elements to increase the transcription of associated protein-coding genes, are referred to as enhancer RNAs (eRNAs). With a common length shorter than 2000 nucleotides, eRNAs are transcribed bidirectionally by Pol II from enhancers, generating nearly equal quantities of RNA in both directions. The functionality of the majority of eRNAs is still uncertain, however, an enhancer-like gene regulatory role is suspected[119,128–130].

1.2.2 Functions of lncRNAs

The genomic location-based classification of lncRNAs does not provide direct insight into their functions, which are highly diverse and depend on their binding to DNA, proteins, or RNA. These interactions enable lncRNAs to perform various crucial roles within cells, including the regulation of gene expression[131].

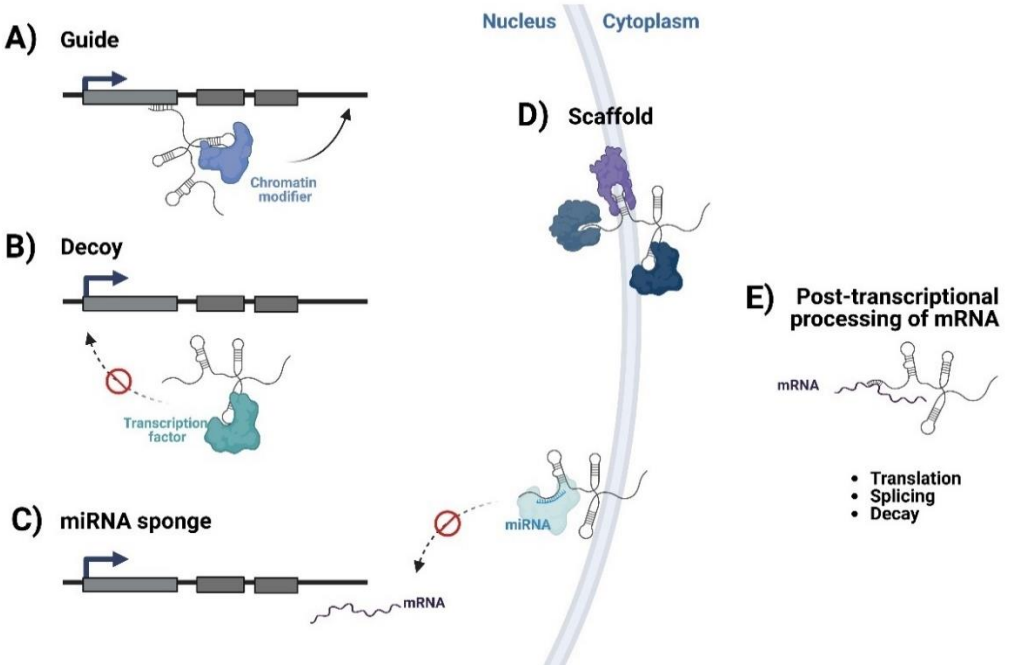

***Figure 6: Overview of lncRNA mechanisms to regulate target molecules**. lncRNAs can act as guide elements, a mechanism where chromatin modification enzymes are recruited to DNA target sites by a direct RNA-DNA interaction. Numerous lncRNAs exhibit decoy functions by directly binding to transcription factors, preventing their interaction with DNA target sites. Another decoy function of lncRNAs is the sponging of miRNA, thus preventing the interaction with its mRNA targets. As scaffold elements, lncRNAs can bring a defined combination of proteins into close proximity to facilitate the assembly of multiprotein complexes. Additionally, lncRNAs can influence post-transcriptional processes, including mRNA splicing, translation, and degradation or decay. Figure was created using Biorender.com and was adapted from the figure 'Mechanism of lncRNA function' by Khalil et al.[131].*

lncRNAs can act as guide elements that recruit chromatin modifying proteins to their DNA target sites *in cis* or *in trans* by direct DNA-RNA interaction to regulate gene expression (Figure 6A). The most prominent example of a lncRNA that mediates chromatin modification *in cis* is the X-inactive specific transcript (Xist). As indicated by the naming, this lncRNA is a crucial player in dosage compensation during the early embryonic development in female mammalian cells by transcriptional silencing of one X chromosome. This is achieved by the transcription of Xist on one X chromosome, the future inactive X (Xi), and its spreading across the entire Xi. Xist recruits chromatin modifiers, including the key complexes polycomb repressive complex 1 and 2 (PRC1 and 2) to deposit repressing chromatin marks, such as histone H3 lysine 27 trimethylation (H3K27me3), resulting in transcriptional inactivation[132]. Other lncRNAs have decoy-capability on the transcriptional level by sequestering transcription factors from their DNA targets (Figure 6B). lncRNA GAS5 functions as such a transcription factor decoy by binding to the glucocorticoid receptor (GR) and competing with DNA binding of GR-dependent genes, thereby affecting cell growth and metabolism during starvation in human cells[133]. At the post-transcriptional level, lncRNAs employ a decoy function to target miRNAs through complementary sequences, thus competing with their mRNA targets (Figure 6C). This mechanism, referred to as miRNA sponging or competitive endogenous RNA (ceRNA) activity, facilitates the indirect stabilization of target mRNAs. For instance, lncRNA H19, abundant in fetal tissues and adult muscles, was reported to exhibit miRNA sponging activity targeting the let-7 miRNA family, directly influencing muscle differentiation[134]. Regarding ribonucleoproteins (RNPs), various lncRNAs have been described to serve as scaffolds for a specific combination of proteins, bringing chromatin modifiers, transcription factors and/or splicing factors to close proximity (Figure 6D). HOX transcript antisense intergenic RNA (HOTAIR) is one lncRNAs attributed with this function. The 5' and the 3' domain of this lincRNA interacts with the PRC2 and LSD1/CoREST/REST complex, respectively, enabling a coordinated chromatin modification. The combined histone modification pattern of H3K27me3 and lysine 4 (K4) demethylation generated by this complex, results in transcriptional silencing of target genes[135,136]. Although lncRNAs are more commonly recognized for their roles at the transcriptional level, some exert significant post-transcriptional effects of their mRNA targets (Figure 6E). Among them are lncRNAs that modulate mRNA splicing, such as metastasis-associated lung adenocarcinoma transcript 1 (MALAT1), which stabilizes the splicing factors PTBP1 and PSF, thereby regulating alternative splicing and directly affecting cellular function[137,138]. Further, translation can be controlled by lncRNAs as described for lincRNA-p21. Association with the RNA-binding protein HuR results in the recruitment of let-7/Ago2 to lincRNA-p21, in turn negatively affecting its stability. In the absence of HuR, lincRNA-p21 is stable, which allows the interaction with its mRNA targets CTNNB1 and JUNB, repressing their translation potentially by ribosome "drop-off"[139]. Lastly, lncRNAs can have a direct effect on mRNA decay by intervening the so-called Staufen1 (STAU1)-mediated mRNA decay (SMD). SMD is a process in mammalian cells during which target mRNAs are degraded by binding of the double-stranded (ds) RNA-binding protein Staufen homolog 1 (STAU1) to their 3'-untranslated region (3'UTR). dsRNAs recognized by STAU1 are generated by partial complementary base pairing of ALU elements of lncRNAs with their target mRNAs, inducing the decay. Computational studies revealed around 350 lncRNAs with one or more ALU elements, highlighting their significance in SMD-related cellular mechanisms[140,141].

1.2.3 lncRNAs in Cancer

The numerous mechanisms of action attributed to lncRNAs highlight their broad physiological importance. Consequently, aberrant lncRNA expression profiles can profoundly impact cellular processes, leading to various pathologies such as cardiovascular diseases, neurological disorders, and most notably, cancer[142–144]. Dysregulation of lncRNA expression has been shown to contribute to tumor development, progression, and metastasis by acting either as oncogenes or tumor suppressors. Interestingly, the majority of lncRNAs exhibit unique expression profiles in a tissue- and cell type-specific manner. Hence, the functions of lncRNAs and their role in a studied cancer type must be interpreted in a cell type-specific context and are not easily transferable to other cell types[144,145]. However, several lncRNAs are described to have multiple functionalities and tumor-promoting effects in more than one cancer type. One of the most deeply examined lncRNA with oncogenic properties is HOTAIR, that is overexpressed in a large variety of cancer, such as melanoma[146], breast[147], pancreatic[148], gastric[149], and bladder cancer[150]. In addition to the previously described chromatin-regulating and gene silencing effects of HOTAIR, a miRNA sponging activity was reported to regulate several miRNAs. Cellular processes with cancer-promoting effects modulated by aberrantly expressed HOTAIR include cell migration and invasion, EMT and metastasis[151]. Comparable are the consequences of the upregulation of MALAT1 levels, as described in various cancers. With its multi-functionality as a ceRNA for many miRNAs[152–154], a guide element for the chromatin modifying enzyme PRC2[155,156] and as a modulator of alternative splicing[137], cancer cell migration, invasion, EMT, angiogenesis and chemoresistance are among the resulting phenotypes[157–159]. In contrast to oncogenic lncRNAs that are overexpressed in a cancerous context, various lncRNAs exhibit tumor-suppressive functions and are downregulated in cancer cells. A well-studied example of a tumor suppressor lncRNA across various tumors is GAS5. Its downregulation and significance have been documented in breast cancer[160,161], pancreatic cancer[162,163], colorectal cancer[164] and ovarian cancer[165]. The specific molecular mechanisms by which GAS5 suppresses tumorigenesis include miRNA sponging, guiding enzymes for chromatin modification to specific genomic locations, and acting as decoy for transcription factors. Consequently, GAS5 influences cell proliferation, invasion, apoptosis, EMT, and drug resistance in different cancer contexts[166]. Another lncRNA exhibiting anti-tumor effects is tumor suppressor candidate 7 (TUSC7). Meta-analysis validated a reduced expression of TUSC7 in cancer samples and a correlation with poor prognosis across multiple cancer types[167,168]. In colorectal cancer a ceRNA activity towards miR-23b, a target of phosphodiesterase 7A, was uncovered, directly affecting cell migration and invasion[169,170]. In triple-negative breast cancer, *in vitro* studies revealed an inhibiting role of TUSC7 on breast cancer cell growth and metastasis through sponging of miR-1224-3p, regulating MAPK, PI3K/AKT, and NF-κB signaling, pathways promoting cancer development and progression when sysregulated[171]. Taken together, these highlighted cases emphasize the multi-functional and cell type-specific nature of lncRNAs in cancer.

1.2.4 lncRNAs in Melanoma

In the past decade, there has been a continuous increase in the amount of studies on lncRNAs in melanoma, showcasing their involvement in key hallmarks of melanoma biology, such as proliferation, invasion and metastasis, metabolism, immune escape and drug resistance, as reviewed by Melixetian *et al.*[172] (Figure 7).

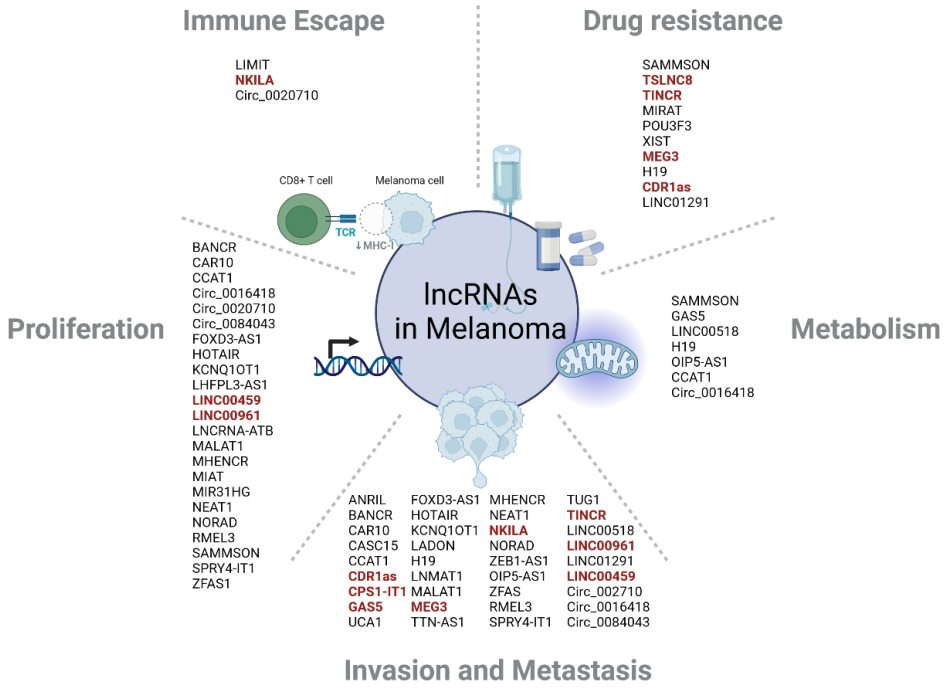

Figure 7: Key hallmarks of melanoma development and progression and lncRNAs involved. *Listed are lncRNAs influencing proliferation, invasion/metastasis, metabolism, drug resistance, and immune evasion processes, contributing to the progression of melanoma pathogenesis. lncRNAs described as tumor suppressors are highlighted in red. Figure is adopted from the Review of Melixetian et al.[172] and was created using Biorender.com.*

Considering their multiple functions, it is unsurprising that differentially expressed lncRNAs often affect multiple hallmarks of melanomagenesis. For instance, the oncogenic, $BRAF^{V600E}$ mutation-induced lncRNAs BANCR and SPRY4-IT1, which are upregulated in melanoma compared to non-cancerous melanocytes, exhibit proliferation- and invasion-promoting effects[173–176]. The former was studied by knockdown experiments *in vitro* and *in vivo*, revealing an inactivation of the MAPK pathway, more specifically ERK1/2 and JNK resulting in decreased tumor growth upon BANCR downregulation[174]. Further, research indicates that BANCR exhibits ceRNA activity on miR-204, which targets Notch2 signaling, leading to increased proliferation and invasion due to lncRNA overexpression[173]. Likewise, the upregulation of lncRNA SPRY4-IT1 is associated with the hallmarks proliferation and invasion/metastasis. Mechanistically, SPRY4-IT1 sponges miR-22-3p, which plays a role in the p38MAPK/MAPKAPK/Hsp27 signaling pathway[175]. SPRY4-IT1 may serve as a prognostic marker, as high abundance in the patient's blood plasma was found to negatively correlate with the overall survival[177]. This is supported by the finding that this lncRNA interacts with lipin-2, a key enzyme in the lipid metabolism. Loss-of-function of SPRY4-IT1 in melanoma cells induces the accumulation of lipin-2

and specific lipid types that may result in cellular lipotoxicity. Accordingly, SPRY4-IT1 is ascribed an anti-apoptotic function[178].

Besides lipid metabolism, lncRNAs have been reported to regulate several other metabolic pathways, such as the mitochondrial or glucose metabolism. For example, the mitochondrial metabolism is controlled by SAMMSON (Survival Associated Mitochondrial Melanoma Specific Oncogenic Non-coding RNA), a lncRNA frequently co-amplified with MITF in melanoma. The mechanism by which SAMMSON interferes with localization and function of mitochondria is a direct lncRNA-protein interaction with p32[179]. Protein p32 is involved in mitochondrial metabolism and the synthesis of mitochondrially encoded peptides, thereby regulating the balance between OXPHOS and glycolysis, crucial for tumor growth in melanoma[180,181]. Downregulation of SAMMSON disrupted the association of p32 to mitochondria, significantly decreasing the membrane potential and thus mitochondrial function[179].

As melanoma continues to demonstrate remarkable resistance to current targeted therapies such as MAPKi, a deep comprehension of the underlying mechanisms driving this drug resistance becomes indispensable for advancing therapeutic strategies. Multiple lncRNAs involved in drug resistance mechanisms in melanoma have been recently uncovered. One example is the tumor suppressor lncRNA TSLNC8 (Tumor suppressive long noncoding RNA on chromosome 8p12), which shows low abundance in BRAFi-resistant melanoma cells. *In vitro* TSLNC8 knockdown in BRAFi-sensitive melanoma cells diminishes BRAFi sensitivity by inhibition of apoptosis in BRAFi-treated cells. In contrast, TSLNC8 overexpression in BRAFi-resistant cells restored the sensitivity towards the inhibitor. Mechanistically, binding of TSLNC8 to the catalytic subunit of protein phosphatase 1α (PP1α) affects its localization, thus inducing the perturbation of MAPK signaling. As BRAFi resistance relies on the re-activation of the MAPK pathway, it is hypothesized that knockdown of TSLNC8 and the accompanying accumulation of PPIα, induces the dephosphorylation of BRAF inhibitory phosphorylation sites to hyper-activate MAPK signaling[182].

Given that immunotherapeutic approaches, particularly ICIs, are the preferred treatment for advanced melanoma, understanding the underlying mechanisms through which melanoma cells evade immune cell recognition is crucial. One of the most prominently studied resistance mechanism is the reduction of HLA-I expression, which allows tumors to evade T cell-specific cytotoxicity. The potential contribution of lncRNAs in ICI resistance was investigated with bioinformatic prediction models using clinical data from melanoma patients, which identified lncRNA signatures linked to ICI response[183,184]. A lncRNA reported to be directly involved in immune escape is LIMIT, which is IFNγ-stimulated and activates the GBP1-HSF1-mediated transcription of the HLA-I-APM. LIMIT perturbation studies revealed that LIMIT enhances HLA-I expression and increases anti-tumor immunity *in vitro* and *in vivo*[185]. Another example for a lncRNA contributing to an immune escape mechanism is circular RNA circ_0020710, whose expression levels positively correlate with poor prognosis and CTL exhaustion. A miRNA sponging activity of this circRNA on miR-37-3p was described, a miRNA that regulates CXCL12 expression. High levels of CXCL12 promote melanoma cell proliferation, migration and invasion *in vitro*, but it is also a known chemoattractant of immune cells. Upregulation of this circRNA was linked to a decreased abundance of CTL infiltration *in vivo*, indicating a resulting immunosuppressive tumor microenvironment, mediated by the circ_0020710/miR-370-3p/CXCL12 axis[186].

1.2.5 lncRNA perturbation

To uncover the function and relevance of lncRNAs and to further explore the complex roles that these molecules fulfil in cellular processes and molecular pathways, extensive studies encompassing loss- and gain-of-function experiments are essential. Within the recent years, methodologies for such lncRNA perturbation studies have facilitated a more comprehensive characterization and aid the elucidation of their significance, particularly in pathological conditions such as cancer[187].

1.2.5.1 Loss-of-function

Among the leading techniques for inducing loss-of-function (Figure 8, left) is CRISPR/Cas-based manipulation, which can operate at the DNA or RNA level to modulate lncRNA expression. The CRISPR/Cas system constitutes the adaptive immune system of prokaryotes, relying on a series of non-coding DNA sequences termed “clustered regularly interspaced short palindromic repeats” (CRISPR) and operating in conjunction with CRISPR-associated (Cas) genes[188]. Within this system, fragments of genetic material from invading pathogens called spacers are integrated into CRISPR loci, transcribed into CRISPR RNA (crRNA) and loaded into Cas nucleases. The crRNA within this ribonucleoprotein complex guides the Cas nuclease to generate double strand breaks (DSBs) in the invader’s nucleic acid[189,190]. Subsequently, the mammalian DNA repair mechanism non-homologous end joining (NHEJ) induces DNA processing and ligation, resulting in the insertion or deletion of 1-3 nucleotides, termed indels. Consequently, frameshift mutations frequently occur, potentially resulting in an early stop codon, which in turn leads to the degradation of mRNA. The remarkable specificity and precision in cleaving target nucleic acids and its high level of programmability position CRISPR-Cas systems as effective tools for genome editing and transcriptional regulation[191,192]. As frameshift mutations within exons are effective solely for protein-coding genes, targeting non-coding RNAs requires modification of the initial CRISPR/Cas technology. Thus, regulatory genomic regions like promoters, or whole exons of the lncRNA gene need to be excised, which can be facilitated by a pair of CRISPR-Cas9 complexes through simultaneous DSBs at sites bordering the target regions[193–195]. Also, the insertion of an early transcription termination signal, such as a synthetic polyadenylation signal, was successfully used to halt transcription of lncRNAs[196,197].

Additional modifications of the CRISPR/Cas system for lncRNA downregulation utilizes a genetically engineered, catalytically ‘dead’ mutant of the Cas9 protein (dCas9), lacking its nuclease activity, while maintaining the capability for DNA binding. The dCas9 protein inhibits transcription initiation through steric hindrance, obstructing the RNA polymerase machinery, hence coining the term CRISPR interference (CRISPRi)[198,199]. Enhanced repression can be attained by fusion of dCas9 protein with transcription repressors, such as the commonly used Krüppel-associated box domain (KRAB). The dCas9-KRAB fusion exhibits robustness and high specificity in both yeast and mammalian cells[200,201]. Further, CRISPRi was successfully used for the identification of functional lncRNA loci in human cells[202]. In addition to CRISPR/Cas systems that function as DNA editing tools, the Cas13 system, containing

single RNA-guided RNA endonucleases, can be used to target single-stranded RNAs without altering the DNA. The Cas13 protein family presently includes 11 members, each differing in size, sequence, and efficiency[203] and Cas13a (C2c2) was the first subtype identified within this family in 2016[204]. However, advantages of the subtype Cas13d over the other Cas13 nucleases regarding efficiency and specificity in RNA cleavage in mammalian cells are described making it the preferred RNA editing tool[205]. Cas13-mediated knockdown as a tool for the discovery of substantial lncRNAs or to uncover lncRNA functions is reported, including studies on the cancer-relevant lncRNAs MALAT1 and HOTTIP[206], as well as MIR497HG[207], or circular RNAs, tested in a large-scale CRISPR-RfxCas13d screen[208].

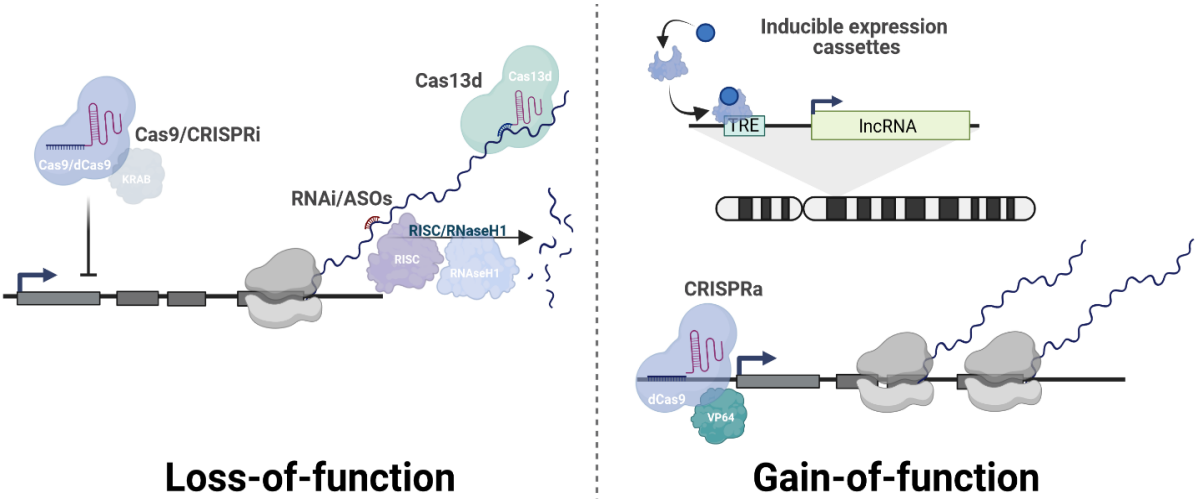

Figure 8: Schematics of lncRNA perturbation methods. *lncRNA loss-of-function tools at the DNA level are either the genome-editing CRISPR/Cas9 system or its catalytically 'dead' dCas9 variant fused to a suppressor protein such as KRAB (CRISPRi). On the RNA level the CRISPR/Cas13d system can be used or the transcribed lncRNA can be targeted by RNA interference (RNAi) or antisense oligonucleotides (ASOs), which results in lncRNA cleavage by either the RISC complex or RNase H (left). Overexpression of lncRNAs can be achieved by stable integration of the expression cassette of the lncRNA of choice into the genome or by CRISPR/dCas9 system fused to an activator protein such as VP64 (CRISPRa) (right). Figure was adapted from the Review of Wang et al.[187] and created using Biorender.com.*

Besides CRISPR/Cas system-based RNA depletion approaches, two other widely used strategies for targeting lncRNAs on the RNA level are RNA interference (RNAi) and antisense oligonucleotides (ASOs). Both methods are based on complementary base-pairing to the target lncRNA by either small interfering RNAs (siRNAs) or small hairpin RNAs (shRNAs) mediating the RNAi effect, or by short, synthetic strands, termed ASOs[187]. RNAi is a natural post-transcriptional gene silencing system that plays a key role in gene regulation by degrading specific mRNAs and also in antiviral defense against foreign double-stranded RNAs (dsRNAs). Mechanistically, RNAi starts with the processing of dsRNA by the endoribonuclease Dicer into siRNAs of around 20-30 nucleotides in length. Incorporation of this siRNAs into the multiprotein complex RNA-induced silencing complex (RISC) results in the guidance of this siRNA to its complementary cellular counterpart that undergoes cleavage by RISC component Argonaute[209–211]. This endogenous RNA degradation pathway can be harnessed to target a lncRNA of interest for its downregulation in the cell by introducing a synthetic siRNA or an shRNA expression vector using established transfection or lentiviral transduction techniques. RNAi-induced lncRNA knockdown

has become a common method to characterize critical functions of lncRNAs in various cellular processes[138,212,213].

A convenient and efficient alternative for si- or shRNAs, are ASOs, which are short, synthetic, single-stranded RNA- or DNA-based sequences designed to target transcripts through complementary base pairing[214]. Mechanistically, ASOs act by either steric hindrance leading to translational arrest or by triggering the Ribonuclease H (RNase H)-mediated RNA cleavage and degradation[215–217]. The RNase H pathway is induced by RNA/DNA hybrids, which can arise during DNA replication or repair, and the involved enzymes specifically cleave the RNA strand of these hybrid structures[218]. In biological systems, unmodified DNA and RNA are prone to rapid degradation, as nucleases are ubiquitously present to cleave their phosphate backbone. The inherent instability of ASOs can be overcome through chemical modifications to their phosphate or sugar moiety of the backbone as well as heterocycle, which improves both, their binding affinity and pharmacokinetics[216]. One of the predominant forms of ASOs for targeting lncRNAs is the gapmeR. It consists of a hybrid structure including a core of unmodified nucleotides, which is required for RNase H activity, and a flanking region of 2′-O-Methyl or LNA-modified synthetic nucleotides[219,220]. LNA gapmeR ASOs were successfully used to target and downregulate oncogenic lncRNA MALAT1 to investigate its significance in multiple myeloma or to knockdown PCAT19 in endothelial cells, illustrating their use in diverse biological contexts[221,222].

To select the most appropriate method, it is essential to consider the distinct mechanisms by which RNAi and ASOs operate. Understanding these differences allows for a more informed choice based on the specific biological context and more importantly the localization of the target lncRNA. Nuclear lncRNAs are reported to be less susceptible to RNAi-mediated degradation compared to cytoplasmic ones. In contrast, ASOs, which rely mainly on RNase H activity, are less affected by the subcellular localization[223]. In contrast to RNA-level silencing approaches like RNAi and ASOs, CRISPR/Cas-based strategies target the genome, which can potentially disrupt nearby DNA elements, such as overlapping/(anti-) sense genes, and influence associated transcriptional processes[224]. Further, targeting lncRNAs at the RNA level is crucial to differentiate their trans-regulatory roles from the cis-regulatory effects they may exert at their native genomic locus. This broader impact underscores the need to carefully consider unintended genomic effects when using CRISPR for lncRNA knockdown studies[187].

1.2.5.2 Gain-of-function

In addition to knockdown studies, overexpression approaches enable researchers to elevate the levels of specific long non-coding RNAs in cells, providing crucial insights into their functional importance in both normal physiology and pathological conditions (Figure 8, right)[187]. Following the development of CRISPR interference (CRISPRi), CRISPR activation (CRISPRa) was introduced, a method that also utilizes the catalytically inactive Cas9 protein (dCas9), fused to RNA polymerase recruiting factors and chromatin remodeling complexes, to promote gene activation rather than repression. A well-established CRISPR/Cas9-based transcriptional activation system in eukaryotic organisms involves the C-terminal VP64 acidic transactivation domain. When co-expressed with optimized guide RNAs, it exhibits a robust

and adaptable strategy for RNA-guided gene activation[225]. It has been effectively applied in the overexpression of lncRNAs, such as MALAT1, to explore their functional roles[226]. Aside from modulating dCas9 alone, further engineering of the sgRNA can enable effector molecule recruitment, leading to a synergistically enhanced level of transcriptional activation. The CRISPRa Synergistic Activation Mediator (SAM) system, developed by Konermann and colleagues, uses the dCas9-VP64 fusion protein. This is combined with engineered sgRNAs containing two bacteriophage MS2 protein-interacting aptamers, which in turn recruit additional transcriptional activators, p65 and HSF1. The three component system consisting of VP64, p65 and HSF1 thus act synergistically to enhance transcription activation compared to using a single activator alone[227]. This dCas9-SAM system has proven effective for lncRNA overexpression screens and experiments aimed at activating specific lncRNAs, facilitating the exploration of their functions[228,229].

Given the limitations of CRISPR/Cas9 technology for studying lncRNAs, particularly due to their potential proximity to neighboring genes, an alternative approach is exogenous overexpression. This involves transient transfection of cells with a plasmid carrying the cDNA of the lncRNA gene of interest and a native or constitutively active promoter, bypassing challenges related to genomic location and off-target effects[230]. This approach is employed not only to investigate the effects of lncRNA overexpression on cells but also regularly in rescue experiments following lncRNA knockdown. The goal is to restore the original phenotype and confirm the validity of the observed effects. However, these experiments are limited to *trans*- and not *cis*-acting lncRNAs, where the functional role is attributed to the RNA molecule itself, rather than the process of transcription[231]. As an alternative to transient overexpression, RNA viral vectors like retro- or lentiviruses can be used for stable integration of a lncRNA expression cassettes with a constitutively active or inducible promoter into the host genome (Figure 8, right)[187]. In recent *in vivo* studies, a doxycycline-inducible allele of lncRNA HOTAIR was introduced into transgenic mice with breast cancer-prone background, revealing HOTAIR as driver of breast cancer progression by modulating the metastatic gene regulatory program[232].

1.3 GRASLND

The primate-specific long non-coding RNA RNF144A-AS1 (RNF144A Antisense RNA 1) has been recognized as a key regulator in mesenchymal stem cell (MSC) chondrogenesis, that is upregulated during this process of cartilage production[233]. As the cartilaginous matrix is abundant in glycosaminoglycans (GAGs)[234], this lncRNA has been designated as Glycosaminoglycan Regulatory Associated Long Non-coding RNA (GRASLND)[233]. In the corresponding study, Huynh *et al.* discovered an essential role of GRASLND on cartilage production in MSCs, as knockdown studies led to a bone-forming profile and a reduction of cartilage, while an overexpression showed enhanced GAG levels. Despite the intrinsic suitability of antisense lncRNAs to regulate their corresponding overlapping sense genes, perturbation of GRASLND did not impact RNF144A RNA or protein levels, suggesting the absence of a regulatory role and that GRASLND acts in *trans*. Additional characterization revealed a cytoplasmic subcellular location. Computational analysis of previously published data suspected the

transcription factor SOX9 as an upstream effector, which was confirmed by transgene overexpression studies in MSCs. Pathway analysis uncovered an association between GRASLND and the type II interferon (IFNγ) JAK-STAT signaling pathway in the context of chondrogenesis. Further research suggests that GRASLND inhibits the IFNγ pathway by a direct lncRNA-protein interaction with interferon-induced, double-stranded RNA-activated protein kinase (PKR). Thus, Huynh *et al.* proposed that a secondary structure of GRASLND might activate PKR, subsequently inhibiting the transcriptional activity of STAT1 within the IFNγ signaling pathway. In the musculoskeletal system, IFNγ-signaling is predominantly acknowledged for its involvement in bone development and homeostasis and its inhibition of chondrocyte proliferation[235–237]. The authors proposed a therapeutic potential of GRASLND for addressing cartilage-related disorders, including osteoarthritis, as it demonstrates a protective effect against IFNγ in engineered cartilage[233].

In the context of cancer, several studies have reported GRASLND as a diagnostic and unfavorable prognostic factor based on bioinformatic risk modelling and survival analysis using clinical data from The Cancer Genome Atlas (TCGA) database. Thus far, GRASLND was found to be associated with poor patient prognosis in papillary renal cell carcinoma[238], osteosarcoma[239], head and neck squamous cell carcinoma[240], glioblastoma[241], bladder[242,243] and gastric cancer[244,245]. In glioma, bladder and gastric cancer, further functional studies of GRASLND were conducted, indicating its role in promoting cancer cell proliferation, migration, and invasion[243,244,246]. Mechanistically, GRASLND was found to act as different miRNA decoys in glioma and gastric cancer, targeting miR-665 and miR-30c-2-3p, respectively. In addition, a bioinformatic survival prediction model in gastric cancer identified an immune-related role of GRASLND, marking it as a negative prognostic factor for immune checkpoint inhibitor (ICI) response[245]. Two studies investigating GRASLND in the melanoma context were published recently, both showing GRASLND's tumor-promoting functions regarding cell proliferation, migration and invasion[247,248]. Specifically, Yang *et al.* uncovered an RBP-mediated mechanism wherein direct binding to RNA-binding protein TAF15 leads to its stabilization, subsequently triggering YAP1 pathway activation, which facilitates the pro-oncogenic effects observed[247]. The other study by Ma *et al.* demonstrated that GRASLND functions as a competing endogenous RNA (ceRNA) by sequestering microRNA miR-218-5p, thus preventing it from suppressing its downstream target STAM2. This upregulation of STAM2 has been linked to enhanced tumor growth and metastasis[248]. Both studies ultimately propose GRASLND as a promising therapeutic target for melanoma treatment, highlighting its role in tumor progression.

2. Aim of work

Melanoma is the most lethal type of skin cancer, marked by both intratumoral heterogeneity and phenotypic plasticity, culminating in an extremely poor prognosis in advanced disease stages. While immune checkpoint blockade has revolutionized melanoma treatment, resistance mechanisms such as impaired antigen presentation and phenotype switching causing immune evasion, limit its success. LncRNAs play critical roles in melanoma biology, including proliferation, metastasis and such immune evasion mechanisms, highlighting the urgent need for novel strategies to address their pathological functions.

For this reason, the aim of this thesis was to characterize lncRNA GRASLND for its potential relevance in melanoma pathogenesis, given its previous identification as a suppressor of the IFNγ signaling pathway in mesenchymal stem cells (MSCs)[233]. Thereby the study focused on three main elements:

(I) Meta-analyses of a large cohort of patient data to examine GRASLND expression in tumor and healthy samples, assess survival outcomes and correlations with melanocytic differentiation markers, and perform gene set enrichment analysis to evaluate a potential clinical significance of GRASLND.

(II) Investigation of GRASLND's functions in relation to the key melanoma hallmarks, such as cell proliferation and growth, cell invasiveness and melanoma cell differentiation. shRNA-mediated GRASLND knockdown studies should provide insights into its role in melanoma. Transcriptomic analysis after GRASLND downregulation, combined with the identification of protein binding partners, should deepen the understanding of pathways affected by GRASLND.

(III) Verification of a suppressive effect on the key immune pathway of IFNγ in melanoma cells, consistent with observations in MSCs through GRASLND knockdown studies under simultaneous cytokine treatment, followed by examination of its impact on the expression of IFNγ-stimulated genes (ISGs). These findings might contribute to hypothesize an adaptive resistance mechanism of melanoma cells evading the immune system by overexpressing lncRNA GRASLND via suppression of IFNγ signaling.

3. Results

The basis for this doctoral research was initially proposed by Prof. Dr. Annette Paschen from the University Hospital Essen (UKE, Department of Dermatology) motivated by findings published by Huynh *et al.* in 2020[233], that identified the long non-coding RNA GRASLND as a suppressor of the IFNγ signaling pathway in mesenchymal stem cells (MSCs). During my Master thesis research, the question of a potential role of GRASLND in IFNγ signaling within melanoma was addressed[249]. This initial work involved the establishment of melanoma cell models with modified GRASLND expression levels through CRISPR/Cas- and RNAi-based perturbation techniques. Although these strategies laid the groundwork for continued research, the question of GRASLND's involvement in IFNγ signaling in melanoma remained unresolved. This doctoral research aims to expand on this work by examining the role of GRASLND in melanoma focusing on a potential impact on the IFNγ signaling pathway and exploring additional roles in cellular processes that could affect the development or progression of melanoma.

3.1 Data Mining and Survival Analysis of GRASLND Expression Profiles

The expression levels of lncRNA GRASLND were subjected to a meta-analysis across a comprehensive set of tumor types and their corresponding healthy tissues utilizing the publicly available Gene Expression Profiling Interactive Analysis (GEPIA) dataset[250]. As represented in Figure 9A, GRASLND expression levels were reduced in tumor compared to normal samples for 14 out of 31 tested paired tissues. However, a subset of tumors exhibited an overexpression of this lncRNA (15/31 tissue types). Subsequent expression analysis of GRASLND in skin cutaneous melanoma (SKCM) was performed by Shashank Tiwari, M.Sc. (Max Planck Institute, Dortmund) using the TCGA-SKCM database as described in section 5.2.12.1. RNA-Sequencing data from 471 melanoma patients were compared with a total of 701 healthy samples sourced from the GTEx database. As expected, principal component analysis (PCA) showed clear clustering patterns of tumor and normal skin samples, accounting for 51.74% variance on PC1 (Figure 9B). Differential gene expression analysis revealed that the expression of GRASLND in SKCM is significantly higher compared to healthy skin tissues (mean Log2FC = 4.56, $p = 3x10^{-153}$, Figure 9C). Further, a Kaplan-Meier survival analysis was conducted to assess whether elevated levels of GRASLND impact the overall patient survival. Human melanoma patient data from the SKCM-TCGA database were categorized based on their GRASLND expression in relation to the overall survival as outlined in section 5.2.12.2, revealing a significant ($p = 0.034$) association between high GRASLND expression and reduced survival outcomes (Figure 9D). These data mining results for GRASLND expression suggest a potential pathological role in the development or progression of melanoma.

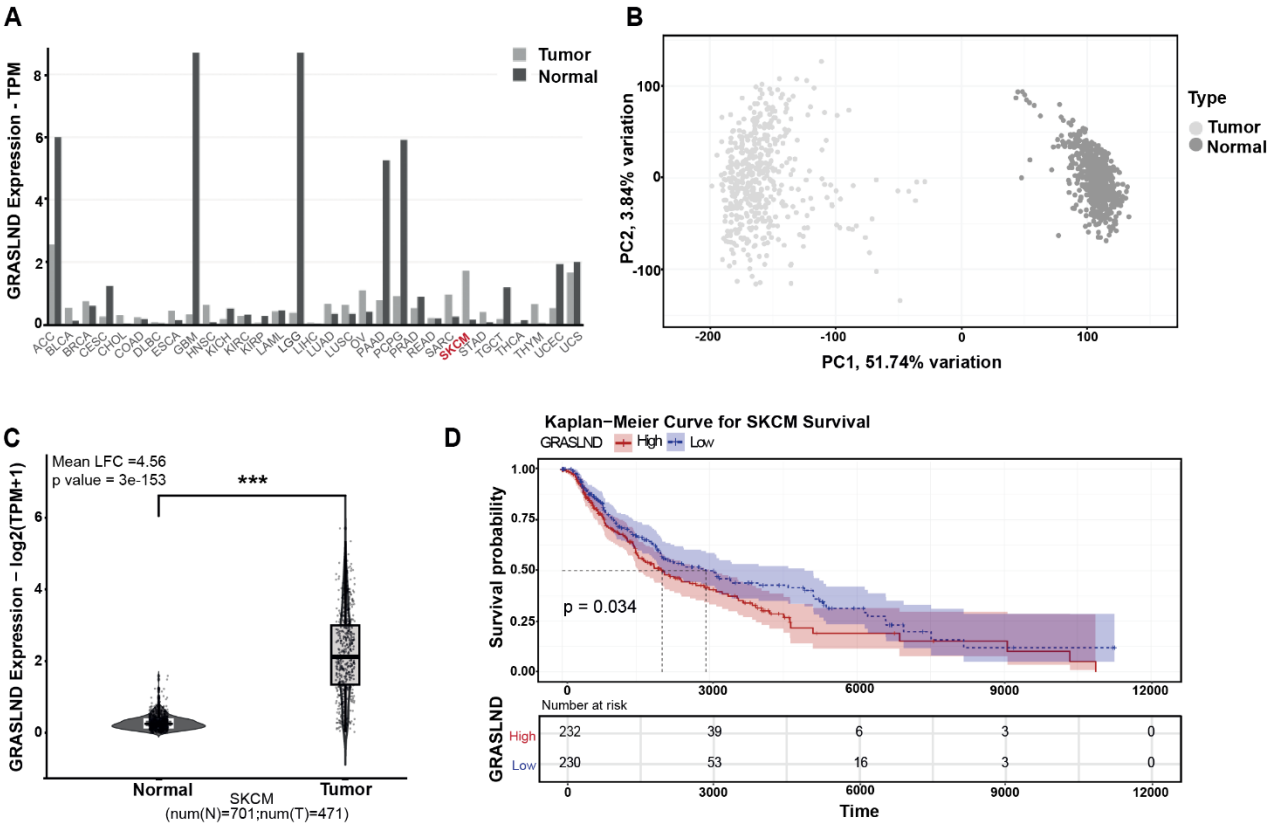

Figure 9: Data Mining and Survival Analysis of GRASLND Expression Profiles. *(A) Gene expression profile of GRASLND across all tumor samples and paired normal tissues analyzed using the publicly available dataset GEPIA. The height of each bar represents the median expression level within a specific tumor type or corresponding normal tissue. (B, C) PCA plot (B) of tumor (TCGA, SKMC, n = 471) and normal skin samples (GTEx database, n = 701) and GRASLND expression in skin tumors compared to healthy skin tissues. p value = $3x10^{-153}$. Wilcoxon's rank-sum test. (D) Kaplan-Meier survival plot (TCGA, SKMC) based on $GRASLND^{high}$ (n = 232) and $GRASLND^{low}$ (n = 230) groups. Two-sided log-rank test for p value.*

3.2 Correlation Analysis of GRASLND Expression and Melanoma Cell Differentiation Status

In melanoma, the cell differentiation status is a critical determinant of both the resistance to therapeutic interventions and the overall aggressiveness of the tumor. Distinct melanoma differentiation cell states exhibit varying sensitivities to treatment, particularly immunotherapy, with dedifferentiation recognized as a mechanism contributing to therapeutic resistance[56,57]. In addition, the differentiation status is closely associated with tumor progression and metastatic potential. A dedifferentiated melanoma phenotype is marked by reduced or absent expression of the key transcription factor of melanocytes MITF and its downstream targets, including MelanA, gp100, and tyrosinase. This phenotype demonstrates an increased metastatic potential due to heightened expression of invasion-related genes[44].

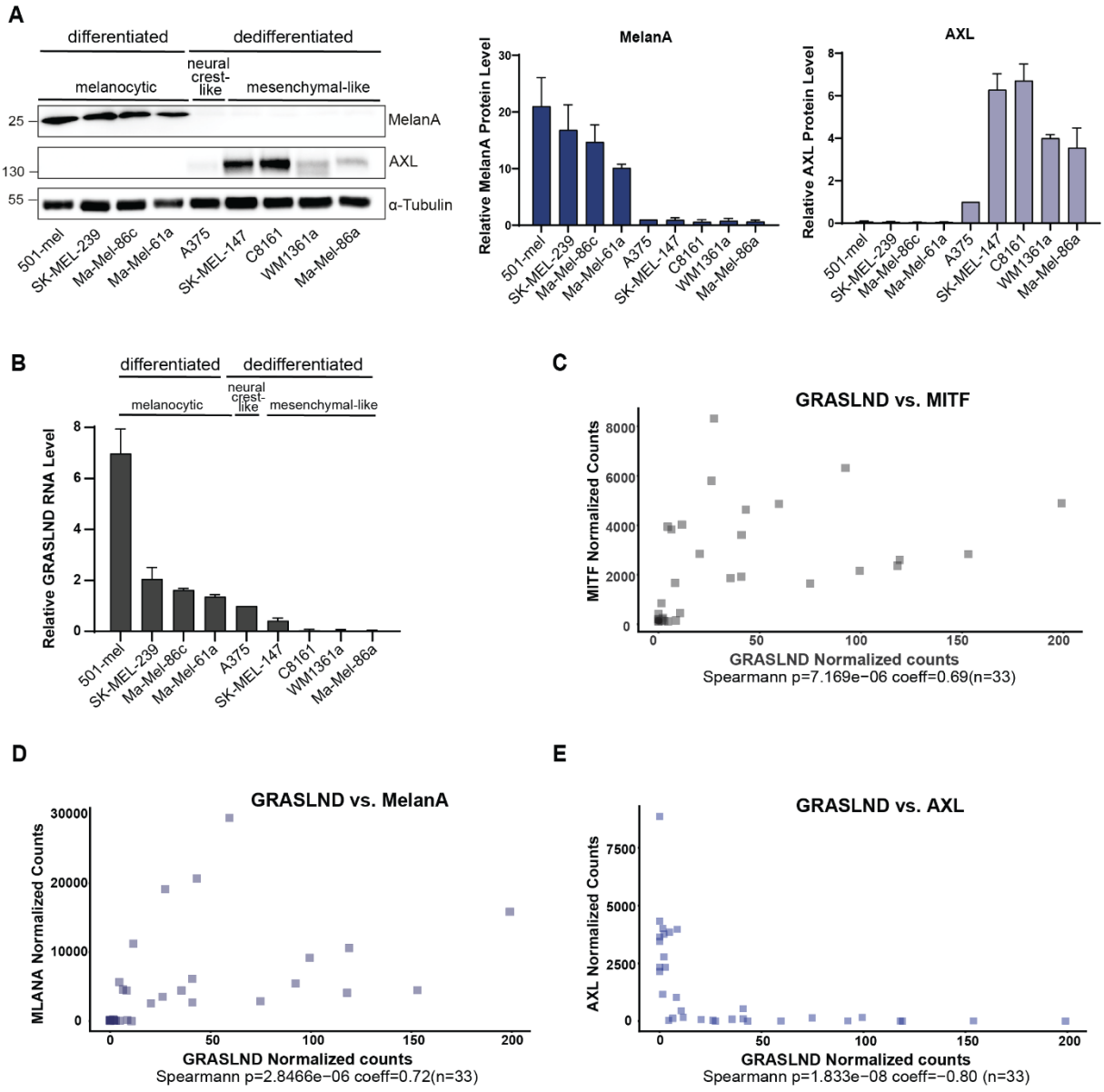

Figure 10: Correlation of GRASLND with the melanoma cell differentiation status. *(A) Protein levels of MelanA and AXL were measured in nine melanoma cell lines using Western blot, with the cell lines categorized into distinct melanoma differentiation states. α-Tubulin served as the loading control (left panel). MelanA and AXL protein levels were quantified, with each replicate normalized to the expression level in cell line A375 (right panel). The blot shown is representative of n = 3 independent biological replicates. (B) Relative GRASLND RNA expression in nine melanoma cell lines was determined using RT-qPCR, with RNA levels normalized to GAPDH mRNA. Each replicate's expression level was further normalized to that of the neural crest-like cell line A375. Data represent three independent biological replicates (n = 3). (C-E) Transcript correlation analysis of GRASLND with MITF (C), MelanA (D), and AXL (E) gene expression was performed on 33 melanoma samples from the Wouters dataset[60]. The Spearman correlation coefficients were 0.69 for MITF, 0.72 for MelanA, and -0.80 for AXL, with p values of 7.2 x 10^{-6}, 2.8 x 10^{-6}, and 1.8 x 10^{-8}, respectively.*

Understanding the importance of the cell state regarding melanoma progression and treatment efficacy, a potential correlation of GRASLND and the melanoma differentiation state was investigated. Accordingly, nine melanoma cells were examined for their cell states through determination of protein levels of melanoma differentiation marker MelanA and AXL, a receptor tyrosine kinase (RTK) linked to the dedifferentiated, mesenchymal-like and drug-resistant phenotype[55] (Figure 10A, left). Melanoma cell

lines were cultured for several days and analyzed by Western blot as detailed in section 5.2.5. Three biological replicates were performed and expression levels of MelanA and AXL were quantified (Figure 10A, right). Concurrently, the expression levels of GRASLND lncRNA in the same melanoma cell lines were analyzed using reverse transcription-quantitative PCR (RT-qPCR) (Figure 10B) and significance tests were performed (Supplementary Table 1). Notably, the differentiated cell lines 501-mel, SK-MEL-239, Ma-Mel-86c, and Ma-Mel-61a, exhibited significantly elevated GRASLND expression compared to the dedifferentiated, mesenchymal-like and AXL-expressing cell lines SK-MEL-147, C8161, WM1361a, and Ma-Mel-86a. Following this finding, Spearman correlation analyses of GRASLND were performed in relation to the lineage-specific key regulator MITF, along with MelanA, and AXL using bulk RNA sequencing data from the Wouters dataset, which includes 33 melanoma cell lines classified into melanocytic, intermediate, neural-crest-like, and mesenchymal-like cell states[60]. This analysis was performed by Shashank Tiwari, M.Sc. as outlined in section 5.2.13. In agreement with the observation in the nine melanoma cell lines (Figure 10A,B), a positive correlation was observed between GRASLND and the melanocytic differentiation markers MITF and Melan, yielding Spearman coefficients of 0.69 (p = 7.2 x 10^{-6}) and 0.72 (p = 2.8 x 10^{-6}), respectively (Figure 10C,D). Consistently, GRASLND shows an inverse correlation with AXL, with a Spearman coefficient of -0.80 (p = 1.8 x 10^{-8}). Together, these data indicate an association between GRASLND expression and melanoma differentiation status, suggesting its cell state dependency.

3.3 Role of GRASLND in Melanoma Phenotype Switching

3.3.1 Generation of Stable Melanoma shRNA Knockdown Cell Lines

For further characterization and investigation for GRASLND's role in melanoma, knockdown studies were performed. Since a correlation of GRASLND expression and the differentiation status of melanoma cells was suspected, the human melanoma cell line 501-mel was chosen as melanocytic cell model, as it displayed the highest GRASLND levels all cell lines analyzed (Figure 10A, B). An RNA interference (RNAi)-mediated lncRNA knockdown approach was selected, that uses artificial short hairpin RNAs (shRNAs) for gene silencing. In the course of my master thesis, an shRNA-based RNAi system was developed for melanoma cell line Ma-Mel-86c[249]. This system utilized the lentiviral, tetracycline-inducible single-vector "pLKO-Tet-On" established by Wiedershain *et al.*, which allows precise temporal control of shRNA expression with the tetracycline derivative doxycycline as inducing agent[251]. In the initial set up, four shRNAs were tested, including two shRNAs with GRASLND target sequences adapted from published data (sh1, sh2)[233] and two newly designed sequences (sh3, sh4). A commercially available non-targeting sequence used as a control in the MISSION® (commercialized TRC) library, was taken as control shRNA. A detailed description on the cloning of the lentiviral, shRNA vectors is outlined in method parts 5.2.1.2-5.2.1.5 and a full list of all shRNA sequences can be found in material sections 5.1.9. For the generation of stable shRNA-expressing Ma-Mel-86c cells, lentiviral particles containing the cloned shRNA vectors were produced according to the protocol described in 5.2.2.4. This was followed by lentiviral transduction of shRNA sequences into parental Ma-Mel-86c cells using these lentiviruses, as

specified in section 5.2.2.5. Transduced cells were selected with puromycin for three days and further treated with doxycycline for additional three days to induce shRNA expression. Afterwards, cells were harvested, total RNA was extracted based on the protocol described in 5.2.3 and RT-qPCR was performed as outlined in 5.2.4 to analyze GRASLND RNA levels. Upon doxycycline induction and compared to the non-targeting control shRNA, GRASLND levels were decreased, with individual shRNAs demonstrating different knockdown efficiencies, ranging from 52.8% (sh2) to 90.3% (sh4) (Figure 11A). These data are reproduced from Fischer, Master thesis, 2021[249]. No additional experiments using the GRASLND-knockdown Ma-Mel-86c cells were conducted as part of the master thesis work. However, as this RNAi system achieved a robust GRASLND knockdown, the existing shRNA-containing lentiviruses were used to generate stable, shRNA-expressing 501-mel cell lines, as this is intended to be the preferred cell model for further studies in this doctoral work. The two most efficient shRNAs, sh3 and sh4, were thus tested in 501-mel cells for their capability to downregulate GRASLND expression. Stable shRNA GRASLND knockdown 501-mel cell lines (sh3, sh4) and an empty vector 501-mel control cell line was produced by lentiviral transduction using the respective lentiviral particles. Three batches of each of these generated cell lines were induced with doxycycline individually for 72 hours to obtain GRASLND knockdown efficiencies from three biological replicates. Compared to induced empty vector control cells, a significant reduced GRASLND expression by 53.6% and 72.4% was observed for shRNA sh3 and sh4, respectively (Figure 11B). Meanwhile, the previously used non-targeting control shRNA (Figure 11A) was reported to exhibit a substantial off-target effect. A study disclosed the targeting of small nuclear ribonucleoprotein Sm D3 (SNRPD3) by the “non-targeting” sequence in several human cell lines, resulting in apoptosis or cell growth arrest caused by p53-dependent mitotic catastrophe[252]. This was tested in a live cell imaging-based cell growth assay using stable Ma-Mel-86c cells containing the non-targeting shRNA control sequence (shNT). Indeed, cell growth was strongly suppressed after shRNA induction (Supplementary Figure 33), disqualifying this shRNA as a suitable non-targeting control shRNA. Consequently, a new negative control shRNA sequence was selected targeting the lacZ mRNA, which encodes the bacterial β-galactosidase, following its prior use by Feng *et al.*[253]. The new lacZ shRNA control 501-mel cell line was generated as stated earlier and cells were induced for 72 hours and tested for a potential effect of GRASLND RNA levels. In parallel, empty vector 501-mel control cells were induced and a comparable GRASLND expression was measured in both cell lines, confirming the lacZ-targeting shRNA cell line as a valid control for further experiments (Figure 11C). With an efficiency of 72.4%, shRNA sh4 demonstrates a strong knockdown ability. Since shRNA sh3 reduces GRASLND expression by only 53.6%, and similarly high efficiency like sh4 is desired for further experiments, an additional panel of four shRNAs (sh5-sh8) was designed, cloned, and stably introduced into 501-mel cells via lentiviral transduction, as previously described. Newly established stable 501-mel shRNA cell lines harboring shRNA constructs sh5-sh8 along with the 501-mel shRNA lacZ control cell line, were treated with doxycycline for 72 hours to induce shRNA expression, followed by analysis of GRASLND RNA levels. Compared to the lacZ control, sh5 and sh8 achieved a reduction of GRASLND levels by 67%, sh6 by 44% and sh7 by 19% (Figure 11D). In three independent experiments, the knockdown efficiencies of stable 501-mel shRNA knockdown cell lines containing the most efficient shRNAs sh4 and sh8, together with the empty vector and the new lacZ control cell line were determined. Both doxycycline-induced knockdown shRNAs sh4 and sh8

significantly reduced GRASLND expression by 65.9% and by 64.1%, respectively, compared to control cells (Figure 11E). Thus, two highly efficient shRNAs (sh4 and sh8) were validated as biological replicates alongside the new lacZ control.

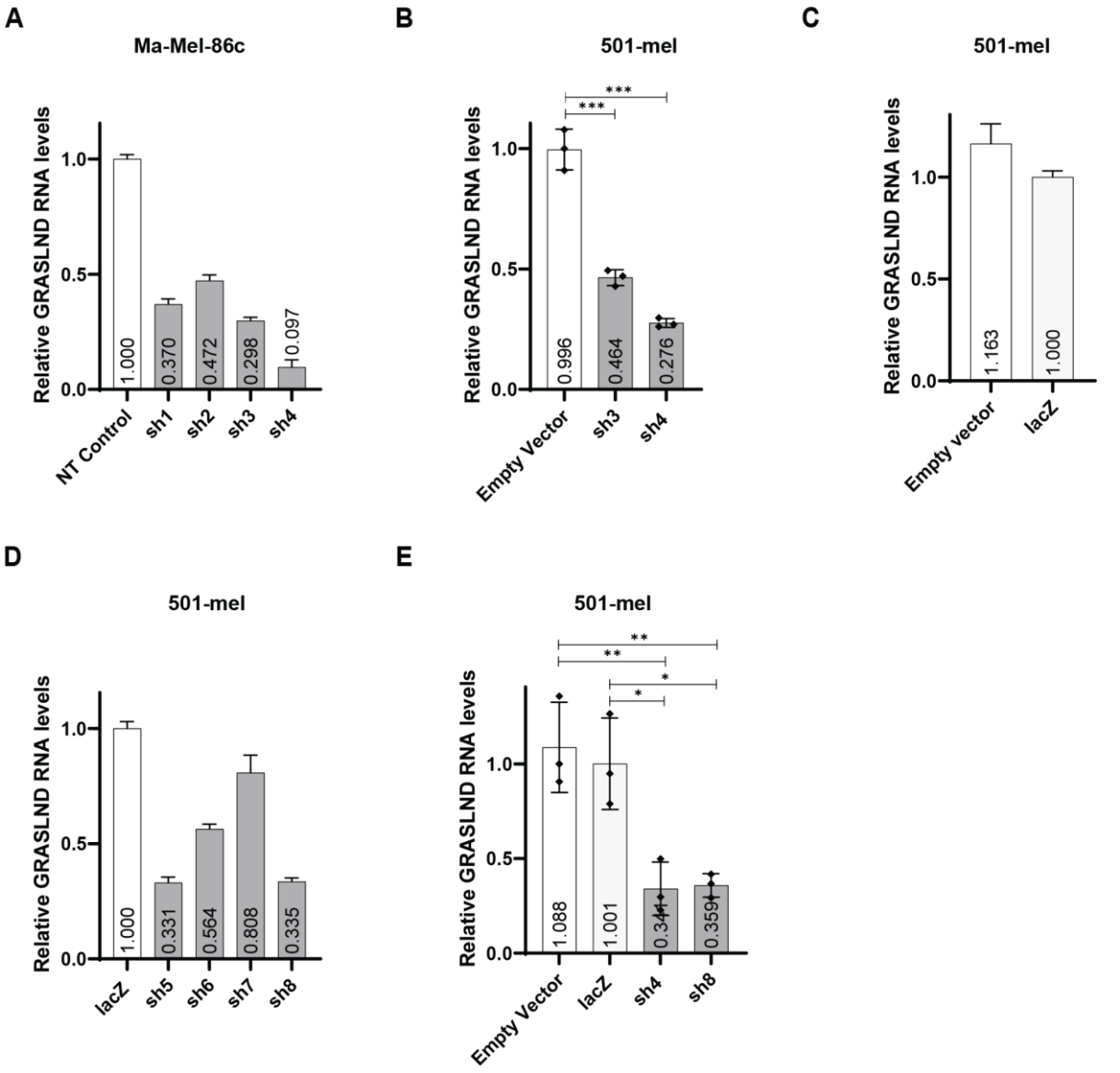

Figure 11: shRNA-mediated GRASLND knockdown in melanoma cell lines Ma-Mel-86c and 501-mel. *(A) Stable Ma-Mel-86c shRNA-expressing cell lines and a non-targeting shRNA expressing cell line were induced with doxycycline (3 µg/mL) for 72 hours. Relative GRASLND expression levels were analyzed by RT-qPCR. Data are normalized to GAPDH mRNA and represented as mean ± SD of n = 3 technical replicates. Data are reproduced from Fischer, Master thesis, 2021[249] (B) Stable 501-mel shRNA knockdown and empty vector control cells were induced with doxycycline (2 µg/mL) for 72 hours and subjected for RT-qPCR analysis. Relative GRASLND RNA levels are normalized to GAPDH mRNA levels and given as mean ± SD of n = 3 independent biological replicates. (C) Stable 501-mel empty vector and 501-mel shRNA lacZ control cell lines were treated with doxycycline (2 µg/mL) for 72 hours and GRASLND abundance was determined by RT-qPCR. Data were normalized to GAPDH mRNA levels and given as mean ± SD of n = 3 technical replicates. (D) Stable 501-mel shRNA GRASLND knockdown and lacZ shRNA control cell lines were induced for shRNA expression for 72 hours using doxycycline (2 µg/mL). GRASLND abundance was measured using RT-qPCR, data were normalized to GAPDH mRNA levels and represented as mean ± SD of n = 3 technical replicates. (E) Stable 501-mel shRNA knockdown, empty vector control and lacZ shRNA control cell lines were induced with doxycycline (2 µg/mL) for 72 hours and subjected for RT-qPCR analysis. Relative GRASLND expressions were normalized to GAPDH mRNA levels and given as mean ± SD of n = 3 independent biological replicates.*

3.3.2 Effects of GRASLND Knockdown on Cell Growth and Viability

With two highly efficient shRNAs available (sh4 and sh8), experiments were conducted to evaluate how GRASLND downregulation influences cell growth and viability. The effects of reduced GRASLND levels on cellular growth was assessed using live cell imaging monitoring. Stable shRNA knockdown and control 501-mel cells were plated, induced with doxycycline or left untreated (stock) and real-live monitoring for a duration of five days was performed as described in section 5.2.6. GRASLND knockdown appears to impair cell proliferation, as a marked reduction in the cell growth rate was observed approximately 48 hours post-induction in sh4 and sh8 cells, but not in the empty vector or shLacZ control cells (Figure 12A). To evaluate the effect of GRASLND knockdown on cell viability, a PARP1 (Poly (ADP-ribose) polymerase 1) cleavage assay was carried out. PARP1 plays a crucial role in DNA repair and the restoration of DNA integrity, thus maintaining genomic stability. PARP1 cleavage into fragments of 89 and 24 kDa is catalyzed by caspases and serves as an indicator of apoptotic cell death[254,255]. 501-mel knockdown and control cells were induced or left untreated for seven days followed by Western blotting with an anti-PARP1 antibody. For the positive control, cells were exposed to the apoptosis-inducing agent etoposide. Of note, during cell harvest adherent cells were detached and analyzed and also the culture media was collected to detect the presence of any potentially suspended and dead cells. Interestingly, cleaved PARP1 was either not detected or was essentially negligible in GRASLND knockdown and control cells (Figure 12B). Further, the live cell imaging studies did not reveal an increase in cell death following GRASLND knockdown. This observation suggests, that downregulation of GRASLND prompted a transition to a slow-proliferating melanoma phenotype without triggering apoptotic cell death.

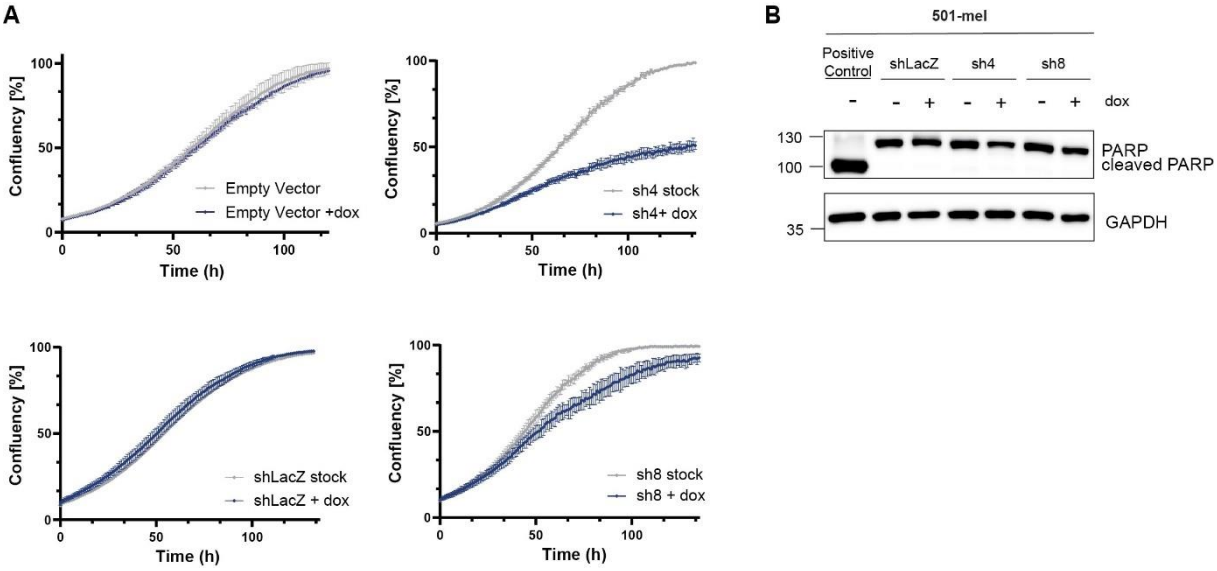

***Figure 12: Effects of GRASLND downregulation on Cell Growth and Viability**. (A) Live-cell imaging of stable shRNA knockdown 501-mel cells. Cells were either exposed to doxycycline (2 µg/mL) or left untreated (stock). Cell confluency was analyzed with the IncuCyte S3 system. One representative growth curve of each knockdown cell line is displayed. n = 3 independent biological replicates per knockdown cell line. (B) PARP cleavage assay. GRASLND knockdown cells were treated with doxycycline (2 µg/mL) for 7 days, followed by Western blot analysis with an anti-PARP antibody. Cells exposed to the apoptosis-inducing agent etoposide (150 µM, Sigma Aldrich) were included as a positive control. GAPDH served as the loading control. Shown is a representative blot from n = 3 independent biological replicates.*

3.3.3 Impact of GRASLND Knockdown on Melanoma Cell Invasiveness

Recognizing cell invasiveness is central to both metastatic spreading and thus melanoma progression, an *in vitro* Transwell invasion assay was performed to investigate a potential effect of GRASLND knockdown on the cell invasion capability. In this widely used Boyden Chamber Assay, the invasive potential of cells is measured by using a two-chamber system in which the two medium-filled compartments are separated by a porous membrane coated with an extracellular matrix layer. Chemotaxis through the matrix towards a chemoattractant is exhibited exclusively by cells possessing invasive capabilities. The protocol, as outlined in section 5.2.7, was adapted from the established method by Justus *et al*.[256] and was optimized regarding seeding density, chemoattractant reagent, incubation time and assay duration by Stavroula Petroulia, PhD (Max Planck Institute, Dortmund) for improved performance in our lab setting. Thus, solely the seeding density of the used cell lines required modification. Prior to the assay, stable shRNA knockdown (sh3 and sh4) and empty vector control 501-mel cells were induced with doxycycline for shRNA expression for 72 hours. Of note, at the time of conducting these initial invasion assays, sh8 and shLacZ control cells had not yet been tested. After 48 hours of incubation on the matrix on the upper chamber, transmigrated cells were stained and imaged. Seeding densities of 4×10^4, 4.5×10^4, 5×10^4 and 6×10^4 cells/insert were tested, all of which allowed thorough processing, cell counting and analysis of the results (Figure 13A, B). Each test experiment with different seeding densities was conducted once, including two technical replicates per condition (Empty vector, sh3, sh4). Interestingly, a consistent trend of enhanced invasiveness is observed in each assay following GRASLND knockdown with both shRNAs compared to the empty vector control.

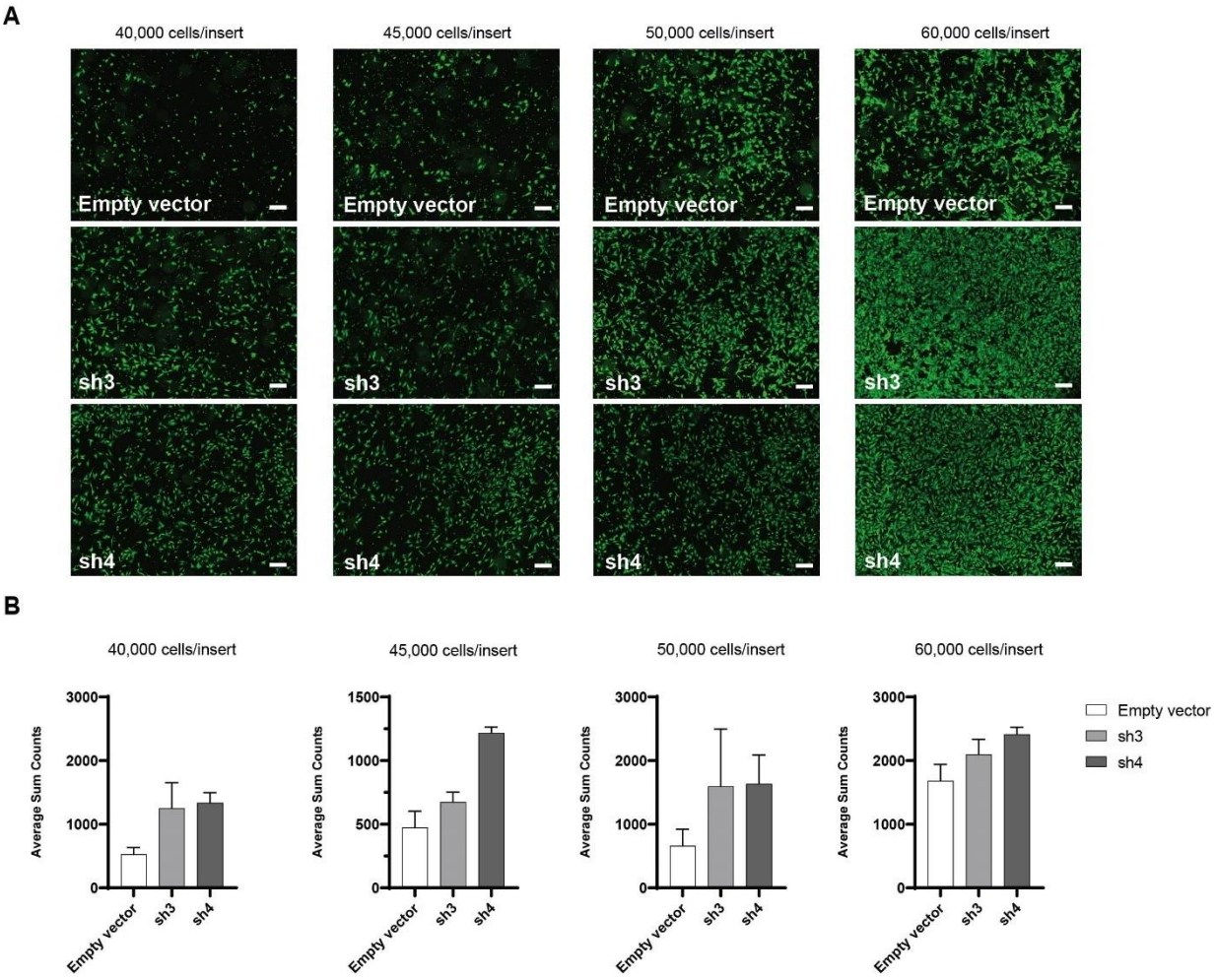

Figure 13: Transwell invasion assay assessing cell invasion following GRASLND knockdown. *(A) Stable shRNA GRASLND knockdown (sh3, sh4) and empty vector control 501-mel cells were induced for 72 hours with doxycycline (2 µg/mL) prior to a Transwell invasion assay with varying seeding densities. Representative images after cell staining (4X objective) for each condition (Empty vector, sh3, sh4) are shown. Scale bar = 50 µm (B) Quantitative analysis of transmigrated cells for each condition is shown. Data represent n = 2 technical replicates per experiment with different seeding numbers.*

In the course of the project, shRNA sh8 was identified as a more effective shRNA than sh3 and a non-targeting control shRNA (shLacZ) 501-mel cell line was generated (Figure 11E). As part of her bachelor thesis work under my supervision[257], Lin Christina Qiu, B.Sc., performed a Transwell invasion assay using stable shRNA 501-mel cell lines containing the most effective shRNAs, sh4 and sh8, as well as the non-targeting shLacZ control shRNA. Following a doxycycline-induction for 72 h, the cell lines were tested in a Transwell invasion assay. An optimized seeding density of 5×10^4 cells/insert were plated on the matrix and incubated for 48 hours. Transmigrated cells were stained and images were analyzed as explained in sections 5.2.7.1 and 5.2.7.2 in more detail. Two independent biological replicates with two technical replicates of each condition (shLacZ, sh4, sh8) were carried out. Compared to the control shRNA, the invasion capacity of 501-mel cells was enhanced by both shRNAs sh4 and sh8, resulting in fold changes of 48.8 ± 2.5 SD and 28.5 ± 10.8 SD, respectively (Figure 14). In line with the previous test experiments (Figure 13), the results indicate an effect of GRASLND on the invasion capability of melanoma cells.

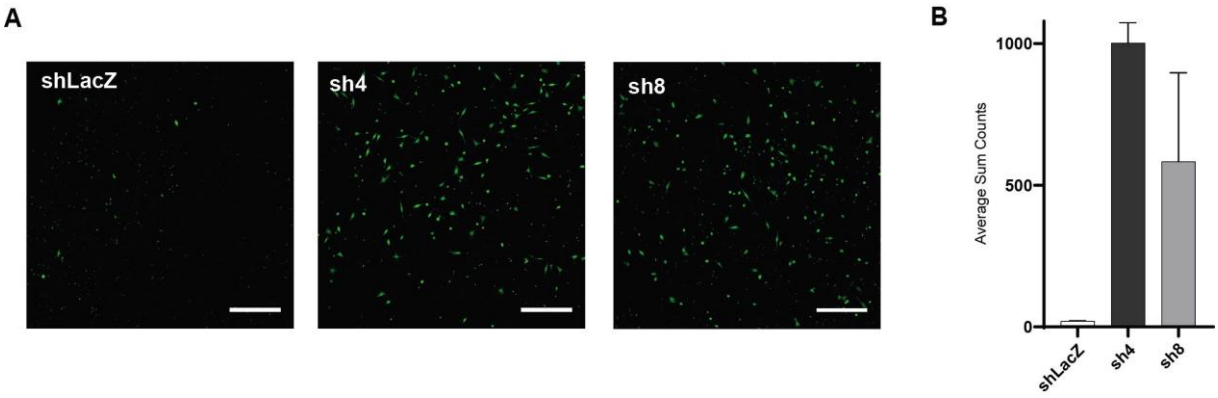

Figure 14: Effect of GRASLND knockdown on cell invasiveness assessed by Transwell invasion assay. *(A) 501-mel GRASLND knockdown (sh4 and sh8) and control (shLacZ) shRNA cells were induced with doxycycline (2 µg/mL) for 72 hours, followed by a Transwell invasion assay. Representative images of n = 2 independent biological replicates are depicted. Scale bar = 25 µm. (B) Quantitative analysis of the Transwell invasion assay. Data represent n = 2 independent biological replicates.*

3.3.4 Influence of GRASLND Knockdown on Melanoma Differentiation

3.3.4.1 shRNA-mediated GRASLND knockdown

Based on these prior results of a transition to a slower-proliferating, more invasive cell state following GRASLND downregulation (Figure 12, Figure 14), the process of phenotype switching was suspected. Initially proposed by Hoek *et al*. and later confirmed and refined, melanoma cell phenotypes are characterized by distinct gene expression profiles, primarily determined by the expression levels of the melanocytic, lineage-specific transcription factor MITF. Accordingly, the slow-growing and highly invasive phenotype is characterized by low MITF levels. In contrast, the $MITF^{high}$ melanoma cell state is less prone to metastasize, being lowly invasive yet highly proliferative[44,45,58]. Thus, a phenotype switch from a differentiated to a dedifferentiated cell state is expected to reduce cell proliferation and increase cell invasiveness, both of which were observed following GRASLND knockdown in 501-mel cells. For this reason, MITF expression levels and those of its target gene MelanA, were examined following GRASLND downregulation. Stable shRNA GRASLND knockdown and empty vector control 501-mel cells were induced for shRNA expression for a duration of 72 hours and MITF and MelanA levels were analyzed using Western blot technique. Three independent biological replicates of this experiment were performed. Indeed, both melanocytic markers were significantly decreased in GRASLND knockdown cells and not empty vector control cells (Figure 15A). For validation, a second differentiated melanoma cell line with high GRASLND levels, Ma-Mel-86c (Figure 10A, B) was tested for a dedifferentiation after GRASLND knockdown. Therefore, stable shRNA GRASLND knockdown and control Ma-Mel-86c cell lines were generated, following the same protocol used for 501-mel, as detailed in section 5.2.2.5. After 72 hours induction of these stable cell lines for shRNA expression, the MITF and MelanA levels were detected by Western blot. Three independent biological replicates of this experiment were performed. Similar to the findings in 501-mel, both shRNAs in Ma-Mel-86c cells exhibit a significant decrease in MelanA levels. A reduction in MITF levels is also observed. Notably, a previous experiment using the less effective shRNA variant, sh3, also demonstrated a reduction in MelanA protein levels, though to a much lesser extent (Supplementary Figure 34). This suggests that the efficiency of the knockdown is

correlated with the extent of downregulation of the melanocytic marker MelanA. Collectively, these findings indicate that GRASLND knockdown induced phenotype switching of a differentiated, MITF^{high} and highly proliferative cell state towards a MITF^{low}, slow-proliferative and highly invasive melanoma phenotype. Thus, it is reasonable to assume that GRASLND has a role in modulating melanoma plasticity.

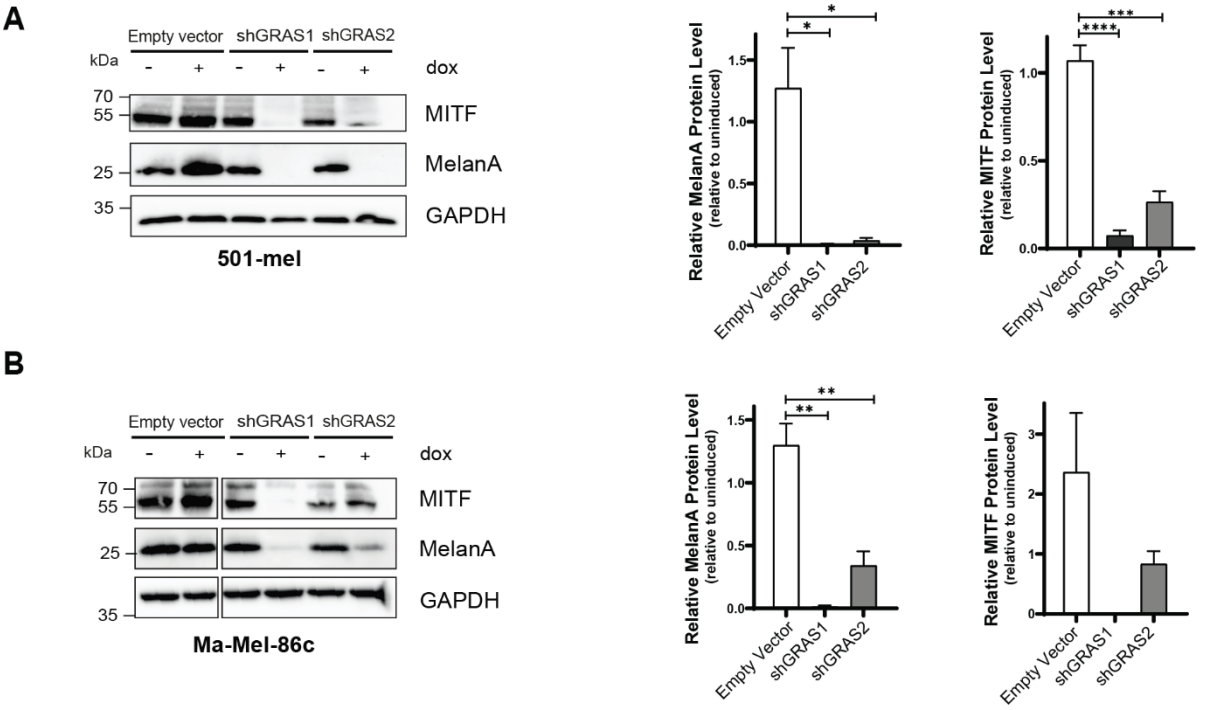

Figure 15: GRASLND downregulation leads to a dedifferentiation in differentiated melanoma cell lines. *(A) Expression levels of melanocytic markers MITF and MelanA upon GRASLND knockdown were analyzed by Western blotting. Stable shRNA GRASLND knockdown and empty vector control 501-mel cells were induced with doxycycline (2 µg/mL) for 72 h and expression was measured. GAPDH served as a loading control. Representative blot (left) and relative quantification of MITF and MelanA levels (right) from n = 3 independent biological replicates. Relative expression is given as mean ± SEM. p values by two-sided t-test. (B) Expression levels of MITF and MelanA upon GRASLND downregulation in Ma-Mel-86c stable shRNA knockdown and empty vector cells were analyzed by Western blotting after cells were induced with doxycycline (2 µg/mL, 72 h). GAPDH served as loading control. Representative blot (left) and relative quantification of MITF and MelanA levels (right) from n = 3 independent biological replicates. Relative expression is given as mean ± SEM. p values by two-sided t-test.*

3.3.4.2 Validation of GRASLND Knockdown-mediated Melanoma Dedifferentiation

3.3.4.2.1 siRNA-mediated GRASLND knockdown

In order to validate the previous findings on a GRASLND knockdown-mediated melanoma phenotype switch from a differentiated and MITF^{high} to a dedifferentiated, MITF^{low} cell state, an additional knockdown strategy was tested. Therefore, a commercially available siRNA pool consisting of four GRASLND-targeting siRNAs (Horizon Discovery) and a non-targeting (NT) siRNA as control (Horizon Discovery) was used. Transfection was performed using the reverse transfection protocol as described in section 5.2.2.6.2. Firstly, parental Ma-Mel-86c cells were subjected to transfection with either 10 nM of the siRNA pool or the non-targeting control siRNA, or the cells were only treated with transfection

reagent as additional control. After incubation for one and three days, the cells were harvested and the GRASLND knockdown efficiency was determined using RT-qPCR (Figure 16A). Compared to the non-targeting control cells, a knockdown of 32% and 22% was achieved after one and three days, respectively. To assess whether increasing siRNA concentration enhances knockdown efficiency, three concentrations (30 nM, 60 nM, and 100 nM) were evaluated and GRASLND levels were measured after 3 days of incubation (Figure 16B). Based on prior observations of shRNA-mediated effects, such as dedifferentiation and reduced cell proliferation occurring only after 48 hours post-induction, the Day 3 timepoint was selected. However, RT-qPCR data of GRASLND levels demonstrate that higher concentrations do not result in improved knockdown efficiency. Further, siRNA knockdown was tested in parental 501-mel cells using two siRNA concentrations and knockdown efficiencies were determined three days post transfection (Figure 16C). GRASLND expression was reduced by 37% and 41% by using either 10 nM or 30 nM siRNA, respectively. Since a correlation between knockdown efficiency and the extent of melanoma dedifferentiation was already suspected, the achieved siRNA efficiencies appear to be insufficient. When comparing the efficiencies of the tested shRNAs, a substantial difference was observed between the less efficient sh3 and the more efficient sh4 and sh8 (Figure 15, Supplementary Figure 34). The siRNA-mediated downregulation of GRASLND achieved less than 50%, which is even lower than that of shRNA sh3. Consequently, further experiments on dedifferentiation, cell proliferation, and invasion were not pursued.

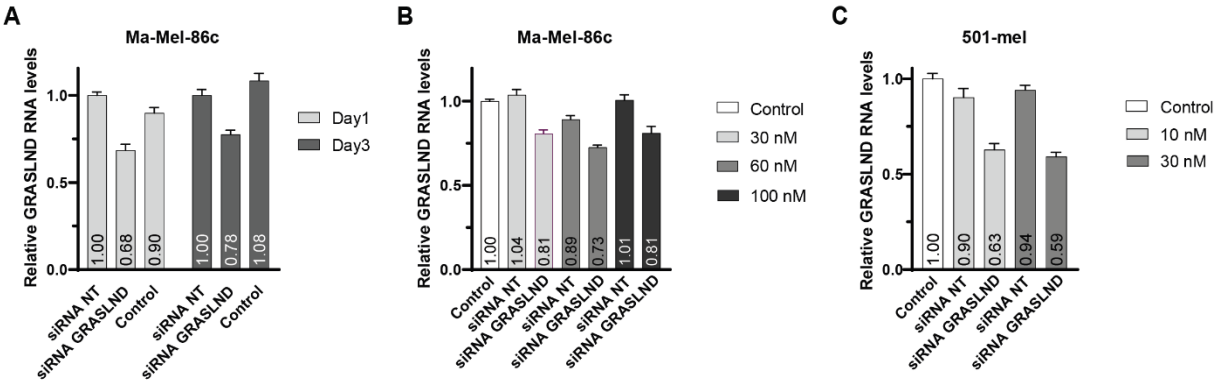

Figure 16: siRNA-mediated GRASLND knockdown in melanoma cell lines Ma-Mel-86c and 501-mel. *(A) Relative GRASLND levels in Ma-Mel-86c cells after Day 1 and Day 3 post siRNA transfection with either a commercial pool of four GRASLND targeting siRNAs or a non-targeting (NT) control siRNA. Control cells were treated with transfection reagent only. GRASLND levels were analyzed by RT-qPCR and normalized to GAPDH mRNA levels. Relative expression is given as mean ± SD from n = 3 technical replicates. (B) Testing of three different siRNA concentrations (30, 60, 100 nM) in parental Ma-Mel-86c cells. RT-qPCR to determine GRASLND levels after three days of incubation. GRASLND expression is normalized to GAPDH mRNA levels. Relative expression is given as mean ± SD from n = 3 technical replicates. (C) Relative GRASLND expression after siRNA transfection in parental 501-mel cells using concentrations of 10 and 30 nM. Analysis was performed by RT-qPCR and GRASLND levels were normalized to GAPDH mRNA levels. Relative expression is given as mean ± SD from n = 3 technical replicates.*

3.3.4.2.2 CRISPRi-mediated GRASLND knockdown

As an alternative approach for lncRNA knockdown, CRISPR interference (CRISPRi), a method well-established in the lab, was selected. As part of my Master thesis work[249], this technique was established in Ma-Mel-86c cells. The CRISPRi system used, involved the catalytically "dead" Cas9 (dCas9) protein, which was fused to the Krüppel-associated box (KRAB), a powerful transcription repressor protein domain[258]. As a first step, lentiviral particle production was performed using the lentiviral vector lenti-TetOn-dCas9-KRAB (Supplementary Figure 35) as described in section 5.2.2.4. Engineered Ma-Mel-86c cells stably expressing the dCas9-KRAB-mCherry fusion protein were generated by lentiviral transfection as detailed in section 5.2.2.5. GRASLND-targeting single guide RNAs (sgRNAs), named sgRNA i4-i7, were designed to meet the criteria for targeting within the range of -50 to +300 bp relative to the transcription start site (TSS) for efficient transcriptional repression[259]. Details on the design and construction of sgRNA plasmids using the backbone vector pLVx-U6se-EF1a-sfPac (Supplementary Figure 36) are given in methods part 5.2.1.1 and required oligonucleotide sequences are listed in section 5.1.9. Lentiviral particles containing sgRNA sequences were produced, followed by lentiviral transductions of harvested lentiviral particles into Ma-Mel-86c-dCas9-KRAB cells. Prior to infections with sgRNAs, the cells were cultured under doxycycline treatment for 72 hours to induce dCas9-KRAB expression. Selection with puromycin was performed for three days, after which cells were harvested for further analysis by RT-qPCR to determine GRASLND levels (Figure 17A). These data are reproduced from Fischer, Master Thesis, 2021[249].

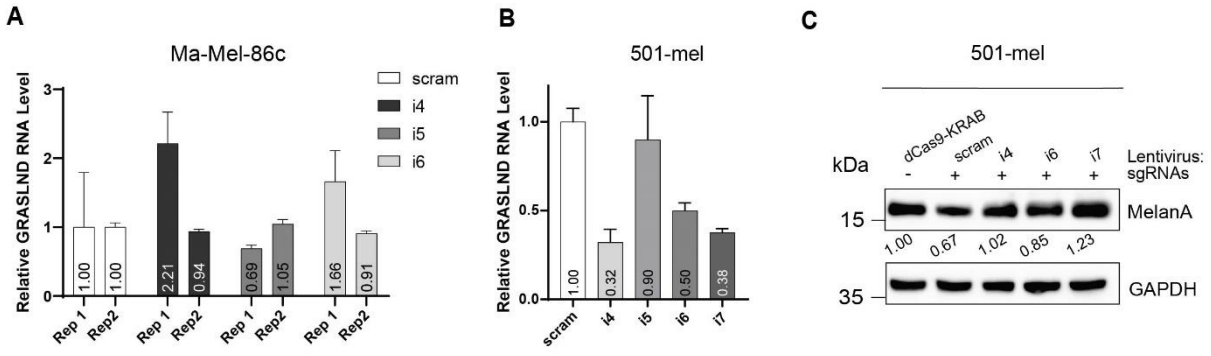

Figure 17: CRISPR interference in Ma-Mel-86c and 501-mel. *(A) Relative GRASLND expression in Ma-Mel-86c-dCas9-KRAB knockdown cells compared to scrambled sgRNA control cells. Ma-Mel-86c-dCas9-KRAB cells were treated with doxycycline (2 µg/mL) for 72 h to induce dCas9-KRAB protein expression, followed by transduction with lentivirus for the incorporation of sgRNAs. After selection with puromycin (5 µg/mL) for 72 h, the relative GRASLND expression was determined by RT-qPCR and normalized to GAPDH mRNA levels. Fold change of GRASLND levels are given as mean ± SD from n = 3 technical replicates. As indicated, n = 2 biological replicates per sgRNA was performed, each normalized to the scrambled control sgRNA. These data were generated during my Master thesis research[249]. (B) 501-mel-dCas9-KRAB cells were seeded one day prior to lentiviral transduction to introduce sgRNAs. Selection with puromycin (5 µg/mL) was performed for 24 hours, followed by doxycycline treatment (5 µg/mL) for the expression of dCas9-KRAB protein for six days. GRASLND expression levels were determined using RT-qPCR and normalized to GAPDH mRNA levels. Data are represented as mean ± SD from n = 3 technical replicates. (C) MelanA protein levels were analyzed following CRISPRi-mediated knockdown using Western blotting. GAPDH served as loading control. Image including relative quantification, normalized to GAPDH protein levels, of measured MelanA levels from one experiment.*

The results reveal that no sufficient GRASLND knockdown was achieved, despite the expression of both components, dCas9-KRAB (fused to mCherry) and the sgRNA (co-expressed with GFP), as validated by Western blot using an anti-Cas9 antibody and visualization of the co-expression of mCherry and GFP by fluorescence microscopy (data not shown). Solely in replicate 1 (Rep 1) using sgRNA i5, a small GRASLND downregulation was measured (0.69-fold ± 0.05). For the other two sgRNAs (i4 and i6) even an upregulation of GRASLND is observed. In replicate 2 (Rep 2) no fold change compared to the control cells was determined. Thus, no potent sgRNA for efficient GRASLND knockdown in Ma-Mel-86c was found.

Nevertheless, as this CRISPRi method is frequently used for lncRNA knockdown within the lab, a validated 501-mel-dCas9-KRAB cell line from Stavroula Petroulia, PhD was available. Consequently, the four sgRNAs were tested in melanoma cell line 501-mel. As part of her Bachelor thesis under my supervision[257], Lin Christina Qiu, B.Sc. examined a potential dedifferentiation in 501-mel following CRISPRi-mediated GRASLND knockdown. Provided 501-mel-dCas9-KRAB cells were seeded one day prior to lentiviral transduction for introduction of the sgRNAs, as explained earlier. This was followed by antibiotic selection for 24 hours with puromycin and doxycycline treatment to induce the expression of the dCas9-KRAB fusion complex. The cells were maintained under doxycycline induction for six days, with the medium refreshed every two days. This was followed by harvest and the cells were divided equally for analysis by RT-qPCR and Western blotting. GRASLND levels were determined (Figure 17B), revealing a reduced GRASLND expression compared to the scrambled control sgRNA by 68%, 10%, 50% and 62% for sgRNAs i4-i7, respectively. As efficient knockdown was achieved using sgRNAs i4, i6 and i7, the MelanA levels of these samples were analyzed by Western blot. In addition, 501-mel-dCas9-KRAB cells served as controls (Figure 17C). Contrary to expectations, no reduced expression of the melanocytic marker MelanA was observed in this experimental setup, despite sufficient knockdown efficiencies, that were comparable to GRASLND downregulations caused by shRNA sh4 and sh8 (Figure 11E).

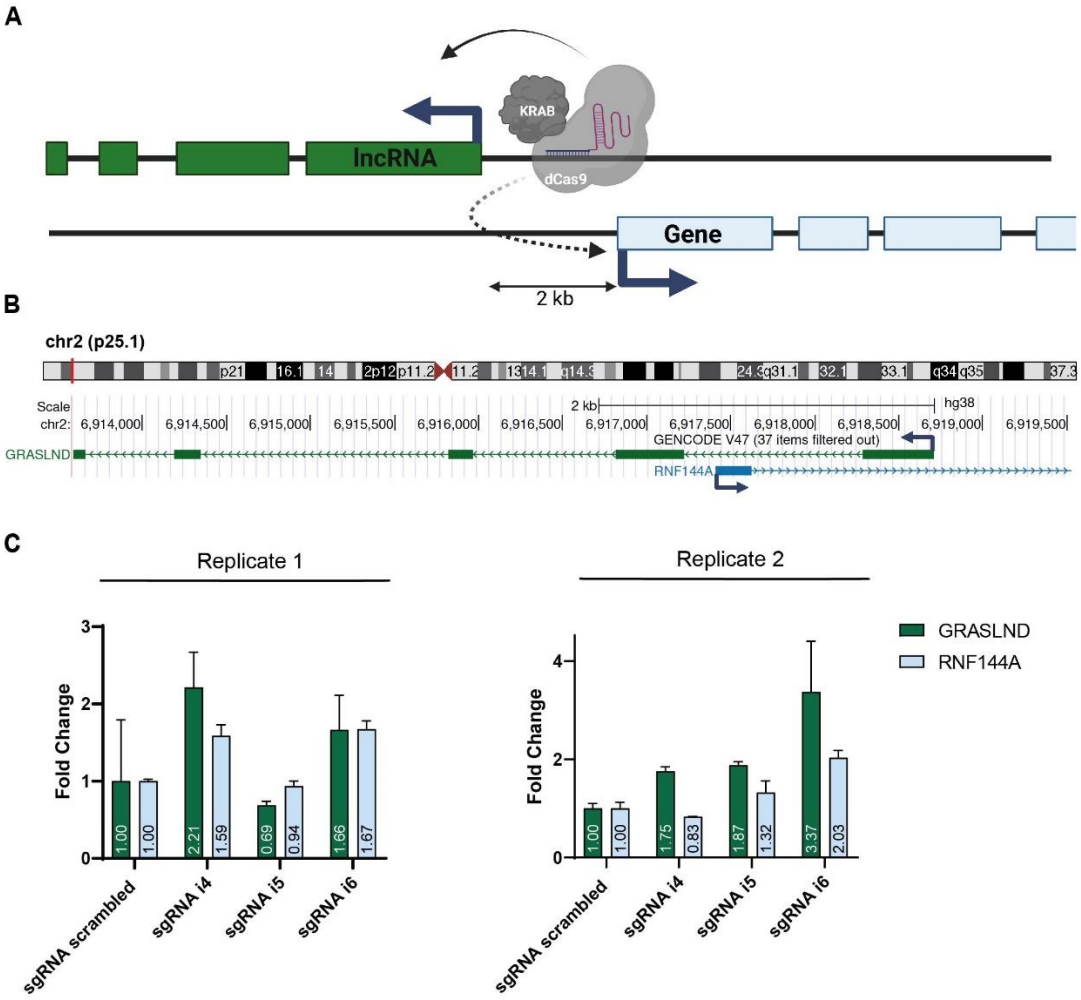

Figure 18: CRISPRi-mediated GRASLND knockdown affects its sense gene RNF144A. *(A) Schematic illustration of a potential effect of CRISPRi targeting antisense lncRNAs on its sense gene. Promoters of lncRNAs and their sense genes, arranged in a head-to-head orientation and located within 2000 basepairs, can be considered as bidirectional. In the case of bidirectional promoters, the lncRNA is not targetable using CRISPRa/i, as the adjacent sense gene might be affected. Illustration is adapted from Goyal et al. (Figure 1)[224]. (B) Schematic representation of the genomic locus of antisense lncRNA GRASLND and its sense gene RNF144A depicted in the UCSC genome browser. (C) CRISPRi-mediated GRASLND knockdown in Ma-Mel-86c cells. Ma-Mel-86c-dCas9-KRAB cells were induced with doxycycline (2 µg/mL) for 72 hours, followed by transduction with 25 µL (left) and 50 µL (right) of each lentivirus for the incorporation of sgRNAs. Selection with puromycin (5 µg/mL) was performed for 72 hours. Relative GRASLND and RNF144A RNA expression levels after CRISPRi perturbation using sgRNAs i4-i6. Data were normalized to GAPDH mRNA levels and given relative to scrambled sgRNA control cells. Fold change of GRASLND levels are given as mean ± SD from n = 3 technical replicates.*

An extensive literature research on the limitations and challenges of CRISPR/Cas9-based methods for targeting lncRNAs, led to the recognition of a genome-wide study by Goyal and colleagues, assessing the "CRISPRability" of lncRNAs[224]. This study highlighted that both, CRISPRa and CRISPRi rely on the recruitment of dCas9 and effector proteins to the promoter proximal region of the target gene that potentially impact nearby genes. Antisense lncRNA promoters and those of their sense gene arranged in a head-to-head orientation, which are located within 2 kb, were considered as bidirectional promoters (Figure 18A). Goyal *et al*. found lncRNAs with bidirectional promoters, or with promoters located in close proximity (< 2 kb) to the transcription start site (TSS) of the sense gene, to be 'non-CRISPRable'[224]. Investigating the genomic locus of GRASLND and its sense gene RNF144A using the UCSC genome

browser revealed the overlapping of both genes and the near distance of both promoters in a range < 2 kb (Figure 18B)[260]. Based on this, the RNA levels of RNF144A were determined after CRISPRi-mediated GRASLND knockdown in Ma-Mel-86c cells. Two independent replicates, differing in the amount of lentiviral particles used for the transduction with sgRNAs i4-i6 (25 or 50 µL), were tested for their GRASLND and RNF144A levels, three days after doxycycline treatment to induce the dCas9-KRAB effector complex (Figure 18C). As previously observed (Figure 17A, Rep 1), GRASLND levels are upregulated in both experiments and also show inconsistency between the replicates, but interestingly, the expression of the sense gene RNF144A is affected to the same extent in most samples. This indicates the suspected influence due to promoter proximity, in line with previously published CRISPRi limitations[224]. Consequently, the CRISPRi approach for knockdown of GRASLND is unsuitable with regard to a direct effect on RNF144A expression, as such sense-antisense pairs are assumed to potentially share common regulatory mechanisms or participate in related signaling pathways[261]. Considering this limitation of applying the CRISPR-based approach to GRASLND downregulation studies, we concluded that employing the doxycycline-inducible shRNA system is the most suitable method to pursue. This system allows parallel experimental groups, with and without doxycycline induction, that can be conducted under identical conditions, providing built-in internal controls, enhancing both, the reliability and interpretability of the results.

3.3.4.2.3 shRNA-mediated GRASLND knockdown – alternative shRNA

The effect of a phenotypic switch observed in the differentiated cell lines 501-mel and Ma-Mel-86c towards a dedifferentiated, lowly proliferative and strongly invasive cell state induced by GRASLND knockdown was demonstrated using two efficient shRNA, though it could not be replicated with the CRISPRi approach. This finding prompts consideration of whether both sh4 and sh8 might share a common off-target effect, leading to dedifferentiation. Although this probability is minimal, to eliminate this option and confirm that the found phenotype switching is due to a specific GRASLND knockdown, an additional shRNA should be tested. Among the panel of tested shRNAs, sh5 exhibited efficiency comparable to that of sh8 (Figure 11D) and was further evaluated for its potential in GRASLND knockdown-induced dedifferentiation. This investigation was also carried out by Lin Christina Qiu, B.Sc. as part of her Bachelor thesis under my supervision[257].

501-mel cells carrying the shRNA constructs for sh4, sh8, sh5 and the non-targeting shLacZ control were seeded and subsequently treated with doxycycline for four days with refreshing the medium after two days containing the same concentration of the induction agent. Afterwards, the cells were harvested and divided for parallel analysis by RT-qPCR and Western blotting. GRASLND levels were measured, showing lncRNA downregulation by 65%, 52%, and 62% by shRNAs sh4, sh5, and sh8, respectively, each relative to their corresponding uninduced controls (Figure 19A). Further analysis of the protein levels of melanocytic marker MelanA upon GRASLND knockdown confirms the shRNA-mediated decrease of MelanA levels for all three shRNAs tested and not the control shRNA, suggesting a dedifferentiation of 501-mel cells (Figure 19B). As previously suspected, a correlation can be observed

between the suppression efficiencies of shRNAs and the degree of melanoma dedifferentiation, as indicated by MelanA levels (Figure 19A, B).

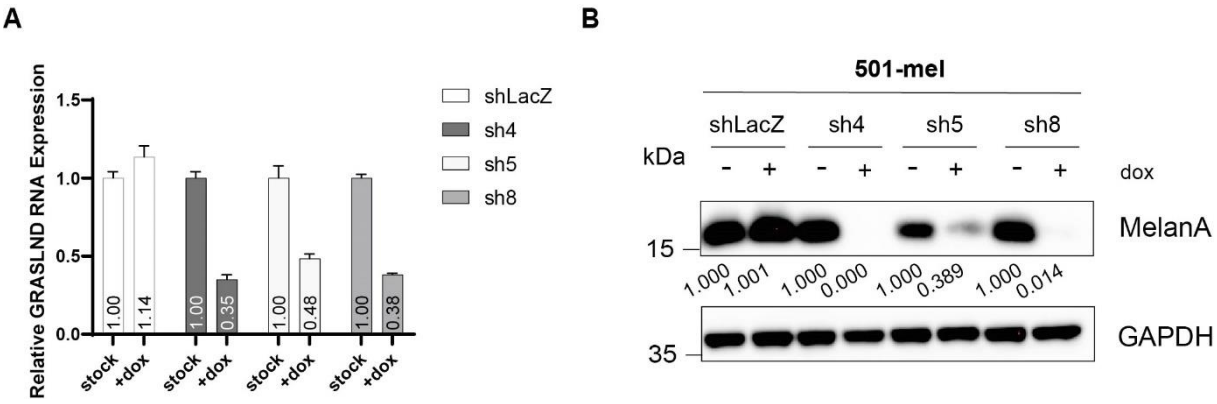

Figure 19: Validation of GRASLND knockdown-mediated dedifferentiation of 501-mel cells using shRNAs. *(A) Stable shRNA GRASLND knockdown and shRNA control 501-mel cells were treated with doxycycline (2 µg/mL) for four days. GRASLND RNA levels were determined by RT-qPCR by normalizing to GAPDH mRNA. Data are shown as mean ± SD from n = 3 technical replicates. (B) The same 501-mel knockdown cells were analyzed for their MelanA protein levels by Western blotting. GAPDH served as a loading control. One blot was performed. For relative quantification of MelanA protein levels, the expression was normalized to GAPDH protein levels and shown in relation to their corresponding uninduced (stock) internal controls.*

In summary, the phenotypic switch could not be confirmed using alternative knockdown methods, including siRNAs or CRISPRi, likely due to insufficient knockdown strength or still unknown factors, potentially issues related to lentiviral transduction or co-targeting of the sense gene RNF144A. However, a third shRNA in addition to the previously used shRNAs (sh4, sh8) was tested, validating the previous results on a dedifferentiation in 501-mel cells. The probability of a shared off-target effect among the three shRNAs is extremely low, supporting the reliability and credibility of the observed phenotypic switch in differentiated cell lines 501-mel and Ma-Mel-86c following GRASLND knockdown.

3.4 Investigation of Pathways Influenced by GRASLND

3.4.1 Transcriptomic Analysis upon GRASLND Knockdown

To investigate the transcriptional changes following GRASLND knockdown, RNA sequencing (RNA-Seq) was conducted to profile differential gene expression and identify pathways impacted by the downregulation of lncRNA activity. Stable shRNA GRASLND knockdown (sh4, sh8) and non-targeting shRNA control (shLacZ) 501-mel cell lines were treated with doxycycline to induce shRNA expression for 72 hours with media refreshed daily to maintain a constant inducer reagent concentration. The cells were harvested and RNA was extracted as described in method part 5.2.3. A portion of the extracted RNA was used for cDNA synthesis to enable the validation of efficient GRASLND knockdown prior to RNA-Seq by using RT-qPCR (Figure 20A). For each cell line, three distinct batches of cells were used as independent biological replicates, each representing separate cell cultures prepared under identical conditions to ensure reproducibility and account for biological variability. Efficient GRASLND knockdown

was confirmed, achieving a minimum downregulation by 55 %. For the subsequent transcriptomic analysis, all three replicates of shLacZ samples and the two replicates for each GRASLND knockdown cell line, which show the highest knockdown efficiency, were selected. The procedures for library preparation and the analysis were performed as outlined in section 5.2.9, the latter carried out by Shashank Tiwari, M. Sc. A list of detailed quality control information of all RNA-Seq samples is given in Supplementary Table 2. A PCA plot was generated from the RNA sequencing results to visualize sample clustering and variation among the conditions (Figure 20B). PCA reveals distinct clustering of control cells compared to both GRASLND knockdown samples explaining 64% variance, whereas replicates are clustered closely together, indicating consistency within each sample group. In this analysis, the four GRASLND knockdown samples (2X sh4, 2X sh8) were combined and treated as four replicates that were compared to the three replicates of control cells. Differentially expressed genes were represented in a volcano plot, revealing a total 549 genes (Fold change >1 and ≤1, adjusted p value < 0.05), of which 393 were upregulated and 156 genes were downregulated (Figure 20C). Further, gene set enrichment analysis (GSEA) of these differentially expressed genes was performed using the HALLMARK pathway gene sets (Figure 20D), and the top 15 enriched pathways for downregulated as well as the top 16 enriched pathways for upregulated genes are depicted. In accordance with the experimental findings of a phenotype switch from a differentiated, highly proliferative towards a slow-growing, highly invasive, dedifferentiated cell state, the epithelial to mesenchymal transitions (EMT) is in the top three of the most upregulated gene set. EMT, in the melanoma context more precisely termed phenotype switching, describes the dynamic ability of melanoma cells to alternate between proliferative and invasive cell states[44]. This distinction arises because melanocytes are not epithelial cells, and when they adopt a dedifferentiated state, they may not exhibit the typical mesenchymal traits associated with EMT. However, these similar processes both function to promote tumor metastasis by losing cell adhesion, enabling tumor cells to disconnect from their original structure and infiltrate the basement membrane[46]. The impact of GRASLND downregulation on proliferation (Figure 12) is evident from the top downregulated gene sets, many of which are involved in regulating the cell cycle, such as G2M checkpoint, E2F and MYC targets. Examination of the genes associated with these gene sets (Supplementary Table 3) reveals downregulation of CDK1 and CDK4, indicating an inhibitory effect of GRASLND knockdown on cell cycle progression[262]. Among the top 16 enriched pathways for upregulated genes, gene sets associated with melanoma dedifferentiation, such as JAK-STAT3-, TNFα- and WNT signaling, were found[263–265]. Detailed investigation of specific genes within these gene sets showed enhanced expression of key regulators of these pathways, STAT3, NFKB2 and LEF1, respectively (Supplementary Table 4). Overall these transcriptomic data of GRASLND knockdown in 501-mel cells support a role of this lncRNA in regulating melanoma differentiation and highlight potential key pathways involved in this process.

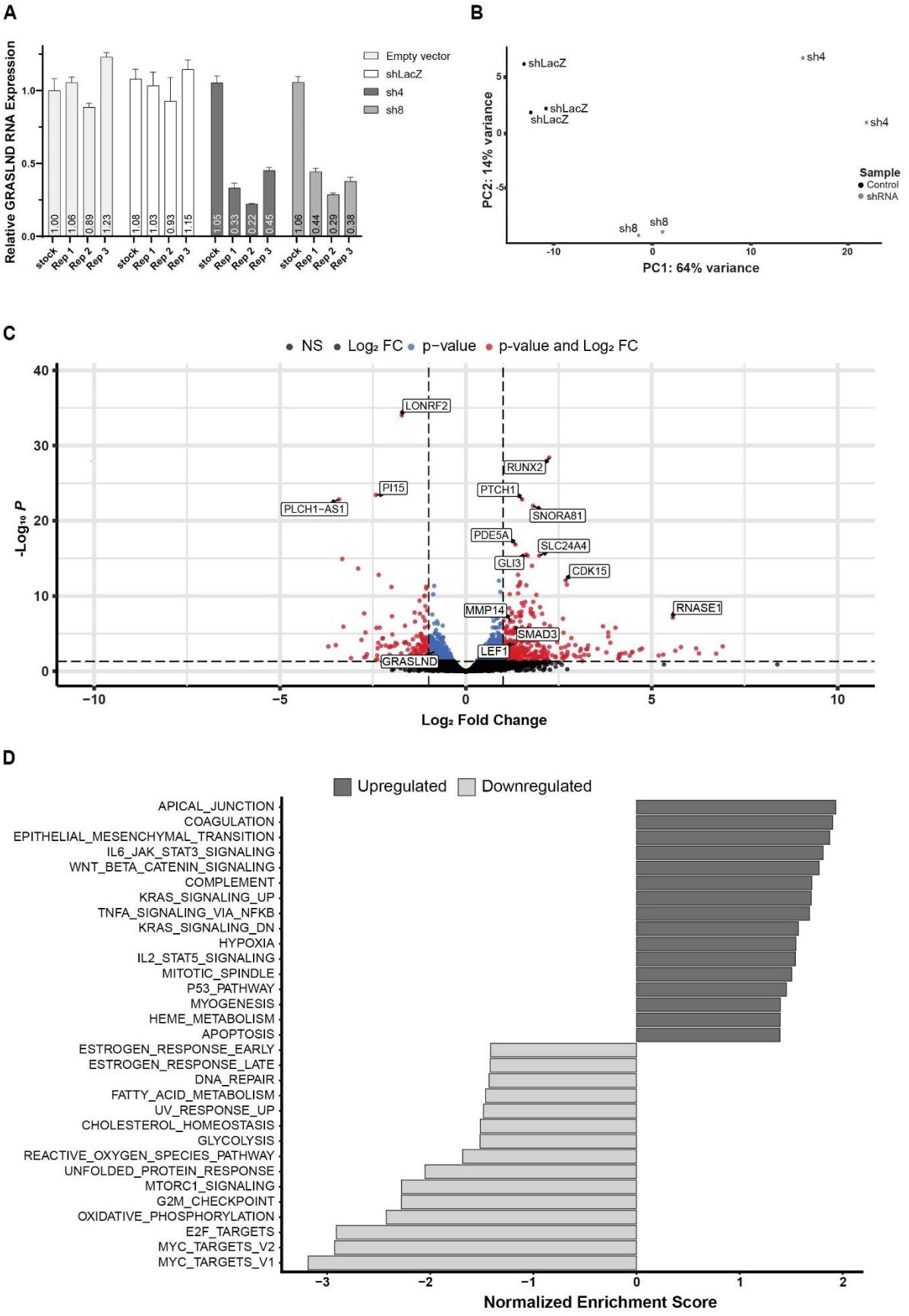

Figure 20: Transcriptomic analysis of 501-mel cells after shRNA-mediated GRASLND knockdown. *(A) Validation of GRASLND knockdown by RT-qPCR. Stable shRNA GRASLND knockdown (sh4, sh8), empty vector control and non-targeting shRNA control (shLacZ) 501-mel cells were induced with doxycycline (2 µg/mL) for 72 hours and GRASLND levels were analyzed using RT-qPCR. Expression levels were normalized to GAPDH*

mRNA levels and given relative to uninduced (stock), empty vector control cells. Data from n = 3 independent biological replicates are represented and given as mean ± SD from n = 3 technical replicates. (B) PCA plot of 501-mel shRNA knockdown and control cell lines used in RNA-Seq. Represented are three replicates of shLacZ and two replicates for each GRASLND knockdown cell line (sh4, sh8). (C) Volcano plot of RNA-Seq results illustrating differentially expressed genes following GRASLND knockdown in 501-mel cells using shRNAs sh4 and sh8 compared to shLacZ samples. Vertical lines mark log2FoldChange thresholds, the horizontal line represent the statistical significance cutoff ($p < 0.05$). Red dots demonstrate genes significantly up- or downregulated. NS = non-significant, FC = Fold Change. (D) Gene set enrichment analysis (GSEA) showing pathways influenced by GRASLND knockdown compared to control samples using the Hallmark pathway gene sets (https://CRAN.R-project.org/package=msigdbr). Displayed are the top 16 enriched pathways for upregulated genes and the top 15 enriched pathways for downregulated genes.

3.4.2 Identification of Protein Interaction Partners via GRASLND RNA Pulldown

3.4.2.1 Validation of GRASLND-PKR interaction

Given the elucidation of relevant pathways and demonstrated phenotypic effects following GRASLND downregulation, identifying potential protein interaction partners represents an essential next step in the characterization of GRASLND to understand the scope of its biological function and potentially insights into the mechanism. In a pivotal study on GRASLND in mesenchymal stem cells (MSCs), Huynh and colleagues performed a GRASLND RNA pulldown followed by mass spectrometry, identifying interferon-induced, double-stranded RNA-activated protein kinase R (PKR) as a binding partner. They proposed that this GRASLND-PKR interaction leads to an inhibition of the JAK-STAT-IFNγ pathway[233]. As a validation of this interaction in melanoma cells, GRASLND RNA pulldown experiments were carried out, followed by direct verification by Western blotting in accordance with the experimental procedures described in the methods sections 5.2.10 and 5.2.5. The used approach was adapted from a protocol established by Dimartino *et al*., that utilizes two sets of biotinylated antisense DNA oligonucleotides (named “odd” and “even”), each containing five probes, to pulldown GRASLND from cytoplasmic extraction of parental 501-mel cells (Supplementary Figure 37)[266]. As a control, a probe set consisting of five biotinylated antisense DNA oligonucleotides targeting lacZ mRNA was taken. Successful and specific enrichment of GRASLND was confirmed through RT-qPCR analysis, revealing a fold change of 24.5 and 8.3 of GRASLND levels with probe set “odd” and “even”, respectively, relative to the input control (Figure 21A). In contrast, the control lncRNA MALAT1 exhibited no enrichment. Subsequent Western blotting was performed to check for the expected abundance of PKR. Indeed, PKR abundance was detected in both RNA pulldown samples, whereas the lacZ control pulldown sample showed a PKR protein signal only at background levels. Two additional independent biological replicates were performed, confirming these findings (Supplementary Figure 38) and indicating a direct GRASLND-PKR interaction in 501-mel melanoma cells as previously reported in MSCs (Figure 21B)[233].

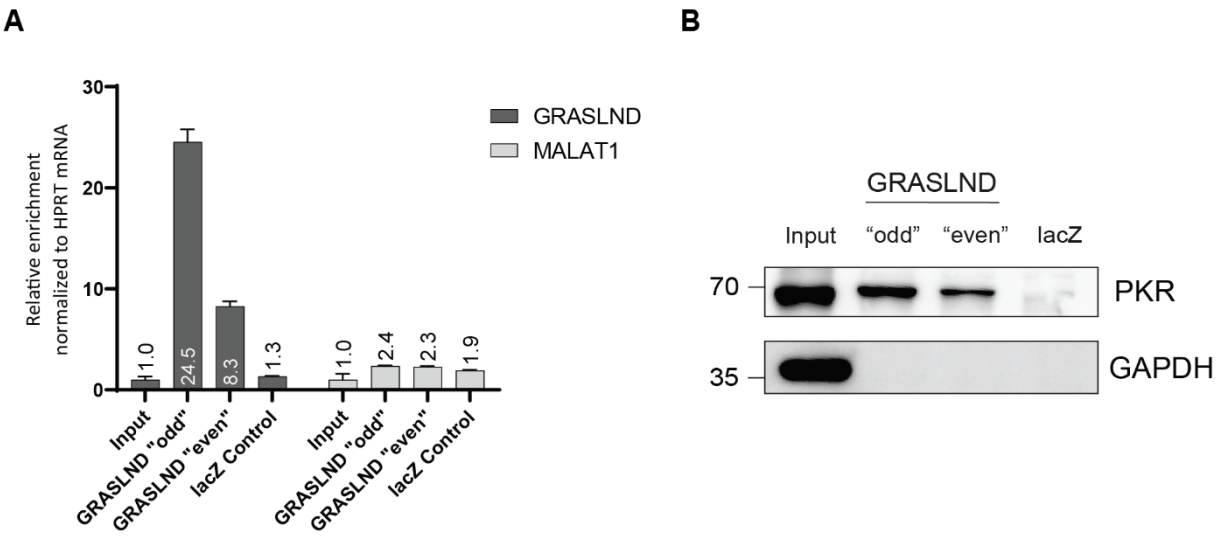

***Figure 21: Validation of GRASLND-PKR interaction by RNA Pulldown**. (A) GRASLND RNA pulldown using biotinylated antisense DNA oligonucleotides and cytoplasmic extracts from parental 501-mel cells. Two probe sets targeting GRASLND lncRNA (“odd”, “even”) and a probe set targeting the lacZ gene (negative control) were used in the experimental setup. GRASLND and MALAT1 levels were analyzed using RT-qPCR and the expression was normalized to HPRT mRNA levels and given relative to Input control. Data are represented as mean ± SD from n = 3 technical replicates. (B) GRASLND pulldown samples were used for PKR detection in a Western blot using anti-PKR antibody. GAPDH served as a control. Representative blot of n = 3 independent biological replicates. The other blots of the two additional biological replicates are presented in the supplement (Figure 38).*

3.4.2.2 Mass Spectrometry-Based GRASLND Pulldown

The multifunctional characteristics of lncRNAs contribute to their ability to associate with numerous protein partners, a common feature that highlights their extensive regulatory potential in cellular systems[117]. Consequently, the next step should involve identifying additional potential binding partners for GRASLND using mass spectrometry to further elucidate its interaction network. Referring to the previous section 3.4.2.1, a GRASLND pulldown was carried out successfully, achieving strong and specific GRASLND enrichment for both pulldown probe sets (Figure 21A, Supplementary Figure 38). For the proteomics-based GRASLND pulldown, an additional four biological replicates were performed, and GRASLND enrichment was verified by RT-qPCR before proceeding with mass spectrometry analysis (Figure 22A). A significant enrichment of 45.2 ± SD = 3.4 and 34.4 ± SD = 8.9 compared to the lacZ control was achieved for the probe sets “odd” and “even”, respectively. This was followed by an on-bead tryptic digestion of proteins bound to bead-immobilized GRASLND RNA, as detailed in methods section 5.2.11.1. For mass spectrometric analysis of the proteins, the service of the mass spectrometry group of Department 4 of the Max Planck Institute, Dortmund was used. Measurement of the tryptic and dried peptides was conducted by the facility using nano-HPLC-MS/MS and further analysis of the proteomics data was carried out by Dr. Petra Janning according to the procedure outlined in methods parts 5.2.11.2 and 5.2.11.3. For quality control of the obtained data, a principal component analysis on the log2-transformed label-free quantification (LFQ) intensities was performed. As expected, the samples cluster rightly according to the replicates (Supplementary Figure 39). Afterwards, all samples and replicates were evaluated using an ANOVA analysis (S_0 = 0, permutation-based FDR, FDR = 0.05). Visualization of the proteins showing significance together with a hierarchical clustering for both, the

samples and the proteins, also reveal a good clustering of the replicates (Supplementary Figure 40). Subsequently, a pairwise comparison of the GRASLND pulldown samples “odd” and “even” against the lacZ control samples were performed individually using a two-sided t test (FDR = 0.01 and S_0 = 1). Volcano plots were created and proteins with log2-fold changes > 1.5 and -Log10 *p* > 3 were considered as statistically significant enriched (Figure 22B). A number of 28 significantly enriched proteins in the GRASLND pulldown sample “odd” was observed, whereas for the “even” samples, seven proteins were identified. Five of these proteins, namely RBM45, XRCC5 and 6, RBMS1 and DHX36 were identified also in the “odd” samples, suggesting an actual interaction of these proteins with lncRNA GRASLND (Figure 22C).

It is worth noting that the previously validated GRASLND binding partner PKR was not detected in this proteomics-based analysis. To clarify this finding, an in-depth re-analysis of the raw data was performed, with an explicit search for PKR peptides in the samples to uncover the reason behind the absence of PKR enrichment. Re-analysis was carried out by Siska Führer, M.Sc. (Max Planck Institute, Dortmund) according to the description in method section 5.2.11.3. Visualization of individual PKR peptide levels throughout all samples reveal the detection of only one “unique” peptide in all samples (“control”, “odd” and “even”), with one missing value from four replicates in the samples “control” and “odd” (Supplementary Figure 41). In the analysis, proteins not identified in at least one run with two or more “razor+unique” peptides were filtered out, explaining that PKR enrichment was not observed.

In summary, this experiment successfully identified potential protein binding partners of GRASLND through targeted lncRNA pulldown and mass spectrometry, providing initial insights into its potential functional interaction network and molecular roles. However, future studies require validation experiments to proof the actual binding of these proteins to GRASLND.

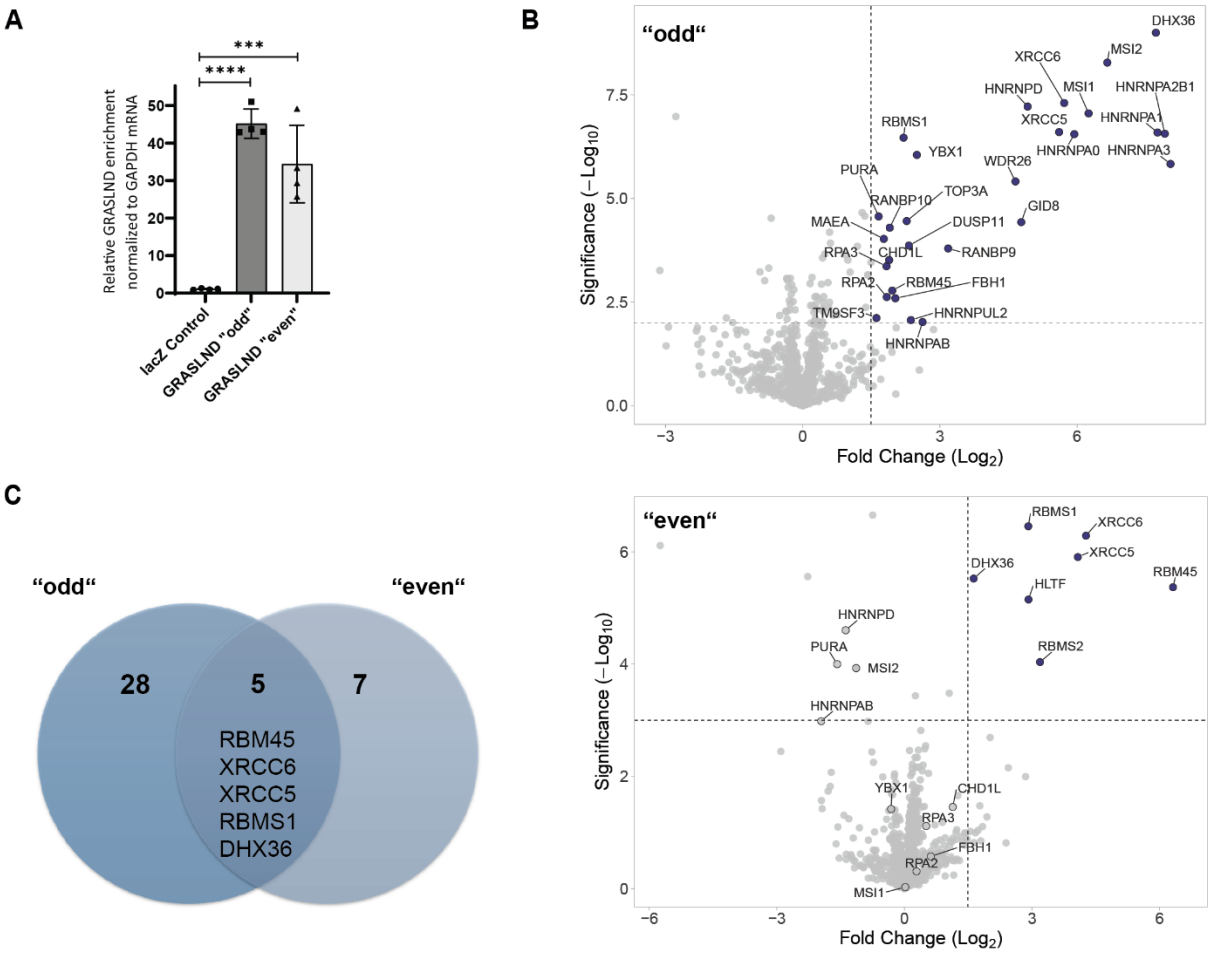

Figure 22: GRASLND lncRNA pulldown followed by mass spectrometry in 501-mel cells. *(A) Cytoplasmic extracts from parental 501-mel cells were used for GRASLND lncRNA pulldown using two probe sets each with five biotinylated antisense DNA oligonucleotides ("odd" and "even") and a control probe sets targeting lacZ mRNA. GRASLND enrichment was confirmed using RT-qPCR. GRASLND levels were normalized to GAPDH mRNA levels and represented relative to one replicate of the lacZ control sample. Data are given as mean ± SD from n=4 independent biological replicates. (B) Mass spectrometry was performed subsequent to GRASLND pulldown. Volcano plots represent the statistical analysis of the obtained proteomics data. A pairwise comparison between the GRASLND pulldown samples "odd" (top) and "even" (bottom) against the lacZ control samples were performed individually using a two-sided t test (FDR = 0.01 and s0 = 1). Volcano plots were created using the VolcaNoseR web app265. Proteins with log2-fold changes > 1.5 and -Log10 (p) > 3 were considered as statistically significant enriched. (C) Venn diagram depicting the overlapping proteins found to be significantly enriched in both GRASLND pulldown probe sets "odd" and "even".*

3.4.3 Investigating Dedifferentiation Pathways by Analyzing Key Protein Levels

3.4.3.1 PKR Pathway

To evaluate pathways potentially involved in the observed phenotype switching, protein levels of key components within these pathways were investigated. As targeted GRASLND lncRNA pulldown confirmed PKR as protein binding, this prompted the question of whether PKR is implicated in the dedifferentiation process. Firstly, the impact of GRASLND downregulation on the expression level of PKR was studied. Therefore, shRNA-mediated GRASLND knockdown in 501-mel cells was conducted, with PKR protein levels determined at timepoints 72 hours and 7 days post shRNA induction. In an initial

experiment, PKR levels were reduced by 48% and 31% after 72 hours, and by 100% and 99.94% after seven days using sh4 and sh8, respectively (Figure 23A,B). In an independent biological replicate using solely shRNA, sh4, a decrease in PKR abundance was observed in GRASLND knockdown cells after 72 hours, but not after seven days (Supplementary Figure 42). This discrepancy may be due to potential feedback loop or compensatory mechanism in the cells, that likely occurred at an earlier time point in this replicate. Nevertheless, these data suggest that GRASLD knockdown is accompanied by a decline in PKR protein expression levels.

As one of the four eIF2α (eukaryotic Initiation Factor 2 alpha) kinases alongside ERK, HRI, and GCN2, PKR serves as a central player in the process of integrated stress response (ISR). Besides its canonical activator, double-stranded RNA (dsRNA) to facilitate its key role in anti-viral response, PKR can also be activated by other stressors such as bacterial lipopolysaccharides (LPS), cytokines (e.g. TNF-α, IFNγ), ER stress, irradiation or reactive oxygen species (ROS)[267]. Once activated, PKR phosphorylates eIF2α, the central mechanism of the ISR. This in turn causes a broad inhibition of Cap-dependent translation, while selectively promoting the translation of specific ISR-related mRNA, including the key effector of ISR, ATF4[268]. In order to examine downstream targets of PKR, an impact of GRASLND knockdown on the ATF4 protein abundance was performed in two independent biological replicates. 501-mel shRNA knockdown cells were induced for shRNA expression for 72 hours and ATF4 levels were determined using Western blotting (Figure 23C,D). The obtained blots reveal a strong loss of ATF4 protein expression in one replicate using both GRASLND knockdown cell lines, however, in the second replicate, a decrease in ATF4 levels was solely observed for knockdown cells using shRNA sh4. An additional downstream target in the PKR-mediated ISR pathway is the transcription factor NF-κB, a protein complex consisting of dimers of NF-κB family members, such as p50 and p65, which regulates genes affecting inflammatory and immune responses, cell differentiation and apoptosis[269–271]. To assess an effect of GRASLND downregulation on this transcription factor, 501-mel GRASLND knockdown cells, which were induced for 72 hours, were subjected to Western blotting using anti-phospho-p65 and anti-p65 antibodies. In line with the previous results, the expression levels of activated (phosphorylated) p65 were decreased in GRASLND knockdown cells. Of note, in shRNA control cells, an approximately 2-fold increase of phospho-p65 levels is observed compared to uninduced control cells (Figure 23E,F). In contrast, the general levels of p65 remain constant in shLacZ, as well as GRASLND knockdown cells after shRNA induction for 24 and 72 hours (Figure 23G,H).

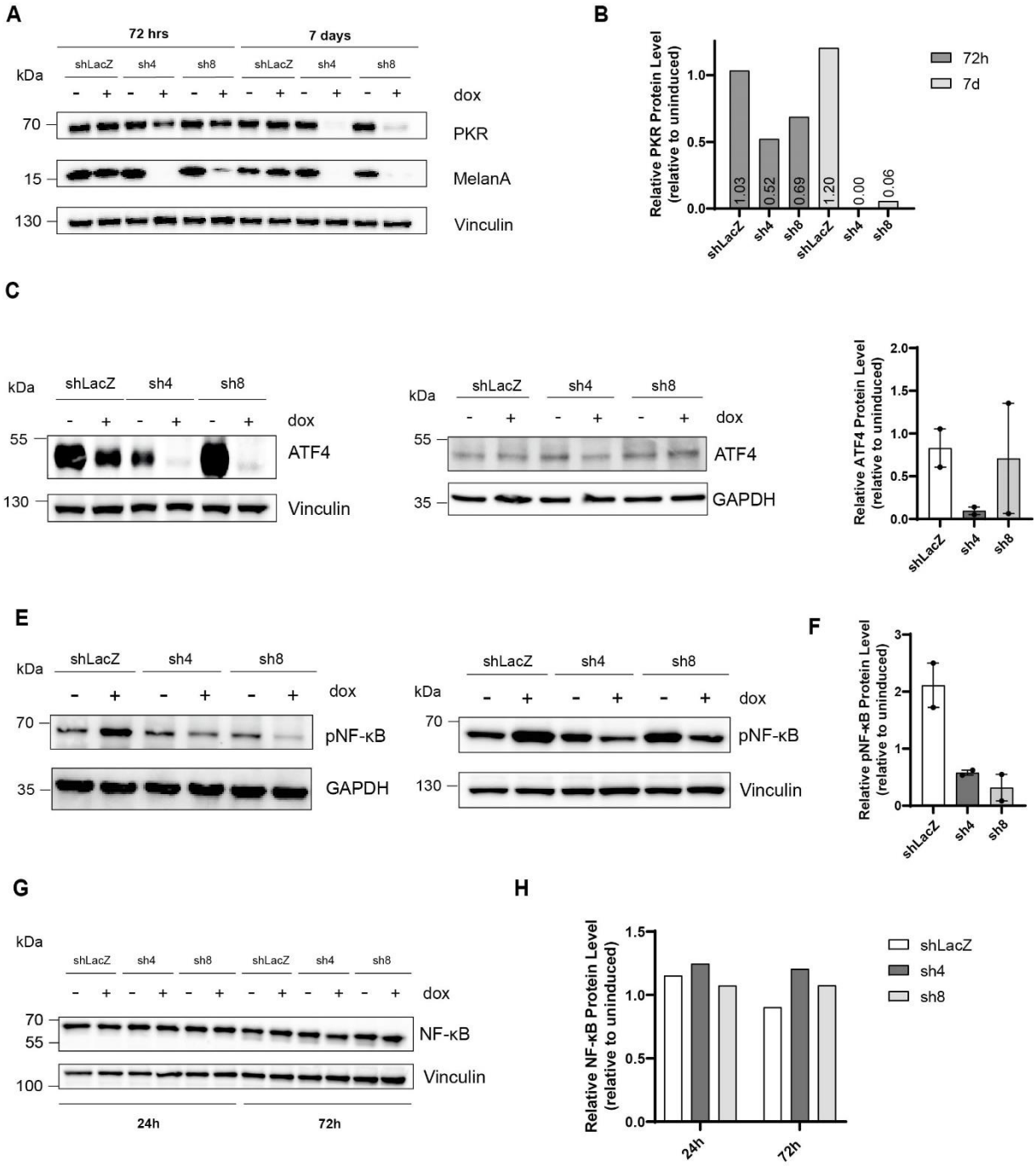

Figure 23: Impact of GRASLND downregulation of key components of PKR downstream targets. *(A, B) Detection of PKR protein levels after shRNA-mediated GRASLND knockdown in 501-mel cells using Western blotting. Stable shRNA GRASLND knockdown and control shRNA 501-mel cells were induced with doxycycline (2 µg/mL) for 72 hours and 7 days. Western blot was performed using anti-PKR antibody. MelanA was used to validate dedifferentiation and vinculin was used as loading control. Blot from one experiment is depicted (A). Relative quantification of PKR levels by normalization to the loading control. Data are represented in relation to the uninduced cells for each knockdown cell line (shLacZ, sh4, sh8) (B). (C, D) Detection of ATF4 protein levels after shRNA-mediated GRASLND knockdown in 501-mel cells using Western blotting. Stable shRNA GRASLND knockdown and control shRNA 501-mel cells were induced with doxycycline (2 µg/mL) for 72 hours. Western blot was performed using anti-ATF4 antibody. Vinculin and GAPDH were used as loading control for one replicate each. n = 2 independent biological replicates were performed and both blots are shown (C). Relative quantification of ATF4 levels by normalization to the loading control. Data are represented in relation to the uninduced cells for each knockdown cell line (shLacZ, sh4, sh8). Data are given as mean ± SEM (D). (E, F) Measurement of phospho-NF-κB (p65) protein levels after shRNA-mediated GRASLND knockdown in 501-mel cells using Western blotting. Stable shRNA GRASLND knockdown and control shRNA 501-mel cells were induced with doxycycline (2 µg/mL, 72 h). Western blot was performed using anti-phospho-NF-κB antibody. Vinculin and GAPDH were used as loading control for one replicate each. n = 2 independent biological replicates were performed and both blots are shown (E). Relative quantification of phospho-NF-κB levels by normalization to the loading control. Data are shown in relation*

to the uninduced cells for each knockdown cell line (shLacZ, sh4, sh8). Data are given as mean ± SEM (F). (G,H) Determination of NF-κB (p65) protein levels after shRNA-mediated GRASLND knockdown in 501-mel cells. Stable shRNA GRASLND knockdown and control shRNA 501-mel cells were induced with doxycycline (2 µg/mL) for either 24 or 72 hours. Western blots were performed using anti-NF-κB antibody. Vinculin was used as loading control. n = 2 independent biological replicates were carried out and both blots are represented (G). Relative quantification of NF-κB levels by normalization to the loading control. Data are shown in relation to the uninduced cells for each knockdown cell line (shLacZ, sh4, sh8). Data are given as mean ± SEM (H).

Overall, these findings reveal that a shRNA-mediated GRASLND knockdown in 501-mel cells may negatively affect the expression of PKR and its downstream target ATF4, as well as the phosphorylation of the NF-κB component p65, which though requires further validation. Accordingly, the suppression of the ISR appears to be a potential effect of GRASLND downregulation. However, the PKR/ATF4-ISR axis is described in the literature to repress MITF expression and to induce a phenotype switch towards a highly invasive, dedifferentiated cell state[51,272]. Since a reduction in both, PKR and ATF4 protein levels after GRASLND knockdown was observed, an ISR/PKR/ATF4-mediated dedifferentiation mechanism may be excluded in this experimental and cellular setup.

3.4.3.2 JAK-STAT Pathway

An additional signaling pathway suspected to be implicated in the process of dedifferentiation occurring in 501-mel GRASLND knockdown cells might be the IL-6-JAK-STAT3 signaling. Transcriptomic analysis revealed this pathway among the top 4 enriched signaling pathway for upregulated genes (Figure 20C). Focused analysis of the individual genes within this gene set showed the upregulation of key regulator STAT3 on the RNA level (Supplementary Table 4). To confirm an increase in STAT3 expression also on the protein level, 501-mel GRASLND knockdown cells were induced for shRNA expression for 72 hours, and Western blot was performed. Indeed, GRASLND knockdown resulted in increased expression of STAT3 protein by 2- and 1.5-fold compared to the uninduced condition using sh4 and sh8, respectively (Figure 24A). STAT3 is reported as a driver of melanoma metastasis by CEPB-mediated repression of MITF transcription *in vivo*[263]. Interestingly, a direct interaction with PKR and its inhibitory effect on this kinase are documented in the literature[273]. This makes a STAT3-mediated mechanism of phenotype switching after GRASLND knockdown in 501-mel conceivable.

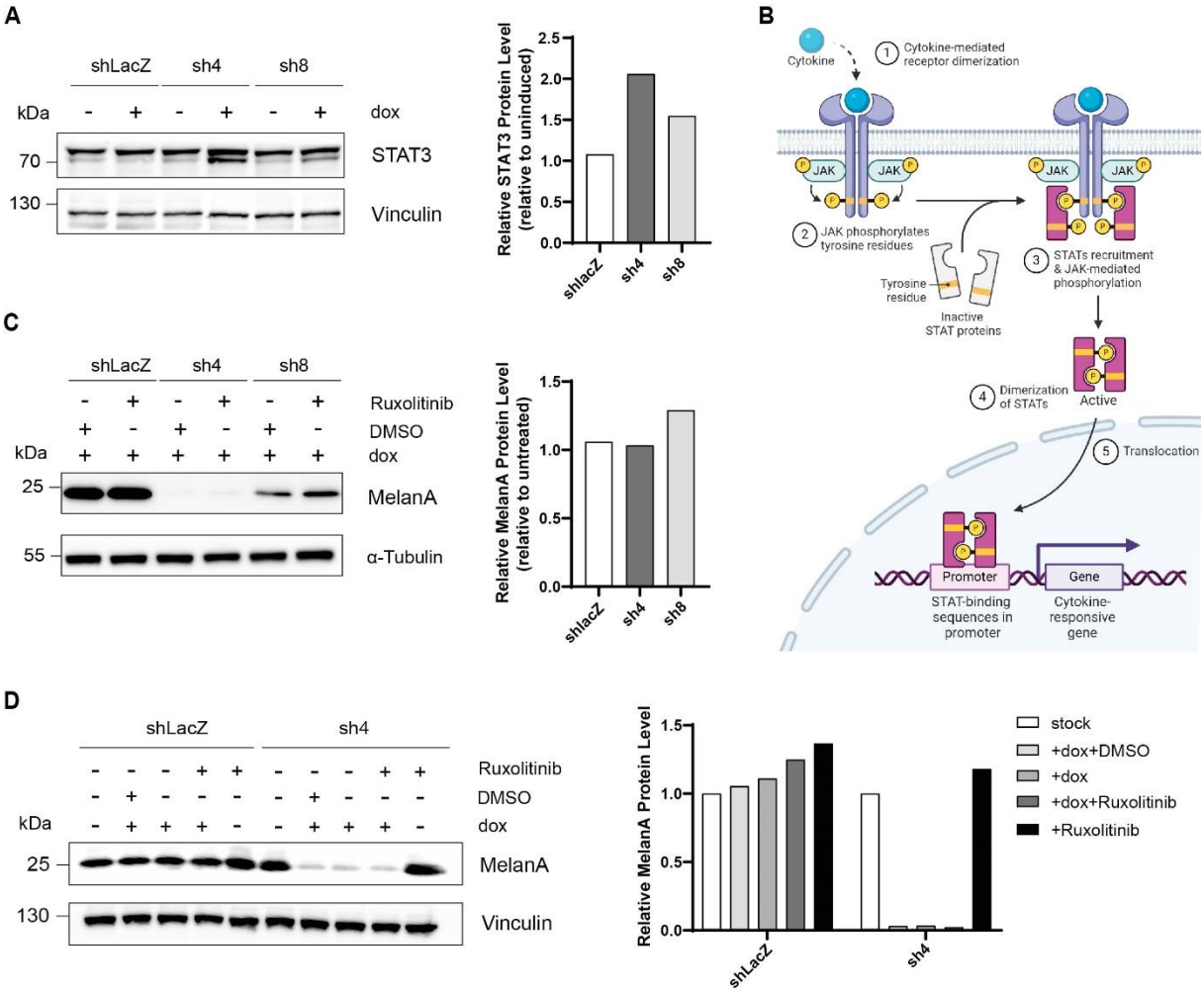

Figure 24: Effect of GRASLND knockdown of JAK-STAT3 signaling. *(A) Detection of STAT3 protein levels after shRNA-mediated GRASLND knockdown in 501-mel cells using Western blot. Stable shRNA GRASLND knockdown and control shRNA 501-mel cells were induced with doxycycline (2 µg/mL) for 72 hours. Western blot was performed using anti-STAT3 antibody. Vinculin served as loading control. Blot of one experiment is shown (left). Relative quantification of STAT3 levels by normalization to the loading control. Data are represented in relation to the uninduced cells for each knockdown cell line (shLacZ, sh4, sh8) (right). (B) Illustration of cytokine signaling through the JAK-STAT pathway. Cytokine binding to their receptor induces its dimerization and subsequent activation of receptor-associated JAK (Janus kinase) enzymes by phosphorylation. Inactive STAT proteins are recruited and activated by JAK-mediated phosphorylation. Phosphorylated STATs dimerizes followed by translocation to the nucleus, where the gene expression of cytokine responsive genes is regulated, affecting diverse immunological functions. Image was created by Ruslan Medzhitov with the help of Akiko Iwasaki and Jung-Hee Lee and was available at Biorender.com. This scheme is published in the 10th Edition of Cellular and Molecular Immunology, Elsevier (2022)[274] (C) Measurement of MelanA levels after shRNA-mediated GRASLND knockdown and treatment with JAK inhibitor Ruxolitinib using Western blotting. Stable shRNA GRASLND knockdown and control 501-mel cells were treated simultaneously with doxycycline (2 µg/mL) and Ruxolitinib (2 µM) for 72 hours. Anti-MelanA antibody was used to detect MelanA protein levels, anti-α-tubulin antibody was used for the loading control. Blot of one experiment is shown (left) and relative quantification (right) is given by normalization to the loading control in relation to the untreated cells of each condition (shLacZ, sh4, sh8). n = 1. (D) Second experiment of MelanA detection after shRNA-mediated GRASLND knockdown and treatment with Ruxolitinib using Western blotting. As performed in (C), stable shRNA GRASLND knockdown (sh4) and control (shLacZ) 501-mel cells were treated simultaneously with doxycycline (2 µg/mL) and Ruxolitinib (2 µM) for 72 hours. Anti-MelanA antibody was used to detect MelanA protein levels, anti-vinculin antibody was used for the loading control. Blot of one experiment is shown (left) and relative quantification (right) is given by normalization to the loading control and in relation to the uninduced and untreated (stock) cells of each condition (shLacZ, sh4). n =1.*

To investigate whether GRASLND has an effect solely on STAT3 or acts upstream of the JAK-STAT3 signaling, GRASLND knockdown experiments in combination with JAK inhibitor ruxolitinib was performed next. Ruxolitinib is a potent and selective Janus kinase 1 (JAK1) and Janus kinase 2 (JAK2) inhibitor and thus inhibits dysregulated JAK signaling[275]. JAK-STAT signaling translates cell external signals from cytokines, such as IFNγ or IL-6, into cell responses by controlling gene expression. Respective receptors undergo cytokine-mediated dimerization, followed by phosphorylation and thus activation of associated JAK enzymes. Subsequent recruitment and phosphorylation of inactive STAT proteins by the JAK enzymes leads to its dimerization and translocation to the nucleus, where gene expression of cytokine responsive genes is controlled (Figure 24B)[274,276]. To test whether GRASLND knockdown-mediated dedifferentiation in 501-mel melanoma cells is due to a general dysregulated JAK-STAT signaling, GRASLND knockdown cells were treated simultaneously with doxycycline and ruxolitinib for 72 hours to induce shRNA expression and inhibit JAK enzymes, respectively. In an initial experiment, the reduction of MelanA levels was observed in both GRASLND knockdown cell lines (sh4, sh8), but not shLacZ cells upon shRNA induction and ruxolitinib was not able to rescue the downregulation of melanoma differentiation (Figure 24C). The potency of ruxolitinib was tested on 501-mel-shLacZ cells, that were treated with IFNγ and the levels of phosphorylated STAT1 (pSTAT1) served as indicator of a functioning JAK-STAT signaling. An explicit reduction in p-STAT1 was detected, confirming a suppression of this pathway by ruxolitinib (Supplementary Figure 43). In a second experiment, the more efficient shRNA sh4 was used and compared to control cells (shLacZ) with the experimental setup remaining consistent with the previous one, however, untreated control cells (stock) were added as additional controls. Detection of MelanA and subsequent relative quantification of the protein levels confirmed the initial results of the inability of JAKi ruxulitinib to prevent melanoma cell dedifferentiation in 501-mel GRASLND knockdown cells (Figure 24D). This indicates that GRASLND does not act upstream of STAT3 on JAK enzymes, but rather seems to have a direct effect on STAT3 expression via a mechanism that requires further investigation. Future studies should thus focus on the validation of the suggested impact of GRASLND knockdown on STAT3 transcription. To evaluate a potential STAT3-mediated dedifferentiation in 501-mel GRASLND knockdown cells, simultaneous STAT3 inhibition using specific small molecule inhibitors or parallel STAT3 knockdown application could be considered.

Altogether, these experiments on key protein levels of suspected dedifferentiation pathways upon GRASLND knockdown, give initial hints on a potential pathway involved in phenotype switch, that is suspected to be STAT3-mediated. Further a PKR/ATF4-ISR-mediated cell state transition mechanism might be excluded based on these preliminary results. However, further and detailed investigation is required to validate these assumptions made in this section.

3.5 Data Mining for Investigation of Immune-Related Effects of GRASLND in Melanoma

LncRNA GRASLND is described to affect the adaptive immune responses by suppressing IFNγ signaling potentially by a direct interaction with PKR as shown in MSCs[233]. Further, GRASLND was identified as an immune-related lncRNA in melanoma based on bioinformatic predictive risk models using patient samples provided in the TCGA-SKCM database[277]. A similar survival prediction model was used for gastric cancer samples, revealing potential immune related effects of GRASLND and suspected it as a negative prognostic factor for response to immune checkpoint inhibitors (ICIs)[245].

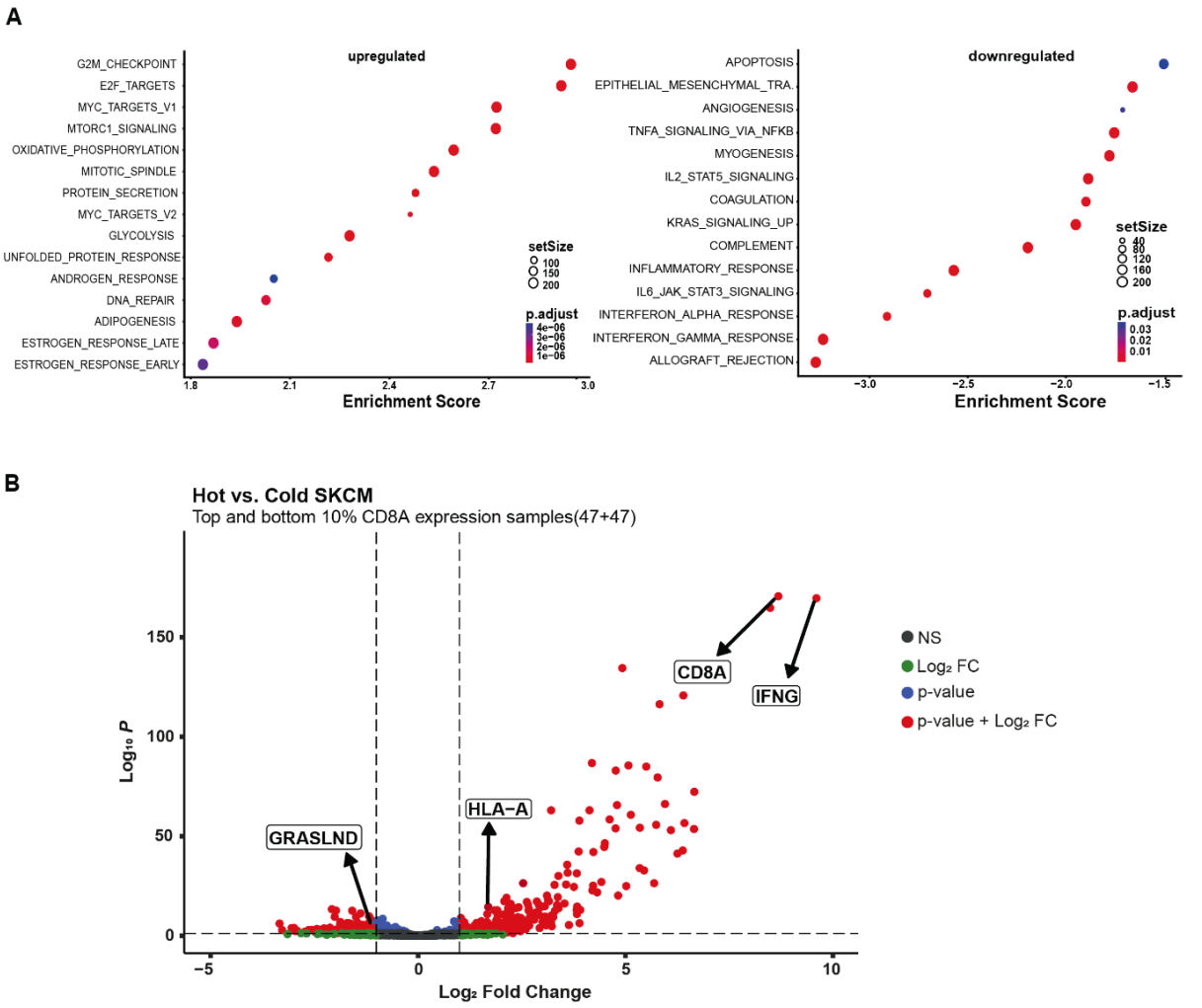

Figure 25: Immune-related role of lncRNA GRASLND. *(A) Gene set enrichment analysis (GSEA) of the GRASLND^{high} subgroup of TCGA-SKCM melanoma patient samples (n = 232) using the Hallmark pathway gene sets. Top 15 upregulated (left) and top 14 downregulated (right) pathways are illustrated. (B) TCGA-SKCM tumor data (n = 471) were grouped in immunological "hot" and "cold" tumors based on the abundance of CD8A transcripts. Volcano plot depicts the fold changes and p values of transcripts in the top and bottom 10% CD8A subgroups as described by Li et al.[185]. Two-sided t-tests for statistical analysis.*

In order to confirm these initial findings on a potential immunoregulatory role of GRASLND in melanoma, bioinformatic analyses using the TCGA-SKCM dataset were performed, realized by Shashank Tiwari, M.Sc. First, TCGA-SKCM tumor data from 471 patients were grouped in GRASLND^{high} and GRASLND^{low} melanoma samples (Supplementary Figure 44). This was followed by a gene set enrichment analysis using the subgroup of 232 GRASLND^{high} melanoma patient samples by utilizing the Hallmark pathway gene sets. Detailed information are given in methods section 5.2.12.3. Top 15 upregulated and top 14 downregulated pathways are illustrated (Figure 25A). Indeed, the top downregulated pathways in GRASLND^{high} melanoma samples include immune pathways, such as IL2-STAT5- and IL6-STAT3-signaling, as well as IFNα-, IFNγ-, and inflammatory responses. Interestingly, the majority of the pathways align with the previously results of the transcriptomic analysis in 501-mel cells upon GRASLND silencing (Figure 20D). Thus, a positive correlation of GRASLND and pathways regulating the cell cycle, such as G2M checkpoint, E2F and MYC targets, as well as a negative correlation with the EMT gene set was found in a large patient cohort, supporting the previous findings on GRASLND's involvement in melanoma phenotype switching.

In addition, all tumor data from the TCGA-SKCM data set (n = 471 patients) were grouped in immunological "hot" and "cold" tumors based on CD8A transcript abundance, that served as an indicator of the infiltration of CD8+ T lymphocytes into the tumor[278]. The analysis was performed as described by Li *et al.*[185] and as outlined in section 5.2.12.3. The transcripts in the top and bottom 10% of CD8A transcript expression groups (47 samples each) are represented, revealing the presence of GRASLND in immunological "cold" tumors (Figure 25B).

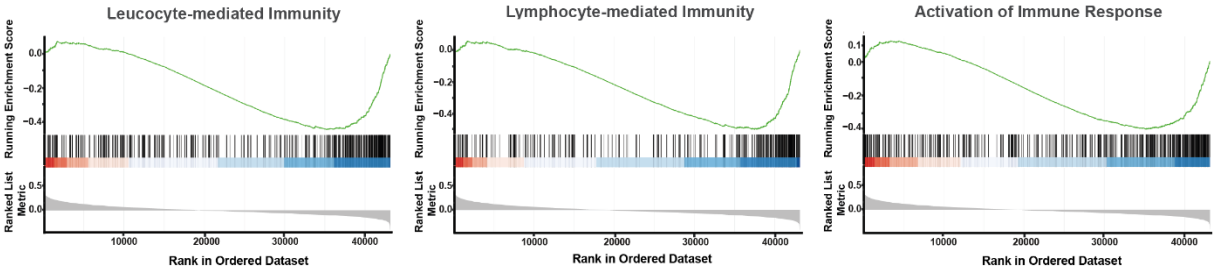

Figure 26: Single GSEA on GRASLND^{high} subgroup of the TCGA-SKCM data (n = 232) set on immune-related gene sets. *Genes involved in leucocyte- and lymphocyte mediated immunity, as well as the activation of immune response were analyzed. Green curve depict the running sum of the enrichment scores. Bars illustrate the gene position within the specific pathways. The distribution of the fold change along with the list of genes is depicted in the bottom part.*

Lastly, single gene set enrichment analysis was performed on the GRASLND^{high} melanoma patient subgroup (n = 232 samples) with the gene sets of leucocyte-mediated immunity, lymphocyte-mediated immunity and the activation of immune response (Figure 26). These GSEA results demonstrate an inverse association between GRASLND and gene expression profiles linked to these pro-inflammatory cellular processes.

Overall, these bioinformatic analyses of the TCGA-SKCM data set in regards to immune-related effects, indicate GRASLND's immune-regulatory role in melanoma and that high GRASLND expression might

support immune escape mechanisms of melanoma tumors. The recently published data by Ma *et al.* on GRASLND in melanoma, validate our findings on a negative correlation between GRASLND expression and CD8+ T lymphocyte infiltration[248].

3.6 Experimental Analysis of GRASLND's Impact on IFNγ Signaling

3.6.1 Transcriptomic Analysis of IFNγ-stimulated Genes (ISGs) upon GRASLND Knockdown under IFNγ

Based on the bioinformatic analysis conducted (Figure 25, Figure 26) and supported by findings from other studies, GRASLND showed a negative correlation with the immune response and cytotoxic CD8+ T cell infiltration in melanoma[248,277]. Additionally, as GRASLND appears to suppress the crucial immune pathway of IFNγ in MSCs, further experimental investigation into its role in modulating IFNγ signaling in melanoma is a clear next step. In MSCs, the inhibition of the JAK-STAT1-IFNγ pathway was suspected to be mediated by PKR, which may be activated by GRASLND and in turn repress STAT1 transcriptional activity[233]. A direct interaction between GRASLND and PKR in melanoma cell line 501-mel was previously validated (Figure 21, Supplementary Figure 38), which makes an inhibitory effect on IFNγ signaling in the melanoma context conceivable. In this case, GRASLND silencing would be expected to result in an overall upregulation of IFNγ-stimulated genes (ISGs) under IFNγ treatment. To test this, a transcriptomic analysis of GRASLND knockdown cells under IFNγ exposition was performed. 501-mel shRNA GRASLND knockdown (sh4, sh8) and control cells (shLacZ) were treated either with IFNγ alone or were induced with doxycycline for shRNA expression in addition to IFNγ treatment. Two independent biological replicates for each cell line (shLacZ, sh4, sh8) and condition (IFNγ, IFNγ + doxycycline) were taken. After six days of continuous treatment, RNA sequencing analysis was conducted as described in method section 5.2.9 and analysis was carried out by Shashank Tiwari, M.Sc. The PCA plot reveals distinct clustering of both, control cells compared to GRASLND knockdown cells, but also IFNγ-treated cells compared to IFNγ-treated and doxycycline-induced cells, clarifying 77% variance on PC1. The replicates, however, are grouped closely, reflecting consistency within each sample group (Supplementary Figure 45A). Differential expression analysis of IFNγ-treated versus IFNγ-treated plus doxycycline-induced cells was performed, revealing a significant up- and downregulation ($p < 0.05$) of a high number of genes for the GRASLND knockdown cells, but a comparatively very low number in the control cells (Supplementary Figure 45B,C). For this analysis, both GRASLND knockdown cell lines (sh4 and sh8) were combined and treated as four replicates. Strikingly, among the significantly upregulated genes, HLA genes (B2M, HLA-B, HLA-C) were found, known to be stimulated by IFNγ[279–281]. To assess, whether additional ISGs are upregulated upon GRASLND downregulation, a selective differential expression analysis for ISGs was carried out. Indeed, a significantly increased expression ($p < 0.05$) of multiple ISGs was observed in GRASLND knockdown samples and not the control samples (Figure 27A, Supplementary Figure 46). ISGs associated with CD8+ T cell recognition and inhibition (B2M and CD274/PD-L1)[106,282], immune cell recruitment (CXCL9, CXCL11)[283,284], the immunoproteasome

(PSMB8, PSMB9)[285] and the antigen processing and presenting machinery (TAP1, TAPBP)[286] were identified.

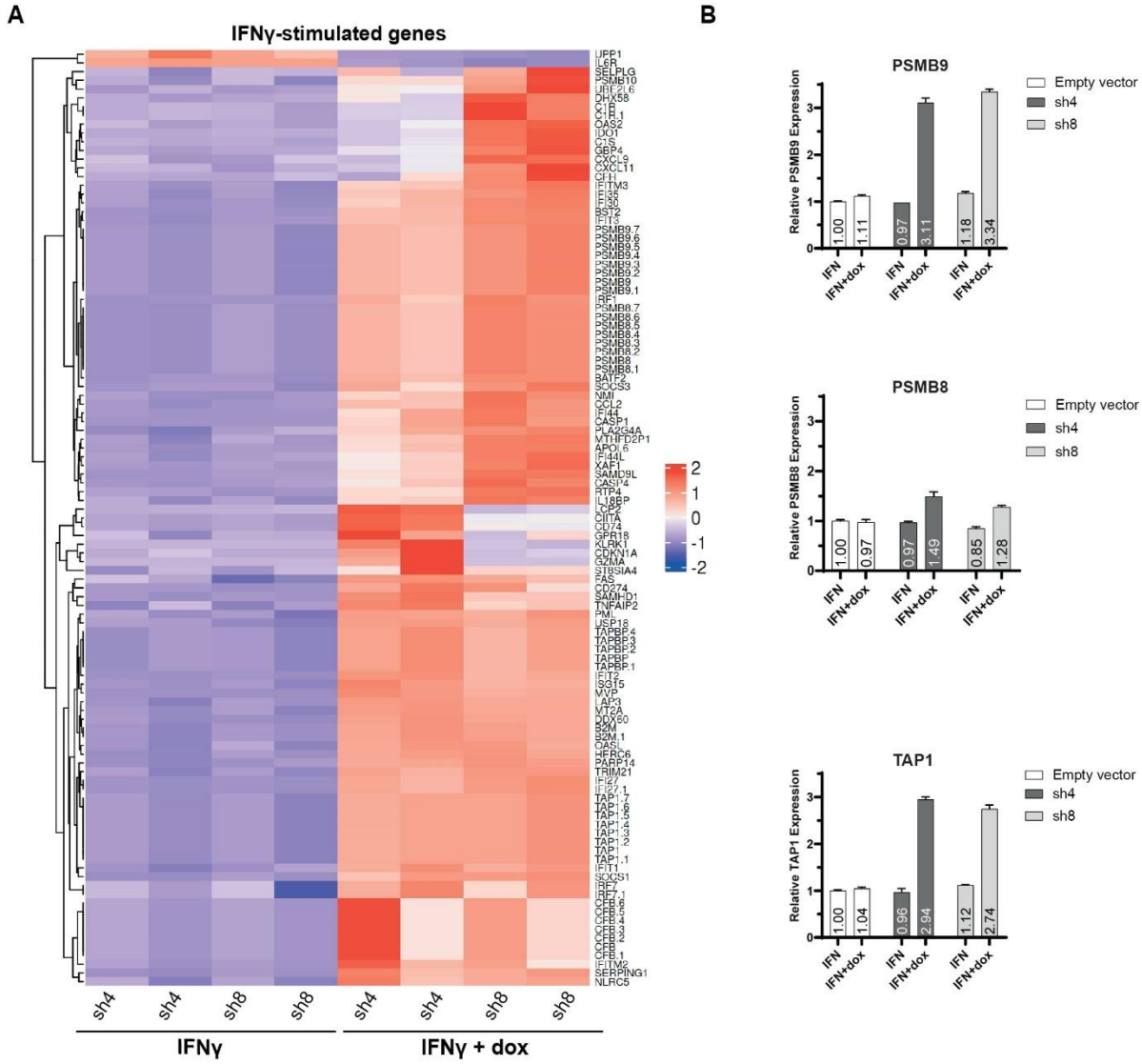

Figure 27: Upregulation of IFNγ-stimulated genes (ISGs) upon GRASLND knockdown under IFNγ. *(A) Heatmap of differentially expressed ISGs after GRASLND knockdown under IFNγ. 501-mel shRNA GRASLND knockdown and control cells were treated with either IFNγ (500 U/mL) alone or in combination with doxycycline (2 µg/mL) for six days and subjected to RNA-seq. (B) Relative RNA expression of ISG examples PSMB9, PSMB8 and TAP1 after GRASLND knockdown under IFNγ treatment. 501-mel shRNA GRASLND knockdown and empty vector control cells were treated with either IFNγ (500 U/mL) alone or simultaneously with doxycycline (2 µg/mL) for three days and mRNA levels were determined using RT-qPCR after normalization to GAPDH mRNA levels. Data are given as mean ± SD from n = 3 technical replicates.*

To validate the findings of the transcriptomic analysis, the experiment was repeated and three ISG examples were chosen to be tested using RT-qPCR. 501-mel shRNA GRASLND knockdown and empty vector control cells were treated with IFNγ alone or with IFNγ and doxycycline for three days. The expression of all three ISGs was upregulated after GRASLND knockdown and not in the control cells treated with doxycycline. The relative expression of PSMB9 and TAP1 mRNA showed a fold change of about 3.2 and 2.8, respectively, using both shRNAs sh4 and sh8. A modest increase in mRNA levels, with a fold change of approximately 1.5, was observed for the immunoproteasome gene PSMB8,

following knockdown with both GRASLND-targeting shRNAs and not the empty vector control (Figure 27B). These findings suggests a suppressive effect of this lncRNA on the IFNγ signaling also in melanoma as previously described in MSCs[233].

3.6.2 Evaluation of HLA I Protein Levels via Flow Cytometry After GRASLND Knockdown under IFNγ

The overall upregulation of ISGs on the mRNA levels indicates an inhibitory effect of GRASLND on the IFNγ pathway and in turn a potential relevance on the HLA-I-mediated antigen processing and presentation to cytotoxic CD8+ T lymphocytes. Given that HLA-I is the essential molecule for the recognition of malignant cells by CD8+ T cells and downregulation of HLA-I by tumor cells is a major immune evasion mechanism, the impact of GRASLND silencing on the HLA-I surface expression was of particular interest[68]. Therefore, in an initial experiment, 501-mel GRASLND knockdown and empty vector control cells were treated with either IFNγ alone or simultaneously with doxycycline to induce shRNA expression, and HLA-I surface protein expression was determined at two timepoints by flow cytometry (method section 5.2.8). After treatment of the cells for three days, IFNγ-exposed cells with concurrent GRASLND knockdown showed an increase in HLA-I levels by 1.38-fold and 1.70-fold relative to the respective uninduced cells, when using sh4 and sh8, respectively, which was not observed in the control cells (Figure 28A, C). With seven days of treatment, an even more pronounced upregulation of HLA-I surface expression was detected (Figure 28B). An elevation of HLA-I protein expression by 3.16-fold using sh4 and 2.52-fold with sh8 in relation to the respective uninduced cells was measured (Figure 28C). To verify successful and efficient GRASLND knockdown, a fraction of the cell suspension used for flow cytometry measurements was allocated for RT-qPCR, confirming a downregulation of lncRNA levels in both GRASLND knockdown cell lines after both, three and seven days of treatment (Figure 28D).

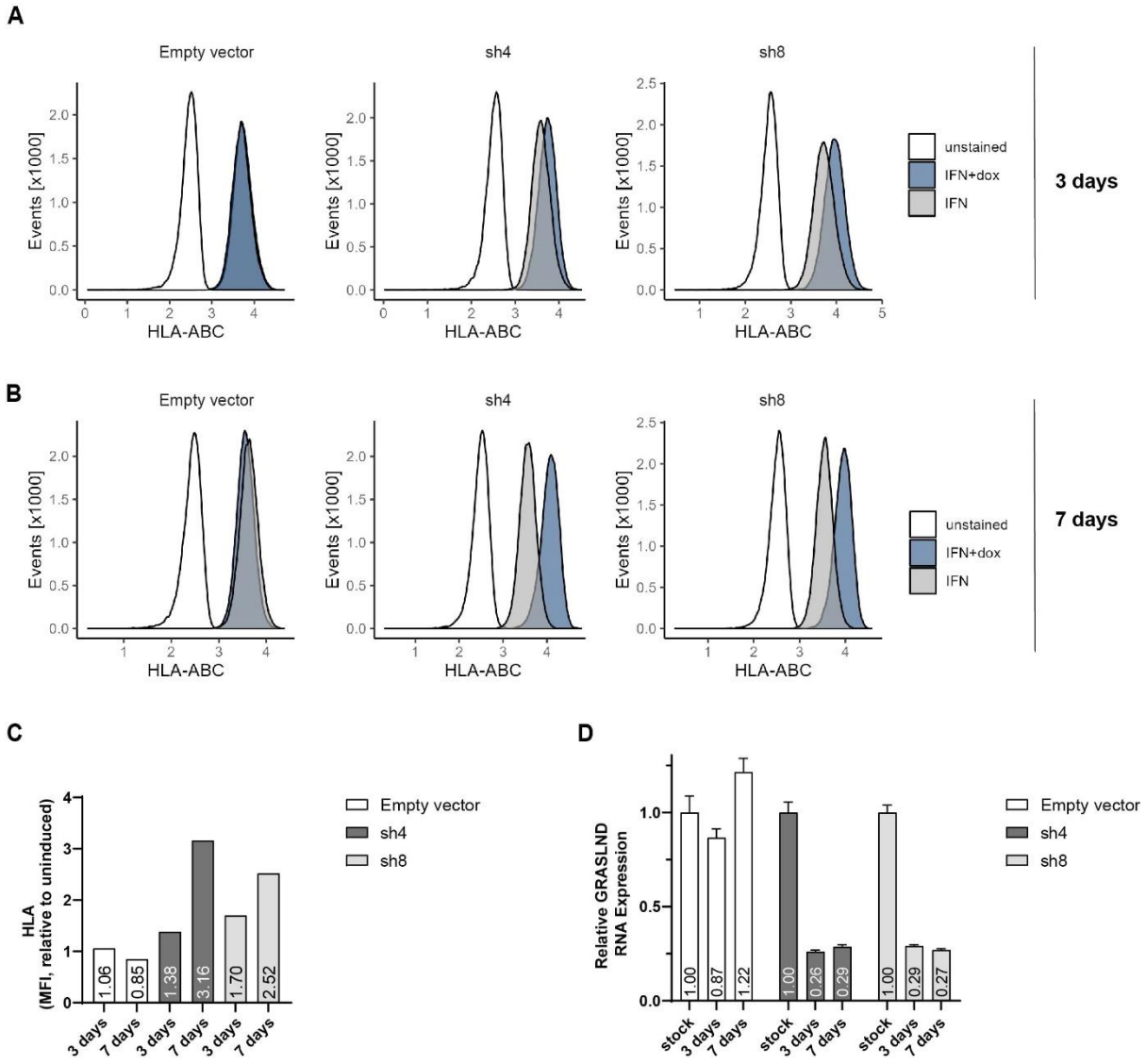

Figure 28: HLA-I surface expression after GRASLND knockdown and under IFNγ treatment in melanoma cell lines 501-mel at different time points*. (A) HLA-I surface expression in 501-mel cells determined by flow cytometry. 501-mel shRNA GRASLND knockdown and empty vector control cells were treated either with only IFNγ (500 U/mL) or simultaneously with doxycycline (2 µg/mL) to induce shRNA expression for three days. Histograms of control and GRASLND knockdown cell lines from one experiment is shown (n = 1). (B) HLA-I surface expression in 501-mel cells analyzed by flow cytometry. 501-mel shRNA GRASLND knockdown and empty vector control cells were treated either with IFNγ (500 U/mL) alone or simultaneously with doxycycline (2 µg/mL) to induce shRNA expression for seven days. Histograms of control and GRASLND knockdown cell lines from one experiment is shown (n = 1). (C) Fold change of MFI of IFNγ-only to IFNγ+dox-treated 501-mel shRNA knockdown cells. Both experiments with timepoints of three or seven days treatment are represented. (D) Relative GRASLND RNA levels after induction with doxycycline (2 µg/mL) for three and seven days determined by RT-qPCR. A fraction of the cell suspension used for flow cytometry measurements was allocated for RT-qPCR analysis to determine GRASLND levels. Data are represented as mean ± SD (n = 3 technical replicates).*

Based on these preliminary results, indicating a marked upregulation of HLA-I surface expression after IFNγ treatment and doxycycline induction for a duration of seven days, three independent biological replicates were performed with the same experimental design, but replacing the empty vector control with the non-targeting shRNA control (shLacZ). The initial findings could be confirmed, as GRASLND downregulation in IFNγ-treated 501-mel cells significantly enhanced HLA-I surface expression by 2.36-fold (± SD = 0.48) and 2.78-fold (± SD = 0.26) when using each of the shRNAs (Figure 29A,B). Exactly

as for 501-mel, HLA-I surface expression was measured in IFNγ-treated Ma-Mel-86c cells after GRASLND knockdown for six days. A total of four independent biological replicates were performed. Two of these replicates were carried out by Lin Christina Qiu, B.Sc. as part of her Bachelor thesis under my supervision[257]. Likewise, the findings in 501-mel, an upregulation of HLA-I levels was detected in Ma-Mel-86c by 1.90 (±SD = 0.48)- and 1.41 (± SD = 0.41)-fold (Figure 29C, D). For testing a third melanoma cell line, differentiated Ma-Mel-61a cells, which exhibit lower GRASLND levels compared to 501-mel and Ma-Mel-86c cells, were selected (Figure 10A, B). Five independent biological replicates were carried out, revealing slightly but not significantly increased HLA-I levels in the GRASLND knockdown cells with fold changes of 1.47 (± SD = 0.34) and 1.35 (± SD = 0.31), compared to their respective uninduced cells. Increased HLA-I levels were observed in four out of five replicates for sh4 and only three out of five replicates for sh8 (Figure 29E, F).

Taken together, these experimental data of GRASLND downregulation under IFNγ treatment in different melanoma cell lines indicate a suppressive role of this lncRNA on IFNγ signaling, as an upregulation of multiple IFNγ-stimulated genes was observed. Importantly, HLA-I surface expression is positively affected by GRASLND silencing. As downregulation of the HLA-I molecule is a key mechanism to evade cytotoxic CD8+ T cell recognition, these results point towards an immune escape strategy of melanoma cells by overexpression of GRASLND[68].

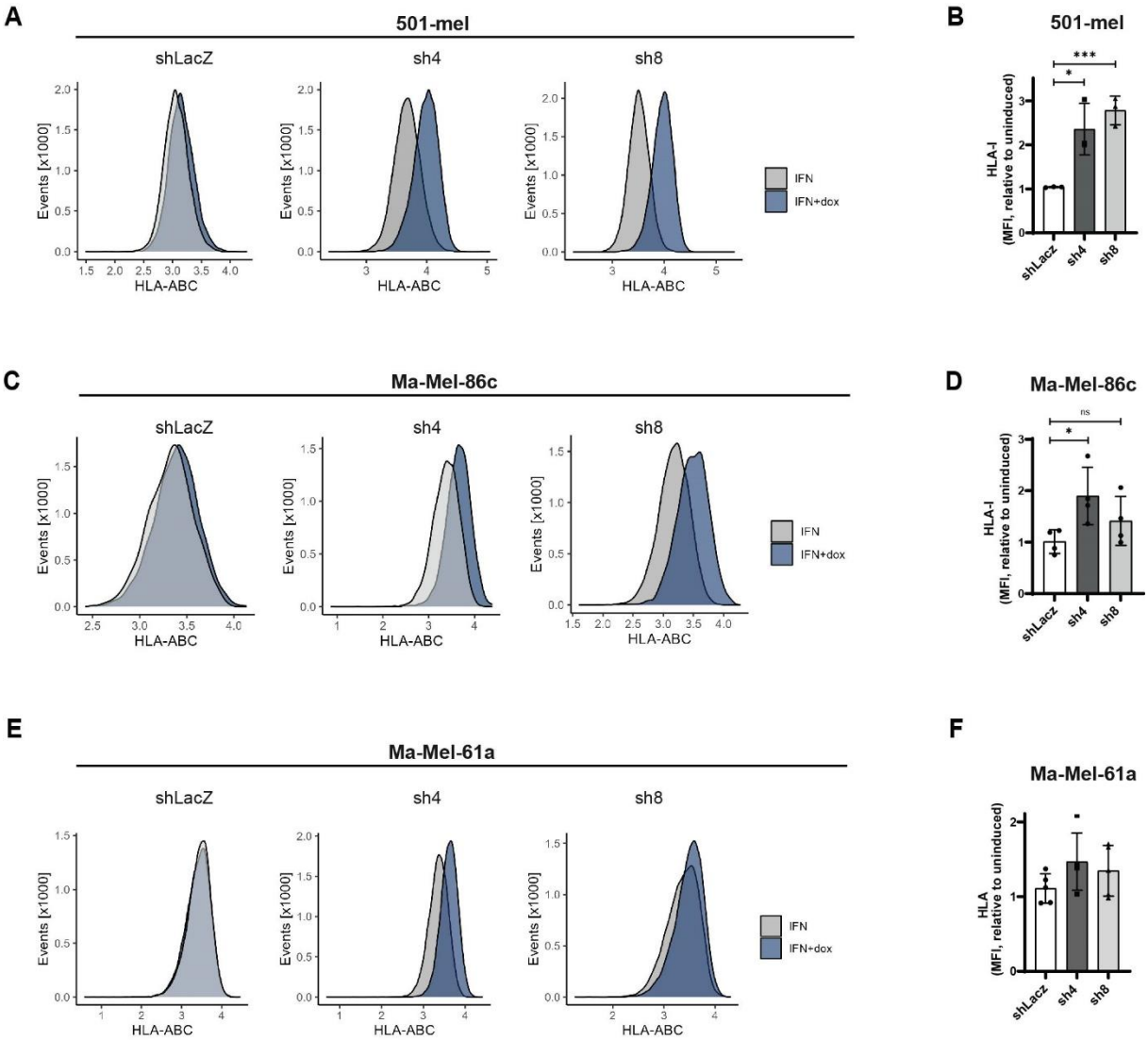

Figure 29: HLA-I surface expression after GRASLND knockdown and under IFNγ treatment in melanoma cell lines 501-mel, Ma-Mel-86c and Ma-Mel61a by flow cytometry. *(A) HLA-I surface expression in 501-mel cells analyzed by flow cytometry. 501-mel shRNA GRASLND knockdown and non-targeting shRNA control cells were treated either with only IFNγ (500 U/mL) or simultaneously with doxycycline (2 µg/mL) to induce shRNA expression for seven days. Representative histograms of GRASLND knockdown and shLacZ control cell lines are shown from independent biological replicates (n = 3). (B) Fold change of MFI of IFNγ-only to IFNγ+dox-treated cells given as mean ± SD in 501-mel cells. (C) HLA-I surface expression in Ma-Mel-86c cells measured by flow cytometry. Ma-Mel-86c shRNA GRASLND knockdown and non-targeting shRNA control cells were treated for six days either with IFNγ (500 U/mL) alone or simultaneously with doxycycline (2 µg/mL) to induce shRNA expression. Representative histograms of GRASLND knockdown and shLacZ control cell lines from four independent biological replicates (n = 4) are shown. (D) Fold change of MFI of IFNγ-only to IFNγ+dox-treated cells given as mean ± SD in Ma-Mel-86c cells. (E) HLA-I surface expression in Ma-Mel-61a cells analyzed by flow cytometry. Ma-Mel-61a shRNA GRASLND knockdown and non-targeting shRNA control cells were treated for six days either with only IFNγ (50 U/mL) or simultaneously with doxycycline (2 µg/mL) to induce shRNA expression. Representative histograms of GRASLND knockdown and shLacZ control cell lines from five independent biological replicates (n = 5) are illustrated. (F) Fold change of MFI of IFNγ-only to IFNγ+dox-treated cells given as mean ± SD in Ma-Mel-61a cells.*

3.6.3 T Cell Activation Experiment

As the previous findings indicate the inhibitory effect of GRASLND on the IFNγ pathway and its silencing caused an upregulated ISGs mRNA levels and HLA-I surface protein expression, a diminished recognition of CTLs towards those melanoma cells could be suspected. Thus, a CD8+ T cell activation experiment using autologous T cells in collaboration with the lab of Prof. Dr. Annette Paschen (UKE, Department of Dermatology) was initiated, which was performed by Dr. Beatrice Thier (Paschen Lab, UKE, Department of Dermatology). The cell lines provided by the Paschen lab included Ma-Mel-86c and Ma-Mel-61a, both of which have corresponding autologous T cells available from the patients. Although a significant and stronger HLA-I upregulation was found in Ma-Mel-86c- compared to Ma-Mel-61a-GRASLND knockdown cells (Figure 29C-F), the T cell co culture experiment was performed with Ma-Mel-61a cells. The decisive factor for this decision is the observation that autologous T cells from patient Ma-Mel-61 are documented to still trigger a T cell activation despite total dedifferentiation, probably through recognition of other antigens than the lost MDAs[287]. This is particularly relevant because GRASLND knockdown results in a dedifferentiation, suggesting a loss of antigen presentation of these differentiation markers (Figure 15).

For the conduction of the T cell activation assay, cryo-conserved tumor-reactive bulk CD8+ T lymphocytes from peripheral blood of patient Ma-Mel-61 were used. These were co-cultured with treated autologous Ma-Mel-61a cells and T cell activation by tumor cells was analyzed based on IFNγ secretion, as described in methods section 5.2.14. Before co-culturing with T cells, Ma-Mel-61a-sh4 and -shLacZ control cells were treated with IFNγ and doxycycline for six days as performed earlier (Figure 29E,F). On day 7, the cells were harvested and thoroughly washed to remove any residual IFNγ from the treatment. After four hours of co-culture with autologous T cells, their activation by GRASLND knockdown and control Ma-Mel-61a cells was evaluated by intracellular IFNγ staining using flow cytometry. Two independent experiments were conducted revealing that treatment of the tumor cells with IFNγ alone already results in a strong T cell activation in both, control and GRASLND knockdown cells (Figure 30A, B). An additional enhancing effect on T cell activation due to GRASLND downregulation is therefore hardly detectable. While the first experiment suggests a minor effect (Figure 30A), this is not validated in the second replicate (Supplementary Figure 47, Figure 30C).

In sum, this initial experiment does not provide conclusive evidence regarding an altered T cell recognition and activation due to GRASLND silencing, and further optimization of the assay is required.

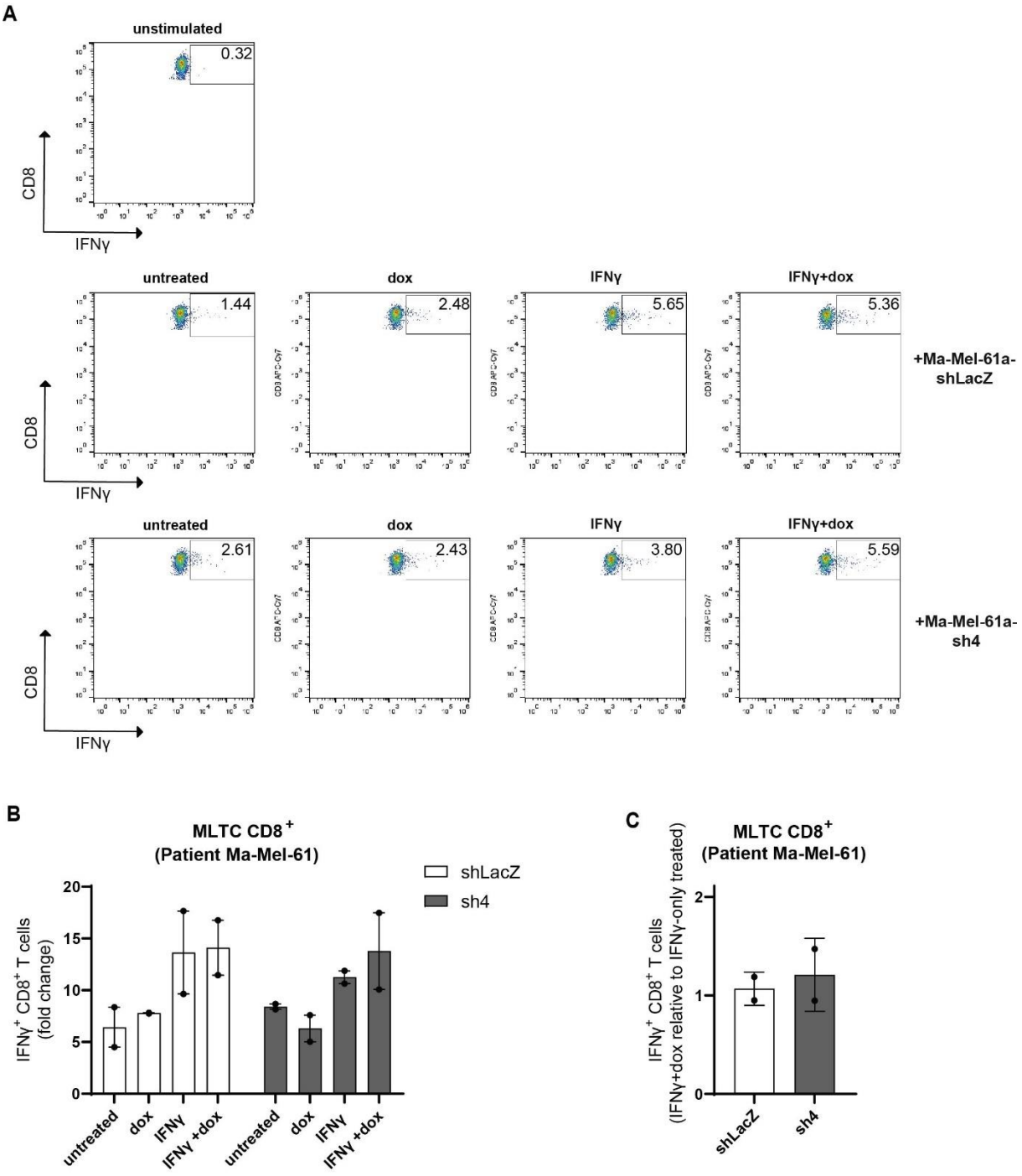

Figure 30: T cell activation assay. *(A) Activation of autologous CD8+ T cells by Ma-Mel-61a cells was analyzed by intracellular IFNγ staining using flow cytometry. Ma-Mel-61a shRNA GRASLND knockdown (sh4) and non-targeting shRNA control cells (shLacZ) were treated for six days either with doxycycline (2 µg/mL), IFNγ (50 U/mL) or simultaneously with IFNγ and doxycycline. Control cells were left untreated. Unstimulated T cells served as control and were used for normalization. Representative dot plots from one experiment out of n = 2 biological replicates are shown. (B) Quantification of IFNγ+ CD8+ T cells. Normalized to unstimulated T cells and fold change given as mean ± SEM from two independent biological replicates. (C) IFNγ+ CD8+ T cells fold changes of IFNγ-only to IFNγ+dox treated Ma-Mel-61a GRASLND knockdown and control cells given as mean ± SEM from two independent experiments (n = 2). MLTC = Mixed Lymphocyte Tumor Cell Culture.*

4. Discussion, Conclusion and Outlook

4.1 Discussion

Over the past years, a relevance of lncRNAs in key hallmarks of melanoma biology has attracted substantial attention, with research uncovering oncogenic and tumor suppressive roles, or their function as biomarkers for diagnostic and prognostic indications, demonstrating their clinical significance in melanoma. By serving as miRNA decoys, scaffolds or regulators of transcription, mRNA stability and translation, lncRNAs exert considerable impacts on critical aspects of melanoma development and progression, including cell proliferation, invasion/metastasis, metabolism, immune escape and drug resistance[131,172]. The continued identification and detailed characterization of additional lncRNAs with functional contributions to melanomagenesis thus remains subject of significant interest to further pave the way for the development of strategies for therapeutic interventions or diagnostic methods for improved melanoma disease management.

Following this reasoning, the objective of this thesis was to investigate lncRNA GRASLND for its potential influence in melanoma biology. This lncRNA has previously been identified as a key regulator of chondrogenesis in MSCs, functioning by inhibiting the IFNγ-JAK-STAT signaling pathway[233]. Acknowledged for its regulation of bone development, homeostasis and its inhibition of chondrocyte proliferation in the musculoskeletal system, the IFNγ signaling is a pivotal immune pathway, with an intact signal transduction being substantial for the responsiveness to immunotherapy[235–237,288]. Beyond its impact on cartilage production in MSCs, GRASLND has been the subject of multiple recent studies investigating its potential role in cancer[289]. On the basis of bioinformatic risk modelling and survival analysis using clinical data, high GRASLND levels has been linked to poor patient prognosis in several cancers, including osteosarcoma, head and neck squamous cell carcinoma, papillary renal cell carcinoma, glioblastoma, bladder cancer, and gastric cancer[238–245]. In glioma, bladder, and gastric cancer, functional studies revealed a driving effect of GRASLND on tumor cell proliferation, migration and invasion through distinct miRNA decoy mechanisms[243,244,246]. An influence of GRASLND on these tumor-promoting functions were further demonstrated in two newly published studies in melanoma from 2024, identifying an RBP-dependent mechanism in the YAP1 pathway and a miRNA decoy function targeting the adaptor molecule STAM2, respectively[247,248]. With knowledge of GRASLND's oncogenic functions in other cancer types, this thesis focused on exploring its functions and relevance in melanoma pathogenesis, focusing on pro-tumorigenic effects and a potential interaction with the IFNγ signaling.

As a first step, the expression of GRASLND was meta-analyzed using skin cutaneous melanoma (SKCM) patient data provided by TCGA program. Compared to healthy skin samples, significantly higher GRASLND expression levels were determined in melanoma samples. Dividing the SKCM-TCGA patient data in GRASLND-high and -low subgroups with subsequent Kaplan-Meier survival analysis revealed a significant association with a lower overall patient survival. Both analyses point towards a potential contribution of GRASLND to the pathological processes underlying melanoma development or progression.

Since the cell differentiation state of melanoma cells play a pivotal role in dictating tumor behavior, particularly its aggressiveness and responsiveness to targeted or immunotherapy, a potential relationship of GRASLND abundance and the melanoma cell state was examined[44,56,57]. Indeed, a positive correlation between GRASLND levels and the expression of melanocytic markers was found, indicating a cell state-dependency for GRASLND abundance in melanoma.

To gain deeper insights into GRASLND's role in melanoma, comprehensive knockdown studies were conducted. These experiments aimed to elucidate a potential contribution of GRASLND on key processes in melanoma, such as proliferation, invasion and differentiation using a shRNA-mediated lncRNA knockdown strategy. Two highly efficient GRASLND-shRNAs and a control shRNA targeting the bacterial lacZ gene were validated and these cell lines were used in further experiments. Firstly, the effect of GRASLND downregulation on cell growth and viability was evaluated. Live cell imaging of both 501-mel GRASLND shRNA knockdown cell lines treated with doxycycline revealed a decrease in cellular growth in response to downregulation of GRASLND, while apoptotic cell death was not induced, as suggested by a PARP1 cleavage assay. Moreover, there were no indications of cell death during cell handling, as the cells consistently remained adherent even after shRNA induction for more than seven days with no detachment observed. Since the transcriptomic analysis following GRASLND knockdown revealed a downregulation of the cell cycle regulating cyclin-dependent kinases CDK1 and CDK4, a cell growth arrest mediated by GRASLND depletion appears plausible. A validation and detailed insights into the underlying process explaining the reduced cell growth could be assessed by a flow cytometry-based cell cycle distribution assay[290]. In a subsequent *in vitro* Transwell invasion assay, the effect of GRASLND knockdown on the invasive potential of 501-mel cells was assessed. Indeed, an increased invasion capacity was observed using both shRNAs, pointing to a role of this lncRNA in modulating the ability of melanoma cells to invade. These observations of a GRASLND knockdown-induced transition toward a slow-proliferating and highly invasive melanoma phenotype, led to the hypothesis that this transition is associated with phenotype switching driven by dedifferentiation accompanied by the loss of melanocytic differentiation markers. The suspected process of an EMT-like phenotype switch of melanoma cells, originally proposed by Hoek *et al*. and confirmed in further studies, describes a reversible transcriptional reprogramming of a melanocytic, $MITF^{high}$ cell state, characterized by a high proliferation rate and low invasive capability, toward a slow-growing and highly invasive, $MITF^{low}$ cell state[44,45,58]. Thus, MITF protein levels and those of its target gene MelanA following GRASLND knockdown, were evaluated. As expected, the abundance of both melanocytic markers was significantly reduced upon knockdown in 501-mel and an additional differentiated cell line Ma-Mel-86c. Together, these findings suggest that GRASLND downregulation triggers phenotype switching, supporting the notion of a regulatory role of this lncRNA in melanoma plasticity.

A comparison of these findings with two recently published studies on GRASLND in melanoma revealed inconsistencies in the observed phenotypes. GRASLND knockdown performed by Yang and colleagues showed an inhibitory effect of this lncRNA on the tumor-promoting processes proliferation, migration, invasion and the EMT capabilities of melanoma cells[247]. Likewise, a downregulation of GRASLND was found to suppress cell migration and invasion in the second melanoma study[248]. Thus, both studies ultimately propose GRASLND as a promising therapeutic target for melanoma treatment by highlighting

its role in tumor progression. Although the reported impact of GRASLND downregulation on melanoma cell proliferation are consistent with the results described in this work, the discrepancy in its influence on melanoma cell invasion is striking. While our results showed that GRASLND knockdown increased the invasion capacity in a differentiated melanoma model cell line, Yang *et al*., as well as Ma *et al*. reported a suppression of cell migration and invasion upon lncRNA silencing[247,248]. The differing phenotypes with respect to melanoma cell invasiveness may result from the distinct cell states of the melanoma models used. In my study, the focus was on differentiated melanoma cell lines, as a positive correlation of GRASLND levels with the differentiated melanoma phenotype was indicated. In contrast, the other studies used SK-MEL-28, A375 and A2058. While the differentiation status of A2058 is unknown, the other two melanoma cell lines SK-MEL-28 and A375 can be classified into the intermediate and neural-crest-like cell state, respectively[60]. In line with the literature, a phenotype switch characterized by the loss of the melanocytic marker MITF, is associated with the transition of highly proliferative, lowly invasive cells to a slow-growing, highly invasive melanoma cell behavior[44,45]. As this process cannot be directly applied to melanoma cells with an intermediate or neural crest-like cell state, these findings on different effects of GRASLND silencing on the invasion capability of melanoma cells of different cell states, are not contradictory. This rather highlights the significance to consider different cellular context and the multifunctional nature of many lncRNAs in experimental investigations[117].

For validation of the GRASLND silencing-induced melanoma phenotype switching, an additional knockdown strategy was employed. Firstly, a commercially provided siRNA pool containing four GRASLND-targeting siRNAs was tested for efficient knockdown capacities in differentiated melanoma cell lines 501-mel and Ma-Mel-86c. For both cell lines transfection with the siRNA pool resulted in a maximum knockdown by 41% and thus further phenotype evaluations on dedifferentiation, cell proliferation, and invasion were not performed. As a second alternative and orthogonal approach for lncRNA knockdown besides shRNAs, CRISPRi was used. Initially evaluated in melanoma cell line Ma-Mel-86c as part of the master thesis work, none of the four tested sgRNAs resulted in any sufficient downregulation of the lncRNA[249]. Nonetheless, the CRISPRi system was applied in 501-mel cells, as a 501-mel-dCas9-KRAB cell line was provided and lentiviral particles for the introduction of the four sgRNAs were available from previous experiments. In 501-mel cells, CRISPRi resulted in substantial GRASLND knockdown efficiencies of 68% and 62% with the most effective sgRNAs, contrasting the results observed in Ma-Mel-86c cells. Unexpectantly, the expression of the melanocytic marker MelanA remained unchanged in this experimental setup, even though knockdown efficiencies were similar to the GRASLND downregulation achieved by shRNA sh4 and sh8. Thus, potential factors contributing to this discrepancy are addressed in the subsequent part of the discussion.

First, the observed phenotype of melanoma dedifferentiation can be induced by off-target effects of both shRNAs as a result of partial pairing to non-intended transcripts. However, a third shRNA with similar knockdown efficiency was tested and confirmed the effect of MelanA downregulation. All three shRNAs targeting GRASLND lncRNA result in a consistent melanoma dedifferentiation across multiple independent biological replicates. This strongly suggests that this phenotype is linked specifically to GRASLND's function, also due to a high correlation of knockdown efficiency and the extent of MelanA loss. In contrast, off-target effects of each individual shRNA would be expected to lead to more variable

phenotypes between different shRNAs, as they are unlikely to consistently impact the same pathways in the same manner.

Second, the CRISPRi technology requires the robust expression of the large dCas9-KRAB-mCherry fusion protein, along with GFP co-expressed with the sgRNAs. Such high demand of cellular resources to express recombinant proteins imposes a significant metabolic burden to the host organism, which may cause cellular stress-induced physiological alterations, such as limited viability and ER stress, as reported in bacterial and mammalian cells[291–293]. In bacterial *E. coli* cells, high dCas9 expression in the absence of gRNAs caused changes in cell morphology and impaired cell division[294]. Although the effects of dCas9 in bacteria cannot necessarily be directly applied to mammalian cell lines, significant physiological changes caused by dCas9 also in human cells cannot be ruled out. This is supported by the findings that the expression of a dCas9 cassette, including a non-targeting gRNA, induced a transient acute stress response in human HEK239T cells, characterized by the activation of genes related to the regulation of cells death, defense response and transcriptional stress[295]. The discrepancy of the lacking melanoma dedifferentiation in CRISPRi-mediated GRASLND knockdown cells might be explained by unexpected cellular alterations caused by the introduction of the recombinant dCas9-KRAB-mCherry and/or GFP protein.

Third and most notably, the usage of the CRISPR/Cas9 technology for targeting lncRNAs is reported to be restricted to lncRNAs whose promoters do not overlap with or are not located in close proximity (< 2 kb) to promoters of neighboring genes and are otherwise termed as being “non-CRISPRable”[224]. Review of the genomic loci of antisense lncRNA GRASLND and its sense gene RNF144A shows that their promoters are positioned less than 2 kb apart, so that CRISPR-dCas9-mediated GRASLND knockdown is expected to additionally simultaneously impact RNF144A expression. This co-regulation of the sense gene with CRISPRi was indicated experimentally. Frequently, antisense lncRNAs regulate their corresponding sense genes and act in the same cellular pathways. Several lncRNAs function by stabilizing its sense gene’s mRNA through direct binding, the recruitment of stabilizing proteins, or by acting as miRNA sponges for sense trancripts[124,261]. RNF144A is an E3 ligase essential in DNA damage repair (DDR) by ubiquitination of DNA-dependent protein kinase, catalytic subunit (DNA-PKcs), promoting its degradation and triggering apoptosis in extensively DNA damaged cells[296]. An immune-related role is suspected, as bioinformatic correlation analysis revealed a correlation of RNF144A levels with immune cell infiltration, including cytotoxic CD8+ T cells, in severe acute pancreatitis[297]. Additionally, it enhances DNA virus- or exogenous cytosolic DNA-induced antiviral immune responses by ubiquitination of stimulator of interferon genes (STING) protein, causing the upregulation of IFNβ, CXCL10, CXCL5 and IL-6[298]. As GRASLND and RNF144A are both implicated in the DNA damage repair pathway and have documented immune-related roles, a regulatory function of GRASLND or a mutual regulatory interplay of this sense-antisense pair is plausible. Unintentional CRISPRi-mediated co-regulation of RNF144A, while desired GRASLND targeting, could counteract the observed phenotypes. Thus, a potential explanation for the lacking dedifferentiation in melanoma cell line 501-mel following CRISPRi-mediated GRASLND knockdown could involve a compensatory mechanism by RNF144A. This hypothesis could be tested by simultaneous transient overexpression of RNF144A and evaluating its impact on MelanA expression levels.

Considering this limitation of co-affecting the sense gene RNF144A, the usage of the CRISPRi technology for GRASLND knockdown experiments is unsuitable. The primary benefit of the used doxycycline-inducible shRNA system in these studies were the integrated internal control groups by parallel handling of uninduced control cells under identical conditions. Therefore, the observed phenotypes can be directly attributed to shRNA expression, eliminating potential confounding effects that lentiviral transduction might have on the cells. This is one of the main advantages of the shRNA system over the CRISPRi strategy, which uses sgRNA introduction in a non-inducible manner. Thus, utilizing the inducible shRNA system to target lncRNA GRASLND represents the most optimal approach.

For the identification of cellular functions affected by GRASLND, transcriptomic analysis after shRNA-mediated GRASLND knockdown was performed. Differential gene expression was profiled and subsequent gene set enrichment analysis highlighted the influenced pathways. Supporting the experimentally observed EMT-like phenotype switch from differentiated, highly proliferative melanoma cells to slow-growing, highly invasive, and dedifferentiated cells upon GRASLND downregulation, the epithelial-to-mesenchymal transition (EMT) is ranked among the top three most upregulated gene sets. This process is accompanied with cellular changes including alterations in cell adhesion, matrix-degrading enzymes, invasive potential and proliferation[46]. This is further validated, as an inhibitory effect of GRASLND silencing on cell proliferation is reflected in the most downregulated gene sets, several of which are essential for cell cycle regulation, such as G2M checkpoint, E2F, and MYC targets. Review of genes involved in these gene sets, demonstrates the downregulation of both key cell cycle-regulating enzymes CDK1 and CDK4[262]. A closer look at the affected signaling pathways reveals that some are well-documented in the literature to induce the phenotypic switch in melanoma[299]. These include JAK-STAT3-, TNFα-, and WNT-signaling, observed among the top16 enriched pathways for upregulated genes and their key regulators, namely STAT3, NFKB2, and LEF1, also showing increased expression[263–265]. However, a more detailed literature research led to the assumption that the canonical Wnt-signaling could be excluded to induce melanoma dedifferentiation, as the upregulated LEF1 mRNA, found after GRASLND knockdown, is reported to be associated with the differentiated melanoma cell state[265]. On the other hand, increased levels of STAT3 are associated with driving melanoma metastasis in a CEPB-mediated manner by repressing the MITF pathway, as reported in *in vivo* studies[263]. In addition to the upregulation of STAT3 mRNA levels observed in the RNA-seq results, increased STAT3 levels were confirmed on the protein levels. This implies that phenotype switching in 501-mel cells in response to GRASLND downregulation could involve a STAT3-mediated mechanism. Moreover, TGFB1 and SMAD3, main components of the TGF-β1/SMAD signaling, were found to be significantly upregulated, a pathway implicated in the promotion of EMT and cancer metastasis[300–302]. Interestingly, GRASLND was identified as an TGF-β1-inducible gene in gastric cancer[244]. Overall, the transcriptomic analysis of GRASLND knockdown in 501-mel cells provides evidence for the involvement of this lncRNA in regulating melanoma differentiation and points to several potential key pathways that may contribute to this process. A complex interaction of multiple of these pathways leading to a phenotype switching can also be assumed, since the multifunctionality of lncRNAs may be applicable for GRASLND[117,303].

With the elucidation of relevant pathways of GRASLND's function, identifying its protein interactome becomes a pivotal step in further characterization of its biological role and to gain potential insights into

underlying mechanisms. In MSCs, GRASLND was determined to bind to interferon-induced, double-stranded RNA-activated protein kinase R (PKR)[233]. This interaction was validated in the melanoma cell line 501-mel through targeted lncRNA pulldown followed by PKR verification using immunoblotting. However, lncRNAs can have multiple protein binding partners, allowing the participation in complex regulatory networks essential for various cellular functions[304,305]. Due to this multifaceted interaction capability, the identification of additional GRASLND binding partners besides PKR was pursued using proteomics-based targeted GRASLND pulldown. Contrary to expectations, PKR was not determined as statistically enriched following analysis of the proteomics data from targeted GRASLND pulldown. In-depth re-analysis revealed the detection of solely one “unique” PKR peptide in all four replicates in all samples “control”, “odd” and “even” (Supplementary Figure 41). For the analysis of the proteomics data, filters were applied, involving the exclusion of proteins identified by fewer than two “razor+unique” peptides, explaining the absence of PKR enrichment. This proteomics-based GRASLND pulldown experiment, however, does not contradict the earlier results that identified PKR as its binding partner. PKR is simply not detectable under the used experimental conditions. For optimization of the experimental setup regarding a detection of PKR in the following mass spectrometry data, increasing the input amount could be considered. Since a limited proteome is analyzed in an enrichment/pulldown experiment, enhanced protein input might lead to the desired finding of PKR. Additionally, multiplexing with TMT labeling would be a good optimization strategy to enhance protein depth, allowing for the detection of more peptides and potentially enabling the identification of PKR with at least two "razor+unique" peptides[306,307]. The same could be achieved by the use of an additional protease with complementary cleavage specificities, such as GluC, alongside the tandem LysC/Trypsin digestion. This may enhance protein sequence coverage, thereby increasing the number of identified unique peptides[308,309].

Nevertheless, analysis of the proteomics data identified five proteins, namely RBM45, XRCC5 and 6, RBMS1 and DHX36, as significantly enriched in both GRASLND pulldown probe sets. This suggests a likely genuine interaction, though further validation is required to confirm these findings. RBM45 is a multifunctional RNA-binding protein (RBP) that interacts with various RBPs forming a complex protein-protein network and participates in numerous cellular processes, such as RNA splicing and translation[310]. Its relevance in cancer is rather unexplored, however, it has been reported in HCC and breast cancer, where it exerts tumor-promoting effects through the BCL2/Twist2-axis or IFNβ, respectively[311,312]. Further, RBM45 is implicated in DNA damage repair (DDR)[313]. Also involved in the process of DDR are the proteins XRCC5 and XRCC6 (also named Ku80 and Ku70), which form a heterodimer and are pivotal for the repair of double strand breaks (DSBs) through the NHEJ pathway, contributing to genome stability and telomere maintenance. Consequently, deficiencies in XRCC5 and XRCC6 can result in genomic instability, thereby increasing the risk of cancer development[314–316]. This evidence for an involvement of GRASLND in DNA repair mechanisms is supported by the results of the transcriptional analysis in response to GRASLND knockdown in 501-mel cells, revealing DNA repair and UV response are among the top 15 most enriched pathways for downregulated genes. With RBMS1 another multifaceted RBP of the RBM family was identified as a GRASLND binding partner. Similar to RBM45, its primary function is post-transcriptional regulation of mRNA stability through direct binding of 3’ UTR’s of a large regulon of mRNAs, observed in the context of colon cancer[317,318]. Interestingly, in

triple negative breast cancer it was reported, that the mRNA stability of the PD-L1 glycosyltransferase B4GALT1 is controlled by RBMS1. A reduction in RBMS1 levels resulted in a suppressed glycosylation of PD-L1, which in turn facilitates its ubiquitination and subsequent degradation. As a consequence of RBMS1 depletion, an increased infiltration of CD8+ T cell and a CTL-mediated anti-tumor immunity was observed *in vitro* and *in vivo*[319]. Further, RBMS1 has been described to drive metastasis in gastric cancer trough transactivation of IL-6 and activation of downstream JAK2-STAT3 signaling, a pathway validated to be also affected by GRASLND knockdown in 501-mel cells[320]. This finding may support the aforementioned proposed STAT3-mediated mechanism of phenotype switching in differentiated melanoma and highlights RBMS1 as a potential additional regulator in this process. The fifth significantly enriched protein found in both GRASLND pulldown samples “odd” and “even” is the ATP-dependent RNA helicase DHX36. Primarily known for its capability to interact with G-quadruplex (G4) structures in DNA and RNA to enable transcriptional regulation and translation control, DHX36 has been reported to physically interact with PKR in a dsRNA-dependent manner to facilitate PKR activation and initiation of innate immunity in response to viral infection[321–323]. The exact mechanism by which GRASLND interacts with these enzymes, remains unclear. It is yet to determined, whether GRASLND might functions as a scaffold, facilitating the interaction between the proteins or acts as a dsRNA mimic to promote DHX36-mediated activation of PKR.

However, since PKR and its binding partner DHX36 are both indicated to interact with GRASLND, PKR downstream signaling known as the integrated stress response (ISR) was further investigated. The PKR-ISR pathway is activated by cellular stresses including viral infections, enhancing the innate immune response by promoting the production of type I interferons and inflammatory cytokines[324]. The key step of the ISR is the phosphorylation of eIF2α by PKR, leading to the widespread inhibition of Cap-dependent translation to prevent viral protein synthesis, but permitting selective translation of ISR-associated mRNAs, such as those of the pathway’s central effector, ATF4[268]. In the context of melanoma differentiation, ATF4 has been reported to transcriptionally repress MITF and an ATF4-mediated feedback loop has been described to sustain the dedifferentiated, MITF^{low} cell state[51,272]. However, experimental data indicated the downregulation of PKR and ATF4 in response to GRASLND knockdown in 501-mel cells. Another downstream target in the PKR signaling, namely the NF-κB family member p65, showed decreased levels of its activated (phosphorylated) form after GRASLND silencing. This suggests that an ISR/PKR/ATF4-dependent mechanism of dedifferentiation observed in 501-mel cells following GRASLND downregulation is unlikely, however, a general PKR involvement in the mechanism of the phenotype switch cannot be ruled out, as shown by the regulation of its protein levels.

As previously mentioned, a STAT3-mediated mechanism inducing the phenotype switch in GRASLND downregulated melanoma cells is suspected. This is based on the observation that IL-6-STAT3 signaling was identified as the fourth most upregulated pathway in the RNA-Seq analysis conducted after GRASLND downregulation and the validation of increased STAT3 protein levels in GRASLND knockdown cells. Together with reported studies demonstrating the antagonistic relationship between STAT3 and MITF, combined with the metastasis-promoting effects of STAT3 in melanoma, an involvement of STAT3 in melanoma phenotype switching after GRASLND knockdown appears conceivable[263,325]. Further literature research revealed STAT3 being a direct interaction partner of PKR

and is thought to function as a competitive inhibitor of the kinase and thus the PKR-mediated ISR[273,326]. Potentially, this interface and the inhibitory function of STAT3 can be translated to the melanoma context. GRASLND knockdown results in an upregulation of STAT3 levels while reducing PKR and ATF4 expression. This raises the hypothesis that GRASLND may regulate PKR activity and thereby modulating STAT3 signaling. Alternatively, STAT3 may influence the expression and activity of PKR. Future studies should prioritize validating the proposed STAT3-mediated dedifferentiation in 501-mel GRASLND knockdown cells potentially through simultaneous STAT3 inhibition using specific small-molecule inhibitors or by employing parallel STAT3 knockdown strategies.

In sum, combining all the experimental data of the transcriptomic analysis revealing affected pathways by GRASLND silencing, the proteomics analysis indicating protein binding partners and analyzing STAT3 protein abundance as well as key components of the PKR pathway, led to a hypothesized complex lncRNA-protein network, potentially including GRASLND, RBMS1, PKR, DHX36 and STAT3 to directly or indirectly influence melanoma dedifferentiation. Thus, this study serves as a solid starting point for further experimental investigations that should aim to uncover the functional mechanisms of GRASLND on melanoma phenotype switching and other processes, including DNA damage repair.

Prior research recognized GRASLND's potential immune-associated function in gastric cancer through bioinformatic prognostic models, indicating it as a part of an immune-related lncRNA (IRL) signature that predicts the effectiveness of immune checkpoint inhibitors (ICIs). This signature is found to be negatively correlated with the infiltration of immune cells including CD8+ T cells and T follicular helper cells, suggesting an influence of GRASLND in the immune microenvironment of gastric cancer[245]. Similarly, an immune-related lncRNAs (immlncRNAs) prognostic risk score model of 46 lncRNAs including GRASLND was constructed by applying melanoma patient samples from the TCGA-SKCM database. These immlncRNAs were linked to multiple immune response signaling pathways, highlighting their potential importance in the immune regulation of melanoma[277]. To validate these initial findings of a potential immunoregulatory role of GRASLND in melanoma, additional bioinformatic analyses of the TCGA-SKCM database were conducted in this thesis. Indeed, gene set enrichment analysis of GRASLND^{high} tumor samples (n = 232) revealed an inverse correlation between this lncRNA and immune response gene signatures, including those involved in inflammation, IFNα-, IFNγ-, IL2-STAT5- and IL6-STAT3-signaling. Additional single-gene set enrichment analysis of the gene sets "leucocyte-mediated immunity", "lymphocyte-mediated immunity" and "activation of immune response" further emphasize this negative relationship. In accordance with this, GRASLND was found to be enriched in immunologically "cold" tumors, which are described to be associated with low immune infiltration and reduced response to ICIs[278]. The studies by Aiwei Ma and colleagues, published in the meantime of this thesis, validates the negative correlation of GRASLND and CD8+ T lymphocyte infiltration[248]. Overall, these bioinformatic data mining results indicate that GRASLND holds immune-regulatory significance in melanoma and propose a role for GRASLND overexpression in immune escape mechanisms. The link between GRASLND overexpression and unfavorable clinical outcomes can thus be explained by its negative impact on tumor immunosurveillance, rather than a metastasis-promoting effect as GRASLND was found to be correlated with the differentiated, highly-proliferative but lowly invasive melanoma cell state.

To explore the immunoregulatory effects of GRASLND in more detail, the previously reported interaction and suppressive effect of GRASLND on the JAK-STAT-IFNγ signaling pathway in MSCs was considered and investigated for a comparable mechanism in melanoma. The inhibition is facilitated through direct binding and potential activation of PKR, which is suspected to suppress transcriptional activity of STAT1[233]. On the basis of our findings of an upregulation of various ISGs observed in response to GRASLND downregulation under IFNγ treatment analyzed by transcriptomic analysis and an increase in HLA-I surface expression, a suppressive impact on IFNγ response also in melanoma was indicated. Mechanistically, PKR associates with STAT1, an interaction that is independent of kinase-substrate binding and PKR's catalytic activity, but depends on its dsRNA-binding domain. This PKR-STAT1 complex is thought to repress STAT1-DNA binding, thereby inhibiting transcriptional activity and its dissociation is suggested to be initiated by IFNγ-induced STAT1 activation[327,328]. Considering published evidence in MSCs[233] and the experimental findings in 501-mel melanoma cells, it can be hypothesized that GRASLND might have a stabilizing effect on the PKR/STAT1 complex during active IFNγ signaling. As a result, GRASLND downregulation causes complex dissociation accompanied by the release of active STAT1 to fulfill further transcription of ISGs (Figure 31). It remains to be elucidated whether GRASLND serves as a mediator of the STAT1-PKR interaction or whether its binding to PKR induces a conformational change that enables the STAT1 interaction in this context.

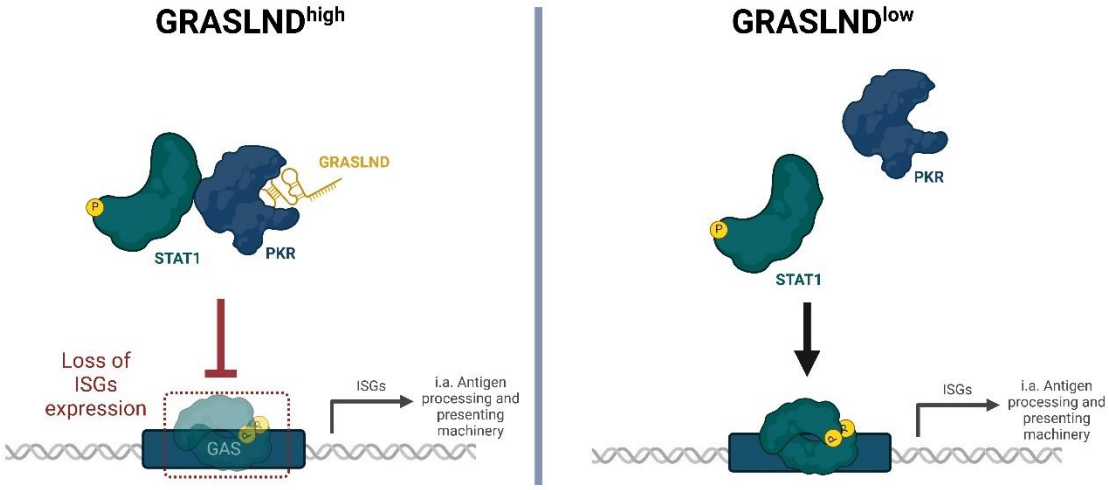

Figure 31: Hypothesized model of GRASLND's stabilizing effect on the PKR-STAT1 complex. *Despite ongoing IFNγ signaling, the PKR-STAT1 complex is stabilized by GRASLND binding, thus inhibiting STAT1 transcriptional activity by preventing its DNA binding capability (left). Downregulation of GRASLND results in dissociation of the complex, releasing active STAT1 for further gene expression of ISGs (right).*

GRASLND knockdown-induced increase of ISGs expression under IFNγ indicates a negative effect of this lncRNA on melanoma HLA-I antigen presentation and thus immunogenicity. A complete loss or downregulation of HLA-I surface expression or other deficiencies impacting the antigen processing and presenting machinery are described as a strategy of tumors to escape immunosurveillance. In addition to the complete loss of HLA-I-APM components due to mutations, downregulation of antigen presentation through epigenetic mechanisms or defects in IFNγ signaling, such as loss-of-function

mutations in JAK1 or JAK2 genes, are frequently observed in melanoma. These alterations are associated with resistance to immunotherapy, especially ICI treatment, by enabling the evasion of CTL recognition[68,329]. Through its direct impact on the key pathway for HLA-I mediated antigen presentation, GRASLND overexpression, as observed in melanoma and correlated with poor clinical outcomes, may indicate an adaptive resistance mechanisms that allows for evasion of CTL-mediated tumor surveillance. This is further supported by the observation that GRASLND is enriched in immunologically "cold" tumors. Uncovering novel immune escape mechanisms are of highest clinical importance to address and overcome resistances to ICI treatment. Although comprehensive research on lncRNAs involved in immunotherapy resistance is still limited, several studies have reported lncRNAs with regulatory functions in immune checkpoints[330]. To name a few, LINC00473 and PCED1B-AS1 regulate PD-L1, while CECR7 modulates CTLA-4 expression via distinct miRNA sponging mechanisms[331–333]. Besides lncRNAs directly impacting ICIs and thereby promoting resistance to this therapy, other lncRNAs are described to indirectly affect ICI responsiveness by regulating HLA-I antigen presentation and thus antitumor immunity. For instance, the IFNγ-stimulated lncRNA LIMIT enhances tumor immunogenicity in melanoma by activating the HLA-I machinery via guanylate-binding protein (GBP) and heat shock factor-1 (HSF1)[185]. This work on GRASLND introduces another lncRNA that may indirectly affect immunogenicity in melanoma by inhibiting IFNγ signaling, resulting in decreased levels of HLA-I surface proteins. Accordingly, future studies should address, whether this also results in an increased recognition by CTLs. An initial CD8+ T cell co-culture experiment using autologous T cells of patient Ma-Mel-61 was performed. However, with this preliminary experiment no conclusive results were obtained. Since this assay involved the treatment of cells with IFNγ, the T cells were activated primarily due to the treatment itself and a potential promoting effect of GRASLND on T cell activation might be overshadowed by the robust, IFNγ-induced T cell activation. Thus, further assay adjustments are required.

Based on the data presented in this work, it appears conceivable that GRASLND could be considered as a potential therapeutic target. However, the therapeutic potential of targeting GRASLND solely lies in its ability to restore HLA-I-mediated antigen presentation and therapeutic intervention should counteract its inhibitory effect on IFNγ signaling. This is because a general downregulation of GRASLND in differentiated melanoma cells led to phenotype switching towards the dedifferentiated cell state that is prone to metastasize and linked to resistance to immunosurveillance and immunotherapy[56,57]. Accordingly, a GRASLND targeting strategy needs to differentiate between the observed phenotypes and specifically address the immunoregulatory, IFNγ-suppressing effects of GRASLND, while preserving its differentiated cell state. To achieve this, underlying molecular mechanisms regarding phenotype switching but also detailed mechanistic information regarding the GRASLND-PKR interaction or those with other protein binding partners have to be resolved completely.

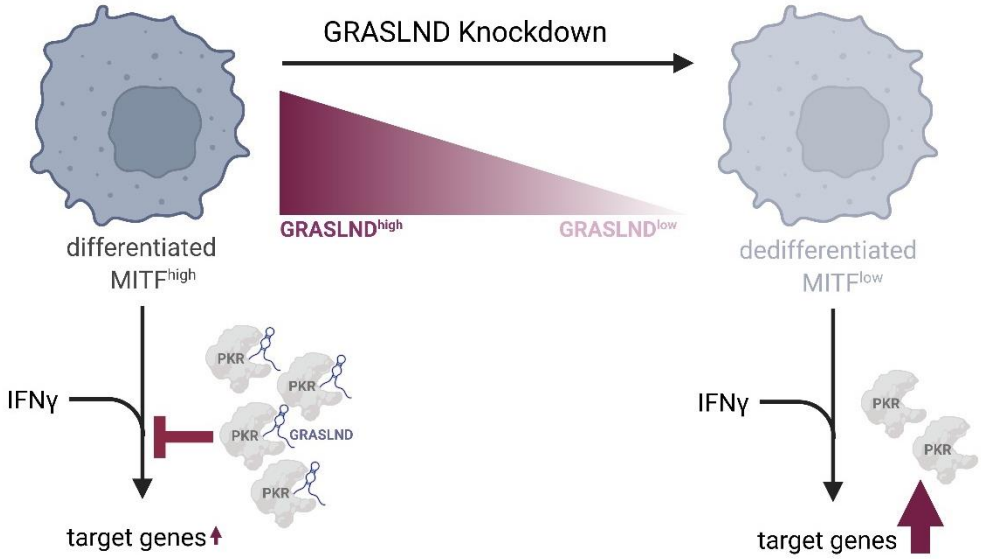

Figure 32: Proposed model of GRASLND's function in melanoma. *LncRNA GRASLND is associated with the differentiated, MITF^{high} melanoma phenotype. Melanomas with low overall GRASLND show a dedifferentiated, MITF^{low} cell state. GRASLND downregulation in differentiated melanoma cells results in their dedifferentiation, accompanied with higher invasion potential, lower cell proliferation and reduced levels of PKR. In addition, high GRASLND abundance is associated with a suppressive effect on the expression IFNγ-target genes by PKR-mediated prevention of STAT1-DNA binding. In contrast, knockdown of GRASLND results in an elevation of the expression of ISGs, indicating an adaptive immune escape strategy of melanoma cells by overexpressing lncRNA GRASLND.*

4.2 Conclusion

In conclusion, this study demonstrated a significance of lncRNA GRASLND in melanoma biology by revealing its overexpression in differentiated melanomas, its association with poor clinical outcome and enrichment in immunologically "cold" tumors. GRASLND downregulation revealed its potential to suppress the invasive melanoma phenotype switching of differentiated, melanocytic melanoma cells towards the dedifferentiated cell state, a process characterized by reduced anti-tumor immunity and immunotherapy responsiveness[56,57]. Initial hints for potential pathways by which GRASLND regulates this dedifferentiation were proposed based on transcriptional analysis upon lncRNA knockdown with subsequent differential gene analysis and GSEA, and proteomics-based GRASLND pulldown to identify its protein binding partners. Together with closer analysis of effects of its silencing on PKR and STAT3 pathway components, the involvement of STAT3 in dedifferentiation was suspected. An immunoregulatory function of GRASLND was indicated by bioinformatic data mining of a large melanoma patient cohort revealing a negative correlation of high GRASLND levels with CD8+ T lymphocyte infiltration and gene signatures of pro-inflammatory processes. Experimentally, this immune-relevant role was confirmed by observing an upregulation of ISGs expression, including HLA-I surface expression upon GRASLND knockdown under IFNγ, indicating an inhibitory effect on the IFNγ-JAK-STAT signaling (Figure 32). Thereupon, GRASLND was hypothesized as an immune-related lncRNA contributing to an immune evasion strategy of melanoma cells towards CTL surveillance, positioning it as a promising prognostic biomarker.

4.3 Outlook

Future perspectives on GRASLND in the melanoma context should focus on uncovering the exact underlying pathway and mechanism(s), by which GRASLND facilitates melanoma dedifferentiation. Considering the potential role of STAT3 in this phenotype, future STAT3 knockdown or inhibitor experiments should be performed to confirm or rule out its influence as a contributing transcription factor to phenotype switching. The same approach can be applied to other key components of different signaling pathways, with a particular focus on the top enriched pathways identified in RNA-Seq analysis of up- and downregulated gene sets. These include several pathways that have been previously described in the literature as drivers of the melanoma phenotype switch. In the case of a more complex interplay of GRASLND across multiple dedifferentiation pathways, combinations of inhibitors and/or genetic manipulations targeting multiple pathways can also be tested. Attention can also be directed towards the potential protein binding partners identified through mass spectrometry following GRASLND pulldown. In regard to the validated GRASLND-PKR interaction in melanoma cell line 501-mel and the proposed PKR-STAT1-complex-stabilizing effect of GRASLND, in-depth mechanistic analysis is needed to verify this hypothesis. Suggested methods to further investigate this lncRNA-protein interaction involves CLIP-seq that can be employed to study genome-wide RBP–RNA binding at single base-pair resolution, thereby uncovering the specific binding site of GRASLND that interacts with PKR[334]. Either mutagenesis of this binding sites or GRASLND knockdown in combination with immunoprecipitation-based PKR-STAT1 formation studies as previously reported by Wong *et al*., may reveal a stabilizing effect of GRASLND on this complex[327]. Moreover, the unexpected downregulation of PKR protein expression following GRASLND knockdown warrants further studies. An initial step to determine whether GRASLND regulates PKR protein expression at the transcriptomic level could be addressed by measuring PKR mRNA levels in GRASLND knockdown cells, as a reduction in PKR transcript levels would indicate a direct transcriptional regulation. If this is the case, a PKR promoter activity assay using a luciferase reporter vector could be performed for validation[335]. To examine potential post-transcriptional regulation of GRASLND on PKR expression, mRNA stability assays could be conducted, for example, using actinomycin D to inhibit transcription in combination with GRASLND knockdown[336]. Another regulatory mechanism to consider is the impact of GRASLND on PKR protein stability, such as through facilitating ubiquitin-mediated degradation that could be evaluated using an immunoprecipitation (IP)-based ubiquitination assay[337]. Nevertheless, indirect effects of GRASLND via upstream regulators of PKR are also possible.

The suppressive effect of GRASLND on IFNγ signaling, observed by upregulation of ISGs expression upon lncRNA knockdown under IFNγ point towards an impaired recognition of melanoma cells towards CTLs that can be further addressed. The T cell activation experiments performed in the Paschen Lab using melanoma cell model Ma-Mel-61a failed to yield definitive evidence of an altered T cell recognition and activation in response to GRASLND silencing, which is a prerequisite for a potential future therapeutic application. Further optimization of the experimental setup is necessary, with a focus on titrating IFNγ to determine the minimal concentration that still allows for significant upregulation of HLA-I. This may help avoid strong T cell activation solely from IFNγ treatment and prevent the potential

masking of any effects on T cell activation induced by GRASLND downregulation. Additionally, different melanoma cell models with available autologous T cells from other patients could be employed, but must first be assessed for a high GRASLND expression and their potential for a GRASLND knockdown-mediated upregulation of HLA-APM under IFNγ. Thereby, it is crucial to ensure that a cell model is chosen in which the recognition and activation of the respective autologous T cells depend on antigens other than the differentiation antigens that are lost due to the phenotypic switch in response to GRASLND downregulation, as described for Ma-Mel-61a.

An alternative strategy to investigate T cell recognition and activation, besides the use of autologous T cells could involve the employment of specifically engineered CAR T cells. These CAR T cells would be designed to target epitopes that remain unaffected or are upregulated under GRASLND knockdown conditions, as determined through prior experimental validation. A potential epitope candidate is B7-H3 (CD276), which transcriptomic analyses indicate is expressed at stable levels regardless of GRASLND perturbation or IFNγ treatment, which has to be confirmed on the protein level. B7-H3-targeting CAR T cells, which have been well-documented in the literature for their ability to suppress tumor growth, may also be employed to investigate immunogenicity in melanoma[338]. However, additional epitopes should be evaluated for their suitability in such assays. The key advantage of using engineered CAR T cells in co-culture experiments is the ability to utilize the melanoma cell line 501-mel. This cell line demonstrated a significant and consistent upregulation of HLA-I protein expression upon GRASLND downregulation across all replicates, contrasting with the Ma-Mel-86c and Ma-Mel-61a cell lines, where autologous T cells are available. A successful execution of such T cell recognition and activation experiments would further strengthen the hypothesis of an immune evasion mechanism mediated by upregulation of lncRNA GRASLND in differentiated melanoma cells.

5. Material and Methods

5.1. Materials

5.1.1 Chemicals and Reagents

Commercial Name	Catalog Number	Supplier
2-chloroacetamide	C0267	Sigma-Aldrich
30 % Acrylamide/Bis Solution, 37.5:1	1610158	Bio-Rad
Acetonitrile, HPLC LC-MS grade	8364029	VWR International GmbH
Agarose Powder	A9539	Sigma-Aldrich
Ammonium Persulfate	A3678	Sigma-Aldrich
Ampicillin Sodium Salt	K029.4	Carl Roth GmbH
Blasticidine S Hydrochloride	15205	Sigma-Aldrich
BSA Molecular Biology Grade	B9000S	New England Biolabs
BSA, Lyophilized Powder	SAB4200541	Sigma-Aldrich
Calcein AM, Fluorescent Dye for Cell Viability	ab141420	Abcam
Calcium Chloride Solution	C-34006	Sigma-Aldrich
Chloroform: Isoamyl Alcohol 24:1 Biotech	C0549	Sigma-Aldrich
Clarity™ Western ECL Substrate	1705060	Bio-Rad
cOmplete™, Mini, EDTA-free Protease Inhibitor Cocktail	4693159001	Sigma-Aldrich
Dimethyl Sulfoxide (DMSO), Cell Culture	sc-358801	Santa Cruz Biotechnology Inc
DL-Dithiothreitol	D9779	Sigma-Aldrich
DMEM, High Glucose, Pyruvate	11594486	Gibco
DNA Ladder 1 kb	N3232S	New England Biolabs
DNA Ladder 100 bp	N3231S	New England Biolabs
Doxycycline Hydrochloride	10224633	Thermo Fisher Scientific
Dynabeads™ MyOne™ Streptavidin C1 magnetic beads	65001	Invitrogen
EDTA, Molecular Biology Reagent	E5134	Sigma-Aldrich
Ethanol, 70 %, For Molecular Biology	BP8201	Sigma-Aldrich
Ethanol, 99.8 %	10644795	Thermo Fisher Scientific
Ethidium Bromide	E1510	Sigma-Aldrich
Etoposide	E1383	Sigma-Aldrich
Fetal bovine serum, heat-inactivated	F9665-500ML	Sigma-Aldrich
Formaldehyde solution, 16 % (w/v), methanol-free	28908	Thermo Fisher Scientific
Formic acid ≥99%, HiPerSolv CHROMANORM®, LC-MS	84865.180	VWR International GmbH
Gel Loading Dye, purple, no SDS (6X)	B7025S	New England Biolabs
Glycerol, 99+%	G/0650/08	Thermo Fisher Scientific
Glycine	G8898	Sigma-Aldrich
GlycoBlue™ Coprecipitant	AM9515	Thermo Fisher Scientific
HBSS, Calcium, Magnesium, No Phenol Red	14025050	Thermo Fisher Scientific
Heparin Sodium Salt	sc-203075	Santa Cruz Biotechnology Inc
HEPES solution, 1M	H3537-100ML	Sigma-Aldrich
Hygromycin B Solution	sc-29067	Santa Cruz Biotechnology Inc
IGEPAL® CA-630	I8896-50ML	Sigma-Aldrich
Immobilon®-P PVDF	IPVH00005	Merck Millipore
Insulin Solution from Bovine Pancreas 1+	I0516-5ML	Sigma-Aldrich
Isopropanol	11398461	Thermo Fisher Scientific

KCl, 2M, RNase-free	AM9640G	Sigma-Aldrich
Leibovitz's L-15 Medium	11415049	Thermo Fisher Scientific
Lincode Human RNF144A-AS1 siRNA SMART Pool	R-027974-00-0005	Horizon Discovery
Lincode Non-targeting siRNA #1	D-001320-01-05	Horizon Discovery
Lipofectamine® RNAiMAX Reagent	13778100	Thermo Fisher Scientific
Lysophosphatidic acid	sc-201053	Santa Cruz Biotechnology Inc
Matrigel®	356234	Corning
Magnesium chloride solution, 1M	M1028-10X1ML	Sigma-Aldrich
MCDB 153 Medium Complete	M7403	Sigma-Aldrich
Methanol	176840010	Thermo Fisher Scientific
N,N,N′,N′-Tetramethylethylenediamine (TEMED)	T7024	Sigma-Aldrich
NEBuffer™ r3.1	B6003S	New England Biolabs
Non-fat Milk Powder	54650	Biomol GmbH
NuPAGE™ LDS Sample Buffer 4X	NP0007	Thermo Fisher Scientific
Opti-MEM™	31985062	Thermo Fisher Scientific
PageRuler™ Prestained Protein Ladder, 10 to 180 kDa	26617	Thermo Fisher Scientific
Penicillin-Streptomycin	P4333	Sigma-Aldrich
Phosphate-Buffered Saline (PBS), 1X	21-040-CV	Corning
Phusion Flash High-Fidelity PCR Master Mix	F548S	Thermo Fisher Scientific
Pierce™ Trifluoroacetic Acid (TFA), LC-MS grade	85183	Thermo Scientific
Polybrene	TR-1003-G	Sigma-Aldrich
Polyethyleneimine (PEI)	408727	Sigma-Aldrich
Ponceau S	33427.01	Serva
Puromycin Dihydrochloride	sc-108071A	Santa Cruz Biotechnology Inc
RNase AWAY	11952385	Thermo Fisher Scientific
RNasin® Ribonuclease Inhibitor	N2615	Promega
RPMI 1640, 1X	10-040-CV	Corning
Ruxolitinib	941678-49-5	Selleckchem
Sodium bicarbonate	S6014	Sigma-Aldrich
Sodium chloride, 5 M Aqua Solution, RNase Free	J60434-AE	Thermo Scientific
Sodium Dodecyl Sulfate (SDS)	L3771	Sigma-Aldrich
Sodium Hydroxide Solution, Molecular Biology, 10 M	2068	Sigma-Aldrich
Tango Buffer	BY5	Thermo Fisher Scientific
Tris Base	10708976001	Roche
Tris base, DNase RNase Protease Free	10103203	Thermo Fisher Scientific
TRIzol Reagent	T9424	Sigma-Aldrich
TRIzol™ Reagent	15596026	Invitrogen
Trypsin-EDTA (0,05 %), phenol red	25300054	Gibco
Tween® 20	P9416	Sigma-Aldrich
UltraPure™ 0.5M EDTA, pH 8.0	15575020	Invitrogen
UltraPure™ 1 M Tris-HCl, pH 8,0	15568025	Invitrogen
UltraPure™ Salmon Sperm DNA Solution (5X)	15632011	Invitrogen
Urea, Sigma Ultra	U0631-500G	Sigma-Aldrich
Water For Cell Culture	H20CC0501	Millipore

5.1.2 Buffers

Name	Components	Method
Alkylation solution	50 mM chloroacetamide in denaturing/reducing buffer	MS
Blocking Buffer	5 % (w/v) Non-fat Dry Milk in TBST Buffer	Western Blot
Blocking Buffer	100 µg/mL salmon sperm DNA, 5% BSA, 0.02 µg/mL heparin in lysis buffer	RNA Pulldown
Coating Buffer	0.01 M Tris-HCl pH 8.0, 0.7 % NaCl	Invasion Assay
Denaturing/reducing Buffer	8 M Urea, 50 mM Tris pH 7.5, 1 mM DTT	MS
FACS Buffer	10% FBS in 1X PBS	Flow Cytometry
Fixing Solution	4 % Paraformaldehyde in 1X PBS	Flow Cytometry
Hybridization Buffer	50 mM Tris-HCl, pH 7.4, 150 mM NaCl, 1 mM MgCl2, 0.05% IGEPAL, 10 mM EDTA, 1 mM DTT)	RNA Pulldown
Lysis Buffer	50 mM HEPES (pH 7.5), 150 mM KCl, 0.5% IGEPAL, 0.5 mM DTT and 2 mM EDTA	RNA Pulldown
Radioimmunoprecipitation assay buffer (RIPA Buffer)[339]	25 mM Tris-base, 150 mM NaCl 1 M, 1 % NP-40, 0.5 % Sodium Deoxycholate (DOC), 0.1 % SDS	Western Blot
SDS Running Buffer	25 mM Tris-base, 192 mM Glycine, 1 % SDS	Western Blot
SDS Separation Gel	8-10 % Acrylamide, 0.1 % SDS, 1.5 M Tris-HCl pH 8.8, 0.1 % APS, 0.004 % TEMED in ddH_2O	Western Blot
SDS Stacking Gel	5 % Acrylamide, 1 M Tris-HCl pH 6.8, 0.1 % SDS, 0.1 % APS, 0.01 % TEMED in ddH_2O	Western Blot
TAE Buffer	0.4 M Tris-base, 0.01 M EDTA-Na_2, 0.2 M Acetic Acid	Gel Electrophoresis
TBS Buffer	20 mM Tris-base, 150 mM NaCl, pH 7.6	Western Blot
TBST Buffer	20 mM Tris-base, 150 mM NaCl, pH 7.6, 0.1 % Tween 20	Western Blot
Transfer Buffer	25 mM Tris-base, 192 mM Glycine, pH 8.3, 10 % Methanol	Western Blot

5.1.3 Antibodies

Name	Catalog Number	Supplier	Clone	Source
Anti-GAPDH	60004-1-Ig	Proteintech	1E6D9	mouse
Anti-Mouse IGG – HRP	A9044	Sigma-Aldrich	polyclonal	rabbit
Anti-Rabbit IGG – HRP	10545	Sigma-Aldrich	polyclonal	goat
Anti-PARP1	9542S	Cell Signaling Technology	polyclonal	rabbit
Anti-AXL	mAb #8661	Cell Signaling Technology	C89E7	rabbit
Anti-STAT3	mAb #12640	Cell Signaling Technology	D3Z2G	rabbit
Anti-PKR	18244-1-AP	Proteintech	polyclonal	rabbit
Anti-β-actin	mAb #4970	Cell Signaling Technology	13E5	rabbit
Anti-ATF4	11815S	Cell Signaling Technology	D4B8	rabbit
Anti-MITF	284M-9	Sigma-Aldrich	C5	mouse
Anti-MelanA	sc-53536	Santa Cruz Biotechnology	M2-7C10	mouse
Anti-phospho-NF-κB p65 (Ser536)	30332S	Cell Signaling Technology	93H1	rabbit
Anti-NF-κB p65 XP	8242S	Cell Signaling Technology	D14E12	rabbit
Anti-Cas9 (Sp.)	34963S	Cell Signaling Technology	7A9-3A3	mouse
Anti-Vinculin	V9131	Sigma-Aldrich	hVIN-1	mouse
Anti-HLA-ABC-APC	17-9983-42	Invitrogen	W6/32	mouse

5.1.4 Enzymes

Commercial Name	Type	Catalog Number	Supplier
AgeI	Restriction Endonuclease	R0552S	New England Biolabs
BsmBI	Restriction Endonuclease	ER0451	Thermo Fisher Scientific
EcoRI	Restriction Endonuclease	ER0271	Thermo Fisher Scientific
rLys-C, Mass Spec grade	Protease	V1671	Promega
Trypsin, sequencing grade modified	Serine protease	V511A	Promega
rAPid Alkaline Phosphatase	Phosphatase	4898133001	Sigma-Aldrich
T4 DNA Ligase	Ligase	M0202S	New England Biolabs
T4 Polynucleotide Kinase	Kinase	EK0032	Thermo Fisher Scientific

5.1.5 Kits

Commercial Name	Catalog Number	Supplier
GoTaq® qPCR Master Mix	A6001	Promega
High-Capacity cDNA Reverse Transcription Kit	4368814	Thermo Fisher Scientific
LookOut® Mycoplasma PCR Detection Kit	MP0035	Sigma-Aldrich
Pierce™ BCA Protein Assay Kit	A55861	Thermo Fisher Scientific
QIAGEN Plasmid Midi Kit	12143	Qiagen
QIAprep Spin Miniprep Kit	27104	Qiagen
QIAquick Gel Extraction Kit	28704	Qiagen
QIAseq FastSelect -rRNA HMR Kit	334386	Qiagen
QIAseq 8-Unique Dual Index Set A	333715	Qiagen
QIAseq Stranded Total RNA Library Kit	180450	Qiagen

5.1.6 Bacterial Strains

Bacterial Strains	Description	Catalog Number
One Shot™ Stbl3™ *E. coli*	Chemical Competent Cells	C737303
One Shot™ TOP10 *E. coli*	Chemical Competent Cells	C404003

5.1.7 Cell Lines

Cell Lines	Specification	Supplier/provided by	RRID
501-mel	Metastatic Melanoma Cell Line	Aifantis Lab, NYU	CVCL_4633
A375	Metastatic Melanoma Cell Line	ATCC	CVCL_0132
C8161	Metastatic Melanoma Cell Line	Mary J. C. Hendrix, Department of Biology, Shepherd University, Shepherdstown, WV, US and West Virginia University Research Corporation	CVCL_6813
Lenti-X™ 293T	HEK 293T Cell Line	Takara, Cat. No. 632180	CVCL_4401
Ma-Mel-61a	Metastatic Melanoma Cell Line	Prof. Dr. Annette Paschen (UKE, Department of Dermatology, Essen, Germany)	CVCL_C291
Ma-Mel-86a	Metastatic Melanoma Cell Line	Prof. Dr. Annette Paschen (UKE, Department of Dermatology, Essen, Germany)	CVCL_A221
Ma-Mel-86c	Metastatic Melanoma Cell Line	Prof. Dr. Annette Paschen (UKE, Department of Dermatology, Essen, Germany)	CVCL_C7TP
SK-MEL-147	Metastatic Melanoma Cell Line	Memorial Sloan Kettering Cancer Center	CVCL_3876
SK-MEL-239	Melanoma Cell Line	Memorial Sloan Kettering Cancer Center	CVCL_6122
WM1361a	Melanoma Cell Line	Aifantis Lab, NYU	CVCL_6788

5.1.8 Plasmids

Plasmid	Description	Resistance	Addgene
Lenti_tetON-dCas9-KRAB	Lentiviral and tet-inducible expressing vector, encoding dCas9-KRAB for CRISPRi, contains mCherry as Fluorescent Protein	Amp, Blast	Unknown
pLVx-U6se-EF1a-sfPac	Lentiviral sgRNA expression vector with modified stem loop driven by U6 Promoter, Puro Resistance and Reporter gene GFP by EF-1alpha Promoter	Amp, Puro	Unknown
pMD2.G	VSV-G Envelope Expressing Plasmid	Ampicillin	#12259
psPAX2	2nd Generation Lentiviral Packaging Plasmid	Ampicillin	#12260
Tet-pLKO-puro	Lentiviral and tet-inducible shRNA expression vector (AgeI/EcoRI cloning)	Amp, Puro	# 21915

5.1.9 Oligonucleotides

Oligo Name	Sequence (5'–3')	Purpose
“odd”, probe 1	tgtaggaatcaggggagtgt	GRASLND pulldown, probe 1, set “odd”
“odd”, probe 2	gcttcgcagatcttagattc	GRASLND pulldown, probe 2, set “odd”
“odd”, probe 3	agacgttacattccacattc	GRASLND pulldown, probe 3, set “odd”
“odd”, probe 4	atgagtagtcaccttccatg	GRASLND pulldown, probe 4, set “odd”
“odd”, probe 5	agaatctacggagcttgcat	GRASLND pulldown, probe 5, set “odd”
“even”, probe 1	ggtgaacagacagactttcc	GRASLND pulldown, probe 1, set “even”
“even”, probe 2	gtactcaaccaggaacttct	GRASLND pulldown, probe 2, set “even”
“even”, probe 3	ctctggcaggaaagtcttgt	GRASLND pulldown, probe 3, set “even”
“even”, probe 4	catgcatagaagatccggtt	GRASLND pulldown, probe 4, set “even”
“even”, probe 5	ccaagggccatattcaattg	GRASLND pulldown, probe 5, set “even”
“lacZ”, probe 1	aatgtgagcgagtaacaacc	GRASLND pulldown, probe 1, set “lacZ Control”
“lacZ”, probe 2	attaagttgggtaacgccag	GRASLND pulldown, probe 2, set “lacZ Control”
“lacZ”, probe 3	aataattcgcgtctggcctt	GRASLND pulldown, probe 3, set “lacZ Control”
“lacZ”, probe 4	aattcagacggcaaacgct	GRASLND pulldown, probe 4, set “lacZ Control”
“lacZ”, probe 5	atcttccagataactgccgt	GRASLND pulldown, probe 5, set “lacZ Control”
GRASLND-shRNA-sh1-FWD	ccggtacaaaggtggcaagataaatctcgag atttatcttgccacctttgtatttttt	RNAi shRNA forward oligo, (Huynh *et al*.[233]), AgeI/EcoRI site
GRASLND-shRNA-sh1-REV	aattaaaaatacaaaggtggcaagataaatc tcgagatttatcttgccacctttgta	RNAi shRNA reverse oligo, (Huynh *et al*.[233]), AgeI/EcoRI site
GRASLND-shRNA-sh2-FWD	ccggggcaagataaatgacaataaactcga gtttattgtcatttatcttgcctttttt	RNAi shRNA forward oligo, (Huynh *et al*.[233]), AgeI/EcoRI site
GRASLND-shRNA-sh2-REV	aattaaaaaggcaagataaatgacaataaa ctcgagtttattgtcatttatcttgcc	RNAi shRNA reverse oligo, (Huynh *et al*.[233]), AgeI/EcoRI site
GRASLND-shRNA-sh3-FWD	ccgggacactcccctgattcctacactcgagt gtaggaatcaggggagtgtcttttt	RNAi shRNA forward oligo, AgeI/EcoRI site
GRASLND-shRNA-sh3-REV	aattaaaaagacactcccctgattcctacact cgagtgtaggaatcaggggagtgtc	RNAi shRNA reverse oligo, AgeI/EcoRI site
GRASLND-shRNA-sh4-FWD	ccgggatccaagcacagcaatttctctcgag agaaattgctgtgcttggatcttttt	RNAi shRNA forward oligo, AgeI/EcoRI site
GRASLND-shRNA-sh4-REV	aattaaaaagatccaagcacagcaatttct ctcgagagaaattgctgtgcttggatc	RNAi shRNA reverse oligo, AgeI/EcoRI site
GRASLND-shRNA-sh5-FWD	ccgggagaacaagggttataataaactcgagttt attataacccttgttctcttttt	RNAi shRNA forward oligo, AgeI/EcoRI site
GRASLND-shRNA-sh5-REV	aattaaaaagagaacaagggttataataaa ctcgagtttattataacccttgttctc	RNAi shRNA reverse oligo, AgeI/EcoRI site
GRASLND-shRNA-sh6-FWD	ccggggatccaagcacagcaatttctcgagaaa ttgctgtgcttggatccttttt	RNAi shRNA forward oligo, AgeI/EcoRI site
GRASLND-shRNA-sh6-REV	aattaaaaaggatccaagcacagcaattt ctcgagaaattgctgtgcttggatcc	RNAi shRNA reverse oligo, AgeI/EcoRI site
GRASLND-shRNA-sh7-FWD	ccgggtgggagtagcatccacataactcgagtta tgtggatgctactcccactttttt	RNAi shRNA forward oligo, AgeI/EcoRI site
GRASLND-shRNA-sh7-REV	aattaaaaagtgggagtagcatccacataa ctcgagttatgtggatgctactcccac	RNAi shRNA reverse oligo, AgeI/EcoRI site
GRASLND-shRNA-sh8-FWD	ccggcttagagaacaagggttataactcgagtta taacccttgttctctaagttttt	RNAi shRNA forward oligo, AgeI/EcoRI site
GRASLND-shRNA-sh8-REV	aattaaaaacttagagaacaagggttataa ctcgagttataacccttgttctctaag	RNAi shRNA reverse oligo, AgeI/EcoRI site
Non-Targeting-shRNA-FWD	ccgggcgcgatagcgctaataatttctcga gaaattattagcgctatcgcgcttttt	RNAi shRNA forward oligo, AgeI/EcoRI site
Non-Targeting-shRNA-REV	aattaaaaagcgcgatagcgctaataattt ctcgagaaattattagcgctatcgcg	RNAi shRNA reverse oligo, AgeI/EcoRI site

lacZ-shRNA-FWD	ccggctcggcgtttcatctgtggctcgagcca cagatgaaacgccgagttttt	RNAi Control shRNA forward oligo, AgeI/EcoRI site
lacZ-shRNA-REV	aattaaaaactcggcgtttcatctgtgg ctcgagccacagatgaaacgccgag	RNAi Control shRNA reverse oligo, AgeI/EcoRI site
GRASLND-gRNA-i4-FWD	caccgaaggcggagcttgcagtgag	CRISPRi sgRNA, TSS -8 nt, BsmBI restriction site overhang
GRASLND-gRNA-i4-REV	aaacctcactgcaagctccgccttc	CRISPRi sgRNA, TSS -8 nt, BsmBI restriction site overhang
GRASLND-gRNA-i5-FWD	caccgaaaaaattagccgggcgcag	CRISPRi sgRNA, TSS +54 nt, BsmBI restriction site overhang
GRASLND-gRNA-i5-REV	aaacctgcgcccggctaatttttc	CRISPRi sgRNA, TSS +54 nt, BsmBI restriction site overhang
GRASLND-gRNA-i6-FWD	caccgaggtcaggagatcgagacca	CRISPRi sgRNA, TSS +103 nt, BsmBI restriction site overhang
GRASLND-gRNA-i6-REV	aaactggtctcgatctcctgacctc	CRISPRi sgRNA, TSS +103 nt, BsmBI restriction site overhang
GRASLND-gRNA-i7-FWD	caccggtagagaggggtttcaccg	CRISPRi sgRNA, TSS +84 nt, BsmBI restriction site overhang
GRASLND-gRNA-i7-REV	aaaccggtgaaacccctctctacc	CRISPRi sgRNA, TSS +84 nt, BsmBI restriction site overhang
scrambled-gRNA-FWD	caccggtattactgatattggtggg	Scrambled CRISPR sgRNA, BsmBI restriction site overhang, forward
scrambled-gRNA-REV	aaaccccaccaatatcagtaatacc	Scrambled CRISPR sgRNA, BsmBI restriction site overhang, reverse

5.1.10 Primers

Primer Name	**Sequence 5'->3'**	**Function**
GRASLND-Fwd	aggattcaggggatgcacag	RT-qPCR
GRASLND-Rev	tgggctgaagatgagacgtt	RT-qPCR
GAPDH-Fwd	agccacatcgctcagacac	RT-qPCR
GAPDH-Rev	gcccaatacgaccaaatcc	RT-qPCR
HPRT1-Fwd	gaccagtcaacaggggacat	RT-qPCR
HPRT1-Rev	gtgtcaattatatcttccacaatcaa	RT-qPCR
MelanA-Fwd	gccactcttacaccacggct	RT-qPCR
MelanA-Rev	cagtaagactcccaggatcactactgtc	RT-qPCR
MALAT1-Fwd	gaaggaaggagcgctaacga	RT-qPCR
MALAT1-Rev	taccaaccactcgctttccc	RT-qPCR
PSMB9-Fwd	atgtctcccgaggagtgcag	RT-qPCR
PSMB9-Rev	gtccacaccggcagctgtaa	RT-qPCR
PSMB8-Fwd	tgatgctcataggaaccccca	RT-qPCR
PSMB8-Rev	gttcctttctccgtccccacc	RT-qPCR
RNF144A-Fwd	ctgctgactctgacatgccc	RT-qPCR
RNF144A-Rev	ctggtgtcctgctgtgctta	RT-qPCR
TAP1-Fwd	tccggaaaccgtgtctactt	RT-qPCR, Huynh *et al*.[233]
TAP1-Rev	tcagggctttcgtacaggag	RT-qPCR, Huynh *et al.*[233]
pLKO-Tet-on seq	ggcagggatattcaccattatcgtttcaga	Sequencing primer pLKO-Tet-on
U6-FWD	ttcccatgattccttcatatttgc	Sequencing primer pLVx-U6se-EF1a-sfPac

5.1.11 Consumables

Commercial Name	Model	Supplier
Amicon® Ultra-15 Centrifugal Filter Unit	UFC910024	Millipore
Aspiration Pipette 2 mL	86.1252.011	Sarstedt AG
AttractSPE™ Disks Bio C18	SPE-Disks-Bio-C18-100.25.40	Affinisep
BioLite Cell Culture Treated Dishes	11815275	Thermo Fisher Scientific
BioLite™ 96-Well, Cell Culture-Treated, Flat-Bottom Microplate	11835275	Thermo Fisher Scientific
Cell culture dish, TC 15 cm	734-2818	VWR International
Cell Strainer, 40 µm, Blue, CS50	431750	Corning BV
Cryotube™ 1.8 mL	479-6843	VWR International
Cytiva Whatman™ Blotting Paper	12425272	Thermo Fisher Scientific
CytoOne® Bottle Top Filtration Unit	CC6032-8233	Starlab
Disposal Bags	HEB-3020	Kisker Biotech
EVE™ Cell Counting Slides	734-2676	NANOENTEK
Falcon Round Bottom Tubes	C-3082	Neo Lab
Falcon® 10 mL Serological Pipet	356551	Corning
Falcon® 14 mL High Clarity PP Test Tube	352059	Corning
Falcon® 25 mL Serological Pipet	357525	Corning
Falcon® 5 mL Serological Pipet	356543	Corning
Falcon® 5mL Round	352054	Corning BV
Fisherbrand Comfort Nitril Gloves	15642367	Thermo Fisher Scientific
Fisherbrand™ Easy Reader™ Conical Polypropylene Centrifuge Tubes, 15 mL	05-539-12	Thermo Fisher Scientific
Fisherbrand™ Easy Reader™ Conical Polypropylene Centrifuge Tubes, 50 mL	05-539-9	Thermo Fisher Scientific
Fisherbrand™ Filter Tips 1-200 µL	10102512	Thermo Fisher Scientific
Fisherbrand™ Top-Line Pipette Filter Tips 0.1-10 µL	10366242	Thermo Fisher Scientific
FluoroBlok™ Insert, 24-well Inserts, 8µm Pore	351152	Corning BV
Hard-Shell® 96-Well PCR Plates	HSP9601	Bio-Rad
Inoculation Spreader	86.1569.005	Sarstedt AG
Microseal 'B' PCR Plate Sealing Film	MSB1001	Bio-Rad
Mr. Frosty™ Freezing Container	10110051	Thermo Fisher Scientific
PCR Tubes 0.5 mL (Flat Cap)	732-3207	VWR International
Protein LoBind Tube, 1.5 mL	0030 108.116	Eppendorf
SafeSeal Microcentrifuge Tube 1.5 mL	72.706	Sarstedt AG
SafeSeal Microcentrifuge Tube 2 mL	72.695.500	Sarstedt AG
Single-Use Syringes, 2-Piece, HENKE-JECT®	613-2009	VWR International
Syringe Filter PES 33mm 0.2 µM	15206869	Thermo Fisher Scientific
TC Dish 100, Standard	83.3902	Sarstedt AG
TC Flask T25, Stand. Vent. Cap	83.3910.002	Sarstedt AG
TC Flask T75, Stand. Vent. Cap	83.3911.002	Sarstedt AG
TC Plate 6-Well, Standard, F	83.3920.005	Sarstedt AG
Tip Filter 1000 µL Micropoint Graduated	613-0992	VWR International
Tip Filter 20 µL Beveled Graduated	613-0988	VWR International
Tip Filter 200 µL Genomic LR RACK	613-0996	VWR International
Tube Strips 0.2 mL Flat Cap	732-3229	VWR International

5.1.12 Lab Equipment

Type	Model	Manufacturer
Biological Safety Cabinet	Thermo Heraeus HERAsafe HS12	Thermo Fisher Scientific
Centrifuge	5415R	Eppendorf
Centrifuge	5804R	Eppendorf
Centrifuge	Fisherbrand™ Mini-Centrifuge	Thermo Fisher Scientific
Electrophoresis Chamber	Wide Mini-Sub Cell GT System 1704405	Bio-Rad
Electrophoresis Chamber	Mini-Sub Cell GT Cell 1664400	Bio-Rad
Wide-Field Fluorescence Microscope	Olympus Cell^R	Olympus Live Science
Automated Cell Counter	Countess™ II automated cell counter	Invitrogen
Fluorescence-activated Cell Sorting	SH800S Cell Sorter	Sony
Fluorescence Microscope	Olympus IX-71 with DeltaVision Elite Imaging System	Olympus Corporation and Cytiva
Gel Visualization System	ChemiDocTM MP Imaging System	Bio-Rad
Incubator	CO_2 Incubator Model CB 170	Binder
Microplate Reader	Spark® Multimode Microplate Reader	Tecan
PCR Cycler	Master Cycler EP Gradient 5341	Eppendorf
Pipette	0.5-10 µL Single Channel Microliter Pipettes LLG-proMLP	LLG Labware
Pipette	2-20 µL Single Channel Microliter Pipettes LLG-proMLP	LLG Labware
Pipette	20-200 µL Single Channel Microliter	LLG Labware
Pipette	Pipettes LLG-proMLP 100-1000 µL Single Channel Microliter Pipettes LLG-pomp	LLG Labware
Power Supply	PowerPacTM Basic Power Supply	Bio-Rad
Magnetic rack	DynaMag™-2 magnet	Invitrogen
qPCR Cycler	CFX Connect™ Real-Time System	Bio-Rad
Shaking Incubator	Incubator Shaking Series I26	New Brunswick Scientific
Spectrophotometer	Nanodrop™ 2000c	Thermo Fisher Scientific
Live cell imager	IncuCyte S3 System	Sartorius
Vortexer	Scientific Industries SI™ Vortex- Genie™ 2	Thermo Fisher Scientific
Wet/Tank Blotting System	Mini Trans-Blot Electrophoretic Transfer Cell 1703930	Bio-Rad
Nano-HPLC system	Ultimate 3000 RSLC nano-HPLC system, coupled with a Hybrid-Orbitrap Q Exactive HF mass spectrometer	Thermo Fisher Scientific
Speed Vacuum Concentrator	Savant™ SpeedVac™ DNA 130 Integrated Vacuum Concentrator System	Thermo Fisher Scientific
HPLC Column	C18 PepMap 100 column	Thermo Fisher Scientific

5.1.13 Software

Name	Purpose	Supplier
Bio Render	Create of scientific illustrations	Bio Render
Fiji	Image processing with software toolkit	Open Source
Adobe Illustrator	Create figures with vector graphics design tool	Adobe
IncuCyte Software 2019B Rev2	Software of IncuCyte S3 System	Sartorius
MaxQuant v.2.2.0.0	Analysis of MS data	Open Source
ChatGPT	Occasional grammar/spelling checking of self-written sentences to enhance synonym usage and word order. This thesis does not incorporate any complete texts created by generative writing tools.	Open Source
Microsoft Office	Data analysis (Excel), writing document (Word)	Microsoft
Graph Pad Prism 9.0	Data Analysis Software	GraphPad Software, USA
CFX Maestro	qPCR Analysis	BioRad
Perseus v.2.0.11.0	Statistical data analysis of MS data	Open Source
softWoRx 7.2.0 software	Software of the DeltaVision Elite Imaging System	Cytiva
RStudio	Analysis and visualization of flow cytometry data	Posit, PBC
ProteoWizard	Conversion and analysis of MS data	Open Source

5.2. Methods

5.2.1 Plasmid Preparation

5.2.1.1 sgRNA Cloning

Single guide RNA (sgRNA) sequences targeting the GRASLND gene locus using dCas9-KRAB-mediated CRISPRi were designed with the free online tool Benchling Life Sciences R&D Cloud (https://www.benchling.com/). Briefly, GRASLND gene DNA sequence was uploaded and with the use of the CRISPR tool, a list of potential sgRNAs was generated. sgRNAs with high on-target and low off-target scores were chosen to balance the efficiency and specificity[340,341]. Oligonucleotides (Integrated DNA Technologies, Inc.) were ordered with overhangs suitable for the insertion into the BsmbI restriction site, specifically designed as follows: Forward oligo: 5'-CACCG-20 bp target-3' and Reverse oligo: 5'-AAAC-20 bp target-C-3'. Lentiviral transfer vector pLVx-U6se-EF1a-sfPac (Supplementary Figure 36) was digested with the BsmBI restriction endonuclease (New England Biolabs) using NE Buffer 3.1 (New England Biolabs) at 55 °C for three hours. For dephosphorylation, rAPid Alkaline Phosphatase (Sigma Aldrich) was added to the reaction, followed by incubation at 37 °C for one hour and agarose gel electrophoresis, as described below (5.2.1.3). The digested backbone vector was gel purified using QIAquick Gel Extraction Kit (Qiagen). For 5' end phosphorylation and annealing of the forward and reverse oligonucleotides, 1 µL of each oligo (100 µM) was combined with 0.5 µL of T4 polynucleotide kinase (10 U/µL, New England Biolabs) and 1 µL of T4 ligase buffer (New England Biolabs) supplemented with 10 mM ATP, and filled to a total volume of 10 µL with H_2O. The reaction was first incubated at 37 °C for 30 minutes, after which the samples were heated to 95 °C for 5 minutes. The samples were cooled to room temperature by turning off the thermocycler. The final ligation reaction required dilution of the oligo duplex 1:200 and 1 µL of this dilution was mixed with 25 ng of digested vector, 1 µL of T4 ligase in respective T4 ligase buffer and filled with H_2O to a total volume of 10 µL. After incubation for 30 minutes at room temperature, 3 µL of the reaction was transformed in Stbl3 *E. coli* bacterial cells as explained in 5.2.1.4, followed by plasmid purification (5.2.1.5) and Sanger sequencing for verification (5.2.1.6). A list of sgRNA oligonucleotides, targeting the GRASLND gene or a scrambled sgRNA as negative control, is presented in 5.1.9.

5.2.1.2 shRNA Cloning

The InvivoGen siRNA Wizard Software 3.1 (https://www.invivogen.com/sirnawizard/design.php) was used to design shRNA sequences targeting the GRASLND lncRNA. Selected sequences were analyzed for specificity to GRASLND through alignment verification using the UCSC Genome Browser (http://genome.ucsc.edu/) to ensure target-specific complementarity[260]. In addition, two target sequences previously utilized for GRASLND knockdown by Huynh *et al.* were selected[233]. A non-targeting and negative control shRNA targeting the lacZ mRNA, as reported by Feng *et al*., was used[253]. Following the protocol "The 'all-in-one' system for the inducible expression of shRNA" by Wiederschain *et al*.[251], selected shRNAs were cloned into the lentiviral vector Tet-pLKO-puro (Addgene #21915), with

minor modifications. In detail, for annealing the oligonucleotides (oligos) encoding the desired shRNA and flanking AgeI/EcoRI sites, 10 µL of oligos (10 µM, Integrated DNA Technologies, Inc.) were combined with 10 µL of 10X Tango Buffer (Thermo Fisher) and 70 µL of H_2O. The reaction was heated for 5 minutes at 95 °C before it was cooled down to room temperature. Meanwhile, the stuffer DNA was removed from the pLKO-Tet-On vector by AgeI/EcoRI double digest (10 µg). Digested vector was loaded on an agarose gel, as described below (5.2.1.3) and gel purified using QIAquick Gel Extraction Kit (Qiagen) according to manufacturer's protocol. The ligation reaction was performed by mixing 20 ng of digested vector with a dilution of the annealed oligos in a final concentration 37.5 nM and T4 ligase (1 µL, 400 U) enzyme in its respective T4 ligase buffer (New England Biolabs) in a total volume of 10 µL. The reaction was incubated for two hours at room temperature and the whole volume was transformed into Stbl3 *E. coli* or TOP10 *E. coli* bacterial cells (see section 5.2.1.4) followed by plasmid purification (5.2.1.5) and Sanger sequencing (5.2.1.6). A full list of shRNA sequences can be found in the materials section 5.1.9.

5.2.1.3 Agarose Gel Electrophoresis

To prepare a 1.5% agarose gel, 1.5 g of agarose was dissolved in 100 mL of 1X TAE buffer by heating in a microwave. After cooling the solution, 5 µL of ethidium bromide solution (10 mg/mL, Sigma Aldrich) was added. The mixture was then poured into a gel casting chamber with a 15-well comb to allow polymerization. Samples were mixed at a 1:6 ratio with 6X DNA Gel Loading Dye (New England Biolabs), and 10 µL of each sample was loaded onto the gel. A standard of 6 µL of either a 1 kb or 100 bp DNA Ladder (New England Biolabs) was used. The gel was submerged in 1X TAE buffer to ensure complete coverage, and electrophoresis was conducted at 100 V for 75 minutes. The results were visualized with the Bio-Rad ChemiDoc™ MP Imaging System.

5.2.1.4 Transformation of Chemically Competent E. coli Cells

Chemically competent One Shot™ Stbl3™ *E. coli* or One Shot™ TOP10 *E. coli* cells (Invitrogen) were thawed on ice and 3-10 µL of ligation reaction mix was added to 100 µL of bacterial cells. The mixture was incubated on ice for 30 minutes before a heat shock was performed at 42 °C for 45 seconds. Subsequently, the tube was placed on ice for two minutes and 500 µL prewarmed super optimal broth with catabolite repression (SOC) medium was added to the cell suspension, which was further incubated for one hour at 37 °C while shaking at 700 rpm. 200 µL of the cell suspension was plated on a pre-warmed lysogeny broth (LB) agar plate with appropriate antibiotic and the plate was incubated overnight at 37 °C.

5.2.1.5 Plasmid Purification

A single colony of transformed *E. coli* bacterial cells was carefully picked from the agar plate and inoculated into 5 mL of LB medium containing 100 µg/mL ampicillin as selection antibiotic. After incubation overnight at 37 °C with shaking at 175 rpm, the culture was centrifuged at 4500 rpm for 10 minutes and the supernatant was discarded. Plasmid purification was performed using QIAprep Spin Miniprep Kit (Qiagen) according to the manufacturer's instructions and the concentration was determined using a NanoDrop™ 2000c (Thermo Fisher). For larger-scale plasmid purification, a colony of transformed *E. coli* bacterial cells was also inoculated into 5 mL of LB medium containing 100 µg/mL ampicillin, however, instead of overnight, it was incubated during the day for approximately 7 hours. This culture was then transferred to 100 mL of LB medium with antibiotic and incubated overnight at 37 °C while gentle agitation at 175 rpm. Next day, the culture was centrifuged at 4500 rpm for 10 minutes and the supernatant was discarded. This is followed by purification using the QIAGEN Plasmid Midi Kit (Qiagen) according to the manufacturer's guidelines and final DNA concentration was measured using a NanoDrop™ 2000c (Thermo Fisher).

5.2.1.6 Sequencing of Plasmids

For Sanger sequencing of plasmids, the service of Microsynth Seqlab was used. According to their guidelines, 12 µL of plasmid DNA at a concentration of 40-100 ng/µL was combined with 3 µL of the appropriate primer (20 µM). Analysis of the received sequencing results was performed using the alignment function of the Benchling Life Sciences R&D Cloud platform. Primer sequences used for sequencing are listed in section 5.1.10.

5.2.2 Cell Culture

5.2.2.1 Cultivation of Mammalian Cells

Human melanoma cell lines 501-mel and WM3161a were kindly received by the Aifantis Lab, NYU, SK-MEL-239 and SK-MEL-147 were provided from the Memorial Sloan Kettering Cancer Center (MSK), cell line C8161 was courteously given by Mary J. C. Hendrix, Department of Biology, Shepherd University, Shepherdstown, WV, United States and West Virginia University Research Corporation and the previously described human melanoma metastasis cell lines Ma-Mel-86a, Ma-Mel-86c and Ma-Mel-61a[342,343] were obtained from Prof. Dr. Annette Paschen (UKE, Department of Dermatology, Essen, Germany). Melanoma cell lines 501-mel, SK-MEL-239, SK-MEL-147, A375, C8161 and the lentiviral packaging and production cell line Lenti-X 293T (purchased from Takara) were cultured as adherent monolayers in Gibco Dulbecco's Modified Eagle Medium (DMEM), high glucose with pyruvate supplemented with 10% (v/v) fetal bovine serum (FBS) and 1% (v/v) penicillin/streptomycin. Ma-Mel-86a, Ma-Mel-86c and Ma-Mel-61a were grown as adherent monolayers in RPMI1640 medium supplemented with 10% (v/v) fetal bovine serum (FBS) and 1% (v/v) penicillin/streptomycin. Melanoma cell line WM1361a cells were cultured in conditioned TU 2 % medium. For the preparation of this medium, one vial of MCDB153 growth medium was dissolved in 900 mL of distilled water and 1.2 g

$NaHCO_3$ were added, followed by a pH adjustment to 7.5 using a 5 M NaOH solution. The total volume was filled up to 1 L with distilled water and sterile filtration was performed using CytoOne® Bottle Top Filtration Unit. This solution was used to produce the TU 2% medium containing 80% (v/v) MCDB153 with L-glutamine and 28 mM HEPES, 20% (v/v) Leibovitz L-15, supplemented 2% (v/v) heat inactivated FBS, $CaCl_2$ (1.68 mM), 5 µg/mL insulin and 1% (v/v) penicillin/streptomycin. All cell lines were cultured in a humidified incubator at 37 °C and 5% CO_2 under sterile conditions. The absence of Mycoplasma bacteria contamination was confirmed using the LookOut® Mycoplasma PCR Detection Kit (Sigma-Aldrich).

5.2.2.2 Passaging and Seeding of Adherent Mammalian Cells

Cells were cultured in the appropriate cell culture growth medium as previously described and grown to 80-90% confluency. The growth medium was then aspirated and the cell monolayer was rinsed with prewarmed 1X PBS. To detach the cells, prewarmed trypsin-EDTA solution (0.05%) was added, followed by incubation for 3 minutes at 37 °C in 5% CO_2 atmosphere. Prewarmed growth medium, at twice the volume of the trypsin-EDTA solution, was used to neutralize the trypsin and the cell suspension was homogenized by repetitive pipetting. The cells were then centrifuged at 500 × *g* for 4 minutes, resuspended in an appropriate amount of prewarmed growth medium, and counted using the Trypan blue exclusion method with the Countess™ II Automated Cell Counter (Thermo Scientific). The required number of cells was transferred to a desired culture vessel containing prewarmed growth medium.

5.2.2.3 Cryopreservation of Mammalian Cells

For long-term storage of mammalian cells, cells were harvested using trypsin-EDTA as described earlier in 5.2.2.2, and centrifuged at 500 × *g* for 4 minutes. The supernatant was aspirated and the cell pellet washed with 1X PBS. The cells were counted as specified above and after another round of centrifugation and aspiration, the cell pellet was resuspended in cryopreservation medium (90% FBS with 10% DMSO) by adjusting the cell concentration to 1-3 × 10^6 cells/mL. The cell suspension was aliquoted into cryovials with a volume of 1 mL each and placed in a Mr. Frosty™ controlled-rate freezing container to be stored at -80 °C overnight. For long-term storage, the cryovials were transferred to a liquid nitrogen storage tank.

For thawing cryopreserved cells, the cryovials were removed from the liquid nitrogen tank and immediately thawed in a water bath at 37 °C. The thawed cells were then transferred to a conical centrifugation tube containing 5 mL of prewarmed growth medium. After centrifugation at 500 × *g* for 4 minutes, the supernatant was aspirated, the cell pellet was resuspended in fresh growth medium and the cells suspension transferred to an appropriate cell culture vessel containing prewarmed growth medium.

5.2.2.4 Lentiviral Particle Production

Lentiviral particles were generated using a well-established three-plasmid transfection method. One day prior to transfection, 4 × 10^6 Lenti-X 293T cells per 10 cm plate were seeded to obtain 80% confluency the next day. For transfection, the following plasmids were combined in 500 µL Opti-MEM™ (Gibco) and incubated for 5 minutes at room temperature: viral envelope plasmid pMD2.G (5.5 µg), viral packaging plasmid psPAX2 (7.4 µg) and the transfer plasmid (11.25 µg). Separately, 500 µL Opti-MEM™ was mixed with 36 µL PEI transfection reagent (Sigma-Aldrich) with a concentration of 1 mg/mL to obtain a PEI to DNA ratio of 1.5:1. This mixture was also incubated for 5 minutes at room temperature. Further, both mixtures were combined by adding the DNA to the transfection reagent solution and incubated for 15 minutes at room temperature before it was dropwise pipetted to the cells in the 6 mL of freshly exchanged growth medium. After gentle swirling, the cell plates were incubated overnight at 37 °C. The PEI-containing medium was replaced with 5 mL of fresh growth medium 12-15 hours post transfection. The lentiviral particles-containing supernatants were collected 48, 72 and 96 hours post-transfection and stored at 4 °C for a maximum of seven days. Further, the supernatants were centrifuged at 500 x *g* for 5 minutes at 4 °C, followed by filtration through 0.2 µm syringe filters (Fisher Scientific) to remove cell debris. Concentration of the filtered supernatants was performed using Amicon® Ultra-15 Centrifugal Filter Unit (Millipore) at 2,000 × *g* for 1-1.5 hours to yield about 500 µL of concentrated virus. Aliquots of the virus were prepared and preserved at -80 °C until further use.

5.2.2.5 Lentiviral Transduction

One day prior to transduction, desired target cells were seeded at 1-3 × 10^5 cells/well in a 6-well plate to obtain an 80% confluency the following day. For transduction, the growth medium was exchanged with fresh medium supplemented with 6 µg/mL of polybrene (Sigma-Aldrich) and 50 µL concentrated lentivirus was added dropwise to the wells. The medium was exchanged to fresh growth medium 16 hours post transfection to remove the polybrene. Another 6-8 hour later, medium was renewed, this time containing the selection antibiotic at the required concentration: Hygromycin B (200 µg/mL), Blasticidine (10 µg/mL) or Puromycin (5 µg/mL). The cells were kept under selection until all control cells died.

5.2.2.6 Cell Treatment

5.2.2.6.1 shRNA induction

Lentiviral stable shRNA knockdown cells were plated one day before being treated with 2 µg/mL doxycycline (Fisher Scientific). Culture medium was replaced every other day, unless otherwise specified. Verification of effective downregulation was performed using RT-qPCR.

5.2.2.6.2 siRNA transfection

Transfection of siRNA was performed using Lipofectamine™ RNAiMAX Transfection Reagent (Thermo Fisher Scientific) according to the manufacturer's protocol. In detail, 36 pmol of RNAi duplex (Horizon Discovery) was diluted in 200 µL Opti-MEM medium without serum in the wells of a 12-well tissue culture plate and gently mixed. This is followed by the addition of 2 µL of transfection reagent to each well containing the diluted siRNAs. The reaction was gently mixed and incubated for 20 minutes at room temperature. Meanwhile, the cells were diluted in 1 mL complete growth medium without antibiotics, with appropriate number of cells to give 20-50% confluence one day after seeding. After incubation of the RNAi-duplex-transfection reagent complexes, the diluted cells were added to obtain a final volume of 1.2 mL and a final RNA concentration of 10 nM. The plate was rocked for thorough mixing. The cells were incubated for 1-3 days at 37 °C in a CO_2 incubator, followed by further analysis.

5.2.2.6.3 Cytokine treatment

One day before treatment, stable shRNA knockdown cells were plated at an appropriate seeding density. The treatment with IFNγ (Imukin, Boehringer Ingelheim) was applied at 500 IU/mL for 501-mel and Ma-Mel-86c cells, and 50 IU/mL for Ma-Mel-61a for the indicated time period. Control samples received no treatment. Cells were harvested and subjected to additional analyses.

5.2.2.6.4 Inhibitor treatment

Stable shRNA knockdown cells were plated one day prior inhibitor treatment at an appropriate seeding density. JAK1/2 inhibitor ruxolitinib (Selleckchem) was used in a concentration of 2 µM on 501-mel knockdown cells. Control cells were treated with the same volume of DMSO. Cells were harvested and the effects on cell differentiation status were analyzed using Western blot.

5.2.3 RNA Extraction

Total RNA was extracted with TRIzol™ reagent (Sigma-Aldrich) according to the manufacturer's protocol as follows: monolayer cells were pelleted and washed with 1X PBS as described above. The cell pellet was lysed by resuspension with 500 µL TRIzol™ reagent for 0.5-3.0 × 10^6 cells and mixing by pipetting. After incubation for 5 minutes at room temperature, 100 µL of chloroform was added and mixed by shaking the tube vigorously, followed by standing for 10 minutes at room temperature. The resulting 3-phase mixture was centrifuged at 12,000 × *g* for 15 minutes at 4 °C and the upper aqueous phase was transferred to a fresh tube. To this, 250 µL isopropanol and 1 µL of GlycoBlue™ Co-precipitant (Thermo Fisher) was added, mixed and incubated for 10 minutes at room temperature. After another centrifugation round (12,000 × *g*, 10 minutes, 4 °C), the supernatant was removed and the RNA pellet washed with 750 µL of 75% ethanol by vortexing. After centrifugation at 12,000 × *g* at 4 °C for 5 minutes, the ethanol was removed and the pellet was air-dried for 5-10 minutes. Afterwards, the RNA pellet was dissolved in 20 µL of RNase-free water and quantified using NanoDrop™2000c (Thermo Fisher).

5.2.4 Reverse Transcription-Quantitative PCR (RT-qPCR)

Reverse transcription was performed subsequent to RNA extraction using High-Capacity cDNA Reverse Transcription Kit (Thermo Fisher) following the manufacturer's instructions. cDNA was synthesized using 1 µg of extracted total RNA and was used either immediately or stored at -20 °C until further use. The following quantitative PCR (qPCR) was performed with the GoTaq® qPCR Master Mix (Promega) by utilizing 50 ng of cDNA following the manufacturer's protocol. In detail: cDNA was diluted 1:20 in PCR grade water and 4 µL of this dilution was combined with 6 µL of GoTaq® qPCR master mix combined with the appropriate qPCR primer pair with a total concentration of 0.5 µM of each primer. A total volume of 10 µL was added to a 96-well plate and technical replicates per target gene were tested. GAPDH or HPRT acted as housekeeping reference genes and the primer pairs are listed in 5.1.10. Data were analyzed with the comparative Ct values (ΔΔCT) method and represented as fold change of the gene expression[344].

5.2.5 Western Blot

Proteins were extracted from 1.5-3.0 × 10^6 cells that were harvested with trypsination as described earlier. The cell pellet was washed once with 1X PBS and was lysed in 100 µL radio-immunoprecipitation assay buffer (RIPA) buffer[345] supplied with cOmplete™ Protease Inhibitor Cocktail (Roche) for 15 minutes on ice. Insoluble material was removed by centrifugation at 13,000 × *g* at 4 °C for 10 minutes and the supernatant transferred into a new microcentrifuge tube. The cell lysate was snap-frozen and kept at -20 °C or -80 °C for short- or long-term storage, respectively, until further use. The quantification of the total protein concentration was performed using the Pierce™ BCA Protein Assay Kit (Thermo

Scientific) according to the manufacturer's protocol. The procedure required the preparation of a series of bovine serum albumin (BSA) standards in the range of 0.025 mg/mL to 2 mg/mL for a standard curve and the samples dilutions that fit within this range. In addition, a working solution was prepared by mixing Reagent A (sodium carbonate, sodium bicarbonate, BCA, sodium tartrate) and Reagent B (copper(II) sulfate pentahydrate) in a 50:1 ratio. Standards and samples (10 µL each) were pipetted into a microplate, followed by the addition of 200 µL of the working solution. The plate was incubated at 37 °C for 30 minutes in the dark and the absorbance at 562 nm was measured using the Spark® Multimode Microplate Reader (Tecan). Protein concentrations of samples were determined by comparing their absorbance values to the standard curve. 20-30 µg of protein was separated by SDS-polyacrylamide gel electrophoresis (SDS-PAGE). Sample preparation was conducted by 1:4 dilution of the desired protein amount with 4X NuPAGE™ LDS Sample Buffer, followed by denaturation at 95 °C for 10 minutes. The samples, together with 8 µL of the protein marker PageRuler™ Prestained Protein Ladder (Thermo Fisher), were loaded on a 10% Tris-glycine polyacrylamide gel and electrophoreses was performed in 1X SDS running buffer for 90 minutes at 120 V. Separated proteins were electroblotted from the gel onto an Immobilon®-P PVDF membrane (Merck Millipore), pre-activated with 100% methanol and equilibrated in 1X transfer buffer, using an electroblotter set at 90 V for 90 minutes. The successful transfer of the proteins to the membrane was checked by incubating the membrane in Ponceau S solution for 2 minutes with gentle agitation. Ponceau S staining was removed by rinsing the membrane with ddH_2O, followed by blocking for 30 minutes at room temperature with either 5% non-fat dry milk or 5% BSA in TBST (Tris-buffered saline, 0.1% Tween 20) buffer, depending on the antibody used. Thereafter, incubation with primary antibody solution was performed overnight at 4 °C under constant, gentle shaking. For washing, the membrane was rinsed three times with TBST buffer for 10 minutes per washing step. Subsequently, the blot was incubated with the appropriate HRP-conjugated mouse or rabbit secondary antibody (Sigma-Aldrich) diluted in the used blocking buffer for one hour at room temperature. After three additional washings in TBST buffer, Clarity™ Western ECL Substrate (Bio-Rad) was used according to the manufacturer's instruction. In detail, the kit components Clarity Western Peroxide Reagent and the Clarity Western Luminol/Enhancer Reagent were mixed in a 1:1 ratio and the membrane was incubated in this substrate solution for 5 minutes in the dark. The Bio-Rad ChemiDoc™ MP Imaging System was used for chemiluminescence detection and visualization. GAPDH, Vinculin or β-actin served as loading controls. All antibodies used are listed in 5.1.3.

5.2.6 Real-time live-cell imaging and analysis

Stable shRNA knockdown 501-mel cells were plated at 1.5×10^3 cells per well in a 96-well plate, one day before induction. The addition of doxycycline occurred to a final concentration of 2 µg/mL, while control cells remained untreated. Cell growth was analyzed over 5 days using the IncuCyte S3 System, and cell confluency was measured as an indicator of growth using the IncuCyte Software 2019B Rev2.

Stable shNT-Ma-Mel-86c cells were plated at 1.5 × 10^3 cells per well in a 96-well plate, one day before induction. Doxycycline (2 µg/mL) was added and control cells remained untreated. The cell growth behaviour was monitored for 6 days using the IncuCyte® ZOOM System (Essen BioScience). Data for growth curves were analyzed using the IncuCyte® ZOOM Software 2018A.

5.2.7 Transwell Invasion Assay

In a Transwell invasion assay, the cell invasion ability of 501-mel shRNA knockdown and cells was evaluated. Therefore, FluoroBlok™ 24-well Transwell inserts were used and the membrane was first pre-coated with 100 µL of the solubilized basement membrane matrix matrigel (Corning) with a concentration of 300 µg/mL diluted in coating buffer solution (0.01 M Tris-HCl pH 8.0, 0.7% NaCl). After incubation for 2 hours at 37 °C, the residual matrigel was removed to fully prepare the membrane for the Transwell assay. One day prior to seeding, cells were starved in serum-free medium overnight. For seeding, the cells were detached, resuspended in serum-free medium and counted. A total of 4-6 × 10^4 cells per condition were gently added to the membrane in 300 µL of serum-free medium, ensuring no direct contact with the membrane surface, and allowed to settle for 10 minutes. The lower chambers were filled with 700 µL medium supplemented with 10% FBS and 1 µM lysophosphatidic acid and the plate was incubated for 48 hours at 37 °C. The inserts containing the transmigrated cells were incubated with 2 µg/mL Calcein AM (Abcam) in HBSS at 37 °C for 10 minutes to stain the cells, followed my imaging using a DeltaVision Elite Imaging System (GE Healthcare) configured with an Olympus IX-71 stand and run with the softWoRx 7.2.0 software. A total of 10 images per insert were taken with the use of a 10X objective to capture all transmigrated cells on the membrane. Two technical replicates per conditions were performed for each independent experiment. GRASLND knockdown- or empty vector/shLacZ control-shRNA 501-mel cells were treated with doxycycline (2 µg/mL) for 72 hours prior to the Transwell invasion assay. Quantification of transmigrated cells including image processing, coloring and cell counting was performed using the following automated macro in ImageJ (FIJI) according to Hanniford *et al.* with slight changes[346].

5.2.7.1 Processing Code

```
macro "Batch Convert to Binary" {
dir = getDirectory("Choose a Directory ");
list = getFileList(dir);
setBatchMode(true);
for (i=0; i<list.length; i++) {
path = dir+list[i];
open(path);
```

```
run("Brightness/Contrast...");
setMinAndMax(157, 2669);
run("Apply LUT");
run("Merge Channels...", "c2=["+list[i]+"]");
run("Sharpen");
' newdir=getDirectory("Choose a Directory");
' MkDir newdir
save(path+"-colourised.png");
setBatchMode(false);
run("Close");
}}
```

5.2.7.2 Counting Code

```
macro “Batch Convert to Binary” {
dir = getDirectory (“Choose a Directory”);
list = getFileList (dir);
setBatchMode (true);
for (i = 0; i < list.length; i++) {
path = dir + list [i];
open (path);
run (“8-bit”);
setAutoThreshold ();
run (“Threshold.”);
setThreshold (20, 255);
run (“Convert to Mask”);
setThreshold (255, 255);
run (“Watershed”);
run (“Analyze Particles.”, “size = 400-Infinity circularity =
0.00–1.00 show = Outlines display clear summarize”);
dotIndex = lastIndexOf(path, “.”);
if (dotIndex! = −1)
path = substring (path, 0, dotIndex);//remove extension
save (path+“−20_bin.tif ”); close ();
}}
setBatchMode (false);
```

5.2.8 Flow Cytometry

5.2.8.1 Cell staining and measurement

Stable shRNA knockdown 501-mel, Ma-Mel-86c and Ma-Mel61a cells were harvested at defined time points after doxycycline induction (2 µg/mL) and IFNγ treatment (50 or 500 IU/mL), followed by two washing steps with 1X PBS. Surface staining was carried out by incubation of the cells with anti-HLA-ABC-APC antibody (25 ng/sample, clone W6/32, Invitrogen) diluted in FACS buffer (10% FBS in 1X PBS) at 4 °C for one hour in the dark. The cells were washed twice with FACS buffer and fixed with 4% paraformaldehyde prior measurement. Flow Cytometry was performed using the SH800S Cell Sorter (Sony Biotechnology). Control samples consisted of unstained and untreated cells. The mean fluorescence intensity (MFI) was analyzed with RStudio as described in 5.2.8.2, and the relative MFI was determined by normalizing the MFI of treated cells to their corresponding control cells, resulting in the fold change.

5.2.8.2 Data analysis using R

Analysis of flow cytometry data was performed using RStudio (Version 4.3.0) and an R script generated by Dr. Tzu-Chen Lin (Technical University of Dortmund). Flow cytometry standard files (FCS) were imported and the following Bioconductor packages were loaded: flowCore (2.0.0)[347], flowClust (3.26.0)[348,349], flowDensity (1.22.0)[350], flowStats (4.0.0)[351] and ggcyto (1.16.0)[352]. The Tidyverse packages (1.3.0) were used to process the fluorescence intensity data collected from selected populations. Initial identification of cell populations was performed using t-mixture models and singlet cells were then gated with a robust linear model (rlm). A boundary filter was implemented and data including mean, median, and standard deviation values were extracted. The data were then visualized as histograms.

5.2.9 RNA Sequencing

5.2.9.1 Library Preparation

Libraries were constructed using QIAseq Stranded RNA Lib Kit UDI (Qiagen) in accordance with the handbook instructions. In detail: total RNA was extracted using TRIzol™ Reagent as described in 5.2.3 RNA Extraction, RNA concentration was determined with the Nanodrop™ 2000c and the quality was evaluated using the 260/280 and 260/230 ratios. The QIAseq FastSelect -rRNA HMR Kit (Qiagen) was used to deplete ribosomal RNA (rRNA) from total RNA samples to enrich for mRNA and other non-ribosomal RNAs. Total RNA (1 µg) was diluted in nuclease-free water and combined with 5X RT buffer to obtain a volume of 37 µL as per the manufacturer's instructions. The reaction was well mixed by pipetting and briefly centrifuged. According to the fragmentation/depletion protocol assuming high quality RNA and a desired insert size of 150-250 bp, the reaction mix was incubated for 15 minutes at 95 °C,

followed by incubation at 75 °C, 70 °C, 65 °C, 60 °C, 55 °C, 37 °C and 25 °C for 2 minutes each and cooled down to 4 °C.

Immediately, the first-strand synthesis was performed by adding 1 µL DTT (0.4 M), 1 µL RT enzyme and 1 µL RNase Inhibitor to the fragmentation/depletion reaction. After mixing by pipetting, this first-strand reaction was incubated at 25 °C for 10 minutes, at 42 °C for 15 minutes and at 70 °C for 15 minutes before it was cooled to 4 °C. Then, 56 µL of resuspended QIAseq Beads were added to each sample, followed by vortexing for 3 seconds and a brief centrifugation. The samples were incubated for 5 minutes at room temperature and placed on a magnetic rack, allowing the solution to clear. The supernatant was carefully removed and discarded, followed by two washing steps of the beads containing the DNA of interest. Each washing step included the addition of 200 µL of 80% ethanol, gentle rotation of the tube three times and careful removal of all traces of ethanol. The beads were air-dried for 5 minutes at room temperature with the tubes uncapped and kept on the magnetic rack. Elution of the DNA from the beads was carried out by adding 40 µL nuclease-free water and thorough mixing by pipetting. With the use of the magnetic rack, 38.5 µL of the DNA-containing supernatant was transferred to a clean tube.

For the second-strand synthesis, end-repair and A-addition, all of the first-strand reaction (38.5 µL) was thoroughly mixed with 5 µL of 10X Second Strand buffer and 6.5 µL Second Strand Enzyme Mix and incubated at 25 °C for 30 minutes and at 65 °C for 15 minutes. Afterwards, 70 µL of resuspended QIAseq beads were added to the sample and mixed by pipetting. Subsequent to incubation for 5 minutes at room temperature, the tubes were placed on a magnetic rack and the supernatant removed carefully after the solution was cleared. The beads were washed twice with 200 µL 80% ethanol and air-dried for 5 minutes, as described earlier. DNA elution from the magnetic beads was carried out by adding 52 µL of nuclease-free water, followed by placing the tube back on the magnetic rack. Once the solution cleared, 50 µL of the supernatant was carefully collected and transferred to a clean tube. The reaction was stored at -20 °C until further use.

The strand-specific ligation was performed using QIAseq Unique Dual-Index (UDI) adapter, which were diluted 1:12.5 with RNase-free water, based on the input RNA of 1 µg. For the reaction, the second-strand reaction was mixed with 2 µL of diluted adapter with a unique adapter for each sample, 25 µL of 4X Ultralow Input Ligation Buffer, 5 µL of Ultralow Input Ligase, 6.5 µL of Ligation Initiator and 11.5 µL of nuclease-free water to have a total volume of 100 µL. After full mixing by pipetting, the reaction was incubated at 25 °C for 10 minutes, followed by the addition of 80 µL resuspended QIAseq beads and incubation for 5 minutes at room temperature. As in the previous steps, the beads were washed twice with 80% ethanol, air-dried and the DNA was eluted using 92 µL nuclease-free water. 90 µL of the supernatant was transferred to a fresh tube and another round of DNA cleaning was performed with 108 µL of resuspended beads. Finally, the DNA was eluted with 25 µL of nuclease-free water and a final of 23.5 µL was transferred to a fresh tube. The samples were stored at -20 °C until further use.

For the CleanStart library amplification, all of the strand-specific ligation reaction was mixed with 25 µL of 2X CleanStart PCR Mix and 1.5 µL of CleanStart PCR Primer Mix. The cycling conditions for the PCR reaction were as follows: CleanStart decontamination by incubation at 37 °C for 15 minutes, initial denaturation at 98 °C for 2 minutes, 11 cycles of the PCR consisting of denaturation (98 °C, 20 s),

annealing (60 °C, 30 s) and extension (72 °C, 30 s) and a final extension at 72 °C for 1 minute. Subsequently, the reaction clean-up was performed using 60 µL of resuspended QIAseq beads and the same procedure as described before. The elution was carried out with 22 µL nuclease-free water to obtain a final amount of 20 µL of the library suitable for RNA sequencing. Libraries were sent to the Sequencing Core Facility at the Max Planck Institute for Molecular Genetics in Berlin for sequencing with an Illumina NovaSeq 6000 PE150, producing a minimum of 3×10^7 reads for each sample (see Supplementary Table 2).

5.2.9.2 Analysis

Analysis of RNA sequencing data were performed by Shashank Tiwari, M.Sc. (Max Planck Institute, Dortmund). Raw fastq files were obtained from the Sequencing Core Facility and processed with the zarp pipeline[353]. FastQC, zpca, and MultiQC (https://github.com/zavolanlab/zpca) are used in this pipeline to perform quality control[354,355]. For the adapter trimming Cutadapt was used[356]. The alignment of reads to the human genome (hg38, Genome Reference Consortium GRCh38) was carried out using STAR, followed by quantification with Salmon[357,358]. A count matrix is produced as the final output and is utilized as input for the R package DESeq2 to detect differentially expressed genes[359]. Genes with a logFoldChange exceeding 1 and an adjusted *p*-value below 0.05 are considered for further analysis. The EnhancedVolcano R-package and the ComplexHeatmap package were used for generating volcano plots and heatmaps, respectively[360,361]. For gene set enrichment analysis (GSEA), gene sets from the msigdbr R package (https://CRAN.R-project.org/package=msigdbr) were needed, as well as clusterProfiler and enrichplot for generating the gene set enrichment plots[362,363].

5.2.10 RNA Pulldown

GRASLND RNA pulldown was carried out using biotinylated antisense DNA probes and following the protocol established by Dimartino *et al.* with some modifications[266]. Antisense DNA probes were designed using an online probe designer (singlemoleculefish.com), with parameters set for target GC content between 40-50%, oligonucleotide length of 20, and spacing length of 40-60. Human melanoma 501-mel cells were grown until confluency in 15 cm plates for each sample needed (probe set “odd,” probe set “even” and probe set “lacZ Control”). The cells were harvested, the pellet was washed twice with 1X PBS and cell lysates were prepared using a lysis buffer consisting of 50 mM HEPES (pH 7.5), 150 mM KCl, 0.5% IGEPAL, 0.5 mM DTT and 2 mM EDTA, supplemented with complete protease inhibitor cocktail (1X, Roche). After incubation of the cells with lysis buffer for 15 minutes on ice, the lysate was centrifuged at 300 × *g* for 5 minutes at 4 °C. The supernatant was carefully removed and transferred into a clean tube. Dynabeads™ MyOne™ Streptavidin C1 magnetic beads (Thermo Fisher) were calibrated for RNA applications according to the manufacturer’s protocol. In detail, the beads were resuspended in 1 mL of a solution of 100 mM NaOH and 50 mM NaCl, incubated for 2 minutes at room

temperature and the tube was placed on a magnetic rack. After a clear solution was obtained, the supernatant was removed and discarded. This washing step was repeated once with the same solution, another time with a 100 mM NaCl solution and once with lysis buffer. These calibrated beads were subsequently blocked (lysis buffer with 100 µg/mL salmon sperm DNA, 5% BSA, 0.02 µg/mL heparin) by incubation at 4 °C for 30 minutes on a rotating wheel. This is followed by three washing steps with 1 mL of hybridization buffer (50 mM Tris-HCl, pH 7.4, 150 mM NaCl, 1 mM $MgCl_2$, 0.05% IGEPAL, 10 mM EDTA, 1 mM DTT) including protease and RNase inhibitor (Promega) using the magnetic rack as described above. Further, 500 µL of lysates were pre-cleared by adding 20 µL blocked beads and 500 µL 2X hybridization buffer, and incubation at 4 °C for 30 minutes while rotating. A combination of five biotinylated oligonucleotides per probe set ("odd," "even" and "lacZ Control"), each at 60 µM, was mixed with the pre-cleared lysates and incubated with rotation at room temperature for 80 minutes. Afterwards, 200 µL of blocked beads were added to each sample and incubated at room temperature for 30 minutes while rotating. The following five washing steps include the resuspension with 1 mL of 1X hybridization buffer, incubation for 4 minutes at room temperature, placing the tube on the magnetic rack and removal and discarding the supernatant. In the last washing step, beads were divided in two tubes for subsequent RNA and protein analysis, respectively. For the RNA sample, the elution from the beads was enabled by the addition of 500 µL TRIzol™ Reagent and RNA extraction was performed as described in 5.2.3. For the protein analysis by Western blot, the beads were incubated with 30 µL 1X NuPAGE LDS sample buffer at 95 °C for 10 minutes. The samples were placed on the magnetic rack and the protein-containing supernatant was transferred to a clean tube, ready to proceed with the protein analysis, described in section 5.2.5. Sequences of the biotinylated oligonucleotides are listed in 5.1.9. The control lacZ sequences were adapted from Dimartino *et al*.[266].

5.2.11 Mass Spectrometry

5.2.11.1 On-bead tryptic digestion of proteins bound to bead-immobilized GRASLND RNA

Following the RNA pulldown described in section 5.2.10, the beads containing the pulled-down proteins were washed detergent-free by performing three additional washing steps with 1X PBS. For on-bead tryptic digestion of proteins bound to the bead-immobilized GRASLND, 50 µL of denaturing/reducing buffer (8 M Urea, 50 mM Tris pH 7.5, 1 mM DTT) was added to the beads and incubated for 30 minutes at room temperature while shaking at 350 rpm. To this solution, 5.55 µL of 10X Alkylation solution (50 mM chloroacetamide in Denaturing/Reducing buffer) was added, to obtain a final chloroacetamide concentration of 5 mM per sample. This mixture was also incubated for 30 minutes at room temperature under gentle shaking at 350 rpm. This was followed by the first digestion with Lys-C, by adding a total amount of 1 µg of this enzyme per sample and incubation for one hour at 37 °C while shaking at 350 rpm. The tube was placed on a magnetic rack and the supernatant was carefully removed and transferred to a new low protein binding tube. 185 µL of 50 mM Tris buffer (pH 7.5) containing 1 µg of trypsin was added to the beads, followed by incubation at 37 °C with shaking at 350 rpm for 1 hour. The tube was placed on a magnetic rack and the supernatant was carefully removed and combined with the previous supernatant containing the Lys-C digest. Another 2 µg trypsin was added and the reaction was incubated

overnight at 37 °C while shaking at 350 rpm. To stop the reaction, 20 µL of 10% trifluoroacetic acid (TFA) was added to obtain a final concentration between 0.5 and 1%. Peptides were desalted using C18 StageTips, as follows. First, the StageTip was created by stacking two C18 disks (Affinisep) in a small Petri dish and by using a specialized syringe for StageTips. The two layers of disks were punched out and transferred into a yellow pipette tip. The StageTip was activated by adding 100 µL of 100% methanol, followed by centrifugation until the solution completely passed through the tip. The subsequent washing step was carried out with 100 µL of a solution of 80% acetonitrile (ACN) and 0.1% formic acid (FA). After centrifugation, two washing steps with 100 µL of 0.1% FA each were performed and the tip was centrifuged without allowing the tip to dry. The samples were loaded onto the StageTip and incubated for one minute before centrifugation, ensuring that the tip did not dry. The tips were washed with 100 µL of 0.1% FA and centrifuged until no solution remained at the top. For elution, 20 µL of a solution of 80% acetonitrile and 0.1% FA was added, followed by a one-minute incubation and centrifugation at 8,000 rpm for 5 minutes to collect the eluate in clean low protein binding tubes. This step was repeated, and the eluates were combined. Samples were then dried in a SpeedVac at 30°C for approximately one hour.

5.2.11.2 Nano-HPLC-MS/MS

The following Nano-HPLC-MS/MS measurement as well as the further analysis of the proteomics data was carried out by Dr. Petra Janning, project group leader of the mass spectrometry group (Department 4 of the Max Planck Institute, Dortmund).

The tryptic and dried peptides were reconstituted in 0.1% TFA (20 µL) and analyzed using nano-HPLC-MS/MS. An Ultimate 3000 RSLC nano-HPLC system, coupled with a Hybrid-Orbitrap Q Exactive HF mass spectrometer was used (Thermo Fisher, Germany). After injection of an aliquot (3 µL) of the peptide solution on a C18 PepMap 100 column (5 mm, 100 Å, 300 mm ID * 5 mm, Dionex), the peptides were enriched using 0.1% TFA at a flow rate of 30 µL/min for 5 minutes. Separation was performed on a C18 PepMap 100 column (3 µm, 100 Å, 75 µm ID × 50 cm) using a linear gradient of 5-20% ACN/H_2O and 0.1% FA over 110 minutes, followed by 20-32% ACN/H_2O and 0.1% FA over 20 minutes, at a flow rate of 300 nL/min. The nano-HPLC system was connected online with the mass spectrometer via a nano-emitter with a 10 µm tip diameter. Mass spectra were recorded in the m/z range of 375 to 1500 with a resolution of 120,000 for full scan, followed by up to fifteen high-energy collision-dissociation (HCD) MS/MS scans of the most intense ions with at least a double charge, at a resolution of 15,000.

5.2.11.3 Data Analysis

Relative protein quantification was performed using MaxQuant v.2.2.0.0, incorporating the Andromeda search algorithm[364]. This software package simultaneously searched the *Homo sapiens* reference proteome from the UniProt database and a built-in contaminants database. In summary, an MS/MS ion search was conducted for tryptic enzymatic cleavage, permitting up to two missed cleavages. Carbamidomethylation was specified as a fixed modification, while methionine oxidation and N-terminal acetylation were considered variable modifications. The mass accuracy threshold was set to 20 parts per million (ppm) for the initial search and 4.5 ppm for the second search. The false discovery rate (FDR) for peptide and protein identification was set to 0.01. Proteins were considered for further analysis only if at least two peptides were quantified. Relative protein quantification was achieved using the label-free quantification (LFQ) algorithm available in MaxQuant. Proteins were filtered out if they were not identified in at least one run with a minimum of 2 "razor+unique" peptides, if they were from the reverse database, or if they were identified solely by side chains.

Statistical data analysis of these proteomics data were carried out using the software platform Perseus v.2.0.11.0[365]. The LFQ intensities were first log-transformed (log2) and replicate samples, four of each (“odd”, “even” and “lacZ”) were grouped. Subsequently, a pairwise comparison between the groups “lacZ” vs. “odd” and “lacZ” vs. “even” were performed individually. All proteins that did not have at least three LFQ quantifications in at least one of the two groups being compared were filtered out. Missing values (original LFQ was “0”) were replaced with small normally distributed values. A width of 0.3 and a downshift of 1.8 were used for this purpose. Afterwards, the groups were compared with each other using a two-sided t-test (FDR = 0.01 and S_0 = 1). Volcano plots were created using the VolcaNoseR web app[366]. Proteins with log2-fold changes > 1.5 and $-\text{Log}_{10}\ p > 3$ were considered as statistically significant enriched.

Re-analysis of proteomics data focusing on PKR peptides was performed by Siska Führer, M.Sc. (Max Planck Institute, Dortmund) using the generated raw files. These were processed to generate mzML format using the MSConvertGUI (64bit) package in ProteoWizard[367]. For the protein identification search, FragPipe V21.1 with MSFragger version 4.0, IonQuant version 1.10.12 and Philosopher version 5.1.0 was used[368–372]. Individual peptide visualization of PKR (E2AK2) was conducted using MSstatsShiny[373].

5.2.12 TCGA Analysis

All bioinformatic analyses was performed by Shashank Tiwari, M.Sc. (Max Planck Institute, Dortmund).

5.2.12.1 GRASLND Expression Analysis

The TCGA-SKCM database provided the RNA-Seq data used for GRASLND expression analysis in skin cutaneous melanoma. Gene expression data from 471 melanoma patients, processed with STAR alignment, was downloaded from the GDC TCGA-SKCM data portal (https://portal.gdc.cancer.gov/projects/TCGA-SKCM), released in August 2023. A total of 701 healthy samples were obtained from the GTEx database (https://gtexportal.org/home/). The differential gene expression analysis was performed using the DESeq2 package[359]. Genes were classified as differentially expressed if they had a Log2FoldChange > 1 and a multiple testing-corrected *p*-value < 0.1. (Benjamini–Hochberg). The TPM counts were used to create the violin plot and the significance level was assessed using the Wilcoxon rank-sum test across 471 tumor samples and 701 healthy control samples.

5.2.12.2 Kaplan-Meier Survival Curve

TCGA-SKCM tumor data were divided into two subsets according to the GRASLND RNA expression level in VST-transformed expression data (from DESeq2), with one group having expression levels ≥ median and the other having expression levels < median. The Kaplan-Meier method was employed for survival analysis of the data, using the TCGA Biolinks package[374].

5.2.12.3 Analysis of Tumor CD8+ T-Cell Infiltration and Immunogenic Gene Correlations

TCGA-SKCM tumor data from 471 patients were grouped based on the presence of CD8A transcripts in immunological hot and cold tumors. The volcano plot was generated using the EnhancedVolcano[360] and shows the fold changes and *p* values of transcripts in hot (CD8A, top 10%) *versus* cold tumors (CD8A, bottom 10%), consistent with the analysis conducted by Li *et al.*[185]. Two-sided t-tests were employed to perform the statistical analysis.

Gene set enrichment analysis of 232 GRASLND^{high} melanoma patient samples (see 5.2.12.2) was performed using the Hallmark pathway gene sets as described in section 5.2.9.2. Top 15 upregulated and top 14 downregulated pathways are illustrated.

Single gene set enrichment analysis was conducted on GRASLND^{high} melanoma patient samples (n = 232) for genes associated with immune response activation, leukocyte-mediated immunity, and lymphocyte-mediated immunity, in accordance with the methods described by Li *et al.*[185]. The curves

illustrate the accumulated enrichment scores, whereas the bars show the positions of genes connected to particular pathways. The bottom section presents the distribution of fold changes in conjunction with the gene list.

5.2.13 Spearman Correlation Analysis

The correlation between GRASLND and other genes was assessed using Spearman correlation analysis on normalized counts obtained from the Wouters dataset[60]. This analysis was performed by Shashank Tiwari, M.Sc. (Max Planck Institute, Dortmund) using R.

5.2.14 T Cell Activation Assay

The CD8+ T cell co-culture experiment was performed in collaboration with the lab of Prof. Dr. Annette Paschen at the University Hospital in Essen (UKE, Department of Dermatology) conducted by Dr. Beatrice Thier. The experiment was carried out using an established protocol as described by Thier *et al.*[287] and Ma-Mel-61a GRASLND shRNA knockdown and control cells generated in this work were provided for this assay. In brief: Tumor-reactive bulk CD8+ T cells derived from the peripheral blood of patient Ma-Mel-61 were isolated using anti-CD8 MicroBeads (Miltenyi Biotec) and 1×10^6 T cells were co-cultured with 1×10^5 irradiated autologous Ma-Mel-61b melanoma cells in AIM-V medium (Gibco/BRL) supplemented with 10% (v/v) human serum at 5% CO_2 and 37°C. Recombinant human IL-2 (500 IU/mL) was added on day 3. Re-stimulation of CD8+ T cells with irradiated melanoma cells was performed at weekly intervals. Ma-Mel-61a GRASLND shRNA knockdown and control cells were treated with IFNγ (500 U/mL) and/or doxycycline (2 µg/mL) for 6 days. Melanoma cells were harvested and washed thoroughly with PBS to remove any residual IFNγ from the treatment and were subjected to co-culturing with T cells on day 7. T cell stimulation with autologous melanoma cells was performed in a 1:1 ratio (5×10^4 cells each) for 4 hours in presence of Brefeldin A (10 µg/mL) at 5% CO_2 and 37°C. To measure CD8+ T cell activation, intracellular IFNγ staining was conducted. Therefore, fixation and permeabilization of the cells was carried out using a Fixation/Permeabilization Kit (eBioscience) followed by staining with an antibody cocktail consisting of anti-CD3-BV421 (clone UCHTI, BioLegend), anti-CD8-APC/Cy7 (clone SK1, BioLegend) and anti-IFNγ-PE (clone B27, BioLegend). Subsequent analysis and data processing were performed using the Gallios flow cytometer and the Kaluza software (Beckman Coulter).

6. Supplementary Data

6.1 Tables

Table 1: Significance testing for GRASLND RNA expression was conducted across nine melanoma cell lines (see Figure 10B). *Mean differences in GRASLND expression, measured by RT-qPCR, were calculated from three independent biological replicates per cell line and statistically compared with all other cell lines using a two-sided unpaired t-test. Statistically significant p-values (p<0.05) are highlighted in bold.*

Cell Line 1	Cell Line 2	p-value	Mean Cell Line 1	Mean Cell Line 2	t-Statistic
501-mel	SK-MEL-239	**0.00970**	6.978	2.062	4.645
501-mel	Ma-Mel-86c	**0.00517**	6.978	1.630	5.547
501-mel	Ma-Mel-61a	**0.00435**	6.978	1.363	5.818
501-mel	SK-MEL-147	**0.00247**	6.978	0.418	6.777
501-mel	C8161	**0.00197**	6.978	0.044	7.200
501-mel	WM1361a	**0.00196**	6.978	0.036	7.209
501-mel	Ma-Mel-86a	**0.00195**	6.978	0.026	7.221
SK-MEL-239	Ma-Mel-86c	0.38569	2.062	1.630	0.973
SK-MEL-239	Ma-Mel-61a	0.19243	2.062	1.363	1.566
SK-MEL-239	SK-MEL-147	**0.02207**	2.062	0.418	3.635
SK-MEL-239	C8161	**0.01027**	2.062	0.044	4.569
SK-MEL-239	WM1361a	**0.01012**	2.062	0.036	4.588
SK-MEL-239	Ma-Mel-86a	**0.00990**	2.062	0.026	4.617
Ma-Mel-86c	Ma-Mel-61a	**0.04752**	1.630	1.363	2.826
Ma-Mel-86c	SK-MEL-147	**0.00053**	1.630	0.418	10.141
Ma-Mel-86c	C8161	**0.00002**	1.630	0.044	22.811
Ma-Mel-86c	WM1361a	**0.00002**	1.630	0.036	23.521
Ma-Mel-86c	Ma-Mel-86a	**0.00002**	1.630	0.026	24.974
Ma-Mel-61a	SK-MEL-147	**0.00173**	1.363	0.418	7.459
Ma-Mel-61a	C8161	**0.00008**	1.363	0.044	16.224
Ma-Mel-61a	WM1361a	**0.00008**	1.363	0.036	16.626
Ma-Mel-61a	Ma-Mel-86a	**0.00006**	1.363	0.026	17.403
SK-MEL-147	C8161	**0.02686**	0.418	0.044	3.417
SK-MEL-147	WM1361a	**0.02446**	0.418	0.036	3.520
SK-MEL-147	Ma-Mel-86a	**0.02105**	0.418	0.026	3.688
C8161	WM1361a	0.88638	0.044	0.036	0.152
C8161	Ma-Mel-86a	0.70266	0.044	0.026	0.410
WM1361a	Ma-Mel-86a	0.80940	0.036	0.026	0.258

Table 2: Detailed quality control information of RNA sequencing samples.

Sample	Sample description	Total reads (millions)	Depth/ Coverage	Mapping rate (% uniquely mapped reads)
lacZR1	shLacZ, dox-induced, Rep1	41.8	2.77	85.99
lacZR2	shLacZ, dox-induced, Rep2	35.1	2.32	83.47
lacZR3	shLacZ, induced, Rep3	38.4	2.54	83.52
lacZ_ifnDoxR1	shLacZ, IFNγ-treated, dox-induced, Rep1	39.3	2.59	82.98
lacZ_ifnR1	shLacZ, IFNγ-treated, uninduced, Rep1	41.1	2.70	82.65
lacZ_ifnR2	shLacZ, IFNγ-treated, uninduced, Rep2	42.3	2.79	82.90
lacz_ifnDoxR2	shLacZ, IFNγ-treated, dox-induced, Rep2	37.2	2.46	84.04
sh4R1	sh4, dox-induced, Rep1	34.8	2.30	84.99
sh4R2	sh4, dox-induced, Rep2	48.6	3.21	84.91
sh4_ifnDoxR1	sh4, IFNγ-treated, dox-induced, Rep1	34.0	2.25	81.28
sh4_ifnDoxR2	sh4, IFNγ-treated, dox-induced, Rep2	37.6	2.48	83.51
sh4_ifnR1	sh4, IFNγ-treated, uninduced, Rep1	38.1	2.52	82.69
sh4_ifnR2	sh4, IFNγ-treated, uninduced, Rep2	46.3	3.05	83.09
sh8R1	sh8, dox-induced, Rep1	33.1	2.18	85.80
sh8R2	sh8, dox-induced, Rep2	40.7	2.69	85.08
sh8_ifnDoxR1	sh8, IFNγ-treated, dox-induced, Rep1	27.8	1.84	84.57
sh8_ifnDoxR2	sh8, IFNγ-treated, dox-induced, Rep2	35.2	2.34	82.65
sh8_ifnR1	sh8, IFNγ-treated, uninduced, Rep1	40.7	2.69	82.14
sh8_ifnR2	sh8, IFNγ-treated, uninduced, Rep2	57.6	3.82	86.28

Table 3: List of downregulated genes from HALLMARK pathways identified through GSEA of RNA-seq data following GRASLND knockdown in 501Mel cells. *Genes strongly associated with the observed phenotypes are highlighted as bold.*

HALLMARK Pathway	**Downregulated genes**
HALLMARK_ESTROGEN_RESPONSE_EARLY	RBBP8, CCND1, FDFT1, SLC22A5, RRP12, RAB17, KAZN, MYC, UNC119, BAG1, NCOR2, SLC16A1, SVIL, NAV2, DHCR7, PPIF, MYBBP1A, SCARB1, FKBP4, ITPK1, NXT1, SLC7A2, FRK, FLNB, FASN, INPP5F, SLC1A4, ADCY1, FOXC1, ABLIM1, HES1, FHL2, SLC7A5, SLC26A2, GREB1
HALLMARK_ESTROGEN_RESPONSE_LATE	RBBP8, RNASEH2A, MOCS2, CCND1, FDFT1, IMPA2, SLC22A5, GALE, BAG1, NCOR2, SGK1, SLC16A1, ISG20, DHCR7, PPIF, SCARB1, GINS2, FKBP4, ITPK1, SORD, NXT1, UGDH, XRCC3, ST6GALNAC2, FRK, CDC6, FLNB, SLC1A4, FOXC1, CKB, SLC7A5, SLC26A2
HALLMARK_DNA_REPAIR	PDE4B, CSTF3, ERCC3, TAF13, SMAD5, POLR1D, ADRM1, POLR2C, POLR1C, POLR2K, NT5C3A, MRPL40, UPF3B, POLR2G, GTF2H3, IMPDH2, SNAPC4, POLA1, POLB, SNAPC5, ERCC2, RFC5, POLR2H, APRT, POLR2J, SF3A3, PNP, SAC3D1, LIG1, POLR2E, POLD1, ADA, RNMT, RPA2, POLA2, RFC2, RAE1, NUDT21, NCBP2, NME1, ZWINT, TYMS, REV3L, POLR2F, TAF12, ALYREF, TMED2, POLR2D, SSRP1, UMPS, RAD51, GTF2H1, FEN1, PCNA, RALA, PRIM1, GTF2A2, RFC3, RFC4
HALLMARK_FATTY_ACID_METABOLISM	UROD, IDH3B, CRYZ, PDHA1, HCCS, HPGD, MDH2, CPOX, DHCR24, HADH, HSPH1, SDHD, MIF, METAP1, ACO2, HMGCS1, ERP29, ADSL, ACAT2, UROS, APEX1, ME1, NTHL1, ECHS1, SLC22A5, CBR1, ALDH9A1, ALDOA, SMS, IDI1, GCDH, HSP90AA1, MDH1, ACSL1, RDH11, FH, ECI1, HSDL2, PRDX6, SUCLG1, UGDH, GLUL, MIX23, FASN, IDH1, LDHA, ODC1, H2AZ1
HALLMARK_UV_RESPONSE_UP	SPR, POLR2H, SLC6A8, CHKA, PDAP1, CASP3, GRPEL1, RAB27A, CNP, E2F5, EIF5, TARS1, IGFBP2, TGFBRAP1, ALDOA, ARRB2, HNRNPU, SIGMAR1, PPIF, DDX21, NUP58, ATP6V1C1, CTSV, AMD1, SOD2, H2AX, FKBP4, FEN1, CCNE1, CEBPG, STIP1, EIF2S3, ASNS, RFC4, TFRC, CHRNA5, PPAT, **CDK2**
HALLMARK_CHOLESTEROL_HOMEOSTASIS	ACTG1, HMGCS1, ACAT2, ERRFI1, CHKA, HMGCR, FDFT1, CBS, MVD, CYP51A1, FDPS, IDI1, LGMN, SQLE, DHCR7, ANXA5, PLSCR1, FASN, TMEM97, LGALS3, SCD, JAG1
HALLMARK_GLYCOLYSIS	AK4, MDH2, HMMR, MIF, RARS1, VEGFA, CENPA, CLN6, HSPA5, ERO1A, SLC25A13, ME1, TPI1, CTH, GLCE, AKR1A1, PPIA, PYGB, GOT2, GALE, CYB5A, CACNA1H, TXN, RRAGD, ALDH9A1, SDC3, ALDOA, CHST6, AURKA, MDH1, ABCB6, PYGL, ISG20, SLC37A4, **CDK1**, GFPT1, ENO1, SLC25A10, POLR3K, PRPS1, PAXIP1, FKBP4, ME2, RPE, B4GALT2, DEPDC1, IDH1, MERTK, HK2, LDHA, MXI1, MET, HOMER1
HALLMARK_REACTIVE_OXYGEN_SPECIES_PATHWAY	ATOX1, NQO1, NDUFB4, PDLIM1, SOD1, HMOX2, FTL, GCLM, ERCC2, PRDX1, TXN, SRXN1, HHEX,

	SBNO2, PRDX6, TXNRD1, MBP, PRDX4, SOD2, ABCC1, GSR
HALLMARK_UNFOLDED_PROTEIN_RESPONSE	EEF2, EIF4A1, CNOT6, VEGFA, RPS14, HSPA5, EIF2S1, LSM4, FUS, ERO1A, EIF4A2, KHSRP, PDIA6, GEMIN4, TARS1, EXOSC9, SDAD1, MTREX, HSPA9, SPCS1, EXOSC4, XPOT, NOP14, EIF4E, IARS1, PARN, NHP2, EXOSC10, RRP9, NPM1, NOP56, H2AX, HSP90B1, ALDH18A1, SERP1, CEBPG, EXOSC2, PSAT1, DKC1, EIF4G1, ATF4, ASNS, SLC1A4, MTHFD2, EIF4A3, EIF4EBP1, NOLC1, SLC7A5
HALLMARK_MTORC1_SIGNALING	GPI, PSMD14, HSPA5, PSMA4, HMGCS1, NUFIP1, NMT1, ERO1A, DDIT3, ME1, PPA1, BUB1, TPI1, PRDX1, HMGCR, PNP, PDAP1, WARS1, PLK1, ABCF2, CTH, CANX, PPIA, PSME3, CYP51A1, ALDOA, IMMT, SDF2L1, IDI1, PHGDH, AURKA, HSPA9, POLR3G, ELOVL6, GGA2, RDH11, EIF2S2, PSMD12, SLC37A4, LGMN, PNO1, SQLE, DHCR7, ACACA, NFKBIB, RRM2, ETF1, SHMT2, RRP9, TXNRD1, ENO1, TUBG1, HSPE1, HSPA4, GTF2H1, MCM2, HSP90B1, SERP1, SORD, HSPD1, DHFR, GMPS, UCHL5, PSAT1, STIP1, NUP205, UNG, IDH1, ACSL3, ASNS, HK2, SLC1A4, EEF1E1, LDHA, GSR, MCM4, TFRC, MTHFD2, CACYBP, TMEM97, TOMM40, PSPH, CCT6A, PSMG1, SCD, IFRD1, CDC25A, SLC7A5
HALLMARK_G2M_CHECKPOINT	KIF22, EZH2, BUB3, LBR, WRN, BIRC5, GSPT1, EWSR1, NASP, POLE, HMGN2, SMC1A, SMARCC1, MKI67, CKS1B, MTF2, E2F2, SMC2, CDC7, MEIS2, XPO1, H2AZ2, G3BP1, SNRPD1, CUL4A, HSPA8, HMMR, ORC6, RAD23B, HIRA, TENT4A, DBF4, CENPA, NSD2, TRA2B, TFDP1, CHEK1, PRIM2, E2F1, SS18, SRSF2, AURKB, SMC4, MCM6, BUB1, BRCA2, RBM14, NUP98, E2F3, PLK1, CCND1, SRSF1, CDKN3, LIG3, SLC12A2, POLQ, KPNA2, CHAF1A, **MYC**, CDC25B, RPA2, POLA2, PRMT5, SFPQ, DTYMK, TACC3, HUS1, KIF23, AURKA, HNRNPD, CKS2, UBE2S, SYNCRIP, HNRNPU, FBXO5, KPNB1, ORC5, SQLE, **CDK1**, LMNB1, UPF1, INCENP, **CDK4**, CCNA2, ESPL1, AMD1, CDC45, EXO1, PTTG1, H2AX, GINS2, MCM2, MCM3, H2BC12, MAD2L1, DKC1, TNPO2, HMGA1, CDC6, NCL, RAD54L, MYBL2, ODC1, NOLC1, H2AZ1, CDC25A, SLC7A5, SLC7A1
HALLMARK_OXIDATIVE_PHOSPHORYLATION	NDUFS7, NDUFV1, ATP5MC2, MRPS11, TIMM9, NDUFS3, NDUFB4, BAX, SDHA, PDHX, UQCRC1, IDH3B, HTRA2, ATP5F1B, PDHA1, NDUFC1, COX5B, COX15, ATP5ME, ACADSB, HCCS, NDUFB6, NDUFC2, MFN2, COX7B, ETFA, MDH2, SLC25A3, NDUFA4, SDHD, ATP5F1C, SLC25A4, ATP5PO, ATP5MC1, CS, UQCRQ, ACO2, COX4I1, GPI, ATP6V0C, NDUFV2, NDUFA8, NDUFAB1, UQCRH, GLUD1, OXA1L, COX7C, TOMM70, SLC25A6, COX11, UQCRC2, ECHS1, UQCRFS1, NDUFA7, GRPEL1, NDUFS6, FDX1, OPA1, SUPV3L1, ATP5MC3, COX5A, AIFM1, IDH3A, GOT2, CYB5A, SDHB, ATP5MF, FXN, COX7A2L, MTRR, OAT, SLC25A11, MTX2, IMMT, SLC25A5, MDH1, POLR2F, HSPA9, CYC1, TIMM17A, TOMM22, MRPL11, FH, MRPS12, ECI1, ACAT1, PRDX3, VDAC2, MRPS30, MRPS15, MRPL34, ATP5F1D, PMPCA, PHB2, ATP5F1A, VDAC1,

	ATP6V1C1, TIMM13, LRPPRC, SUCLG1, LDHB, MRPL35, AFG3L2, IDH1, CYCS, LDHA, DLAT, TIMM50
HALLMARK_E2F_TARGETS	BUB1B, KIF22, EZH2, CCP110, RFC1, CDCA8, LBR, SMC3, BIRC5, GSPT1, CNOT9, NASP, DCK, ZW10, POLE, DCLRE1B, SMC1A, DNMT1, TBRG4, MKI67, CKS1B, RPA1, MLH1, XPO1, DEK, EED, PMS2, HELLS, HMMR, ORC6, ORC2, PAICS, DSCC1, TRA2B, ANP32E, NUP153, CHEK1, EIF2S1, PRIM2, SRSF2, AURKB, SMC4, MCM6, BRCA2, RNASEH2A, RAD1, MRE11, PLK1, LIG1, CIT, SRSF1, DLGAP5, CDKN3, POLD1, MMS22L, USP1, GINS1, E2F8, XRCC6, EXOSC8, ASF1B, SLBP, KPNA2, MYC, PNN, CDC25B, RPA2, POLA2, SHMT1, AK2, RFC2, NUDT21, PHF5A, NME1, TACC3, HUS1, AURKA, HNRNPD, ATAD2, CKS2, UBE2S, KIF18B, SYNCRIP, IPO7, CENPM, SNRPB, DONSON, TK1, NAP1L1, CTPS1, RAN, GINS3, CDK1, LMNB1, MSH2, RRM2, CDK4, BRCA1, ESPL1, WEE1, PRKDC, TUBB, UBE2T, SSRP1, TUBG1, NUP107, NOP56, PTTG1, PRPS1, PRDX4, H2AX, POP7, MCM2, PCNA, CSE1L, CCNE1, DCTPP1, MELK, TIPIN, MCM3, MCM7, MAD2L1, RAD51AP1, PSMC3IP, DEPDC1, CHEK2, POLD2, NUP205, UNG, HMGA1, LYAR, GINS4, RFC3, MCM4, PA2G4, TFRC, MTHFD2, MYBL2, RANBP1, TRIP13, NOLC1, H2AZ1, CDC25A
HALLMARK_MYC_TARGETS_V2	TCOF1, DDX18, TFB2M, PES1, NOC4L, PLK1, RRP12, SUPV3L1, GRWD1, PPAN, MYC, RABEPK, PPRC1, NOP16, SLC19A1, PUS1, WDR74, UTP20, FARSA, GNL3, IMP4, BYSL, MYBBP1A, RCL1, CDK4, AIMP2, RRP9, NPM1, WDR43, SLC29A2, NOP56, HSPE1, IPO4, DCTPP1, SORD, NOP2, HSPD1, PRMT3, NDUFAF4, MRTO4, UNG, HK2, MCM4, PA2G4, TMEM97, SRM, NOLC1
HALLMARK_MYC_TARGETS_V1	EPRS1, BUB3, EIF3D, SNRPB2, RACK1, PCBP1, SRSF7, NCBP1, GSPT1, SRSF3, SF3B3, PSMA1, PSMD1, PSMA2, PSMB2, SMARCC1, MRPS18B, CBX3, MRPL23, IMPDH2, STARD7, XPO1, DEK, G3BP1, ABCE1, EIF4A1, SNRPD1, VBP1, SLC25A3, ILF2, EIF1AX, CSTF2, SF3A1, RPS10, RAD23B, SSBP1, ORC2, EIF4G2, PSMD14, RRM1, PSMA4, TRA2B, PSMD7, DDX18, TFDP1, PSMD3, RNPS1, EIF2S1, NDUFAB1, SNRPD3, UBE2E1, SRSF2, APEX1, MCM6, TOMM70, RPS5, HNRNPR, ACP1, CCT3, CCT7, SRSF1, CNBP, HNRNPC, LSM7, ERH, USP1, CANX, RPL6, PPIA, SSB, UBA2, KARS1, XRCC6, COX5A, AP3S1, PRPF31, KPNA2, GOT2, **MYC**, PPM1G, EIF4H, EEF1B2, TARDBP, RPL22, EIF3J, NOP16, PSMA7, NCBP2, SNRPG, NME1, PABPC1, FBL, RPS6, HNRNPD, TYMS, HDAC2, SERBP1, CYC1, SYNCRIP, HNRNPU, KPNB1, TCP1, XPOT, CCT4, EIF2S2, RPS3, RPLP0, GNL3, NAP1L1, EIF4E, IARS1, PRDX3, CTPS1, RAN, NHP2, RSL1D1, TRIM28, DDX21, PHB2, **CDK4**, SET, PTGES3, ETF1, RPS2, AIMP2, VDAC1, SNRPA1, RRP9, CCNA2, CCT5, HSP90AB1, SRPK1, NPM1, NOP56, HSPE1, CDC45, RUVBL2, RPL14, PRDX4, CCT2, TUFM, MCM2, PCNA, GLO1, MCM7, SNRPA, HSPD1, MAD2L1, POLD2, PABPC4, C1QBP, EXOSC7, HNRNPA1, PRPS2, LDHA, RFC4, MCM4, PA2G4, SRM, RANBP1, ODC1, NOLC1, IFRD1, H2AZ1, CDK2

Table 4: List of upregulated genes from HALLMARK pathways identified through GSEA of RNA-seq data following GRASLND knockdown in 501Mel cells. *Genes strongly associated with the observed phenotypes are highlighted in bold.*

HALLMARK Pathway	**Upregulated genes**
HALLMARK_APICAL_JUNCTION	GNAI1, IRS1, JUP, YWHAH, GNAI2, ITGA10, CDH3, ITGA9, SYK, TRO, CERCAM, FSCN1, ADAM23, MYH9, PBX2, CTNNA1, TMEM8B, ICAM1, ACTN4, B4GALT1, VASP, STX4, NECTIN2, NECTIN3, CRAT, MAPK11, ITGA3, BMP1, MSN, SKAP2, SGCE, SPEG, ITGB1, AKT3, PARVA, MAPK14, THBS3, RSU1, CTNND1, CD99, NECTIN1, IKBKG, SHC1, CD276, NLGN2, ZYX, TJP1, NF1
HALLMARK_COAGULATION	A2M, MMP14, S100A13, CTSB, GSN, LRP1, USP11, MSRB2, SPARC, CRIP2, KLF7, FURIN, TIMP1, BMP1, CPQ, TF, ANXA1
HALLMARK_EPITHELIAL_MESENCHYMAL_TRANSITION	SNTB1, FUCA1, MMP14, MATN3, LGALS1, LRP1, CD59, CCN2, TNFAIP3, SPARC, TPM4, WIPF1, COPA, TIMP1, SGCB, LAMC1, P3H1, BMP1, SERPINE2, COL6A2, ITGB5, RHOB, ITGB1, ECM1, **TGFB1**, EMP3, PCOLCE, GADD45B
HALLMARK_IL6_JAK_STAT3_SIGNALING	A2M, IL6ST, PDGFC, STAT2, IFNAR1, TNFRSF21, IL10RB, HMOX1, **STAT3**, TNFRSF1A, SOCS3, STAM2, **TGFB1**, PIM1, IRF9, TYK2, IL13RA1, ACVR1B
HALLMARK_WNT_BETA_CATENIN_SIGNALING	PTCH1, GNAI1, NKD1, PPARD, LEF1, NUMB, HDAC5, AXIN2, NCSTN, HEY1, HEY2, FRAT1
HALLMARK_COMPLEMENT	CBLB, MMP14, S100A13, DOCK9, CTSB, GNAI2, RASGRP1, LRP1, DOCK4, CD59, TNFAIP3, PLA2G4A, GNG2, CD55, CASP4, PDP1, TIMP1, STX4, CALM3, DGKH, PSEN1, CD46, LIPA, CPQ, CASP7, USP8, VCPIP1, PIM1, CDK5R1, DGKG, USP15, EHD1, CASP9, BRPF3
HALLMARK_KRAS_SIGNALING_UP	GPRC5B, FUCA1, JUP, ETV1, TMEM158, ABCB1, TFPI, ETV5, TNFAIP3, CCSER2, SDCCAG8, RABGAP1L, HDAC9, GLRX, MAP7
HALLMARK_TNFA_SIGNALING_VIA_NFKB	**SMAD3**, PNRC1, NR4A2, TSC22D1, CEBPD, KLF9, SLC2A3, IL6ST, FOSL2, NFIL3, TNFAIP3, LITAF, BCL6, NFAT5, BCL2A1, CFLAR, ICAM1, B4GALT1, TANK, MXD1, KDM6B, DRAM1, ZFP36, SNN, PPP1R15A, SERPINB8, RHOB, PDLIM5, **NFKB2**, SOCS3, FJX1, PER1, DNAJB4, GADD45B, BTG1, EHD1, KLF6, TIPARP, PHLDA1, TNIP1
HALLMARK_KRAS_SIGNALING_DN	PTPRJ, NR4A2, YPEL1, CPEB3, SLC29A3, ADRA2C, MAST3, COQ8A, PDK2, MFSD6, PLAG1, IDUA, SNN, CHST2
HALLMARK_HYPOXIA	SLC2A1, PNRC1, CAV1, PAM, STC1, SLC2A3, HS3ST1, TES, SDC2, WSB1, CCN2, FOSL2, NFIL3, TNFAIP3, MT2A, NDRG1, CITED2, MYH9, P4HA2, CCNG2, KLF7, GLRX, VHL, IDS, RORA, HMOX1, NAGK, ZFP36, PPP1R15A, CHST2, B3GALT6, MAP3K1, ENO3, GBE1, ZNF292, GAA, KLHL24, PIM1, PDK1
HALLMARK_IL2_STAT5_SIGNALING	PTCH1, AHNAK, SNX9, SLC39A8, BMPR2, AHR, ABCB1, SYT11, CTLA4, SPRY4, SLC2A3, NFIL3, NDRG1, SNX14, CDC42SE2, RABGAP1L, ITGA6, FURIN, TNFRSF21, MXD1, ALCAM, RORA, SLC1A5, IFITM3, IKZF4, ITIH5, PRAF2, EOMES, TWSG1, RHOB, ENO3, SOCS2, ECM1
HALLMARK_MITOTIC_SPINDLE	KLC1, PREX1, ARL8A, KIFAP3, SORBS2, GSN, CYTH2, SPTBN1, DOCK4, PKD2, SUN2, NEDD9, CLIP2, FSCN1, DYNLL2, SPTAN1, PLEKHG2, MYH9, CAPZB, CSNK1D, NUMA1, AKAP13, ARHGAP27, ARHGAP5, HDAC6, ARFGEF1, ACTN4, ARHGAP29, RASA2, CLIP1, RICTOR, BCAR1, CNTRL, ALS2, ABI1, CDC42, SOS1, KIF3C, PDLIM5, CD2AP, STK38L, RAB3GAP1

HALLMARK_P53_PATHWAY	FUCA1, MXD4, TSC22D1, SLC7A11, PTPN14, S100A10, ERCC5, PLXNB2, SLC35D1, NDRG1, **CDKN2B**, IP6K2, COQ8A, PITPNC1, ZFP36L1, PERP, SERTAD3, MXD1, PRMT2, PPM1D, BLCAP, DRAM1, EPHA2, HMOX1, TSPYL2, PPP1R15A, CSRNP2, RALGDS, TXNIP, HEXIM1, TGFB1, ABCC5, CDK5R1, TRIB3, JAG2, BTG1, APAF1, RAB40C, DDB2, MKNK2, DEF6
HALLMARK_HEME_METABOLISM	RANBP10, SLC2A1, ATP6V0A1, SLC7A11, CTSB, SIDT2, EZH1, LRP10, LMO2, OPTN, TMCC2, NARF, P4HA2, BCAM, CAT, AGPAT4, ENDOD1, YPEL5, TMEM9B, ELL2, MARK3, KHNYN, PSMD9, LPIN2, NEK7, ACP5, CIR1, EIF2AK1, ARL2BP, RBM5, ADD1, SEC14L1, ALDH6A1, MGST3

6.2 Figures

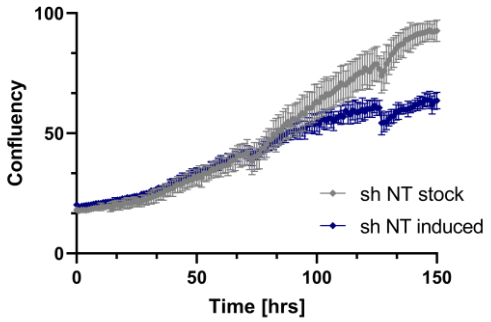

***Figure 33: Live cell monitoring of shNT-Ma-Mel-86c cells**. Ma-Mel-86c cells containing the non-targeting shRNA control sequence (shNT) were seeded one day prior to live cell monitoring. Cells were either induced with doxycycline (2 µg/mL) or left untreated (stock) and cell confluency was monitored with the IncuCyte ZOOM system. Data are represented as mean ± SD of n = 3 technical replicates.*

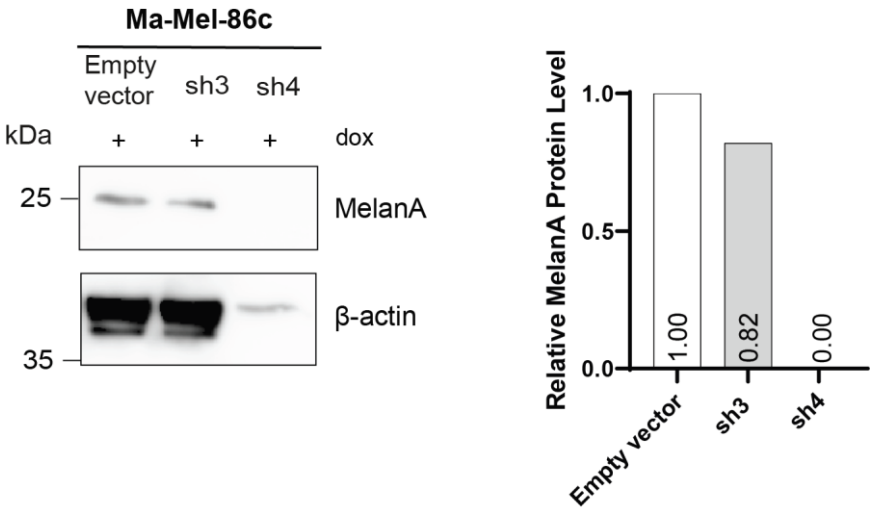

***Figure 34: Effect of GRASLND knockdown on melanocytic marker MelanA.** Stable shRNA GRASLND knockdown and empty vector control Ma-Mel-86c cells were induced for shRNA expression with doxycycline (2 µg/mL) for 72 h and the MelanA levels were analyzed by Western blotting. β-actin served as loading control. Western Blot image (left) and relative quantification (right) of MelanA levels, normalized to β-actin.*

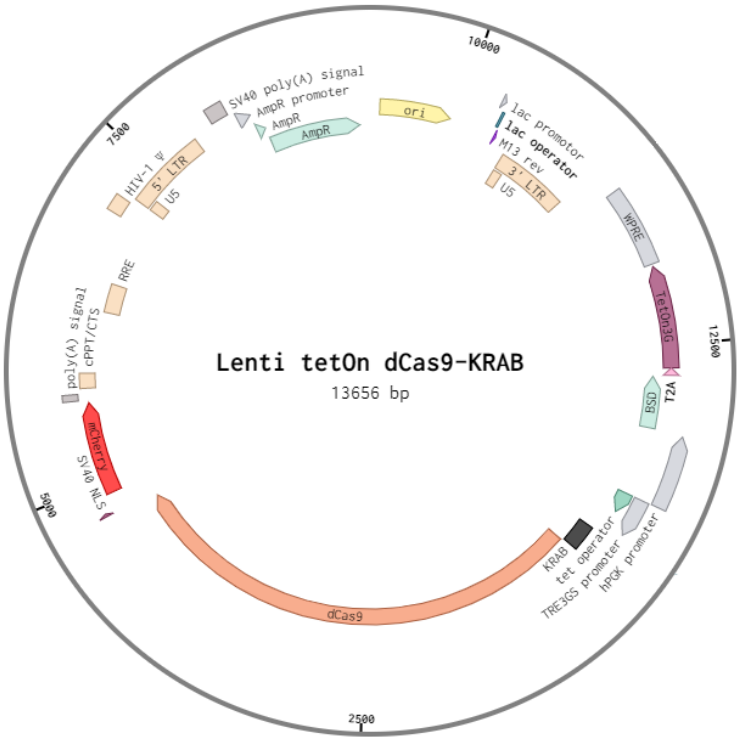

Figure 35: Plasmid map of vector Lenti tetOn dCas9-KRAB for CRISPRi. *This lentiviral expression vector enables inducible expression of a dCas9-KRAB fusion protein for CRISPR interference. It includes an mCherry fluorescent protein fused to dCas9-KRAB for visualization. Expression can be induced by tetracyclines, including doxycycline.*

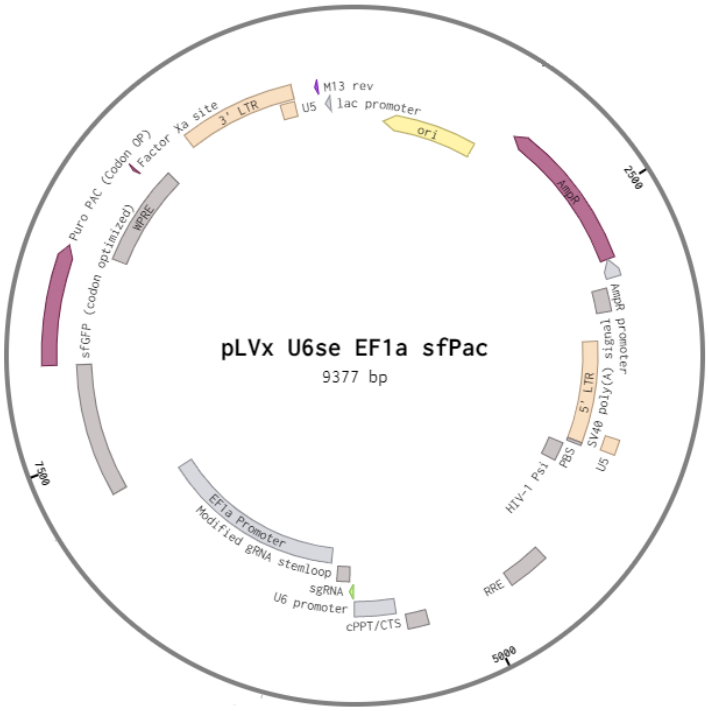

Figure 36: Plasmid map of sgRNA expression vector pLVx-U6se-EF1a-sfPac for CRISPRi. *sgRNA sequence is fused to a modified stem loop and its expression is driven by the U6 promoter. The vector contains a puro resistance (PuroR) and the green fluorescent reporter gene GFP driven by EF-1alpha promoter.*

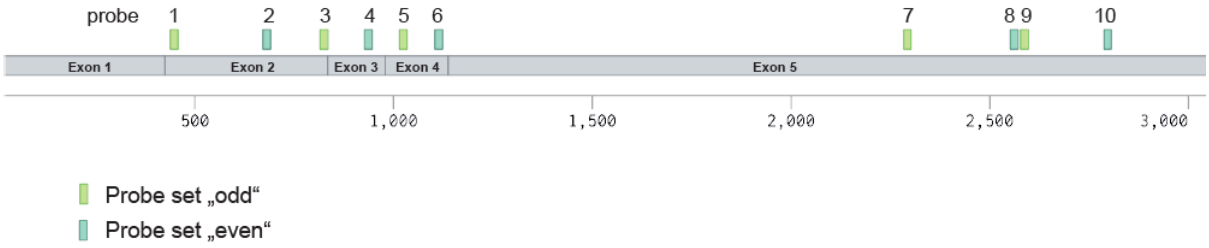

Figure 37: Schematic overview of the GRASLND target sequences of the biotinylated DNA probe sets used in GRASLND RNA pulldown experiment. *Two probe sets “odd” and “even” target GRASLND lncRNA at different exons.*

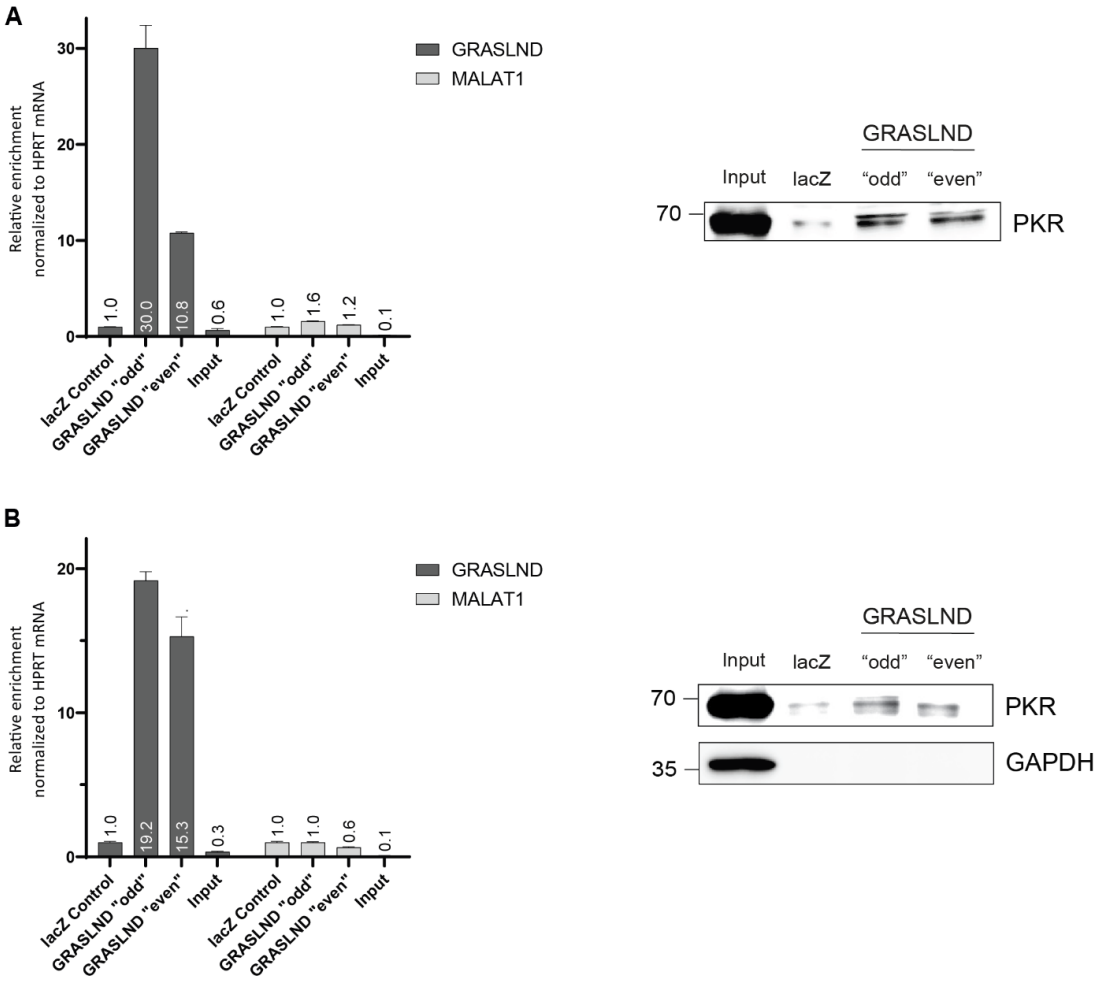

Figure 38: Additional biological replicates of GRASLND RNA Pulldown followed by PKR Western blotting. *(A) Replicate 2 of GRASLND RNA Pulldown. GRASLND and MALAT1 levels were analyzed by RT-qPCR by normalizing the expression to the levels of HPRT mRNA levels. Data are represented as mean ± SD from n = 3 technical replicates (left). GRASLND pulldown probes were subjected to Western blotting to detect PKR levels in the samples (right). (B) Replicate 3 of GRASLND RNA Pulldown. GRASLND and MALAT1 levels were analyzed by RT-qPCR by normalizing the expression to the levels of HPRT mRNA levels. Data are represented as mean ± SD from n = 3 technical replicates (left). GRASLND pulldown samples were subjected to Western blotting to detect PKR levels in the samples (right).*

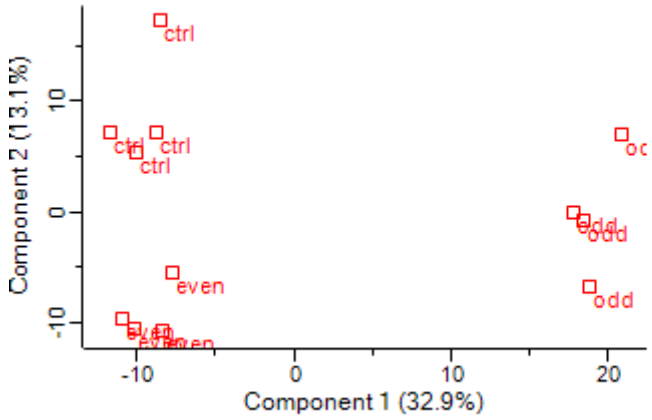

Figure 39: Principal component analysis (PCA) performed on log2-transformed label-free quantification (LFQ) intensities. *LFQ intensities were log2-transformed and the replicates were grouped accordingly. Proteins lacking three LFQ measurements in at least one group were filtered out. Original LFQ values of "0" which become undefined after logarithmic transformation were replaced by randomly generated small values according to the normal distribution of the existing values. A width of 0.3 and a down shift of 1.8 were used for this.*

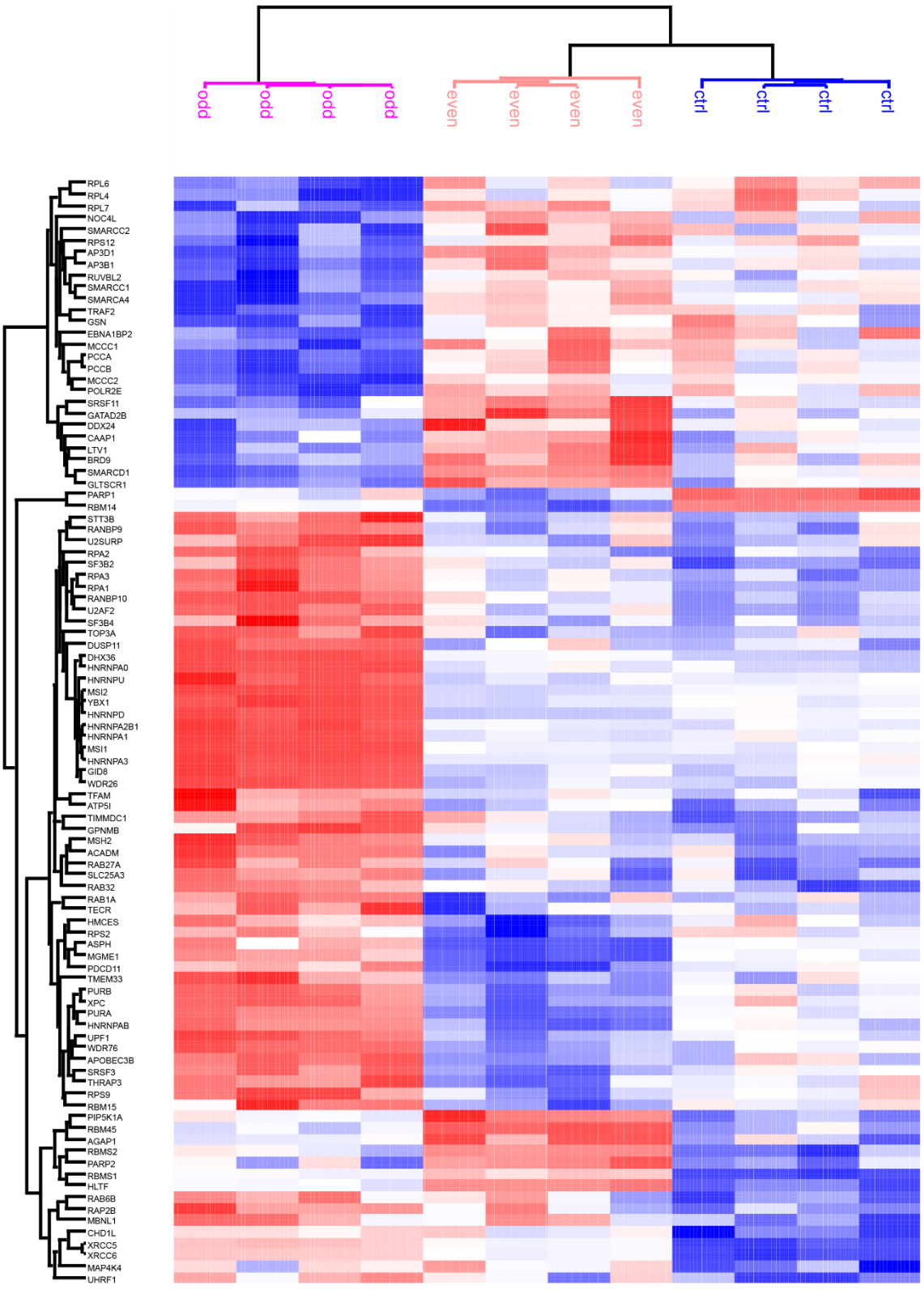

Figure 40: Evaluation of mass spectrometry data upon GRASLND pulldown in 501-mel*. Analysis was conducted across all samples and replicates. Following principal component analysis (PCA), an analysis of variance (ANOVA) was performed (S_0 = 0, using permutation-based false discovery rate (FDR) control with FDR = 0.05). Only proteins with statistically significant differences were included in the graphical representation. The median intensity of each protein is represented in white, with downward deviations in blue and upward deviations in red. Hierarchical clustering was applied to both the samples and proteins.*

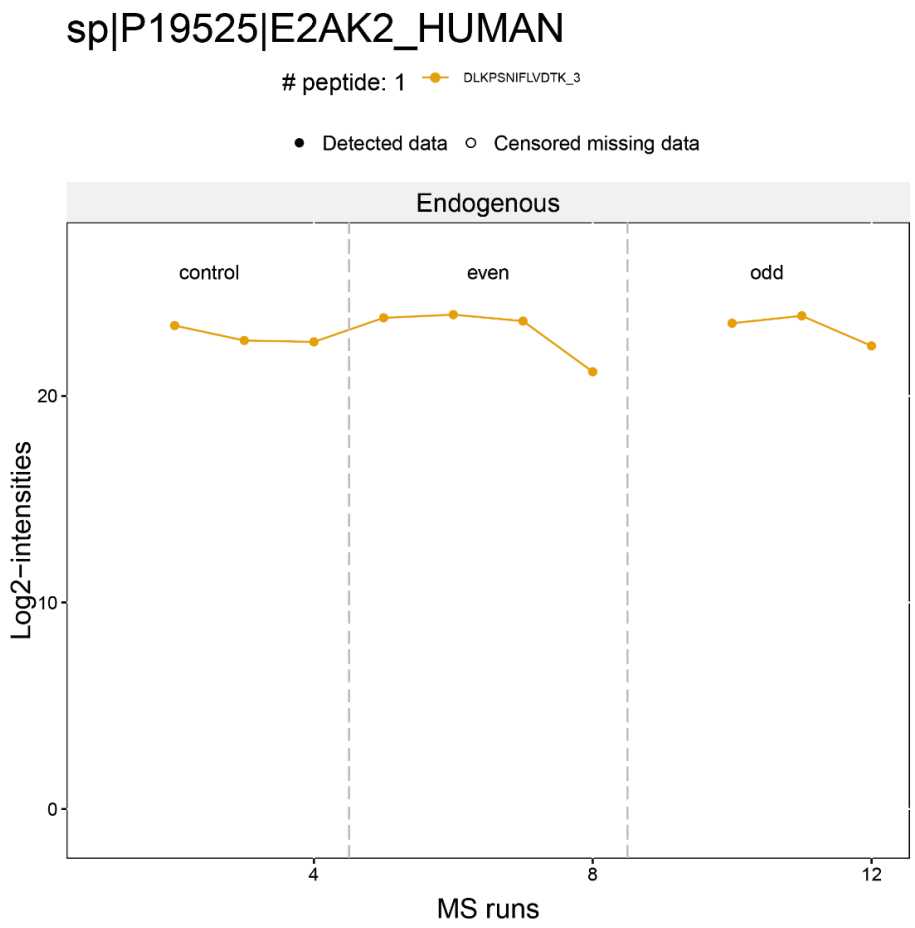

Figure 41: Re-analysis of proteomics data obtained after targeted GRASLND pulldown and mass spectrometry. *Visualized are the individual peptide levels of PKR (E2AK2) in the samples "control", "odd" and "even" with n = 4 biological replicates using MSstatsShiny.*

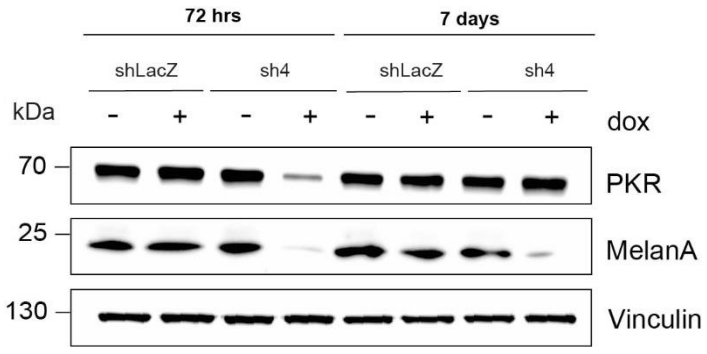

Figure 42: GRASLND downregulation affects PKR levels 501-mel melanoma cells. *PKR protein levels after shRNA-mediated GRASLND knockdown with sh4 and shLacZ in 501-mel cells after induction with doxycycline (2 µg/mL) after 72 hours and 7 days analyzed by Western blotting. MelanA levels served as evidence of dedifferentiation and Vinculin as a loading control.*

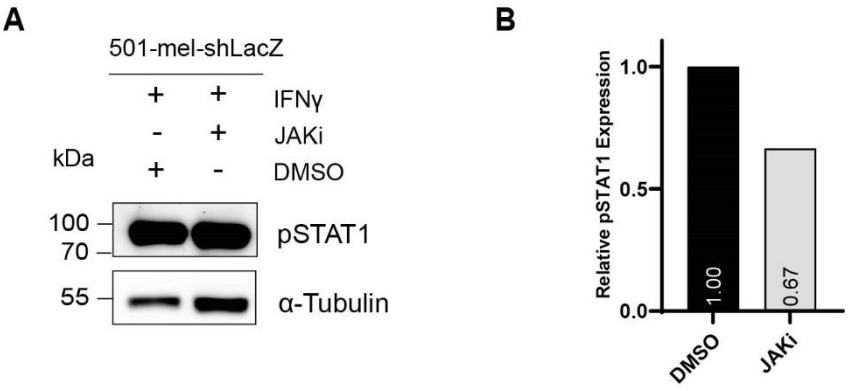

Figure 43: Confirmation of the potency of JAK inhibitor (JAKi) ruxolitinib. *(A) 501-mel-shLacZ cells were treated with IFNγ (500 U/mL) and with ruxolitinib (2 µM) simultaneously and protein levels of phosphorylated STAT1 (pSTAT1) were detected as indicator for functional JAK-STAT signaling using Western blotting. α-tubulin served as loading control. (B) Relative quantification of pSTAT1 expression by normalization to loading control levels.*

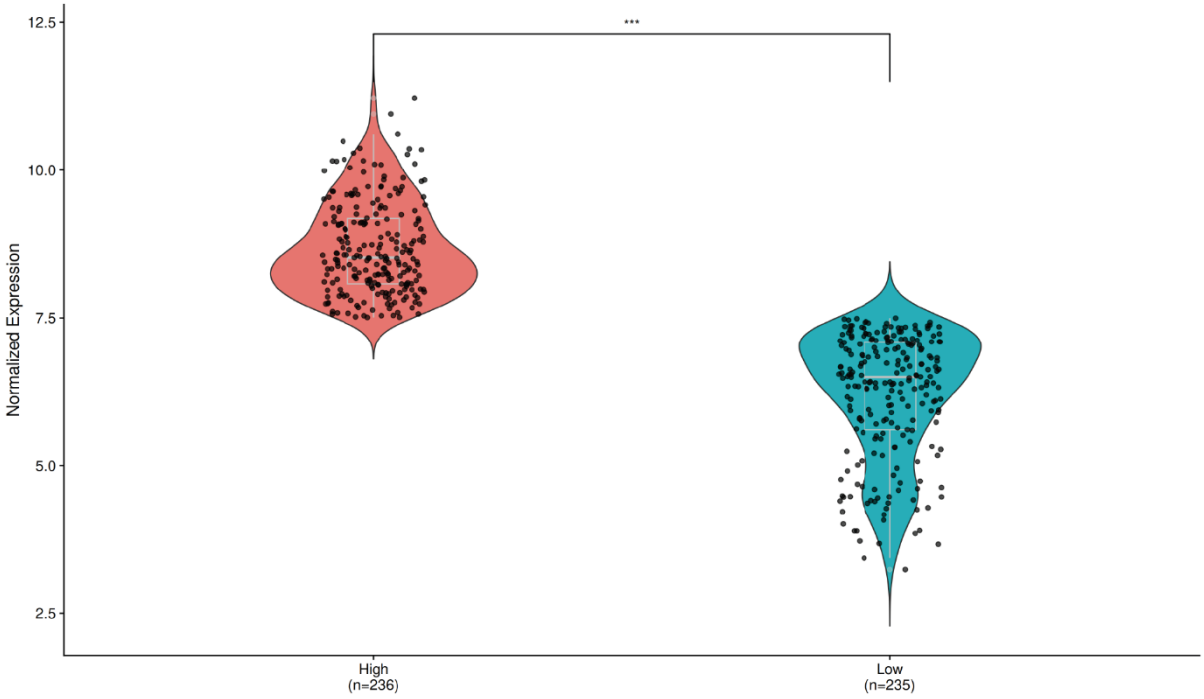

Figure 44: TCGA-SKCM tumor data grouping. *A total of 471 melanoma tumor samples were subdivided into GRASLND^{high} and GRASLND^{low} tumor cells.*

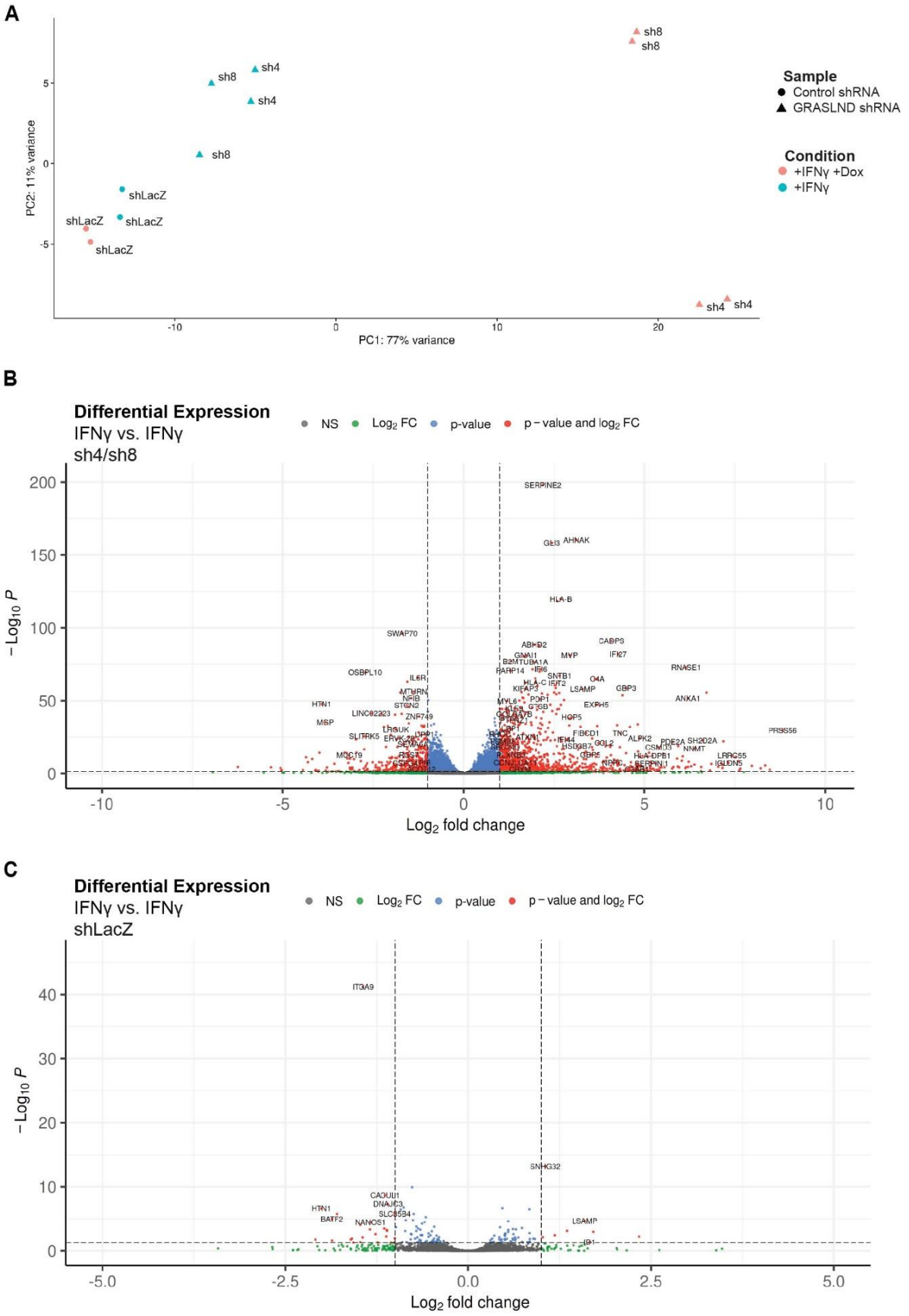

Figure 45: Transcriptomic analysis of ISGs upon GRASLND knockdown and under IFNγ. *(A) PCA plot of 501-mel shRNA knockdown and control cell lines treated with IFNγ used in RNA-Seq. Represented are two independent biological replicates of each condition (IFNγ only, IFNγ + doxycycline) and each cell line (shLacZ, sh4 and sh8). (B) Volcano plot of RNA-seq results showing differentially expressed genes following GRASLND knockdown with sh4 and sh8 in 501-mel cells for 6 days. Compared are samples treated with IFNγ alone versus cells treated with IFNγ*

and doxycycline. Genes with log2-fold changes >1 and ≤1 and an adjusted p value < 0.05 were considered statistically significant and are illustrated as red dots. NS = non-significant, FC = Fold Change. (C) Volcano plot of RNA-seq results showing differentially expressed genes following induction of control shRNA (shLacZ) in 501-mel cells for 6 days. Compared are samples treated with IFNγ alone versus cells treated with IFNγ and doxycycline. Genes with log2-fold changes >1 and ≤1 and an adjusted p value < 0.05 were considered statistically significant and are illustrated as red dots. NS = non-significant, FC = Fold Change.

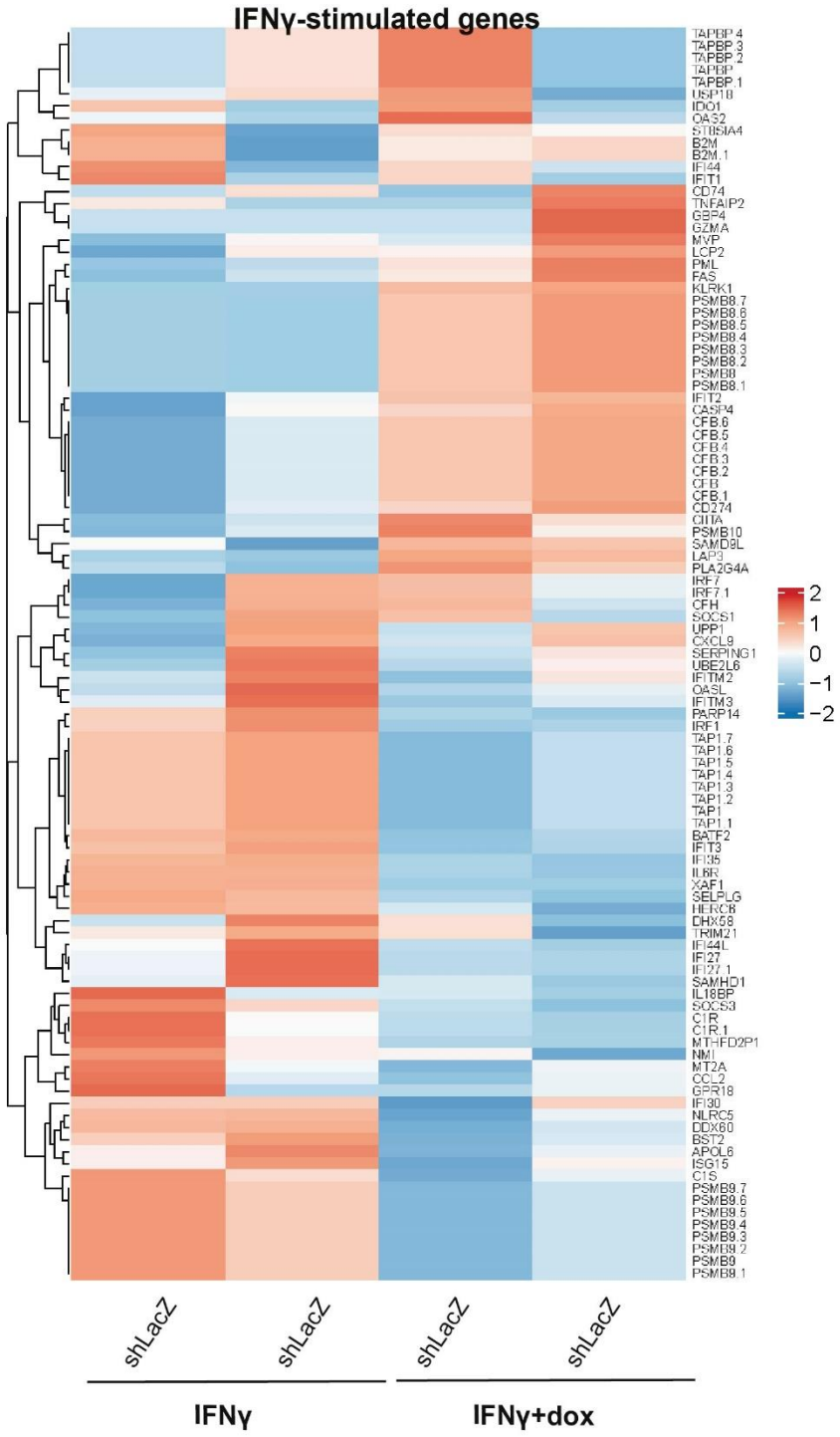

***Figure 46: Heatmap of differentially expressed ISGs of control cells**. After IFNγ treatment (500 U/mL) and doxycycline (2 µg(mL) induction of 501Mel control shRNA (shLacZ) cells for 6 days, transcript was analyzed using RNA-sequencing.*

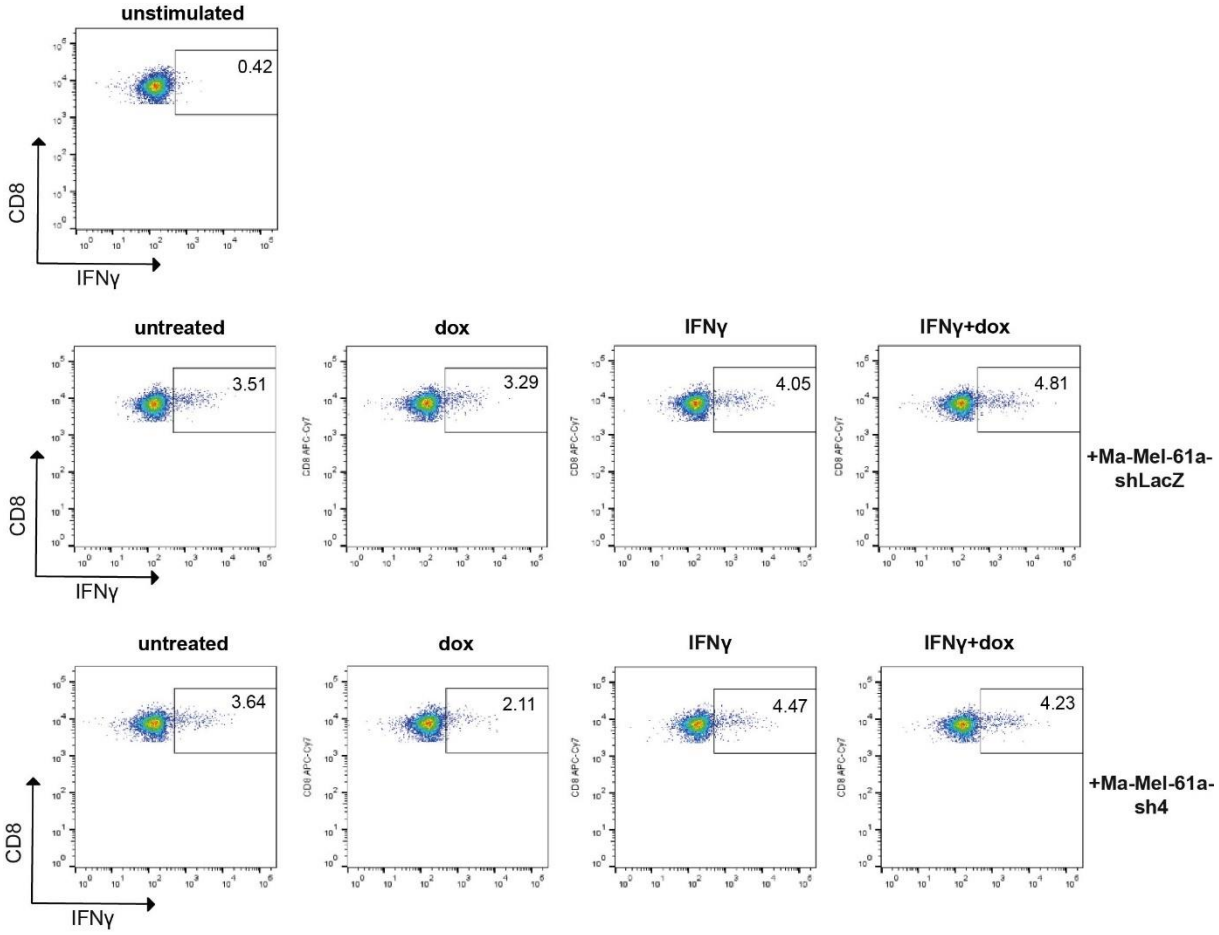

Figure 47: Replicate 2 of T cell activation assay. *Activation of autologous CD8+ T cells by Ma-Mel-61a cells was evaluated through intracellular IFNγ staining analyzed by flow cytometry. Ma-Mel-61a shRNA GRASLND knockdown (sh4) and non-targeting shRNA control cells (shLacZ) were treated for six days either with doxycycline (2 µg/mL), IFNγ (50 U/mL) or a combination of both. Untreated control cells were included, and unstimulated T cells were used as a normalization reference.. Dot plots from the second experiment out of n = 2 biological replicates are depicted.*

7. References

1. Chang, A. E., Karnell, L. H. & Menck, H. R. The National Cancer Data Base report on cutaneous and noncutaneous melanoma. *Cancer* **83,** 1664–1678; 10.1002/(SICI)1097-0142(19981015)83:8<1664::AID-CNCR23>3.0.CO;2-G (1998).
2. Cummins, D. L. *et al.* Cutaneous malignant melanoma. *Mayo Clinic proceedings* **81,** 500–507; 10.4065/81.4.500 (2006).
3. Mort, R. L., Jackson, I. J. & Patton, E. E. The melanocyte lineage in development and disease. *Development (Cambridge, England)* **142,** 620–632; 10.1242/dev.106567 (2015).
4. Clark, Wallace H., Jr., From, L., Bernardino, E. A. & Mihm, M. C. The Histogenesis and Biologic Behavior of Primary Human Malignant Melanomas of the Skin1. *Cancer research* **29,** 705–727 (1969).
5. Breslow, A. Thickness, cross-sectional areas and depth of invasion in the prognosis of cutaneous melanoma. *Annals of surgery* **172,** 902–908; 10.1097/00000658-197011000-00017 (1970).
6. Hout, F. E. M. in 't *et al.* Prognostic importance of the extent of ulceration in patients with clinically localized cutaneous melanoma. *Annals of surgery* **255,** 1165–1170; 10.1097/SLA.0b013e31824c4b0b (2012).
7. Kim, C. J., Reintgen, D. S. & Balch, C. M. The new melanoma staging system. *Cancer control : journal of the Moffitt Cancer Center* **9,** 9–15; 10.1177/107327480200900102 (2002).
8. Schuchter, L. M. Review of the 2001 AJCC staging system for cutaneous malignant melanoma. *Current oncology reports* **3,** 332–337; 10.1007/s11912-001-0086-4 (2001).
9. Ogata, D., Namikawa, K., Takahashi, A. & Yamazaki, N. A review of the AJCC melanoma staging system in the TNM classification (eighth edition). *Japanese Journal of Clinical Oncology* **51,** 671–674; 10.1093/jjco/hyab022 (2021).
10. Keung, E. Z. & Gershenwald, J. E. The eighth edition American Joint Committee on Cancer (AJCC) melanoma staging system: implications for melanoma treatment and care. *Expert Review of Anticancer Therapy* **18,** 775–784; 10.1080/14737140.2018.1489246 (2018).
11. Claps, G. *et al.* The multiple roles of LDH in cancer. *Nat Rev Clin Oncol* **19,** 749–762; 10.1038/s41571-022-00686-2 (2022).
12. Gershenwald, J. E. *et al.* Melanoma staging: Evidence-based changes in the American Joint Committee on Cancer eighth edition cancer staging manual. *CA: a cancer journal for clinicians* **67,** 472–492; 10.3322/caac.21409 (2017).
13. Amin, M. B. *et al.* The Eighth Edition AJCC Cancer Staging Manual: Continuing to build a bridge from a population-based to a more “personalized” approach to cancer staging. *CA: a cancer journal for clinicians* **67,** 93–99; 10.3322/caac.21388 (2017).
14. Rastrelli, M., Tropea, S., Rossi, C. R. & Alaibac, M. Melanoma: epidemiology, risk factors, pathogenesis, diagnosis and classification. *In vivo (Athens, Greece)* **28,** 1005–1011 (2014).
15. Elwood, J. M. & Jopson, J. Melanoma and sun exposure: an overview of published studies. *International journal of cancer* **73,** 198–203; 10.1002/(sici)1097-0215(19971009)73:2<198::aid-ijc6>3.0.co;2-r (1997).
16. Gandini, S. *et al.* Meta-analysis of risk factors for cutaneous melanoma: II. Sun exposure. *European journal of cancer (Oxford, England : 1990)* **41,** 45–60; 10.1016/j.ejca.2004.10.016 (2005).
17. Gandini, S. *et al.* Meta-analysis of risk factors for cutaneous melanoma: I. Common and atypical naevi. *European journal of cancer (Oxford, England : 1990)* **41,** 28–44; 10.1016/j.ejca.2004.10.015 (2005).
18. Titus-Ernstoff, L. *et al.* Pigmentary characteristics and moles in relation to melanoma risk. *International journal of cancer* **116,** 144–149; 10.1002/ijc.21001 (2005).
19. Zocchi, L. *et al.* Familial Melanoma and Susceptibility Genes: A Review of the Most Common Clinical and Dermoscopic Phenotypic Aspect, Associated Malignancies and Practical Tips for Management. *Journal of clinical medicine* **10**; 10.3390/jcm10163760 (2021).
20. Gruis, N. A. *et al.* Homozygotes for CDKN2 (p16) germline mutation in Dutch familial melanoma kindreds. *Nature genetics* **10,** 351–353; 10.1038/ng0795-351 (1995).

21. Zuo, L. *et al.* Germline mutations in the p16INK4a binding domain of CDK4 in familial melanoma. *Nature genetics* **12,** 97–99; 10.1038/ng0196-97 (1996).

22. Rhodes, A. R. Risk Factors for Cutaneous Melanoma. *JAMA* **258,** 3146; 10.1001/jama.1987.03400210088032 (1987).

23. Manson, J. E., Rexrode, K. M., Garland, F. C., Garland Cedric, F. & Weinstrock, M. A. The Case for a Comprehensive National Campaign to Prevent Melanoma and Associated Mortality. *Epidemiology* **11,** 728–734 (2000).

24. Curtin, J. A. *et al.* Distinct sets of genetic alterations in melanoma. *The New England journal of medicine* **353,** 2135–2147; 10.1056/NEJMoa050092 (2005).

25. Viros, A. *et al.* Improving melanoma classification by integrating genetic and morphologic features. *PLoS medicine* **5,** e120; 10.1371/journal.pmed.0050120 (2008).

26. Shain, A. H. & Bastian, B. C. From melanocytes to melanomas. *Nature reviews. Cancer* **16,** 345–358; 10.1038/nrc.2016.37 (2016).

27. Leonardi, G. C. *et al.* Cutaneous melanoma: From pathogenesis to therapy (Review). *International journal of oncology* **52,** 1071–1080; 10.3892/ijo.2018.4287 (2018).

28. Hodis, E. *et al.* A landscape of driver mutations in melanoma. *Cell* **150,** 251–263; 10.1016/j.cell.2012.06.024 (2012).

29. Chappell, W. H. *et al.* Ras/Raf/MEK/ERK and PI3K/PTEN/Akt/mTOR inhibitors: rationale and importance to inhibiting these pathways in human health. *Oncotarget* **2,** 135–164; 10.18632/oncotarget.240 (2011).

30. Pratilas, C. A. *et al.* (V600E)BRAF is associated with disabled feedback inhibition of RAF-MEK signaling and elevated transcriptional output of the pathway. *Proceedings of the National Academy of Sciences of the United States of America* **106,** 4519–4524; 10.1073/pnas.0900780106 (2009).

31. Ascierto, P. A. *et al.* The role of BRAF V600 mutation in melanoma. *Journal of translational medicine* **10,** 85; 10.1186/1479-5876-10-85 (2012).

32. Lovly, C. M. *et al.* Routine multiplex mutational profiling of melanomas enables enrollment in genotype-driven therapeutic trials. *PloS one* **7,** e35309; 10.1371/journal.pone.0035309 (2012).

33. Lee, J.-H., Choi, J.-W. & Kim, Y.-S. Frequencies of BRAF and NRAS mutations are different in histological types and sites of origin of cutaneous melanoma: a meta-analysis. *The British journal of dermatology* **164,** 776–784; 10.1111/j.1365-2133.2010.10185.x (2011).

34. Jakob, J. A. *et al.* NRAS mutation status is an independent prognostic factor in metastatic melanoma. *Cancer* **118,** 4014–4023; 10.1002/cncr.26724. (2012).

35. Goel, V. K., Lazar, A. J. F., Warneke, C. L., Redston, M. S. & Haluska, F. G. Examination of mutations in BRAF, NRAS, and PTEN in primary cutaneous melanoma. *The Journal of investigative dermatology* **126,** 154–160; 10.1038/sj.jid.5700026 (2006).

36. Fedorenko, I. V., Gibney, G. T. & Smalley, K. S. M. NRAS mutant melanoma: biological behavior and future strategies for therapeutic management. *Oncogene* **32,** 3009–3018; 10.1038/onc.2012.453 (2013).

37. Báez-Flores, J., Rodríguez-Martín, M. & Lacal, J. The therapeutic potential of neurofibromin signaling pathways and binding partners. *Communications biology* **6,** 436; 10.1038/s42003-023-04815-0 (2023).

38. Gong, H. Z., Zheng, H. Y. & Li, J. The clinical significance of KIT mutations in melanoma: a meta-analysis. *Melanoma research* **28,** 259–270; 10.1097/CMR.0000000000000454 (2018).

39. Guo, Y. *et al.* TERT Promoter Mutations and Telomerase in Melanoma. *Journal of oncology* **2022,** 6300329; 10.1155/2022/6300329 (2022).

40. Teixido, C., Castillo, P., Martinez-Vila, C., Arance, A. & Alos, L. Molecular Markers and Targets in Melanoma. *Cells* **10**; 10.3390/cells10092320 (2021).

41. Stahl, J. M. *et al.* Loss of PTEN promotes tumor development in malignant melanoma. *Cancer research* **63,** 2881–2890 (2003).

42. Hou, L. & Pavan, W. J. Transcriptional and signaling regulation in neural crest stem cell-derived melanocyte development: do all roads lead to Mitf? *Cell research* **18,** 1163–1176; 10.1038/cr.2008.303 (2008).

43. Steingrímsson, E., Copeland, N. G. & Jenkins, N. A. Melanocytes and the microphthalmia transcription factor network. *Annual review of genetics* **38,** 365–411; 10.1146/annurev.genet.38.072902.092717 (2004).

44. Hoek, K. S. *et al.* Metastatic potential of melanomas defined by specific gene expression profiles with no BRAF signature. *Pigment cell research* **19,** 290–302; 10.1111/j.1600-0749.2006.00322.x (2006).

45. Hoek, K. S. *et al.* In vivo switching of human melanoma cells between proliferative and invasive states. *Cancer research* **68,** 650–656; 10.1158/0008-5472.CAN-07-2491 (2008).

46. Kalluri, R. & Weinberg, R. A. The basics of epithelial-mesenchymal transition. *The Journal of clinical investigation* **119,** 1420–1428; 10.1172/JCI39104 (2009).

47. Rambow, F., Marine, J.-C. & Goding, C. R. Melanoma plasticity and phenotypic diversity: therapeutic barriers and opportunities. *Genes & development* **33,** 1295–1318; 10.1101/gad.329771.119 (2019).

48. Feige, E. *et al.* Hypoxia-induced transcriptional repression of the melanoma-associated oncogene MITF. *Proceedings of the National Academy of Sciences of the United States of America* **108,** E924-33; 10.1073/pnas.1106351108 (2011).

49. Dratkiewicz, E. *et al.* Hypoxia and Extracellular Acidification as Drivers of Melanoma Progression and Drug Resistance. *Cells* **10**; 10.3390/cells10040862 (2021).

50. Ferguson, J., Smith, M., Zudaire, I., Wellbrock, C. & Arozarena, I. Glucose availability controls ATF4-mediated MITF suppression to drive melanoma cell growth. *Oncotarget* **8,** 32946–32959; 10.18632/oncotarget.16514. (2017).

51. Falletta, P. *et al.* Translation reprogramming is an evolutionarily conserved driver of phenotypic plasticity and therapeutic resistance in melanoma. *Genes & development* **31,** 18–33; 10.1101/gad.290940.116. (2017).

52. Pierrat, M.-J., Marsaud, V., Mauviel, A. & Javelaud, D. Expression of microphthalmia-associated transcription factor (MITF), which is critical for melanoma progression, is inhibited by both transcription factor GLI2 and transforming growth factor-β. *The Journal of biological chemistry* **287,** 17996–18004; 10.1074/jbc.M112.358341 (2012).

53. Landsberg, J. *et al.* Melanomas resist T-cell therapy through inflammation-induced reversible dedifferentiation. *Nature* **490,** 412–416; 10.1038/nature11538 (2012).

54. Diazzi, S., Tartare-Deckert, S. & Deckert, M. The mechanical phenotypic plasticity of melanoma cell: an emerging driver of therapy cross-resistance. *Oncogenesis* **12,** 7; 10.1038/s41389-023-00452-8 (2023).

55. Müller, J. *et al.* Low MITF/AXL ratio predicts early resistance to multiple targeted drugs in melanoma. *Nature communications* **5,** 5712; 10.1038/ncomms6712 (2014).

56. Lee, J. H. *et al.* Transcriptional downregulation of MHC class I and melanoma de- differentiation in resistance to PD-1 inhibition. *Nature communications* **11,** 1897; 10.1038/s41467-020-15726-7 (2020).

57. Mehta, A. *et al.* Immunotherapy Resistance by Inflammation-Induced Dedifferentiation. *Cancer discovery* **8,** 935–943; 10.1158/2159-8290.CD-17-1178 (2018).

58. Tsoi, J. *et al.* Multi-stage Differentiation Defines Melanoma Subtypes with Differential Vulnerability to Drug-Induced Iron-Dependent Oxidative Stress. *Cancer cell* **33,** 890-904.e5; 10.1016/j.ccell.2018.03.017. (2018).

59. Boshuizen, J. *et al.* Reversal of pre-existing NGFR-driven tumor and immune therapy resistance. *Nature communications* **11,** 3946; 10.1038/s41467-020-17739-8 (2020).

60. Wouters, J. *et al.* Robust gene expression programs underlie recurrent cell states and phenotype switching in melanoma. *Nature cell biology* **22,** 986–998; 10.1038/s41556-020-0547-3 (2020).

61. Rambow, F. *et al.* Toward Minimal Residual Disease-Directed Therapy in Melanoma. *Cell* **174,** 843-855.e19; 10.1016/j.cell.2018.06.025 (2018).

62. Harbers, F. N. *et al.* Melanoma Differentiation Trajectories Determine Sensitivity toward Pre-Existing CD8+ Tumor-Infiltrating Lymphocytes. *The Journal of investigative dermatology* **141,** 2480–2489; 10.1016/j.jid.2021.03.013 (2021).

63. Peng, S. *et al.* CTLs heterogeneity and plasticity: implications for cancer immunotherapy. *Molecular cancer* **23,** 58; 10.1186/s12943-024-01972-6 (2024).

64. Platanias, L. C. Mechanisms of type-I- and type-II-interferon-mediated signalling. *Nature reviews. Immunology* **5,** 375–386; 10.1038/nri1604 (2005).

65. Castro, F., Cardoso, A. P., Gonçalves, R. M., Serre, K. & Oliveira, M. J. Interferon-Gamma at the Crossroads of Tumor Immune Surveillance or Evasion. *Frontiers in immunology* **9,** 847; 10.3389/fimmu.2018.00847 (2018).

66. Jorgovanovic, D., Song, M., Wang, L. & Zhang, Y. Roles of IFN-γ in tumor progression and regression: a review. *Biomarker research* **8,** 49; 10.1186/s40364-020-00228-x (2020).

67. Leone, P. *et al.* MHC class I antigen processing and presenting machinery: organization, function, and defects in tumor cells. *Journal of the National Cancer Institute* **105,** 1172–1187; 10.1093/jnci/djt184 (2013).

68. Maggs, L., Sadagopan, A., Moghaddam, A. S. & Ferrone, S. HLA class I antigen processing machinery defects in antitumor immunity and immunotherapy. *Trends in cancer* **7,** 1089–1101; 10.1016/j.trecan.2021.07.006 (2021).

69. Shin, D. S. *et al.* Primary Resistance to PD-1 Blockade Mediated by JAK1/2 Mutations. *Cancer discovery* **7,** 188–201; 10.1158/2159-8290.CD-16-1223 (2017).

70. Dzwierzynski, W. W. Managing malignant melanoma. *Plastic and reconstructive surgery* **132,** 446e-460e; 10.1097/PRS.0b013e31829ad411 (2013).

71. Kimbrough, C. W., McMasters, K. M. & Davis, E. G. Principles of surgical treatment of malignant melanoma. *The Surgical clinics of North America* **94,** 973-88, vii; 10.1016/j.suc.2014.07.002 (2014).

72. Wollina, U. Melanoma surgery-An update. *Dermatologic therapy* **35,** e15966; 10.1111/dth.15966 (2022).

73. Schwantes, I. R. *et al.* Metastasectomy for metastatic melanoma in the era of effective systemic therapy. *American journal of surgery* **231,** 65–69; 10.1016/j.amjsurg.2023.04.020 (2024).

74. Padma, V. V. An overview of targeted cancer therapy. *BioMedicine* **5**; 10.7603/s40681-015-0019-4 (2015).

75. Jenkins, R. W. & Fisher, D. E. Treatment of Advanced Melanoma in 2020 and Beyond. *The Journal of investigative dermatology* **141,** 23–31; 10.1016/j.jid.2020.03.943 (2020).

76. Carter, S. K. & Friedman, M. A. 5-(3,3-dimethyl-l-triazeno)-imidazole-4-carboxamide (DTIC, DIC, NSC-45388)--a new antitumor agent with activity against malignant melanoma. *European journal of cancer* **8,** 85–92; 10.1016/0014-2964(72)90087-4 (1972).

77. Atkins, M. B. *et al.* High-dose recombinant interleukin 2 therapy for patients with metastatic melanoma: analysis of 270 patients treated between 1985 and 1993. *Journal of clinical oncology : official journal of the American Society of Clinical Oncology* **17,** 2105–2116; 10.1200/JCO.1999.17.7.2105 (1999).

78. Lee, R. J., Ul-Ain-Tariq, N., Fusi, A., Bowyer, S. & Lorigan, P. The role of chemotherapy in the modern management of melanoma. *Melanoma management* **1,** 173–184; 10.2217/mmt.14.20 (2014).

79. Lo, J. A. & Fisher, D. E. The melanoma revolution: from UV carcinogenesis to a new era in therapeutics. *Science (New York, N.Y.)* **346,** 945–949; 10.1126/science.1253735 (2014).

80. Flaherty, K. T. *et al.* Inhibition of mutated, activated BRAF in metastatic melanoma. *The New England journal of medicine* **363,** 809–819; 10.1056/NEJMoa1002011 (2010).

81. Hauschild, A. *et al.* Dabrafenib in BRAF-mutated metastatic melanoma: a multicentre, open-label, phase 3 randomised controlled trial. *Lancet (London, England)* **380,** 358–365; 10.1016/S0140-6736(12)60868-X (2012).

82. Flaherty, K. T. *et al.* Improved survival with MEK inhibition in BRAF-mutated melanoma. *The New England journal of medicine* **367,** 107–114; 10.1056/NEJMoa1203421 (2012).

83. Long, G. V. *et al.* Combined BRAF and MEK inhibition versus BRAF inhibition alone in melanoma. *The New England journal of medicine* **371,** 1877–1888; 10.1056/NEJMoa1406037 (2014).

84. Guo, W., Wang, H. & Li, C. Signal pathways of melanoma and targeted therapy. *Signal transduction and targeted therapy* **6,** 424; 10.1038/s41392-021-00827-6 (2021).

85. Trojaniello, C., Luke, J. J. & Ascierto, P. A. Therapeutic Advancements Across Clinical Stages in Melanoma, With a Focus on Targeted Immunotherapy. *Frontiers in oncology* **11,** 670726; 10.3389/fonc.2021.670726 (2021).

86. Boutros, A. *et al.* The treatment of advanced melanoma: Current approaches and new challenges. *Critical reviews in oncology/hematology* **196,** 104276; 10.1016/j.critrevonc.2024.104276 (2024).

87. Tangella, L. P., Clark, M. E. & Gray, E. S. Resistance mechanisms to targeted therapy in BRAF-mutant melanoma - A mini review. *Biochimica et biophysica acta. General subjects* **1865,** 129736; 10.1016/j.bbagen.2020.129736 (2021).

88. Paraiso, K. H. T. *et al.* PTEN loss confers BRAF inhibitor resistance to melanoma cells through the suppression of BIM expression. *Cancer research* **71,** 2750–2760; 10.1158/0008-5472.CAN-10-2954 (2011).

89. Whittaker, S. R. *et al.* A genome-scale RNA interference screen implicates NF1 loss in resistance to RAF inhibition. *Cancer discovery* **3,** 350–362; 10.1158/2159-8290.CD-12-0470 (2013).

90. Wagle, N. *et al.* Dissecting Therapeutic Resistance to RAF Inhibition in Melanoma by Tumor Genomic Profiling. *Journal of clinical oncology : official journal of the American Society of Clinical Oncology* **29,** 3085–3096; 10.1200/JCO.2010.33.2312 (2011).

91. Smalley, K. S. M. *et al.* Increased cyclin D1 expression can mediate BRAF inhibitor resistance in BRAF V600E-mutated melanomas. *Molecular cancer therapeutics* **7,** 2876–2883; 10.1158/1535-7163.MCT-08-0431 (2008).

92. van Allen, E. M. *et al.* The genetic landscape of clinical resistance to RAF inhibition in metastatic melanoma. *Cancer discovery* **4,** 94–109; 10.1158/2159-8290.CD-13-0617 (2014).

93. Straussman, R. *et al.* Tumour micro-environment elicits innate resistance to RAF inhibitors through HGF secretion. *Nature* **487,** 500–504; 10.1038/nature11183 (2012).

94. Wilson, T. R. *et al.* Widespread potential for growth-factor-driven resistance to anticancer kinase inhibitors. *Nature* **487,** 505–509; 10.1038/nature11249 (2012).

95. Konieczkowski, D. J. *et al.* A melanoma cell state distinction influences sensitivity to MAPK pathway inhibitors. *Cancer discovery* **4,** 816–827; 10.1158/2159-8290.CD-13-0424 (2014).

96. Kaplan, F. M. *et al.* SHOC2 and CRAF mediate ERK1/2 reactivation in mutant NRAS-mediated resistance to RAF inhibitor. *The Journal of biological chemistry* **287,** 41797–41807; 10.1074/jbc.M112.390906 (2012).

97. Greger, J. G. *et al.* Combinations of BRAF, MEK, and PI3K/mTOR inhibitors overcome acquired resistance to the BRAF inhibitor GSK2118436 dabrafenib, mediated by NRAS or MEK mutations. *Molecular cancer therapeutics* **11,** 909–920; 10.1158/1535-7163.MCT-11-0989 (2012).

98. Villanueva, J. *et al.* Concurrent MEK2 mutation and BRAF amplification confer resistance to BRAF and MEK inhibitors in melanoma. *Cell reports* **4,** 1090–1099; 10.1016/j.celrep.2013.08.023 (2013).

99. Long, G. V. *et al.* Increased MAPK reactivation in early resistance to dabrafenib/trametinib combination therapy of BRAF-mutant metastatic melanoma. *Nature communications* **5,** 5694; 10.1038/ncomms6694 (2014).

100. Poulikakos, P. I. *et al.* RAF inhibitor resistance is mediated by dimerization of aberrantly spliced BRAF(V600E). *Nature* **480,** 387–390; 10.1038/nature10662 (2011).

101. Jiang, C. C. *et al.* MEK-independent survival of B-RAFV600E melanoma cells selected for resistance to apoptosis induced by the RAF inhibitor PLX4720. *Clinical cancer research : an official journal of the American Association for Cancer Research* **17,** 721–730; 10.1158/1078-0432.CCR-10-2225 (2011).

102. Anastas, J. N. *et al.* WNT5A enhances resistance of melanoma cells to targeted BRAF inhibitors. *The Journal of clinical investigation* **124,** 2877–2890; 10.1172/JCI70156 (2014).

103. Sorino, C., Iezzi, S., Ciuffreda, L. & Falcone, I. Immunotherapy in melanoma: advances, pitfalls, and future perspectives. *Frontiers in molecular biosciences* **11,** 1403021; 10.3389/fmolb.2024.1403021 (2024).

104. Sanlorenzo, M. *et al.* Melanoma immunotherapy. *Cancer biology & therapy* **15,** 665–674; 10.4161/cbt.28555 (2014).

105. Xu, J., Mu, S., Wang, Y., Yu, S. & Wang, Z. Recent advances in immunotherapy and its combination therapies for advanced melanoma: a review. *Frontiers in oncology* **14,** 1400193; 10.3389/fonc.2024.1400193 (2024).

106. Pardoll, D. M. The blockade of immune checkpoints in cancer immunotherapy. *Nature reviews. Cancer* **12,** 252–264; 10.1038/nrc3239 (2012).

107. Rowshanravan, B., Halliday, N. & Sansom, D. M. CTLA-4: a moving target in immunotherapy. *Blood* **131,** 58–67; 10.1182/blood-2017-06-741033 (2018).

108. Hodi, F. S. *et al.* Improved survival with ipilimumab in patients with metastatic melanoma. *The New England journal of medicine* **363,** 711–723; 10.1056/NEJMoa1003466 (2010).

109. Lipson, E. J. & Drake, C. G. Ipilimumab: an anti-CTLA-4 antibody for metastatic melanoma. *Clinical cancer research : an official journal of the American Association for Cancer Research* **17,** 6958–6962; 10.1158/1078-0432.CCR-11-1595 (2011).

110. Buchbinder, E. I. & Desai, A. CTLA-4 and PD-1 Pathways: Similarities, Differences, and Implications of Their Inhibition. *American journal of clinical oncology* **39,** 98–106; 10.1097/COC.0000000000000239 (2016).

111. Johnson, D. B., Peng, C. & Sosman, J. A. Nivolumab in melanoma: latest evidence and clinical potential. *Therapeutic advances in medical oncology* **7,** 97–106; 10.1177/1758834014567469 (2015).

112. Deeks, E. D. Nivolumab: a review of its use in patients with malignant melanoma. *Drugs* **74,** 1233–1239; 10.1007/s40265-014-0234-4 (2014).

113. Spain, L., Younger, E., Hatipoglu, E. & Larkin, J. Pembrolizumab in the management of metastatic melanoma. *Melanoma management* **2,** 315–325; 10.2217/mmt.15.33 (2015).

114. Rizzetto, G., Simoni, E. de, Molinelli, E., Offidani, A. & Simonetti, O. Efficacy of Pembrolizumab in Advanced Melanoma: A Narrative Review. *International journal of molecular sciences* **24**; 10.3390/ijms241512383 (2023).

115. Dummer, R. *et al.* Randomized Phase III Trial Evaluating Spartalizumab Plus Dabrafenib and Trametinib for BRAF V600-Mutant Unresectable or Metastatic Melanoma. *Journal of clinical oncology : official journal of the American Society of Clinical Oncology* **40,** 1428–1438; 10.1200/JCO.21.01601 (2022).

116. Sharma, P., Hu-Lieskovan, S., Wargo, J. A. & Ribas, A. Primary, Adaptive, and Acquired Resistance to Cancer Immunotherapy. *Cell* **168,** 707–723; 10.1016/j.cell.2017.01.017 (2017).

117. Kung, J. T. Y., Colognori, D. & Lee, J. T. Long noncoding RNAs: past, present, and future. *Genetics* **193,** 651–669; 10.1534/genetics.112.146704 (2013).

118. Quinn, J. J. & Chang, H. Y. Unique features of long non-coding RNA biogenesis and function. *Nature reviews. Genetics* **17,** 47–62; 10.1038/nrg.2015.10 (2016).

119. Wu, H., Yang, L. & Chen, L.-L. The Diversity of Long Noncoding RNAs and Their Generation. *Trends in genetics : TIG* **33,** 540–552; 10.1016/j.tig.2017.05.004 (2017).

120. Wilusz, J. E., Freier, S. M. & Spector, D. L. 3' end processing of a long nuclear-retained noncoding RNA yields a tRNA-like cytoplasmic RNA. *Cell* **135,** 919–932; 10.1016/j.cell.2008.10.012 (2008).

121. Yin, Q.-F. *et al.* Long noncoding RNAs with snoRNA ends. *Molecular cell* **48,** 219–230; 10.1016/j.molcel.2012.07.033 (2012).

122. Salzman, J., Gawad, C., Wang, P. L., Lacayo, N. & Brown, P. O. Circular RNAs are the predominant transcript isoform from hundreds of human genes in diverse cell types. *PloS one* **7,** e30733; 10.1371/journal.pone.0030733 (2012).

123. Ma, L., Bajic, V. B. & Zhang, Z. On the classification of long non-coding RNAs. *RNA biology* **10,** 925–933; 10.4161/rna.24604 (2013).

124. Zhou, M., Guo, X., Wang, M. & Qin, R. The patterns of antisense long non-coding RNAs regulating corresponding sense genes in human cancers. *Journal of Cancer* **12,** 1499–1506; 10.7150/jca.49067 (2021).

125. Preker, P. *et al.* RNA exosome depletion reveals transcription upstream of active human promoters. *Science (New York, N.Y.)* **322,** 1851–1854; 10.1126/science.1164096 (2008).

126. Preker, P. *et al.* PROMoter uPstream Transcripts share characteristics with mRNAs and are produced upstream of all three major types of mammalian promoters. *Nucleic acids research* **39,** 7179–7193; 10.1093/nar/gkr370 (2011).

127. Lubas, M. *et al.* The human nuclear exosome targeting complex is loaded onto newly synthesized RNA to direct early ribonucleolysis. *Cell reports* **10,** 178–192; 10.1016/j.celrep.2014.12.026 (2015).

128. Melo, C. A. *et al.* eRNAs are required for p53-dependent enhancer activity and gene transcription. *Molecular cell* **49,** 524–535; 10.1016/j.molcel.2012.11.021 (2013).

129. Li, W. *et al.* Functional roles of enhancer RNAs for oestrogen-dependent transcriptional activation. *Nature* **498,** 516–520; 10.1038/nature12210 (2013).

130. Li, Q. *et al.* Enhancer RNAs: mechanisms in transcriptional regulation and functions in diseases. *Cell communication and signaling : CCS* **21,** 191; 10.1186/s12964-023-01206-0 (2023).

131. Khalil, A. M. & Coller, J. *Molecular Biology of Long Non-coding RNAs* (Springer New York, New York, NY, 2013).

132. Koziol, M. J. & Rinn, J. L. RNA traffic control of chromatin complexes. *Current opinion in genetics & development* **20,** 142–148; 10.1016/j.gde.2010.03.003 (2010).

133. Kino, T., Hurt, D. E., Ichijo, T., Nader, N. & Chrousos, G. P. Noncoding RNA gas5 is a growth arrest- and starvation-associated repressor of the glucocorticoid receptor. *Science signaling* **3,** ra8; 10.1126/scisignal.2000568 (2010).

134. Kallen, A. N. *et al.* The imprinted H19 lncRNA antagonizes let-7 microRNAs. *Molecular cell* **52,** 101–112; 10.1016/j.molcel.2013.08.027 (2013).

135. Rinn, J. L. *et al.* Functional demarcation of active and silent chromatin domains in human HOX loci by noncoding RNAs. *Cell* **129,** 1311–1323; 10.1016/j.cell.2007.05.022 (2007).

136. Tsai, M.-C. *et al.* Long noncoding RNA as modular scaffold of histone modification complexes. *Science (New York, N.Y.)* **329,** 689–693; 10.1126/science.1192002 (2010).

137. Miao, H. *et al.* MALAT1 modulates alternative splicing by cooperating with the splicing factors PTBP1 and PSF. *Science advances* **8,** eabq7289; 10.1126/sciadv.abq7289 (2022).

138. Tripathi, V. *et al.* The nuclear-retained noncoding RNA MALAT1 regulates alternative splicing by modulating SR splicing factor phosphorylation. *Molecular cell* **39,** 925–938; 10.1016/j.molcel.2010.08.011 (2010).

139. Yoon, J.-H. *et al.* LincRNA-p21 suppresses target mRNA translation. *Molecular cell* **47,** 648–655; 10.1016/j.molcel.2012.06.027 (2012).

140. Park, E. & Maquat, L. E. Staufen-mediated mRNA decay. *Wiley interdisciplinary reviews. RNA* **4,** 423–435; 10.1002/wrna.1168 (2013).

141. Gong, C. & Maquat, L. E. lncRNAs transactivate STAU1-mediated mRNA decay by duplexing with 3' UTRs via Alu elements. *Nature* **470,** 284–288; 10.1038/nature09701. (2011).

142. Ma, Y., Ma, W., Huang, L., Feng, D. & Cai, B. Long non-coding RNAs, a new important regulator of cardiovascular physiology and pathology. *International journal of cardiology* **188,** 105–110; 10.1016/j.ijcard.2015.04.021. (2015).

143. Zhou, S. *et al.* Long Non-coding RNAs in Pathogenesis of Neurodegenerative Diseases. *Frontiers in cell and developmental biology* **9,** 719247; 10.3389/fcell.2021.719247. (2021).

144. Schmitt, A. M. & Chang, H. Y. Long Noncoding RNAs in Cancer Pathways. *Cancer cell* **29,** 452–463; 10.1016/j.ccell.2016.03.010. (2016).

145. Iyer, M. K. *et al.* The landscape of long noncoding RNAs in the human transcriptome. *Nature genetics* **47,** 199–208; 10.1038/ng.3192 (2015).

146. Cantile, M. *et al.* HOTAIR role in melanoma progression and its identification in the blood of patients with advanced disease. *Journal of cellular physiology* **232,** 3422–3432; 10.1002/jcp.25789 (2017).

147. Shi, Y. *et al.* Current Knowledge of Long Non-Coding RNA HOTAIR in Breast Cancer Progression and Its Application. *Life (Basel, Switzerland)* **11**; 10.3390/life11060483 (2021).

148. Ramya Devi, K. T., Karthik, D., Mahendran, T., Jaganathan, M. K. & Hemdev, S. P. Long noncoding RNAs: role and contribution in pancreatic cancer. *Transcription* **12,** 12–27; 10.1080/21541264.2021.1922071 (2021).

149. Kong, W. *et al.* Long noncoding RNA (lncRNA) HOTAIR: Pathogenic roles and therapeutic opportunities in gastric cancer. *Genes & diseases* **9,** 1269–1280; 10.1016/j.gendis.2021.07.006 (2022).

150. Martínez-Fernández, M. *et al.* Analysis of the Polycomb-related lncRNAs HOTAIR and ANRIL in bladder cancer. *Clinical epigenetics* **7,** 109; 10.1186/s13148-015-0141-x (2015).

151. Bhan, A. & Mandal, S. S. LncRNA HOTAIR: A master regulator of chromatin dynamics and cancer. *Biochimica et biophysica acta* **1856,** 151–164; 10.1016/j.bbcan.2015.07.001. (2015).

152. Zhang, Y., Chen, Z., Li, M.-J., Guo, H.-Y. & Jing, N.-C. Long non-coding RNA metastasis-associated lung adenocarcinoma transcript 1 regulates the expression of Gli2 by miR-202 to strengthen gastric cancer progression. *Biomedicine & pharmacotherapy = Biomedecine & pharmacotherapie* **85,** 264–271; 10.1016/j.biopha.2016.11.014 (2017).

153. Lu, H. *et al.* Long non-coding RNA MALAT1 modulates radiosensitivity of HR-HPV+ cervical cancer via sponging miR-145. *Tumour biology : the journal of the International Society for Oncodevelopmental Biology and Medicine* **37,** 1683–1691; 10.1007/s13277-015-3946-5 (2016).

154. Li, Q. *et al.* Disrupting MALAT1/miR-200c sponge decreases invasion and migration in endometrioid endometrial carcinoma. *Cancer letters* **383,** 28–40; 10.1016/j.canlet.2016.09.019 (2016).

155. Fan, Y. *et al.* TGF-β-induced upregulation of malat1 promotes bladder cancer metastasis by associating with suz12. *Clinical cancer research : an official journal of the American Association for Cancer Research* **20,** 1531–1541; 10.1158/1078-0432.CCR-13-1455 (2014).

156. Hirata, H. *et al.* Long Noncoding RNA MALAT1 Promotes Aggressive Renal Cell Carcinoma through Ezh2 and Interacts with miR-205. *Cancer research* **75,** 1322–1331; 10.1158/0008-5472.CAN-14-2931 (2015).

157. Hou, J., Zhang, G., Wang, X., Wang, Y. & Wang, K. Functions and mechanisms of lncRNA MALAT1 in cancer chemotherapy resistance. *Biomarker research* **11,** 23; 10.1186/s40364-023-00467-8 (2023).

158. Michalik, K. M. *et al.* Long noncoding RNA MALAT1 regulates endothelial cell function and vessel growth. *Circulation research* **114,** 1389–1397; 10.1161/CIRCRESAHA.114.303265 (2014).

159. Sun, Y. & Ma, L. New Insights into Long Non-Coding RNA MALAT1 in Cancer and Metastasis. *Cancers* **11**; 10.3390/cancers11020216 (2019).

160. Mourtada-Maarabouni, M., Pickard, M. R., Hedge, V. L., Farzaneh, F. & Williams, G. T. GAS5, a non-protein-coding RNA, controls apoptosis and is downregulated in breast cancer. *Oncogene* **28,** 195–208; 10.1038/onc.2008.373 (2009).

161. Zheng, S., Li, M., Miao, K. & Xu, H. lncRNA GAS5-promoted apoptosis in triple-negative breast cancer by targeting miR-378a-5p/SUFU signaling. *Journal of cellular biochemistry* **121,** 2225–2235; 10.1002/jcb.29445 (2020).

162. Lu, X. *et al.* Downregulation of gas5 increases pancreatic cancer cell proliferation by regulating CDK6. *Cell and tissue research* **354,** 891–896; 10.1007/s00441-013-1711-x (2013).

163. Liu, B. *et al.* lncRNA GAS5 Reverses EMT and Tumor Stem Cell-Mediated Gemcitabine Resistance and Metastasis by Targeting miR-221/SOCS3 in Pancreatic Cancer. *Molecular therapy. Nucleic acids* **13,** 472–482; 10.1016/j.omtn.2018.09.026 (2018).

164. Song, J., Shu, H., Zhang, L. & Xiong, J. Long noncoding RNA GAS5 inhibits angiogenesis and metastasis of colorectal cancer through the Wnt/β-catenin signaling pathway. *Journal of cellular biochemistry* **120,** 6937–6951; 10.1002/jcb.27743 (2019).

165. Dong, Q. *et al.* LncRNA GAS5 suppresses ovarian cancer progression by targeting the miR-96-5p/PTEN axis. *Annals of translational medicine* **9,** 1770; 10.21037/atm-21-6134 (2021).

166. Yu, Y. & Hann, S. S. Novel Tumor Suppressor lncRNA Growth Arrest-Specific 5 (GAS5) In Human Cancer. *OncoTargets and therapy* **12,** 8421–8436; 10.2147/OTT.S221305 (2019).

167. Li, N., Shi, K. & Li, W. TUSC7: A novel tumor suppressor long non-coding RNA in human cancers. *Journal of cellular physiology* **233,** 6401–6407; 10.1002/jcp.26544 (2018).

168. Shi, X. *et al.* LncRNA TUSC7 affects malignant tumor prognosis by regulating protein ubiquitination: a genome-wide analysis from 10,237 pan-cancer patients. *Transl. Cancer Res* **6,** 834–842; 10.21037/tcr.2017.08.19 (2017).

169. Hao, L., Yun, Y., Liang, R. & Yuan, G. Long non-coding RNA TUSC7 suppressed colorectal cancer progression via regulation of miR-23b/PDE7A Axis. *Clinical and investigative medicine. Medecine clinique et experimentale* **43,** E35-43; 10.25011/cim.v43i4.34703 (2020).

170. Hao, L. & Yu, H. MiR-23b inhibits cell migration and invasion through targeting PDE7A in colon cancer cells. *International Journal of Clinical and Experimental Pathology* **10,** 9436–9443 (2017).

171. Zheng, B.-H. *et al.* The Biological Function of TUSC7/miR-1224-3p Axis in Triple-Negative Breast Cancer. *Cancer management and research* **13,** 5763–5774; 10.2147/CMAR.S305865 (2021).

172. Melixetian, M., Pelicci, P. G. & Lanfrancone, L. Regulation of LncRNAs in Melanoma and Their Functional Roles in the Metastatic Process. *Cells* **11**; 10.3390/cells11030577 (2022).

173. Cai, B. *et al.* BANCR contributes to the growth and invasion of melanoma by functioning as a competing endogenous RNA to upregulate Notch2 expression by sponging miR-204. *International journal of oncology* **51,** 1941–1951; 10.3892/ijo.2017.4173 (2017).

174. Li, R. *et al.* Long non-coding RNA BANCR promotes proliferation in malignant melanoma by regulating MAPK pathway activation. *PloS one* **9,** e100893; 10.1371/journal.pone.0100893 (2014).

175. Li, Z., Tang, X. & Duan, S. Interference from LncRNA SPRY4-IT1 restrains the proliferation, migration, and invasion of melanoma cells through inactivating MAPK pathway by up-regulating miR-22-3p. *International Journal of Clinical and Experimental Pathology* **12,** 477–487 (2019).

176. Khaitan, D. *et al.* The melanoma-upregulated long noncoding RNA SPRY4-IT1 modulates apoptosis and invasion. *Cancer research* **71,** 3852–3862; 10.1158/0008-5472.CAN-10-4460 (2011).

177. Liu, T. *et al.* Clinical significance of long noncoding RNA SPRY4-IT1 in melanoma patients. *FEBS open bio* **6,** 147–154; 10.1002/2211-5463.12030 (2016).

178. Mazar, J. *et al.* The Functional Characterization of Long Noncoding RNA SPRY4-IT1 in Human Melanoma Cells. *Oncotarget* **5,** 8959–8969 (2014).

179. Leucci, E. *et al.* Melanoma addiction to the long non-coding RNA SAMMSON. *Nature* **531,** 518–522; 10.1038/nature17161 (2016).

180. Fogal, V. *et al.* Mitochondrial p32 protein is a critical regulator of tumor metabolism via maintenance of oxidative phosphorylation. *Molecular and cellular biology* **30,** 1303–1318; 10.1128/MCB.01101-09 (2010).

181. Fogal, V., Zhang, L., Krajewski, S. & Ruoslahti, E. Mitochondrial/cell-surface protein p32/gC1qR as a molecular target in tumor cells and tumor stroma. *Cancer research* **68,** 7210–7218; 10.1158/0008-5472.CAN-07-6752 (2008).

182. Han, Y. *et al.* Downregulation of lncRNA TSLNC8 promotes melanoma resistance to BRAF inhibitor PLX4720 through binding with PP1α to re-activate MAPK signaling. *Journal of cancer research and clinical oncology* **147,** 767–777; 10.1007/s00432-020-03484-4 (2021).

183. Yu, Y. *et al.* Association of Long Noncoding RNA Biomarkers With Clinical Immune Subtype and Prediction of Immunotherapy Response in Patients With Cancer. *JAMA network open* **3,** e202149; 10.1001/jamanetworkopen.2020.2149 (2020).

184. Zhou, J.-G. *et al.* Identification of 15 lncRNAs Signature for Predicting Survival Benefit of Advanced Melanoma Patients Treated with Anti-PD-1 Monotherapy. *Cells* **10**; 10.3390/cells10050977 (2021).

185. Li, G. *et al.* LIMIT is an immunogenic lncRNA in cancer immunity and immunotherapy. *Nature cell biology* **23,** 526–537; 10.1038/s41556-021-00672-3 (2021).

186. Wei, C.-Y. *et al.* Circular RNA circ_0020710 drives tumor progression and immune evasion by regulating the miR-370-3p/CXCL12 axis in melanoma. *Molecular cancer* **19,** 84; 10.1186/s12943-020-01191-9 (2020).

187. Wang, G., Lee-Yow, Y. & Chang, H. Y. Approaches to probe and perturb long noncoding RNA functions in diseases. *Current opinion in genetics & development* **85,** 102158; 10.1016/j.gde.2024.102158 (2024).

188. Jansen, R., van Embden, J. D. A., Gaastra, W. & Schouls, L. M. Identification of genes that are associated with DNA repeats in prokaryotes. *Molecular microbiology* **43,** 1565–1575; 10.1046/j.1365-2958.2002.02839.x (2002).

189. Nussenzweig, P. M. & Marraffini, L. A. Molecular Mechanisms of CRISPR-Cas Immunity in Bacteria. *Annual review of genetics* **54,** 93–120; 10.1146/annurev-genet-022120-112523 (2020).

190. Hille, F. *et al.* The Biology of CRISPR-Cas: Backward and Forward. *Cell* **172,** 1239–1259; 10.1016/j.cell.2017.11.032 (2018).

191. Doudna, J. A. & Charpentier, E. Genome editing. The new frontier of genome engineering with CRISPR-Cas9. *Science (New York, N.Y.)* **346,** 1258096; 10.1126/science.1258096 (2014).

192. Jinek, M. *et al.* A programmable dual-RNA-guided DNA endonuclease in adaptive bacterial immunity. *Science (New York, N.Y.)* **337,** 816–821; 10.1126/science.1225829 (2012).

193. Da Silva Santos, R. *et al.* CRISPR/Cas9 small promoter deletion in H19 lncRNA is associated with altered cell morphology and proliferation. *Scientific reports* **11,** 18380; 10.1038/s41598-021-97058-0 (2021).

194. Aparicio-Prat, E. *et al.* DECKO: Single-oligo, dual-CRISPR deletion of genomic elements including long non-coding RNAs. *BMC genomics* **16,** 846; 10.1186/s12864-015-2086-z (2015).

195. Lyu, Q. R., Zhang, S., Zhang, Z. & Tang, Z. Functional knockout of long non-coding RNAs with genome editing. *Frontiers in genetics* **14,** 1242129; 10.3389/fgene.2023.1242129 (2023).

196. Liu, Y. *et al.* Biallelic insertion of a transcriptional terminator via the CRISPR/Cas9 system efficiently silences expression of protein-coding and non-coding RNA genes. *The Journal of biological chemistry* **292,** 5624–5633; 10.1074/jbc.M116.769034 (2017).

197. Paralkar, V. R. *et al.* Unlinking an lncRNA from Its Associated cis Element. *Molecular cell* **62,** 104–110; 10.1016/j.molcel.2016.02.029 (2016).

198. Bikard, D. *et al.* Programmable repression and activation of bacterial gene expression using an engineered CRISPR-Cas system. *Nucleic acids research* **41,** 7429–7437; 10.1093/nar/gkt520 (2013).

199. Qi, L. S. *et al.* Repurposing CRISPR as an RNA-guided platform for sequence-specific control of gene expression. *Cell* **152,** 1173–1183; 10.1016/j.cell.2013.02.022 (2013).

200. Thakore, P. I. *et al.* Highly specific epigenome editing by CRISPR-Cas9 repressors for silencing of distal regulatory elements. *Nature methods* **12,** 1143–1149; 10.1038/nmeth.3630 (2015).

201. Pickar-Oliver, A. & Gersbach, C. A. The next generation of CRISPR-Cas technologies and applications. *Nature reviews. Molecular cell biology* **20,** 490–507; 10.1038/s41580-019-0131-5 (2019).

202. Liu, S. J. *et al.* CRISPRi-based genome-scale identification of functional long noncoding RNA loci in human cells. *Science (New York, N.Y.)* **355**; 10.1126/science.aah7111 (2017).

203. Hu, Y. *et al.* Metagenomic discovery of novel CRISPR-Cas13 systems. *Cell discovery* **8,** 107; 10.1038/s41421-022-00464-5 (2022).

204. Abudayyeh, O. O. *et al.* C2c2 is a single-component programmable RNA-guided RNA-targeting CRISPR effector. *Science (New York, N.Y.)* **353,** aaf5573; 10.1126/science.aaf5573 (2016).

205. Gupta, R. *et al.* Cas13d: A New Molecular Scissor for Transcriptome Engineering. *Frontiers in cell and developmental biology* **10,** 866800; 10.3389/fcell.2022.866800 (2022).

206. Konermann, S. *et al.* Transcriptome Engineering with RNA-Targeting Type VI-D CRISPR Effectors. *Cell* **173,** 665-676.e14; 10.1016/j.cell.2018.02.033. (2018).

207. Zhuang, C. *et al.* Silencing of lncRNA MIR497HG via CRISPR/Cas13d Induces Bladder Cancer Progression Through Promoting the Crosstalk Between Hippo/Yap and TGF-β/Smad Signaling. *Frontiers in molecular biosciences* **7,** 616768; 10.3389/fmolb.2020.616768 (2020).

208. Li, S. *et al.* Screening for functional circular RNAs using the CRISPR-Cas13 system. *Nature methods* **18,** 51–59; 10.1038/s41592-020-01011-4 (2021).

209. Bernstein, E., Caudy, A. A., Hammond, S. M. & Hannon, G. J. Role for a bidentate ribonuclease in the initiation step of RNA interference. *Nature* **409,** 363–366; 10.1038/35053110 (2001).

210. Pratt, A. J. & MacRae, I. J. The RNA-induced silencing complex: a versatile gene-silencing machine. *The Journal of biological chemistry* **284,** 17897–17901; 10.1074/jbc.R900012200 (2009).

211. Hannon, G. J. RNA interference. *Nature* **418,** 244–251; 10.1038/418244a (2002).

212. Stojic, L. *et al.* A high-content RNAi screen reveals multiple roles for long noncoding RNAs in cell division. *Nature communications* **11,** 1851; 10.1038/s41467-020-14978-7 (2020).

213. Huarte, M. *et al.* A large intergenic noncoding RNA induced by p53 mediates global gene repression in the p53 response. *Cell* **142,** 409–419; 10.1016/j.cell.2010.06.040 (2010).

214. Quemener, A. M. *et al.* The powerful world of antisense oligonucleotides: From bench to bedside. *Wiley interdisciplinary reviews. RNA* **11,** e1594; 10.1002/wrna.1594 (2020).

215. Wu, H. *et al.* Determination of the role of the human RNase H1 in the pharmacology of DNA-like antisense drugs. *The Journal of biological chemistry* **279,** 17181–17189; 10.1074/jbc.M311683200. (2004).

216. Bennett, C. F. & Swayze, E. E. RNA targeting therapeutics: molecular mechanisms of antisense oligonucleotides as a therapeutic platform. *Annual review of pharmacology and toxicology* **50,** 259–293; 10.1146/annurev.pharmtox.010909.105654 (2010).

217. Dias, N. *et al.* Antisense PNA tridecamers targeted to the coding region of Ha-ras mRNA arrest polypeptide chain elongation. *Journal of molecular biology* **294,** 403–416; 10.1006/jmbi.1999.3277 (1999).

218. Cerritelli, S. M. & Crouch, R. J. Ribonuclease H: the enzymes in eukaryotes. *The FEBS journal* **276,** 1494–1505; 10.1111/j.1742-4658.2009.06908.x (2009).

219. Dhuri, K. *et al.* Antisense Oligonucleotides: An Emerging Area in Drug Discovery and Development. *Journal of clinical medicine* **9,** 2004; 10.3390/jcm9062004 (2020).

220. Roux, B. T., Lindsay, M. A. & Heward, J. A. Knockdown of Nuclear-Located Enhancer RNAs and Long ncRNAs Using Locked Nucleic Acid GapmeRs. *Methods in molecular biology (Clifton, N.J.)* **1468,** 11–18; 10.1007/978-1-4939-4035-6_2 (2017).

221. Amodio, N. *et al.* Drugging the lncRNA MALAT1 via LNA gapmeR ASO inhibits gene expression of proteasome subunits and triggers anti-multiple myeloma activity. *Leukemia* **32,** 1948–1957; 10.1038/s41375-018-0067-3 (2018).

222. Oo, J. A. *et al.* Long non-coding RNA PCAT19 safeguards DNA in quiescent endothelial cells by preventing uncontrolled phosphorylation of RPA2. *Cell reports* **41,** 111670; 10.1016/j.celrep.2022.111670 (2022).

223. Lennox, K. A. & Behlke, M. A. Cellular localization of long non-coding RNAs affects silencing by RNAi more than by antisense oligonucleotides. *Nucleic acids research* **44,** 863–877; 10.1093/nar/gkv1206 (2016).

224. Goyal, A. *et al.* Challenges of CRISPR/Cas9 applications for long non-coding RNA genes. *Nucleic acids research* **45,** e12; 10.1093/nar/gkw883 (2017).

225. Perez-Pinera, P. *et al.* RNA-guided gene activation by CRISPR-Cas9-based transcription factors. *Nature methods* **10,** 973–976; 10.1038/nmeth.2600 (2013).

226. Xie, H. *et al.* LncRNA MALAT1 Inhibits Apoptosis and Promotes Invasion by Antagonizing miR-125b in Bladder Cancer Cells. *Journal of Cancer* **8,** 3803–3811; 10.7150/jca.21228 (2017).

227. Konermann, S. *et al.* Genome-scale transcriptional activation by an engineered CRISPR-Cas9 complex. *Nature* **517,** 583–588; 10.1038/nature14136. (2015).

228. Bester, A. C. *et al.* An Integrated Genome-wide CRISPRa Approach to Functionalize lncRNAs in Drug Resistance. *Cell* **173,** 649-664.e20; 10.1016/j.cell.2018.03.052 (2018).

229. Yamazaki, T., Fujikawa, C., Kubota, A., Takahashi, A. & Hirose, T. CRISPRa-mediated NEAT1 lncRNA upregulation induces formation of intact paraspeckles. *Biochemical and biophysical research communications* **504,** 218–224; 10.1016/j.bbrc.2018.08.158 (2018).

230. Robinson, E. K., Covarrubias, S. & Carpenter, S. The how and why of lncRNA function: An innate immune perspective. *Biochimica et biophysica acta. Gene regulatory mechanisms* **1863,** 194419; 10.1016/j.bbagrm.2019.194419 (2020).

231. Bassett, A. R. *et al.* Considerations when investigating lncRNA function in vivo. *eLife* **3,** e03058; 10.7554/eLife.03058 (2014).

232. Ma, Q. *et al.* Inducible lncRNA transgenic mice reveal continual role of HOTAIR in promoting breast cancer metastasis. *eLife* **11**; 10.7554/eLife.79126 (2022).

233. Huynh, N. P. *et al.* Long non-coding RNA GRASLND enhances chondrogenesis via suppression of the interferon type II signaling pathway. *eLife* **9**; 10.7554/eLife.49558 (2020).

234. Mackay, A. M. *et al.* Chondrogenic differentiation of cultured human mesenchymal stem cells from marrow. *Tissue engineering* **4,** 415–428; 10.1089/ten.1998.4.415 (1998).

235. Sahni, M. *et al.* FGF signaling inhibits chondrocyte proliferation and regulates bone development through the STAT-1 pathway. *Genes & development* **13,** 1361–1366; 10.1101/gad.13.11.1361 (1999).

236. Sahni, M., Raz, R., Coffin, J. D., Levy, D. & Basilico, C. STAT1 mediates the increased apoptosis and reduced chondrocyte proliferation in mice overexpressing FGF2. *Development (Cambridge, England)* **128,** 2119–2129; 10.1242/dev.128.11.2119 (2001).

237. Rostovskaya, M. *et al.* Clonal Analysis Delineates Transcriptional Programs of Osteogenic and Adipogenic Lineages of Adult Mouse Skeletal Progenitors. *Stem cell reports* **11,** 212–227; 10.1016/j.stemcr.2018.05.014 (2018).

238. Chen, B., Di Dong, Yao, Q., Zou, Y. & Hu, W. A novel prognostic cancer-related lncRNA signature in papillary renal cell carcinoma. *Cancer cell international* **21,** 545; 10.1186/s12935-021-02247-6 (2021).

239. Rothzerg, E. *et al.* Upregulation of 15 Antisense Long Non-Coding RNAs in Osteosarcoma. *Genes* **12**; 10.3390/genes12081132 (2021).

240. Hu, Y., Guo, G., Li, J., Chen, J. & Tan, P. Screening key lncRNAs with diagnostic and prognostic value for head and neck squamous cell carcinoma based on machine learning and mRNA-lncRNA co-expression network analysis. *Cancer biomarkers : section A of Disease markers* **27,** 195–206; 10.3233/CBM-190694 (2020).

241. Liu, Y. *et al.* H19- and hsa-miR-338-3p-mediated NRP1 expression is an independent predictor of poor prognosis in glioblastoma. *PloS one* **16,** e0260103; 10.1371/journal.pone.0260103 (2021).

242. Zhong, W., Qu, H., Yao, B., Wang, D. & Qiu, J. Analysis of a Long Non-coding RNA associated Signature to Predict Survival in Patients with Bladder Cancer. *Cureus* **14,** e24818; 10.7759/cureus.24818 (2022).

243. Wang, Y. *et al.* A nomogram combining long non-coding RNA expression profiles and clinical factors predicts survival in patients with bladder cancer. *Aging* **12,** 2857–2879; 10.18632/aging.102782. (2020).

244. Li, Z. *et al.* RNF144A-AS1, a TGF-β1- and hypoxia-inducible gene that promotes tumor metastasis and proliferation via targeting the miR-30c-2-3p/LOX axis in gastric cancer. *Cell & bioscience* **11,** 177; 10.1186/s13578-021-00689-z (2021).

245. Ding, Z. *et al.* Identification of an Immune-Related LncRNA Signature in Gastric Cancer to Predict Survival and Response to Immune Checkpoint Inhibitors. *Frontiers in cell and developmental biology* **9,** 739583; 10.3389/fcell.2021.739583 (2021).

246. Tong, X., Yang, Z., Wang, Q. & Zhang, D. RNF144A-AS1 promotes the development of glioma cells by targeting miR-665/HMGA1 axis. *Neuroscience letters* **765,** 136259; 10.1016/j.neulet.2021.136259 (2021).

247. Yang, S. *et al.* RNF144A-AS1 stabilizes TAF15 and promotes malignant biological behaviors of skin cutaneous melanoma. *Molecular and cellular biochemistry*; 10.1007/s11010-024-05045-6 (2024).

248. Ma, A. *et al.* GRASLND regulates melanoma cell progression by targeting the miR-218-5p/STAM2 axis. *Journal of translational medicine* **22,** 684; 10.1186/s12967-024-05397-z (2024).

249. Kim Denise Fischer. *Investigation of lncRNA GRASLND in the context of IFNγ signalling in melanoma.* Master Thesis (Technical University Dortmund, 2021).

250. Tang, Z. *et al.* GEPIA: a web server for cancer and normal gene expression profiling and interactive analyses. *Nucleic acids research* **45,** W98-W102; 10.1093/nar/gkx247 (2017).

251. Wiederschain, D. *et al.* Single-vector inducible lentiviral RNAi system for oncology target validation. *Cell cycle (Georgetown, Tex.)* **8,** 498–504; 10.4161/cc.8.3.7701 (2009).

252. Czarnek, M., Sarad, K., Karaś, A., Kochan, J. & Bereta, J. Non-targeting control for MISSION shRNA library silences SNRPD3 leading to cell death or permanent growth arrest. *Molecular therapy. Nucleic acids* **26,** 711–731; 10.1016/j.omtn.2021.09.004 (2021).

253. Feng, S. *et al.* Atp6v1c1 is an essential component of the osteoclast proton pump and in F-actin ring formation in osteoclasts. *The Biochemical journal* **417,** 195–203; 10.1042/BJ20081073 (2009).

254. Aslan Koşar, P. *et al.* The efficiency of Poly(ADP-Ribose) Polymerase (PARP) cleavage on detection of apoptosis in an experimental model of testicular torsion. *International journal of experimental pathology* **96,** 294–300; 10.1111/iep.12137 (2015).

255. Schreiber, V. *et al.* A dominant-negative mutant of human poly(ADP-ribose) polymerase affects cell recovery, apoptosis, and sister chromatid exchange following DNA damage. *Proceedings of the National Academy of Sciences of the United States of America* **92,** 4753–4757; 10.1073/pnas.92.11.4753 (1995).

256. Justus, C. R., Marie, M. A., Sanderlin, E. J. & Yang, L. V. Transwell In Vitro Cell Migration and Invasion Assays. *Methods in molecular biology (Clifton, N.J.)* **2644,** 349–359; 10.1007/978-1-0716-3052-5_22 (2023).

257. Lin Christina Qiu. *LncRNA GRASLND expression perturbation to investigate its role on melanoma cell transition and IFNγ sensitivity.* Bachelor Thesis (Technical University Dortmund, 2023).

258. Didovyk, A., Borek, B., Tsimring, L. & Hasty, J. Transcriptional regulation with CRISPR-Cas9: principles, advances, and applications. *Current opinion in biotechnology* **40,** 177–184; 10.1016/j.copbio.2016.06.003 (2016).

259. Gilbert, L. A. *et al.* Genome-Scale CRISPR-Mediated Control of Gene Repression and Activation. *Cell* **159,** 647–661; 10.1016/j.cell.2014.09.029 (2014).

260. Kent, W. J. *et al.* The human genome browser at UCSC. *Genome research* **12,** 996–1006; 10.1101/gr.229102 (2002).

261. Das, S., Zea Rojas, M. P. & Tran, E. J. Novel insights on the positive correlation between sense and antisense pairs on gene expression. *Wiley interdisciplinary reviews. RNA* **15,** e1864; 10.1002/wrna.1864 (2024).

262. Malumbres, M. & Barbacid, M. Cell cycle, CDKs and cancer: a changing paradigm. *Nature reviews. Cancer* **9,** 153–166; 10.1038/nrc2602 (2009).

263. Swoboda, A. *et al.* STAT3 promotes melanoma metastasis by CEBP-induced repression of the MITF pathway. *Oncogene* **40,** 1091–1105; 10.1038/s41388-020-01584-6 (2021).

264. Rossi, S. *et al.* TNF-alpha and metalloproteases as key players in melanoma cells aggressiveness. *Journal of experimental & clinical cancer research : CR* **37,** 326; 10.1186/s13046-018-0982-1 (2018).

265. Eichhoff, O. M. *et al.* Differential LEF1 and TCF4 expression is involved in melanoma cell phenotype switching. *Pigment cell & melanoma research* **24,** 631–642; 10.1111/j.1755-148X.2011.00871.x (2011).

266. Dimartino, D. *et al.* The Long Non-coding RNA lnc-31 Interacts with Rock1 mRNA and Mediates Its YB-1-Dependent Translation. *Cell reports* **23,** 733–740; 10.1016/j.celrep.2018.03.101 (2018).

267. Gal-Ben-Ari, S., Barrera, I., Ehrlich, M. & Rosenblum, K. PKR: A Kinase to Remember. *Frontiers in molecular neuroscience* **11,** 480; 10.3389/fnmol.2018.00480 (2018).

268. Pakos-Zebrucka, K. *et al.* The integrated stress response. *EMBO reports* **17,** 1374–1395; 10.15252/embr.201642195 (2016).

269. Ghosh, S., May, M. J. & Kopp, E. B. NF-kappa B and Rel proteins: evolutionarily conserved mediators of immune responses. *Annual review of immunology* **16,** 225–260; 10.1146/annurev.immunol.16.1.225. (1998).

270. Verma, I. M., Stevenson, J. K., Schwarz, E. M., van Antwerp, D. & Miyamoto, S. Rel/NF-kappa B/I kappa B family: intimate tales of association and dissociation. *Genes & development* **9,** 2723–2735; 10.1101/gad.9.22.2723 (1995).

271. García, M. A. *et al.* Impact of protein kinase PKR in cell biology: from antiviral to antiproliferative action. *Microbiology and molecular biology reviews : MMBR* **70,** 1032–1060; 10.1128/MMBR.00027-06 (2006).

272. Vivas-García, Y. *et al.* Lineage-Restricted Regulation of SCD and Fatty Acid Saturation by MITF Controls Melanoma Phenotypic Plasticity. *Molecular cell* **77,** 120-137.e9; 10.1016/j.molcel.2019.10.014 (2020).

273. Shen, S. *et al.* Cytoplasmic STAT3 represses autophagy by inhibiting PKR activity. *Molecular cell* **48,** 667–680; 10.1016/j.molcel.2012.09.013 (2012).

274. Abbas, A. K., Lichtman, A. H. & Pillai, S. *Cellular and molecular immunology* (Elsevier, Philadelphia, Pennsylvania, 2022).

275. Mesa, R. A. Ruxolitinib, a selective JAK1 and JAK2 inhibitor for the treatment of myeloproliferative neoplasms and psoriasis. *IDrugs : the investigational drugs journal* **13,** 394–403 (2010).

276. Hu, X., Li, J., Fu, M., Zhao, X. & Wang, W. The JAK/STAT signaling pathway: from bench to clinic. *Signal transduction and targeted therapy* **6,** 402; 10.1038/s41392-021-00791-1 (2021).

277. Ma, Y., Wang, N. & Yang, S. Skin cutaneous melanoma properties of immune-related lncRNAs identifying potential prognostic biomarkers. *Aging* **14,** 3030–3048; 10.18632/aging.203982 (2022).

278. Gajewski, T. F. *et al.* Cancer Immunotherapy Targets Based on Understanding the T Cell-Inflamed Versus Non-T Cell-Inflamed Tumor Microenvironment. *Advances in experimental medicine and biology* **1036,** 19–31; 10.1007/978-3-319-67577-0_2. (2017).

279. Boehm, U., Klamp, T., Groot, M. & Howard, J. C. Cellular responses to interferon-gamma. *Annual review of immunology* **15,** 749–795; 10.1146/annurev.immunol.15.1.749 (1997).

280. Lanza, L. *et al.* Interferons up-regulate with different potency HLA class I antigen expression in M14 human melanoma cell line. Possible interaction with glucocorticoid hormones. *Cancer immunology, immunotherapy : CII* **41,** 23–28; 10.1007/BF01788956 (1995).

281. Friedman, R. L., Manly, S. P., McMahon, M., Kerr, I. M. & Stark, G. R. Transcriptional and posttranscriptional regulation of interferon-induced gene expression in human cells. *Cell* **38,** 745–755; 10.1016/0092-8674(84)90270-8 (1984).

282. Jhunjhunwala, S., Hammer, C. & Delamarre, L. Antigen presentation in cancer: insights into tumour immunogenicity and immune evasion. *Nature reviews. Cancer* **21,** 298–312; 10.1038/s41568-021-00339-z (2021).

283. Wang, J. *et al.* Exploring Tumor Immune Microenvironment and Its Associations With Molecular Characteristics in Melanoma. *Frontiers in oncology* **12,** 821578; 10.3389/fonc.2022.821578 (2022).

284. Tokunaga, R. *et al.* CXCL9, CXCL10, CXCL11/CXCR3 axis for immune activation - A target for novel cancer therapy. *Cancer treatment reviews* **63,** 40–47; 10.1016/j.ctrv.2017.11.007 (2018).

285. Kalaora, S. *et al.* Immunoproteasome expression is associated with better prognosis and response to checkpoint therapies in melanoma. *Nature communications* **11,** 896; 10.1038/s41467-020-14639-9 (2020).

286. Pishesha, N., Harmand, T. J. & Ploegh, H. L. A guide to antigen processing and presentation. *Nature reviews. Immunology* **22,** 751–764; 10.1038/s41577-022-00707-2 (2022).

287. Thier, B. *et al.* Innate immune receptor signaling induces transient melanoma dedifferentiation while preserving immunogenicity. *Journal for immunotherapy of cancer* **10**; 10.1136/jitc-2021-003863 (2022).

288. Han, J., Wu, M. & Liu, Z. Dysregulation in IFN-γ signaling and response: the barricade to tumor immunotherapy. *Frontiers in immunology* **14,** 1190333; 10.3389/fimmu.2023.1190333 (2023).

289. Wu, W. *et al.* The Role of Long Non-Coding RNF144A-AS1 in Cancer Progression. *Cell biochemistry and biophysics* **82,** 2007–2017; 10.1007/s12013-024-01411-9 (2024).

290. Kim, K. H. & Sederstrom, J. M. Assaying Cell Cycle Status Using Flow Cytometry. *Current protocols in molecular biology* **111,** 28.6.1-28.6.11; 10.1002/0471142727.mb2806s111. (2015).

291. Glick, B. R. Metabolic load and heterologous gene expression. *Biotechnology advances* **13,** 247–261; 10.1016/0734-9750(95)00004-A (1995).

292. Jones, J. *et al.* Optimization of tetracycline-responsive recombinant protein production and effect on cell growth and ER stress in mammalian cells. *Biotechnology and bioengineering* **91,** 722–732; 10.1002/bit.20566 (2005).

293. Li, Z. & Rinas, U. Recombinant protein production associated growth inhibition results mainly from transcription and not from translation. *Microbial cell factories* **19,** 83; 10.1186/s12934-020-01343-y (2020).

294. Cho, S. *et al.* High-Level dCas9 Expression Induces Abnormal Cell Morphology in Escherichia coli. *ACS synthetic biology* **7,** 1085–1094; 10.1021/acssynbio.7b00462 (2018).

295. Johnston, A. D. *et al.* A Cellular Stress Response Induced by the CRISPR-dCas9 Activation System Is Not Heritable Through Cell Divisions. *The CRISPR journal* **3,** 188–197; 10.1089/crispr.2019.0077 (2020).

296. Ho, S.-R., Mahanic, C. S., Lee, Y.-J. & Lin, W.-C. RNF144A, an E3 ubiquitin ligase for DNA-PKcs, promotes apoptosis during DNA damage. *Proceedings of the National Academy of Sciences of the United States of America* **111,** E2646-55; 10.1073/pnas.1323107111 (2014).

297. Xiao, S., Han, X., Bai, S. & Chen, R. Analysis of immune cell infiltration characteristics in severe acute pancreatitis through integrated bioinformatics. *Scientific reports* **14,** 8711; 10.1038/s41598-024-59205-1 (2024).

298. Yang, B. *et al.* RNF144A promotes antiviral responses by modulating STING ubiquitination. *EMBO reports* **24,** e57528; 10.15252/embr.202357528 (2023).

299. Hossain, S. M. & Eccles, M. R. Phenotype Switching and the Melanoma Microenvironment; Impact on Immunotherapy and Drug Resistance. *International journal of molecular sciences* **24**; 10.3390/ijms24021601 (2023).

300. Wrana, J. L. Signaling by the TGFβ superfamily. *Cold Spring Harbor perspectives in biology* **5,** a011197; 10.1101/cshperspect.a011197 (2013).

301. Hao, Y., Baker, D. & Dijke, P. ten. TGF-β-Mediated Epithelial-Mesenchymal Transition and Cancer Metastasis. *International journal of molecular sciences* **20**; 10.3390/ijms20112767 (2019).

302. Tuncer, E. *et al.* SMAD signaling promotes melanoma metastasis independently of phenotype switching. *The Journal of clinical investigation* **129,** 2702–2716; 10.1172/JCI94295 (2019).

303. Graf, J. & Kretz, M. From structure to function: Route to understanding lncRNA mechanism. *BioEssays : news and reviews in molecular, cellular and developmental biology* **42,** e2000027; 10.1002/bies.202000027. (2020).

304. Ferrè, F., Colantoni, A. & Helmer-Citterich, M. Revealing protein-lncRNA interaction. *Briefings in bioinformatics* **17,** 106–116; 10.1093/bib/bbv031 (2016).

305. Shang, D. *et al.* A global view of network of lncRNAs and their binding proteins. *Molecular bioSystems* **11,** 656–663; 10.1039/c4mb00409d. (2015).

306. Liu, X., Fields, R., Schweppe, D. K. & Paulo, J. A. Strategies for mass spectrometry-based phosphoproteomics using isobaric tagging. *Expert review of proteomics* **18,** 795–807; 10.1080/14789450.2021.1994390 (2021).

307. Thompson, A. *et al.* Tandem Mass Tags: A Novel Quantification Strategy for Comparative Analysis of Complex Protein Mixtures by MS/MS. *Analytical Chemistry* **75,** 1895–1904; 10.1021/ac0262560 (2003).

308. Giansanti, P., Tsiatsiani, L., Low, T. Y. & Heck, A. J. R. Six alternative proteases for mass spectrometry-based proteomics beyond trypsin. *Nature protocols* **11,** 993–1006; 10.1038/nprot.2016.057. (2016).

309. Swaney, D. L., Wenger, C. D. & Coon, J. J. Value of using multiple proteases for large-scale mass spectrometry-based proteomics. *Journal of proteome research* **9,** 1323–1329; 10.1021/pr900863u. (2010).

310. Li, Y. *et al.* Immunoprecipitation and mass spectrometry defines an extensive RBM45 protein-protein interaction network. *Brain research* **1647,** 79–93; 10.1016/j.brainres.2016.02.047 (2016).

311. Han, L., Wang, L. & Wu, F. *RBM45 Promoted HCC Growth and Metastasis by Stabilizing BCL2 and Twist1 mRNA* (2021).

312. Lv, Y. *et al.* Loss of RBM45 inhibits breast cancer progression by reducing the SUMOylation of IRF7 to promote IFNB1 transcription. *Cancer letters* **596,** 216988; 10.1016/j.canlet.2024.216988 (2024).

313. Gong, J. *et al.* RBM45 competes with HDAC1 for binding to FUS in response to DNA damage. *Nucleic acids research* **45,** 12862–12876; 10.1093/nar/gkx1102 (2017).

314. Thacker, J. & Zdzienicka, M. Z. The XRCC genes: expanding roles in DNA double-strand break repair. *DNA repair* **3,** 1081–1090; 10.1016/j.dnarep.2004.04.012 (2004).

315. Wang, Z., Lin, H., Hua, F. & Hu, Z. Repairing DNA damage by XRCC6/KU70 reverses TLR4-deficiency-worsened HCC development via restoring senescence and autophagic flux. *Autophagy* **9,** 925–927; 10.4161/auto.24229. (2013).

316. Thacker, J. & Zdzienicka, M. Z. The mammalian XRCC genes: their roles in DNA repair and genetic stability. *DNA repair* **2,** 655–672; 10.1016/S1568-7864(03)00062-4. (2003).

317. Goodarzi, H., Warren, R. S., Yu, J. & Fish, L. A regulatory program that promotes metastasis in colorectal cancer (CRC) through modulation of mRNA stability. *Journal of clinical oncology : official journal of the American Society of Clinical Oncology* **37,** 3523; 10.1200/JCO.2019.37.15_SUPPL.3523 (2019).

318. Yu, J. *et al.* RBMS1 Suppresses Colon Cancer Metastasis through Targeted Stabilization of Its mRNA Regulon. *Cancer discovery* **10,** 1410–1423; 10.1158/2159-8290.CD-19-1375. (2020).

319. Zhang, J. *et al.* Loss of RBMS1 promotes anti-tumor immunity through enabling PD-L1 checkpoint blockade in triple-negative breast cancer. *Cell death and differentiation* **29,** 2247–2261; 10.1038/s41418-022-01012-0 (2022).

320. Liu, M. *et al.* RBMS1 promotes gastric cancer metastasis through autocrine IL-6/JAK2/STAT3 signaling. *Cell death & disease* **13,** 287; 10.1038/s41419-022-04747-3 (2022).

321. Schult, P. & Paeschke, K. The DEAH helicase DHX36 and its role in G-quadruplex-dependent processes. *Biological chemistry* **402,** 581–591; 10.1515/hsz-2020-0292. (2021).

322. Srinivasan, S., Liu, Z., Chuenchor, W., Xiao, T. S. & Jankowsky, E. Function of Auxiliary Domains of the DEAH/RHA Helicase DHX36 in RNA Remodeling. *Journal of molecular biology* **432,** 2217–2231; 10.1016/j.jmb.2020.02.005. (2020).

323. Yoo, J.-S. *et al.* DHX36 enhances RIG-I signaling by facilitating PKR-mediated antiviral stress granule formation. *PLoS pathogens* **10,** e1004012; 10.1371/journal.ppat.1004012 (2014).

324. Dalet, A., Gatti, E. & Pierre, P. Integration of PKR-dependent translation inhibition with innate immunity is required for a coordinated anti-viral response. *FEBS letters* **589,** 1539–1545; 10.1016/j.febslet.2015.05.006 (2015).

325. Suwei, D. *et al.* Metformin inhibits melanoma cell metastasis by suppressing the miR-5100/SPINK5/STAT3 axis. *Cellular & molecular biology letters* **27,** 48; 10.1186/s11658-022-00353-5 (2022).

326. Niso-Santano, M. *et al.* Direct interaction between STAT3 and EIF2AK2 controls fatty acid-induced autophagy. *Autophagy* **9,** 415–417; 10.4161/auto.22910 (2013).

327. Wong, A. H. *et al.* Physical association between STAT1 and the interferon-inducible protein kinase PKR and implications for interferon and double-stranded RNA signaling pathways. *The EMBO journal* **16,** 1291–1304; 10.1093/emboj/16.6.1291 (1997).

328. Wong, A. H. *et al.* Enhanced antiviral and antiproliferative properties of a STAT1 mutant unable to interact with the protein kinase PKR. *The Journal of biological chemistry* **276,** 13727–13737; 10.1074/jbc.M011240200 (2001).

329. Zaretsky, J. M. *et al.* Mutations Associated with Acquired Resistance to PD-1 Blockade in Melanoma. *The New England journal of medicine* **375,** 819–829; 10.1056/NEJMoa1604958 (2016).

330. Saadi, W., Fatmi, A., Pallardó, F. V., García-Giménez, J. L. & Mena-Molla, S. Long Non-Coding RNAs as Epigenetic Regulators of Immune Checkpoints in Cancer Immunity. *Cancers* **15**; 10.3390/cancers15010184 (2022).

331. Zhou, W.-Y. *et al.* Long noncoding RNA LINC00473 drives the progression of pancreatic cancer via upregulating programmed death-ligand 1 by sponging microRNA-195-5p. *Journal of cellular physiology* **234,** 23176–23189; 10.1002/jcp.28884 (2019).

332. Fan, F. *et al.* Dual targeting of PD-L1 and PD-L2 by PCED1B-AS1 via sponging hsa-miR-194-5p induces immunosuppression in hepatocellular carcinoma. *Hepatology international* **15,** 444–458; 10.1007/s12072-020-10101-6 (2021).

333. Yao, K., Wang, Q., Jia, J. & Zhao, H. A competing endogenous RNA network identifies novel mRNA, miRNA and lncRNA markers for the prognosis of diabetic pancreatic cancer. *Tumour biology : the journal of the International Society for Oncodevelopmental Biology and Medicine* **39,** 1010428317707882; 10.1177/1010428317707882 (2017).

334. Wang, Z., Tollervey, J., Briese, M., Turner, D. & Ule, J. CLIP: construction of cDNA libraries for high-throughput sequencing from RNAs cross-linked to proteins in vivo. *Methods (San Diego, Calif.)* **48,** 287–293; 10.1016/j.ymeth.2009.02.021 (2009).

335. Solberg, N. & Krauss, S. Luciferase assay to study the activity of a cloned promoter DNA fragment. *Methods in molecular biology (Clifton, N.J.)* **977,** 65–78; 10.1007/978-1-62703-284-1_6. (2013).

336. Ratnadiwakara, M. & Änkö, M.-L. mRNA Stability Assay Using transcription inhibition by Actinomycin D in Mouse Pluripotent Stem Cells. *Bio-protocol* **8,** e3072; 10.21769/BioProtoc.3072 (2018).

337. Choo, Y. S. & Zhang, Z. Detection of protein ubiquitination. *Journal of visualized experiments : JoVE*; 10.3791/1293 (2009).

338. Du, H. *et al.* Antitumor Responses in the Absence of Toxicity in Solid Tumors by Targeting B7-H3 via Chimeric Antigen Receptor T Cells. *Cancer cell* **35,** 221-237.e8; 10.1016/j.ccell.2019.01.002 (2019).

339. RIPA Lysis Buffer. *Cold Spring Harb Protoc* **2017,** pdb.rec101428; 10.1101/pdb.rec101428 (2017).

340. Doench, J. G. *et al.* Optimized sgRNA design to maximize activity and minimize off-target effects of CRISPR-Cas9. *Nature biotechnology* **34,** 184–191; 10.1038/nbt.3437 (2016).

341. Hsu, P. D. *et al.* DNA targeting specificity of RNA-guided Cas9 nucleases. *Nature biotechnology* **31,** 827–832; 10.1038/nbt.2647 (2013).

342. Zhao, F. *et al.* Melanoma Lesions Independently Acquire T-cell Resistance during Metastatic Latency. *Cancer research* **76,** 4347–4358; 10.1158/0008-5472.CAN-16-0008 (2016).

343. Stupia, S. *et al.* HLA Class II Loss and JAK1/2 Deficiency Coevolve in Melanoma Leading to CD4 T-cell and IFNγ Cross-Resistance. *Clinical cancer research : an official journal of the American Association for Cancer Research* **29,** 2894–2907; 10.1158/1078-0432.CCR-23-0099. (2023).

344. Livak, K. J. & Schmittgen, T. D. Analysis of relative gene expression data using real-time quantitative PCR and the 2(-Delta Delta C(T)) Method. *Methods (San Diego, Calif.)* **25,** 402–408; 10.1006/meth.2001.1262 (2001).

345. DeCaprio, J. & Kohl, T. O. Detergent Lysis of Tissue Culture Cells for Immunoprecipitation. *Cold Spring Harb Protoc* **2017,** pdb.prot098558; 10.1101/pdb.prot098558 (2017).

346. Hanniford, D. *et al.* Epigenetic Silencing of CDR1as Drives IGF2BP3-Mediated Melanoma Invasion and Metastasis. *Cancer cell* **37,** 55-70.e15; 10.1016/j.ccell.2019.12.007 (2020).

347. B. Ellis, P. Haaland, F. Hahne, N. Le Meur, N. Gopalakrishnan, J. Spidlen, M. Jiang. *flowCore* (Bioconductor, 2017).

348. Lo, K., Brinkman, R. R. & Gottardo, R. Automated gating of flow cytometry data via robust model-based clustering. *Cytometry. Part A : the journal of the International Society for Analytical Cytology* **73,** 321–332; 10.1002/cyto.a.20531 (2008).

349. Lo, K., Hahne, F., Brinkman, R. R. & Gottardo, R. flowClust: a Bioconductor package for automated gating of flow cytometry data. *BMC bioinformatics* **10,** 145; 10.1186/1471-2105-10-145 (2009).

350. Malek, M. *et al.* flowDensity: reproducing manual gating of flow cytometry data by automated density-based cell population identification. *Bioinformatics (Oxford, England)* **31,** 606–607; 10.1093/bioinformatics/btu677 (2015).

351. Florian Hahne, Nishant Gopalakrishnan, Alireza HadjKhodabakhshi, Chao-Jen Wong, Kyongryun Lee. *flowStats* (Bioconductor, 2017).

352. Van, P., Jiang, W., Gottardo, R. & Finak, G. ggCyto: next generation open-source visualization software for cytometry. *Bioinformatics (Oxford, England)* **34,** 3951–3953; 10.1093/bioinformatics/bty441 (2018).

353. Katsantoni, M. *et al. ZARP: An automated workflow for processing of RNA-seq data* (2021).

354. Andrews, S. FASTQC. A quality control tool for high throughput sequence data (2010).

355. Ewels, P., Magnusson, M., Lundin, S. & Käller, M. MultiQC: summarize analysis results for multiple tools and samples in a single report. *Bioinformatics (Oxford, England)* **32,** 3047–3048; 10.1093/bioinformatics/btw354 (2016).

356. Martin, M. Cutadapt removes adapter sequences from high-throughput sequencing reads. *EMBnet j.* **17,** 10; 10.14806/ej.17.1.200 (2011).

357. Dobin, A. *et al.* STAR: ultrafast universal RNA-seq aligner. *Bioinformatics (Oxford, England)* **29,** 15–21; 10.1093/bioinformatics/bts635 (2013).

358. Patro, R., Duggal, G., Love, M. I., Irizarry, R. A. & Kingsford, C. Salmon provides fast and bias-aware quantification of transcript expression. *Nature methods* **14,** 417–419; 10.1038/nmeth.4197 (2017).

359. Love, M. I., Huber, W. & Anders, S. Moderated estimation of fold change and dispersion for RNA-seq data with DESeq2. *Genome biology* **15,** 550; 10.1186/s13059-014-0550-8 (2014).

360. Kevin Blighe. *EnhancedVolcano* (Bioconductor, 2018).

361. Gu, Z., Eils, R. & Schlesner, M. Complex heatmaps reveal patterns and correlations in multidimensional genomic data. *Bioinformatics (Oxford, England)* **32,** 2847–2849; 10.1093/bioinformatics/btw313 (2016).

362. Wu, T. *et al.* clusterProfiler 4.0: A universal enrichment tool for interpreting omics data. *Innovation (Cambridge (Mass.))* **2,** 100141; 10.1016/j.xinn.2021.100141 (2021).

363. Guangchuang Yu. *enrichplot* (Bioconductor, 2018).

364. Cox, J. & Mann, M. MaxQuant enables high peptide identification rates, individualized p.p.b.-range mass accuracies and proteome-wide protein quantification. *Nature biotechnology* **26,** 1367–1372; 10.1038/nbt.1511 (2008).

365. Tyanova, S. & Cox, J. Perseus: A Bioinformatics Platform for Integrative Analysis of Proteomics Data in Cancer Research. *Methods in molecular biology (Clifton, N.J.)* **1711,** 133–148; 10.1007/978-1-4939-7493-1_7 (2018).

366. Goedhart, J. & Luijsterburg, M. S. VolcaNoseR is a web app for creating, exploring, labeling and sharing volcano plots. *Scientific reports* **10,** 20560; 10.1038/s41598-020-76603-3 (2020).

367. Holman, J. D., Tabb, D. L. & Mallick, P. Employing ProteoWizard to Convert Raw Mass Spectrometry Data. *Current protocols in bioinformatics* **46,** 13.24.1-13.24.9; 10.1002/0471250953.bi1324s46 (2014).

368. Da Veiga Leprevost, F. *et al.* Philosopher: a versatile toolkit for shotgun proteomics data analysis. *Nature methods* **17,** 869–870; 10.1038/s41592-020-0912-y (2020).

369. Käll, L., Canterbury, J. D., Weston, J., Noble, W. S. & MacCoss, M. J. Semi-supervised learning for peptide identification from shotgun proteomics datasets. *Nature methods* **4,** 923–925; 10.1038/nmeth1113 (2007).

370. Kong, A. T., Leprevost, F. V., Avtonomov, D. M., Mellacheruvu, D. & Nesvizhskii, A. I. MSFragger: ultrafast and comprehensive peptide identification in mass spectrometry-based proteomics. *Nature methods* **14,** 513–520; 10.1038/nmeth.4256 (2017).

371. Teo, G. C., Polasky, D. A., Yu, F. & Nesvizhskii, A. I. Fast Deisotoping Algorithm and Its Implementation in the MSFragger Search Engine. *Journal of proteome research* **20,** 498–505; 10.1021/acs.jproteome.0c00544 (2021).

372. Yang, K. L. *et al.* MSBooster: improving peptide identification rates using deep learning-based features. *Nature communications* **14,** 4539; 10.1038/s41467-023-40129-9 (2023).

373. Kohler, D. *et al.* MSstatsShiny: A GUI for Versatile, Scalable, and Reproducible Statistical Analyses of Quantitative Proteomic Experiments. *Journal of proteome research* **22,** 551–556; 10.1021/acs.jproteome.2c00603 (2023).

374. Colaprico, A. *et al.* TCGAbiolinks: an R/Bioconductor package for integrative analysis of TCGA data. *Nucleic acids research* **44,** e71; 10.1093/nar/gkv1507 (2016).